Localisation of key proteases involved in the assembly and repair of Photosystem II in cyanobacterium *Synechocystis* sp. PCC 6803

Joanna Sacharz

A thesis submitted for the degree of Doctor of Philosophy in the University of London

School of Biological and Chemical Sciences

Queen Mary University of London

2014

Declaration

I certify that unless otherwise stated in the text, this thesis is written entirely by myself and that the research to which it refers is my own. Any ideas or quotations from the work of other people, published or otherwise are fully acknowledged in accordance with the standard referencing practices of the discipline.

The research was carried out with guidance and support my supervisor, Professor Conrad Mullineaux.

Joanna Sacharz

"a naturalist's life would be a happy one if he had only to observe and never to write"

Charles Darwin

Abstract

All photosynthetic organisms use light as a source of energy, however prolonged excessively high light causes irreversible damage to the main photosynthetic complexes. In particular the D1 polypeptide of Photosystem II is susceptible to damage and must be degraded and replaced. While the concept of PSII repair has attracted intensive research, important details remain to be determined. The sub-cellular localisation of proteases involved in PSII repair and assembly is investigated here in the model cyanobacterium *Synechocystis* sp. PCC 6803, by employing fluorescent protein tagging and fluorescence imaging *in vivo*. Results show that all FtsH protease homologues in *Synechocystis* are localised to distinct regions of the plasma membrane (FtsH1) and thylakoids (FtsH2, FtsH3, FtsH4). Importantly, FtsH2, involved in PSII repair, remains within distinct thylakoid membrane zones when activated by high light, leading to the hypothesis of localised PSII repair centres in the thylakoid membranes.

In order to assess composition of the FtsH2-defined membrane zones, a novel technique for isolating membrane sub-fractions by anti-GFP pull-downs was employed. Mass spectrometry identified potentially interacting and neighbouring proteins within the repair centres, whose content changes under different light exposure. Furthermore, observed changes in FtsH2 and FtsH4 distributions under iron and copper deprivation suggest functions in responses to other stress conditions. To find the locations of D1 synthesis during PSII repair and *de novo* assembly, the D1 C-terminal processing peptidase CtpA was similarly GFP-tagged and observed *in vivo*. Results suggest that D1 synthesis for PSII repair takes place in the thylakoid

membranes, while D1 synthesis for *de novo* PSII biogenesis takes place in specialised regions at both edges of the thylakoid system, adjacent to the plasma membrane and protruding into the central cytoplasm. By localising crucial cellular enzymes *in vivo*, this study demonstrates functional compartmentalisation and membrane heterogeneity in a prokaryote.

Acknowledgements

I am deeply thankful to all, who contributed to this project as well as supported me throuhgout the whole period. Mainly my sincere gratitude to my supervisor, Prof. Conrad Mullineaux for giving me opportunity to work in his group. His open-minded attitude and encouragement during these years guided me well. His belief in my abilities helped me become independent and follow my own ideas. I will keep it as a life dogma to always be as easy-going as Conrad.

This project would not be started or completed without the great support of a former postdoc Dr Samatha Bryan and Dr Edward Spence. They opened a mysterious door for me by leading me hand-in-hand, teaching me basics of molecular biology, and inspiring me with ideas. I owe them both not only for being such great mentors but for being amazing friends. Last year I had a great opportunity to learn from the best, by being watched and looked after by Dr Tchern Lenn I managed to master new skills in molecular biology. His relaxed attitude and encouragement were irreplace- able during my final year.

A meaningful part of this project was performed under supervision of Prof. Peter Nixon at Imperial College of London. His priceless advice and comments contributed to remarkable improvements in biochemical data. Work would not be completed if not for the great help of Dr Jianfeng Yu who accompanied me with marathon slots of experiments. He is a great support in every day life and his tea makes every long day bearable. Thanks to Prof Josef Komenda and Prof Bryan Diner for their help with antibodies.

Prof Nigel Burroughs contributed to this project with his expertise in data

analysis, he prepared algorythms used in this study.
I also wish to thank for the support to my PhD panel members, Prof Alexander Ruban and Prof Richard Pickersgill.

In my final year I had a great opportunity by being awarded with a funding for a short-term fellowship by Japan Society for the Promotion in Science (JSPS). I spent three months working at the University of Tokyo, under supervision of Prof Hajime Wada, analysing lipids in the cyanobacterial membranes. It was a life experience, Wada's sen-sei support, warm and friendly attitude made my time in Japan unforgettable. With accompanied by his amazing and skilled group listing: Kobayashi sen-sei, Okazaki-san, Saito-san, Tanoue-san, Endo-san, Fuji-san, Hori-san and Sasaki-san I have managed to master the subject of lipid analysis and started a new project. All members have their special place in my heart. Special mention to Prof Ikaubashi and Prof Murata who spent their time with me talking on most exciting and interesting subjects of science.
During these nearly four years, I have worked with a group of collegues, listing among: Giulia, Dennis, Gianna, Petra, Tomasz, Luning, Fang, Anja, Yumi, Ruth and Shuang my great apprecitations and thanks to them.
Additionally, I wish to thank my dear friends of Queen Mary: Paolo, Gianna, Miao, Shuang, Fang, Fabrizio, Phil, Freida, Lucia, who I was lucky to meet during these 3 years.

Finally, thanks to my family, my parents who always believed in me and encouraged me. And mostly I am grateful to my partner Greg and our little daughter Matilda, who have always been by my side in good and bad times, supported, understood and motivated me to push through the hard times and made me believe in miracles. Thank you.

My last but not least thanks goes to Queen Mary University of London, for being my home for the last four years. I wish to acknowledge Queen Mary for the travel grant funding. Finally, I would like to thank the HARVEST Marie Curie ACTIONS (with special acknowledgement of Prof Jan Dekker) for funding my studies, supporting my living in London and letting me become a part of a talented photosynthetic research group, being honoured to attend numerous meetings and workshops.

***

In both life and science "whatever it is you're seeking won't come in the form you're expecting" (Haruki Murakami).

Contents

List of Figures

List of Tables

Abbreviations

AFM -atomic force microscopy

ATP - adenosine triphosphate

ADP - adenosine diphosphate

CCD - charge-coupled device

DCBQ - 2,6 dichloro-p-benzoquinone

DGDG - digalactosyl diacylglycerol

DM - dodecyl maltoside

EDTA - ethylenediaminetetraacetate

FRAP - fluorescence recovery after photobleaching

GFP - green fluorescent protein

HL - high light

LL - low light

LPS - lipopolysaccharide

MGDG - monogalactosyl diacylglycerol

NA - numerical aperture

NADH - reduced nicotinamide adenine dinucleotide

OD - optical density

PAGE - polyacrylamide gel electrophoresis

PC - phosphotidylcholine

PC - phycobilisomes

PC - phycocyanin

PG - phosphatidylglycerol

PE - phosphotidylethanolamine

PL - phosholipids

PMT - photomultiplier

SbtA - sodium dependent bicarbonate transporter

SQDG - sulfoquinovosyl diacylglycerol

Chapter 1

Introduction

This work combines two important biological issues; clearly it is a meaningful piece of work on photosynthesis *per se*, giving the answers to some intruding questions concerning photosystem II repair and assembly. Furthermore, studying membrane proteins *in vivo* contributes to a better understanding of structure and functions of biological membranes.

In vivo techniques have an outstanding advantage of observing processes in real time in a living organism and are indispensible to neatly complement and confirm data collected in *in vitro* studies.

We chose the cyanobacterium *Synechocystis* sp. PCC 6803 (hereafter *Synechocystis*) for this study, firstly because cyanobacteria are considered to be the progenitors of the chloroplasts in green plants and algae. *Synechocystis*, is also an advantageous model organism for photosynthetic studies, mainly due to its sequenced genome, ease in generating mutants and relatively simple structure. The large protein complexes of the photosynthetic and respiratory electron transfer chains reside in the internal system of thy-

lakoid membranes. These features adopted a geometry of multiple concentric shells (Nierzwickibauer *et al*., 1983). It is unclear if in such arrangement any connections between thylakoid and cytoplasmic membranes exist. Hence, all lipids and proteins originating in the cytoplasm are very carefully designed to ensure their proper translocation and assembly into the correct lipid bi-layer in this extraordinary membrane-enriched system. One of the most convenient and straightforward approaches to study protein localisation is to employ minimally invasive *in vivo* techniques, such as the approach developed in this study.

1.1 Photosynthesis

> ...the life of the planet began the long, slow process of modulating and regulating the physical conditions of the planet. The oxygen in today's atmosphere is almost entirely the result of photosynthetic living, which had its start with the appearance of blue-green algae among the microorganisms
>
> Lewis Thomas (In Late Night Thoughts on Listening to Mahler Ninth Symphony (1984)

The Lewis Thomas's quote simply sums up the importance of photosynthetic organisms, which evolved round 3 billion years ago and transformed the Earth's atmosphere composition by increasing oxygen level (Blankenship and Hartman, 1998). Plants as the accessible source of energy have always been in human interest. However, the relation between sunlight and plant growth has been proposed only in 1774. Joseph Priestley for the

first time mentioned in his short reports the impact of solar energy and built foundation for later great minds in the magnificent field of photosynthesis. Based on above, in 1779 Jan Ingenhousz was honoured with the title *the father of photosynthesis* in recognition to his discovery of plant respiration.

> I observed that plants not only have a faculty to correct bad air in six to ten days, by growing in it...but that they perform this important office in a complete manner in a few hours; that this wonderful operation is by no means owing to the vegetation of the plant but to the influence of light of the sun upon the plant.
>
> Jan Ingenhousz

It is now known that photosynthesis is simply an endothermic chemical reaction triggered by light and according to Le Chatelier's principle:

> heat, either by conduction or radiation, promotes the equilibrium in the direction of plant (carbohydrate) growth

$$6\ CO_2 + 12\ H_2O + 18\ ATP + 12\ NADPH + 48\ h\nu \rightarrow$$
$$C_6H_{12}O_6 + 18\ ADP + 18\ P_i + 12\ NADP^+ + 12\ H^+ + 6\ O_2$$

The equation describes the overall biochemistry of photosynthesis for the formation of one glucose molecule from six CO_2 molecules. The oxygenic (i.e. aerobic) photosynthesis is common for cyanobacteria, algae and plants. However, in 1941 van Niel discovered that green sulfur and purple bacteria exhibits similar metabolic process, where water was replaced with other hydrogen compounds as an electron donor and where hydrogen is the new

by-product, proposing to call these reactions the anoxygenic (i.e. anaerobic) photosynthesis. The principles for both types of processes remain alike and results in capturing the sunlight energy into chemical bonds energy of NADPH and ATP, fuel useful for cellular processes.

1.2 Photosynthesis in cyanobacteria and plants

There were long periods of time in evolution of cyanobacteria, algae and plants, however most of the photosynthetic components remain preserved. Algae and plants developed a specialised organelle the chloroplast, according to the endosymbiothic theory it originated after cyanobacteria engulfed by a bigger eukaryotic cell became a progenitor of the protoplast (Merchant *et al.,* 1905; Schimper *et al.,* 1883). Nevertheless, in both chloroplast and cyanobacteria all light-dependent reactions of photosynthesis, together with the electron transport chain happen within the membranes called thylakoid. However, along with the progressive specialisation, some distinct differences in arrangements of the thylakoid membranes (Mullineaux, 1999) have been adjusted. One of remarkable differences in both systems are the structure of light-harvesting complexes in cyanobacteria and plants (Grossman *et al.,* 1993; Grossman *et al.,* 1995). In a simple cell of cyanobacterium *Synechocystis* all photosynthetic complexes (Photosystem II, cytochrome b_6f, Photosystem I and ATP synthase) required for the light-driven reactions reside in the thylakoid membranes, which form concentric sheets following the periphery of the cell in a number of three to ten. These thylakoid membranes converged in some places and form structures called: thylakoid centres. High-resolution imaging techniques have also reported that some

populations of ribosomes are attached along the internal membrane to small rod-like structures within the thylakoid membranes (van de Meene *et al.*, 2006). Cyanobacteria similarly to higher plants house both photosystem I (PSI) and photosystem II (PSII). The distribution of both complexes is likely to be homogeneous within the thylakoid, however in mutants lacking PSI and PSII sheet-like membranes were disturbed, such impact was not observed for strains lacking exclusively PSI, suggesting PSII indispensible function in the formation of photosynthetic membranes (van de Meene *et al.*, 2012). Another great difference distinguishing cyanobacteria from photosynthetic higher plants is the antenna protein complex, in order to maximise the number of photons utilised in the electron chain cyanobacteria use large membrane-extrinsic phycobilisomes. Phycobilisomes are present in number of six biliprotein rods sitting on top of the core biliprotein, such complex is peripherally attached to the cytoplasmic side of the thylakoid membrane, in close proximity to the photosystems (Grossman *et al.*, 1993). This system allows absorption in a specific wavelength range (500-650 nm) out of chlorophyll absorption, which is an important advantage for organisms living in aqueous environment (Glazer *et al.*, 1985). Eukaryotic phototrophs, (i.e. algae and plants) contain highly organised chloroplast, which not only holds the photosynthetic system but also hosts independent from nuclear genetic information, called plastome (Whitney *et al.*, 2001) and small ribosomes, allowing for independent protein synthesis. Lens-shape chloroplasts contain system of thylakoid membranes gathered into discs-shape stacks interconnected by much thinner membranes lamellae (Andersson and Anderson, 1980). The matrix filling the chloroplast space stroma is enriched in proteins and its alkaline environment corresponding to the

cyanobacterial cytosol (Wise *et al.*, 2006). The distribution of PSI and PSII is diverse and heterogeneous with major predominance of PSII complexes within the grana, whilst large complexes of PSI and ATPases sterically not fitting into the appressed grana space are found in stroma lamellae (Andersson and Anderson, 1980; Mustardy, 2008). Additionally, plants depend on chlorophyll a/b and their light harvesting complexes (LHCI for PSI and LHCII for PSII). *Synechocystis* is an advantageous model organism for this study, its genome has been fully sequenced and transformation occurs spontaneously (Keneko and Tabata 1997). Foreign DNA is integrated to genomic by double-homologous recombination. The cyanobacterial thylakoids compared to plant chloroplast lack grana stacks and this feature makes *in vivo* imaging and data analysis more reliable (Garab and Manella, 2008).

1.3 Light-depended reactions and electron transport

The Reaction Centre (RC) complexes constitute as the key drivers of photosynthesis. RC is aptly described as mega-complex of proteins, pigments and cofactors all involved in the light-dependent reactions, using light energy to oxidize water via a redox electron transport chain to form reducing NADH/NADPH, produce ATP and to release molecular oxygen. Two types of RC are distinguished in the phototrophic organisms: I and II, whilst anoxygenic phototrophs contain only one of either of RC type, the oxygenic phototrophs contain both (Blankenship, 2002). The fundamental difference between types I and II refers to the early electron acceptor cofactor, FeS for type I RC and pheophytin/quinone for type II RC. In plants, al-

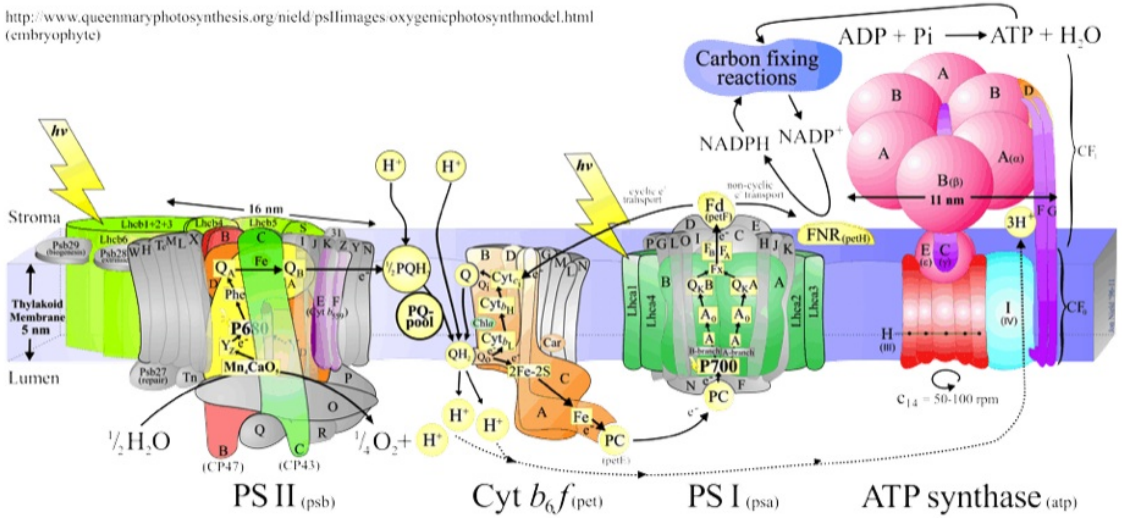

Figure 1.1: **Electron transport chain diagram with five main photosynthetic complexes**
A cartoon of the Z-scheme of oxygenic photosynthesis in the thylakoid membrane of plants. Drawing includes structural details on the organisation of proteins within the photosynthetic complexes (photosystem II, cytochrome b6f, photosystem I and ATP synthase), all protein subunits are annotated with appropriate standardized letter (e.x. A for PsbA of PSII and A for PsaA of PSI), the light harvesting complexes are marked as LHCII for PSII and LHCI for PSI. The black arrows indicate both the path of electron transport chain in the thylakoid membrane and the proton gradient formation. The yellow arrows symbolise photons, all protein subunits chain. Thanks to courtesy of Jon Nield, Queen Mary, University of London, UK

gae and cyanobacteria there are two photosystems (PSI and PSII) catalysing the cascade of reactions, functionally connected by a set of proteins (i.e. complex cyt b_6f) and low molecular mass subunits (PQ) that constitute an electron transport chain. The light-dependent reactions begin with excitation of chlorophyll or phycobilisome with a single photon. The excited chlorophyll molecule reaches a higher energy level and carries an impaired single electron. Such excited molecule returns to the ground state by energy transmission to the neighbouring chlorophyll molecule, this creates the resonance energy and the process is repeated until the transfer reaches the last two key chlorophyll molecules proximity to PSII. When RC is excited two electrons are transferred to the secondary acceptor quinone (QB), together with two protons derived from water oxidation on manganese cluster on the other side of PSII. Simultaneously, two electrons lost by PSII are replaced by electrons derived from water molecule, together with hydrogen ions, which are released into the lumen, contributing to the hydrogen ion gradient (pH) and oxygen molecules (per every two molecules of water). Plastoquinone PQ transfers the two electrons to the cytochrome b_6f, two protons are released into the lumen, this process is coupled with pumping two more hydrogen ions into the lumen space by cytochrome b_6f. The electrons are then transported to the mobile carrier plastocyanin (PC) or the redox carrier cytochrom c_6 in cyanobacteria and algae, which delivers the electrons to the PSI complex (Sandmann et al., 1983, Merchant and Dreyfuss, 1998). On the other side, PSI is simultaneously excited by photons at 700 nm and transfers the electrons to the Ferredoxin (NADP) Reductase (FNR), every two electrons reaching FNR results in one NADPH. The gradient created by the electron transport chain is utilised by the ATPase (ATP

hydrolase) to produce ATP from ADP and Pi. The concept of electron flow between two photochemical systems in series, where the product of one becomes the substrate of the other, was formulated in the 1960s (Hill 1960) and it is known as $Z-$ *scheme* of oxygenic photosynthesis presented by Figure 1.1.

1.4 Photosystem II structure and function

Photosystem II is the light-driven water:plastoquinone oxidoreductase of photosynthesis. PSII is one, if not the most important enzyme in nature. The PSII crystal at 3.5 Å resolution provided the first reliable information on the complex structure (Ferreira et al. 2004). The most recent published structure of PSII obtained at the high resolution of 1.9 Å yielded a detailed picture of the Mn_4CaO_5 cluster for the first time (Umena, *et al.*, 2011) Figure 1.2.

PSII is an integral-membrane multi-subunit complex, which initiates the electron flow in the oxygenic photosynthesis of plants, algae and cyanobacteria. Although there are some fundamental differences between cyanobacterial and plant oxygenic photosynthesis, the core and structure of PSII remain similar. PSII with a molecular mass of 250 kDa, consists of at least 20 protein subunits, 35 chlorophylls, 2 pheophytins, 11 β -carotens, 2 plastoquinoes, 1 bicarbonate, 1 heme (2 in cyanobacteria), 1 non-heme iron and Mn_4CaO_5 cluster, which catalyses water oxigation and lipids (Umena *et al.*, 2011). Identification of the polypeptides in the highly active detergent-isolated preparation was obtained from spinach and *Synechocystis* sp. PCC

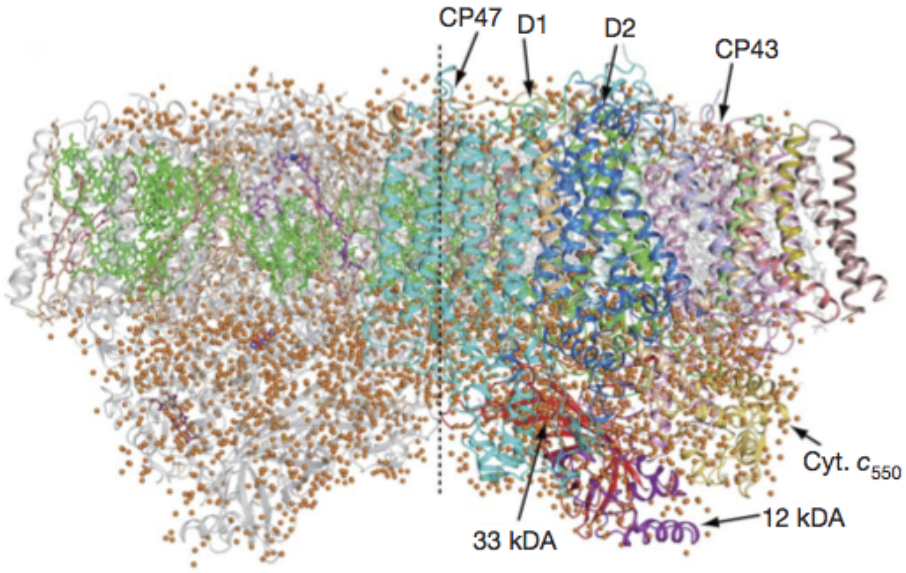

Figure 1.2: **The structure of PSII complex at 1.9 Å**
Structure of PSII dimer from *T. vulcanus* at a resolution of 1.9 Å. The protein subunits: CP47, D1, D2 and CP43 are coloured, two left and right monomers are seperated by the central line, and the cofactors are in colour exclusively in the left-hand monomer. Gold colour balls represent water molecules. Reproduced from Umena *et al.*, 2011.

6803 by stepwise removal of single subunits allowed defining the bare minimum of PSII complex composition capable of O_2 production (Berthold *et al.,* 1981; Kuwabara *et al.,* 1983; Bricker *et al.,* 1996). The heart of PSII holds a 10 transmembrane α - helices heterodimer composed of two highly conserved homologues proteins D1 (encoded by three genes: *psbA1*, *psbA2*, *psbA3*) and D2 (*psbD1*, *psbD2*) (Golden *et al.,* 1986; Golden *et al.,* 1988). The D1 and D2 dimer play a key role in the PSII complex. D1 alone provides the scaffolding for the majority of cofactors involved in the electron transport including: Mn_4Ca cluster, the primary electron donor (P680), Chl_{D1}, $Pheo_{D1}$, non-heme iron and external acceptor Q_B. Therefore D1 is highly susceptible to damage and its turnover is considerably faster than that of any other thylakoid polypeptide in a light-dependent process (Ohad, *et al*., 1984). Closely associated with the core of PSII are the chlorophyll binding intrinsic proteins CP47 (PsbB) and CP43 (PsbC), often referred to as the inner antenna proteins. Both of the CP47 and CP43 are anchored in the membrane by 6 transmembrane helices and bind 29 to 30 Chl *a* molecules, which are aligned in two layers near the cytoplasmic and luminal side of the membrane (Ferreira *et al.,* 2004). Moving outside of the PSII core three extrinsic proteins are found on the luminal side of the thylakoid: Psb O, Psb P and Psb Q (Psb O, Psb U and cyt c-550 (Psb V) in cyanobacteria) (Shen *et al.,* 1993), which form a cap over the catalytic site where oxygen evolution occurs. Other smaller subunits located at the periphery of PSII core help to stabilise the binding of Chl *a* and β -carotene to the complex. However, two of smaller subunits PsbE and PsbF provide histidine ligands for the heme of Cyt b_{559}, whilst PsbL, Psb M and Psb T found at the monomer-monomer binding sites probably stabilise the dimeric nature of PSII complex (Thorn-

ton *et al.*,2005).

1.4.1 PSII assembly

The assembly of large protein complexes seems to happen in a sequential and highly coordinated process. PSII assembly happens in the same manner and order in all photosynthetic organisms (Figure 1.3). However, there are two pathways of PSII assembly, first *de novo* and second assembly of the damaged and repaired active PSII complexes. Different concepts on localisation of these two processes have been proposed. Recent studies state that synthesis of new complexes and their repair take place rather in different cell compartments. There are indictions, that PSII synthesis *de novo* originates in *Synechocystis* in the cylindrical structures located at the cell periphery in close proximity to the cytoplasmic membrane (CM), called thylakoid centres (van de Meene *et al.*, 2006), whilst assembly of repaired PSII complexes happens continuously within the mature thylakoid membranes.

Apart from the polypeptides subunits building up the complex there are a large number of auxiliary factors involved in the whole assembly process. The early stage of PSII construction begins with incorporation of RC subunits (i.e. D1, D2 and cyt b_{559} and PsbI) directly into the membrane bilayer in a cotranslational manner (Zhang *et al.*, 1999). Precursor of D1 (pD1) is therefore assembled into the membrane by proteins from the group of insertases Alb3/Oxa1/YidC family, which fold the incorporated protein ahead (Ossenbuhl *et al.*, 2004; Ossenbuhl *et al.*, 2006). After pD1 insertion into the membrane, it is predicted that soluble PratA protein from

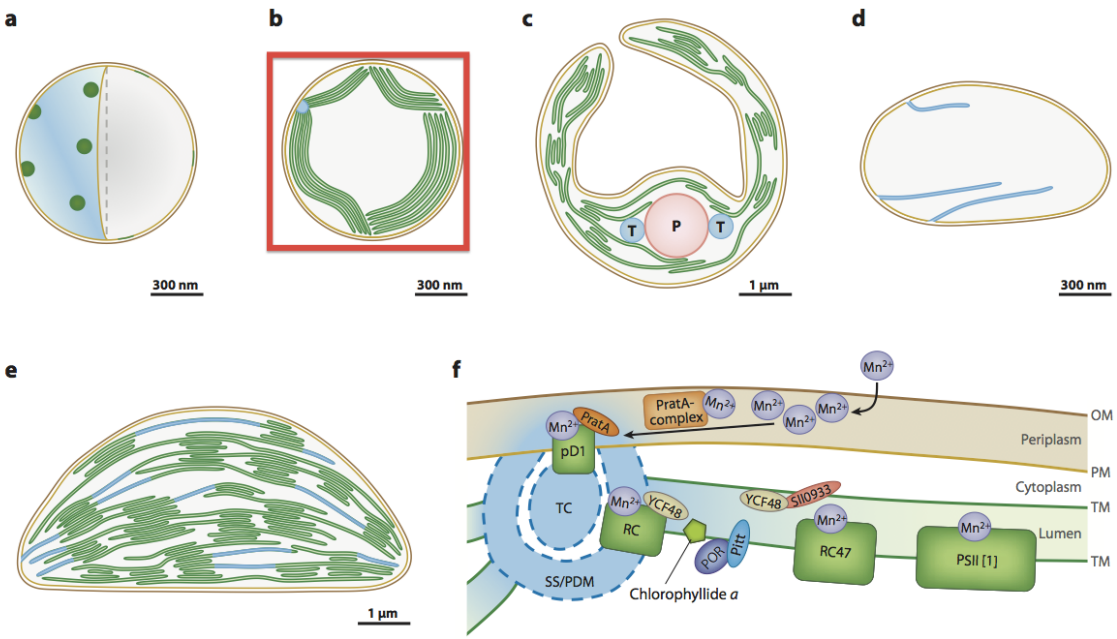

Figure 1.3: **Organisation of PSII assembly *de novo***
in (a) *Gleobacter violaceus*, (b and f) *Synechocystis* sp. PCC 6803, (c) *Chlamydomonas reainhardtii*, (d) plant proplastid and (e) plant chloroplast. Green colour represents the photosynthetically active areas in all cells, blue symbolises the thylakoid centre (TC) of *Synechocystis* and the translation zones in *Chlamydomonas reainhardtii*. Cartoon (f) shows a detailed scheme of PSII assembly in the thylakoid centre of *Synechocystis*, auxiliary factors are marked with oval contours while PSII subunits in the bars. Manganese ions (purple) are bounded by periplasmic PratA protein and loaded onto the pD1 polypeptide in TC. The TC is surrounded by semicircular structures (SS) and PDM (PratA-defined membranes). Assembled new PSII complex leaves the TC into the thylakoid membrane through membrane interconnections. The remaining subunits are incorporated into the growing complex by assembling factors: YCF48, Pitt, Sll0933. Details in the text. Reproduced from Nickelsen and Rengstl (2013).

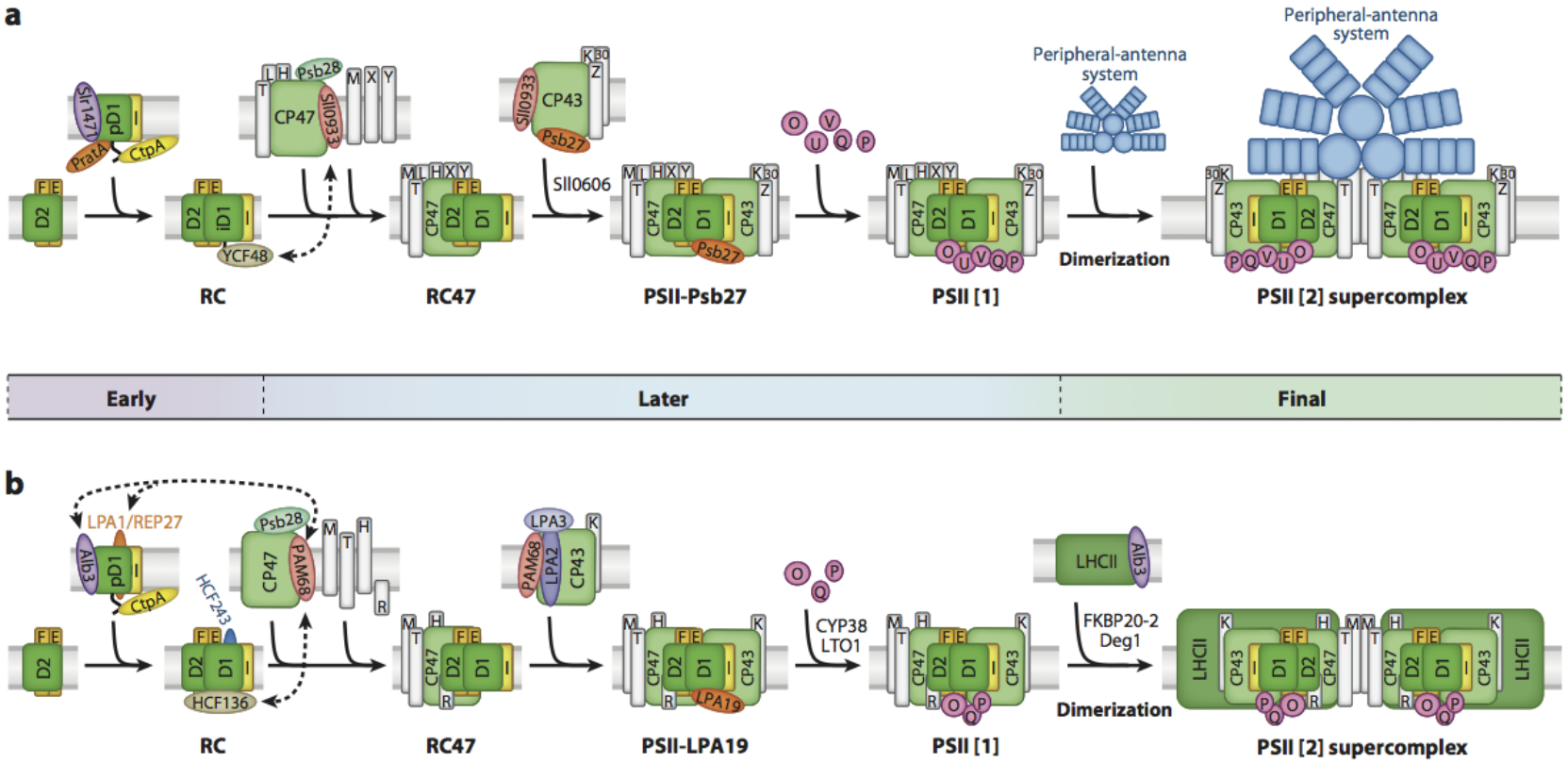

Figure 1.4: **PSII assembly** (a) in cyanobacterium *Synechocystis* 6803 and (b) plant chloroplast. The construction of PSII is divided into three stages: early, later and final. Auxiliary assembly factors are marked by oval contours, the same colours in both schemes represent the homologues or factors performing the same role. Green bars present the Reaction Centre (RC), while the extrinsic low-molecular mass subunits (grey bars) are designated by a conventional abbreviation. Black arrows indicate the direction of progress, dotted arrows mark known or presumed interactions between the auxiliary factors. Detailed description found in the text. Reproduced from Nickelsen and Rengstl (2013).

TPR (tetratricopeptide repeat) family interacts with pD1 α -helical structure from C-terminal site, where the cluster of Mn_4CaO_5 is bound (Klinkert *et al.,* 2004). The TPR family is known to act as scaffold due to its superhelical structure (D'Andrea *et al.,* 2003). Additionally PratA has shown a high affinity binding manganese ions, suggesting its involvment in delivering Mn^{2+} to the PSII at the very early stage of *de novo* assembly (Klinkert *et al.,* 2004; Schottkowski *et al.,* 2009; Stengel *et al.,* 2012). Obvious homologues of PratA were not found in plants, however factors of TPR family LPA1 of *Arabidopsis thaliana* and REP27 in *C. reinhardtii* show some similar features to PratA (i.e. binding Mn^{2+} and interacting with D1). pD1 requires processing and cleavage of its C-terminal extension in order to bind the Oxygen Evolving Complex (OEC) and other extrinsic proteins (Roose *et al.,* 2004). Although it is not clear whether the cleavage occurs before or after manganese cluster binding, it was confirmed that CtpA (C-terminal processing protease) is involved in this process. In plants 9 amino acids are cleaved from pD1 C-terminus extension, while in cyanobacteria the extension of 16 residues is removed in a two-step manner, forming an intermediate form of D1 (i.e. iD1) (Nixon *et al.*, 1992; Anbudurai *et al.*, 1994) (for details refer to Chapter 5 of this work). Interestingly, in most of Dinoflagellates the C-terminal extension is absent (Satoh *et al.*, 2007). Further steps of assembly depend on the stability of assembled subunits within the membrane. Another factor was associated with PSII construction, in *A. thaliana* soluble HCF13 and in *Synechocystis* 6803 YCF48 participate in RC formation in two ways, firstly it stabilizes the pD1 and binds it to the D2-cyt b_{559} receptor complex (Plucken *et al.,* 2002; Komenda *et al.,* 2002). Furthermore, YCF48 seems to be involved in the replacement of damaged D1 during the repair

cycle (Komenda *et al.,* 2002) (Figure 1.4). D2 polypeptide is the consecutive subunit incorporated into the growing RC, however, with the exception of two proteins folding D2 (encoded by genes: *slr0286* and *slr2013*) in *Synechocystis* 6803, no other assembly factors in any of the model organisms have been yet reported (Kufryk *et al.,* 2001; Kufryk *et al.,* 2003). Later on, in order to convert the RC into the mature large PSII complex PAM68 in *A. thaliana* and *Sll0933* in *Synechocystis* were reported to be essential providing the bridge between RC- and PSII[1]-complex formation (Armbruster *et al.,* 2010; Rengstl *et al.,* 2013). The RC is enriched by two inner-antenna proteins CP47 and CP43, following assembly of extrinsic subunits protecting the Mn_4CaO_5 cluster. The process of CP47 and CP43 incorporation is aided by three identified proteins: Psb27, Psb28 and Psb29 (Kashino *et al.,* 2002; Shi, *et al.,* 2012). CP47 binding is promoted by Psb28, which binds to the stromal/cytoplasmic surface of the subunit. Psb29 is predicted to be a peripheral sub-unit bound to the cytoplasmic side of the TM (Keren *et al.*,2005). Other unpublished studies proposed that Psb29 might be involved in the assembly and repair of PSII in *Synechocystis* 6803. On the contrary to Psb29, the function of luminal lipoprotein Psb27 in *Synechocystis* and its homologue in *A. thaliana* (Thf1) have been well established. Both forms bind transiently to the large luminal loop of CP43, as well as to the monomeric and dimeric PSII and PSI (Nowaczyk *et al.,* 2006; Roose and Pakrasi, 2008). First presumed function of Psb27 is to prevent from premature binding of extrinsic subunits assuring all stages of D1 preparation have been completed (Roose and Pakrasi, 2008). Secondly, binding to CP43 allows its assembly into the RC47. Interestingly, two homologues of Psb27 in *A. thaliana* showed to play different roles, with LPA19 involved in the

PSII synthesis *de novo* (Wei *et al.*, 2010), whilst the Psb27-H1 is rather essential for the recovery of photoinhibited PSII (Chen *et al.*, 2006). Finally, given that PSII in nature is found in a dimeric form with the attachment of peripherical antennae, a couple of factors have been assigned to perform this action: the Alb3 insertase, FKBP20-2 in *A. thaliana* and the thylakoid protease Deg1 with its chaperone activity accumulates increased number of RC47 and PSII complexes (Lima *et al.*, 2006; Moore *et al.*, 2000; Sun *et al.*, 2010). The integration of organic and non-organic compounds of PSII (e.g. Ca^{2+}, Cl^{-}, Fe^{2+}, pigments) is not clear. It is however known that chlorophyll a and β - carotene molecules are loaded onto CP47 and CP43 subcomplexes prior to being assembled into the PSII (Boehm *et al.*, 2011).

1.4.2 The more, the better? Photoinhibition

Light intensities differ across all latitude, but the most rapid changes are observed in changeable conditions within the same location. Hence the photosynthetic organisms must have developed a large variety of strategies and mechanisms allowing survival in both the optimal and extreme conditions. In order to live nearly everywhere where sunlight can penetrate, the photosynthetic organisms developed variety of mechanisms on macro- and micro-scale. A perfect survival solution for an autotrophic organism would be to maximise light harvesting and minimize deleterious effects. One of solutions is the large system of antenna exceeding the chance of excitation. In plants, the LHCII proteins of light-harvesting complex present with PSII constitute for up to 50% of the total thylakoid proteins (Anderson, 1986), similarly in cyanobacteria phocobilisomes fraction reaches up to 50% (Grossmann *et al.*, 1993). However, the photosynthetic efficiency in the

function of light intensity increases gradually to the maximum (saturation) and then declines rapidly. Such light induced decline of photosynthetic activity is referred to as photoinhibition (Vass, 2011). Photoinhibition phenomenon is a complicated process and there are probably as many views as minds. However, it has been established that major part of photoinhibition affects directly PSII site, as a consequence the electron transport is inhibited and protein structure damaged (Aro *et al.,* 1993). Thus, PSI may be damaged by light indirectly while electron transport is limited (Scheller, et al., 2005; Kudoh *et al.,* 2002).

PSII megacomplex catalyses the light-driven oxidation of water, evolving one molecule of oxygen and four protons per every two molecules of water. In undisturbed electron transport, the charge separation between the excited chlorophyll ($P680^+$) and the pheophytin (Phe^-) acceptor leads to the production of the intermediate primarily charged separated radial states $P680^+$ $Pheo^-$ rapidly stabilised by electron transport to both acceptor and donor of PSII. The electron of the reduced Phe is transferred first to Q_A and then to Q_B electron acceptor of plastoquinone (PQ) molecules. On the site of the donor, the $P680^+$ is reduced by Tyr-Z, an active tyrosine residue of D1 protein, which then fills the impaired electron shell by extracting electron from water-oxidising complex (Styring *et al.,* 2012). PSII activity strongly depends on the electron donors, acceptors as well as the activation of Mn_4Ca cluster, it is therefore prone to photodamage caused by any failure of these substrates. It is evident that the main mechanism leading to photoinhibition of PSII is associated with the production of ROS (Reactive Oxygen Species) such $^1O_2$, $O_2^{\cdot -}$, $OH^{\cdot -}$, H_2O_2 and their catastrophic impact on both the manganese cluster and proteins. Although the molec-

ular mechanisms of photoinhibition caused by ROS are still under intense debates, there are several theories trying to explain the underlying mechanisms of this phenomenon.

Not exclusively UV

The spectrum of the solar radiation striking Earth s atmosphere spans a broad range of 100 nm to about 1 mm. Not surprisingly, intense work focused on the impact of the high frequency UV part of radiation on the photodamage of PSII. The following conclusions have been drawn (1) UV targets in photosynthetic organisms nucleic acid, Calvin-Benson cycle enzymes and PSII complex (Vass *et al.*, 1996a), (2) importantly the absorption of UV by quinone electron acceptor, Mn_4Ca and the tyrosine electron donors implies that these are main targets of UV-induced PSII damage (Vass *et al.*, 1996b; Yerkes *et al.*, 1990), (3) UV-A (315-400 nm) damaging effect was close to the UV-B (280-315 nm) (Turcsanyi *et al.*, 2000), while the most dangerous UV-C (200-280 nm) radiation is not relevant, as it is mostly absorbed in the atmosphere not reaching the Earth surface, (4) UV-B radiation is 50% more efficient in damaging the PSII structure compare to UV-A, however UV-A intensity in the sun light spectra is significantly higher than UV-B (Turcsanyi *et al.*, 2000). Visible light (400-700 nm) carrying less energy, nevertheless visible light leads to PSII photoinhibition. However, the damaging mechanism differs and it is more complicated from the direct damage induced by UV, and several model mechanisms have been suggested.

Photoinhibition Models

Figure 1.5 presents the sites of photodamage in the PSII complex. There

are several proposed models explaining the PSII photodamage. The classic model of *At the acceptor site* mechanistically explains the photoinhibition resulting in a halt of the electron flow from PSII to further acceptors. Under strong continuous illumination, there is an increased possibility of over-reduction of plastoquinone-pool, which results in double reduction of Q_A and its dissociation from the D1. In consequence, excited electron of $Pheo^-$ cannot enter electron chain and it enhances formation of the P680 triplet state ($^3P680$) (Vass, 1992). Potentially the P680 triplet may transfer the energy to triplet oxygen ($^3O_2$) resulting in a highly reactive singlet oxygen ($^1O_2$). Singlet oxygen reacts with D1 polypeptide causing its irreversible damage. However, this model fails to explain the photoinhibition under anaerobic conditions (Hakala *et al.*, 2005). Similary to the first model, model of *low-light* photoinhibition supports the hypothesis that light-driven damage of PSII and D1 protein turnover occurs under low light (Mattoo *et al.*, 1997). The difference between this and the previous model regards ROS being produced as a consequence of excited electrons flowing back from Q_B to the S- state of OEC (Keren *et al.*, 1997).

The donor-side model on the other hand describes photoinhibition, which happens independently from oxygen. Manganese compounds used in both *in vitro* and *in vivo* tests appeared to be susceptible to the light-induced damage (Antal *et al.*, 2009; Hakala *et al.*, 2006). Manganese cluster damage in the PSII leads to the inactivation of OEC. Consequently, without supply of electrons from OEC, highly oxidizing radicals ($Y_{Z^{\cdot}}$, $P680^+$) are formed, which will then fill the electron holes by extracting electrons from the surrounding proteins, causing damage inflicted on D1 protein (Klimov *et al.*, 1990; Chen *et al.*, 1992). The three putative models of photoinhibition ex-

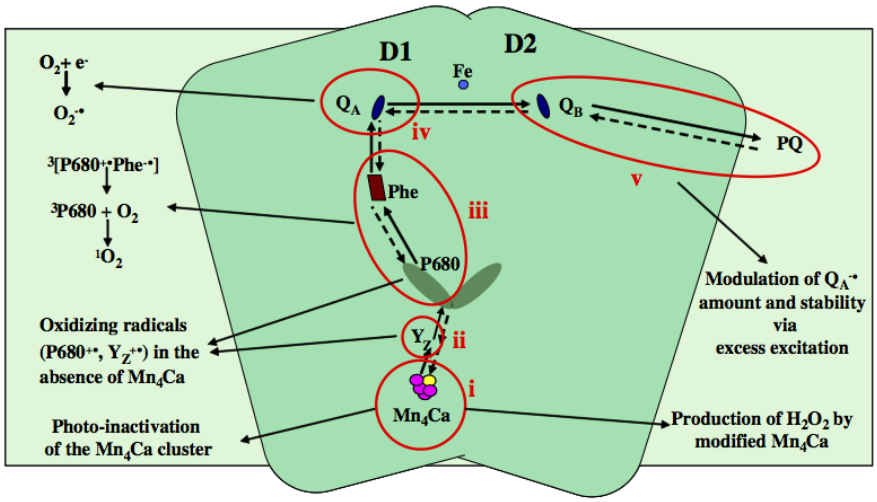

Figure 1.5: **The sites of photodamge in PSII complex**
(i) Mn_4Ca damage is caused by both UV and visible light, such modifications of water oxidizing complex lead to the formation of H_2O_2, which initiates production of highly reactive OH^- (ii) damage of Mn_4Ca may cause as well the accumulation of $P680^{+\cdot}$ and $Tyr^{-\cdot}$. (iii) Recombination of $P680^{+\cdot}$ and $Phe^{-\cdot}$ results in highly reactive singlet oxygen $^1O_2$ (iv) if Q_A become doubly reduced then the electron flow is blocked by $Pheo^-$ not entering the electron chain, this enhances the formation of the P680 triplet state (^{3}P680) and further 1O2 synthesis. (v) The reduction in the PQ pool in the lipid phase of the membrane and QB creates a negative pressure causing the flow of electron backwards to the S-state of OEC, this stabilises the $Q_A{}^{-\cdot}$, which results in ^{3}P680 and $^1O_2$ formation. Figure reproduced from Vass, 2011.

plain photodamage based exclusively on *in vitro* studies, where the whole PSII complexes were isolated and the effect of ROS was observed. However, more recent *in vitro* studies in both plants and cyanobacteria stress the importance of impaired PSII repair cycle, which *in vivo* seems to be inhibited by ROS (Nishiyama *et al.*, 2001; Nishiyama *et al.*, 2004).

1.4.3 Photoprotection

Light varies in intensity throughout the day. All photosynthetic organisms aim to maximise the amount of captured light utilised in the photosynthetic electron transport chain, this has been accomplished by incorporation of large harvesting systems capable of efficient absorption and delivery photon energy to the RC. Although this enhancement system has advantages in low light, elevated light inevitably inflicts damage. To alleviate its harmful effects and prevent photoinhibtion, several effective protective mechanisms have been developed by photoautotrophs.

Elimination of ROS

Each electron donor and acceptor in the electron transfer chain from chlorophyll to the complex oxidising water is the potential substrates catalysing formation of ROS. Oxygen alone might become a final electron acceptor giving rise to superoxide $O_2^{-\cdot}$ easily converted to hydrogen peroxide H_2O_2 and then to hydroxyl radicals $^{\cdot}OH$ (Asada, 1999; Asada, 2000). One type of the protection mechanisms evolved in plants and cyanobacteria relies on elimination and protection from the harmful radical states, this may be accomplished via (1) non-radiative charge recombination, by modulation of redox potential charges of Phe and Q_A, (Vass *et al.*, 2009; Vass, 2011a), or alternatively changing the redox potential of Q_A and Q_B which

decreases the $^1O_2$ production and overall PSII damage (Krieger-Liszkay *et al.,* 1998; Fufeza *et al.,* 2002). (2) ROS-scavenging by inducible antioxidatvie enzymes: superoxide dismutase and ascorbate peroxidase (APX) present in bacteria and plant chloroplasts, contributing to reduction of the H_2O_2 and other ROS (Asada, 1999; Miyagawa *et al.,* 2000; Nishiyama *et al.,* 2001). Additionally, common antioxidants such α-tocopherol and β- carotene aid to decrease the oxidative stress and damage of PSII damage and repair mechanism (1.5.4) by scavenging the intercellular $^1O_2$ (Neely *et al.,* 1988; Di Mascio *et al.,* 1990; Havaux *et al.,* 2005).

Non-photochemical Quenching (NPQ)

Prevention of photoinhibition by dissipation of absorbed light energy in the antenna system before it reaches the PSII Reaction Centre (RC) is known as non-photochemical quenching (NPQ). Such reductions of the chlorophyll fluorescence yields are divided into three categories depending on the relaxation kinetics: (1) *energy-dependent quenching* ***(qE)*** is among all three the major and the fastest response to high-light (Horton and Ruban, 1992). The quenching mechanism is not clear and it varies among the photosynthetic organisms. However, several proteins and cofactors were assigned to the qE-mediated heat dissipation. The principle for qE is to redirect the energy from chlorophyll of light-harvesting antenna protein complexes to carotenoids, which will then be subsequently dissipated in a form of heat (Demmig-Adams *et al.,* 1996). Cyanobacteria thermally dissipate excess absorbed energy at the level of the phycobilisome, the light-collecting antenna. The photoactive orange carotenoid protein (OCP) plays an important role in cyanobacterial qE and it is likely that OCP-dependent NPQ evolved first. OCP binds a single xanthophyll molecule (Kerfeld *et al.,*

2003), which absorbs in a range of blue-green wavelengths. Such excitation of xanthophyll switches on the OCP^0 to active red form OCP^R, which is able to bind to the phycobilisome (Gwizdala *et al.*, 2011). The energy of phycobilisome is transferred on the xanthophyll molecule at OCP^R (Niyogi and Truong, 2013). Reversibility of this process may be achieved by upregulation of the Fluorescence Recovery Protein (FRP), which leads to dissociation of OCP from the phycobilisomes and reversion of OCP^R to OCP^0 (Gwizdala *et al.*, 2011).

In plants and algae, however the process of qE seems to have evolved separately, phycobilisomes were lost in the green and secondary red plastid lineages and the three-helix light-harvesting complex (LHC) antenna proteins diversified (Niyogi and Truong, 2013). Under high light the electron transport is increased, ATP overproduced, causing the accumulation of protons in the chloroplast lumen. Such increased ΔpH triggers the qE quenching by initiating the xanthophyll cycle via activation of violaxantin de-epoxidase, which converts violaxantin to zeaxantin via the intermediate antheraxanthin (Demmig-Adams *et al.*, 1996). Zeaxanthin is the key carotenoid capable of quenching the energy of excited chlorophyll by absorbing it and dissipating as heat. It has recently been shown that the plant LHCII has the ability to switch rapidly between a state of efficient light use and the one in which excess excitation energy is harmlessly dissipated as heat (Kruger *et al.*, 2012). Protonation of PsbS protein binding the chlorophyll a/b at PSII complex promotes the rearrangements of PSII complexes in the chloroplast grana lamellae (Goral *et al.*, 2012) and it appears likely that it is aiding the conformational changes of the LHCII complexes (Ruban *et al.*, 1993). Nevertheless, studies *in vitro* on the thylakoid membranes isolated from

mutant lacking PsbS have shown that when increased ΔpH in the environment, LHCII were undergoing conformational changes, suggesting other unknown factors involved in the process of qE (Johnson and Ruban, 2011). Therefore, the precise mechanisms and details of qE NPQ in plants remain unsolved.

2) *state-transition quenching* ***(qT)*** another system of protection works when strong prolong illumination occurs, such condition maintain for period of minutes switches on the qT NPQ. To cope with long-lasting high light plants, algae and cyanobacteria all adjust the size and position of light-harvesting antennas either by decreasing the gene expression or by protein degradation (Anderson, 1986; Escoubas*et al.,* 1995; Lindahl *et al.,* 1995; Reuter and Muller, 1993). During the state-transition, which described the short-term acclimation, antenna proteins migrate between PSI and PSII in order to regulate the electron flow chain (Murata and Sugahara, 1969), this mechanisms differs in plants and cyanobacteria (Mullineaux and Emlyn-Jones, 2004). Plant responses during the state transition are regulated by redox state of reduced plastoquinone pool, which leads to activation of kinase phosphorylating the light-harvesting complexes at PSII. This step allows for migration of antenna complexes from PSII in the grana lamellae to PSI in the stroma lamellae in so-called: state 2 (Allen 2003; Bonardi *et al.,* 2005; Kanervo *et al.,* 2005). State 1 happens *vice versa* regulated by opposite enzyme phosphatase (Pribil *et al.,* 2010; Allen and Forsberg, 2001; Gal *et al.,* 1997; Mullineaux and Emlyn-Jones, 2005).

In cyanobacteria the qT is associated with state 2, however the movement of phycobilisomes does not seem to require phosphorylation (Mullineaux and Emlyn-Jones, 2005), though the detailed mechanism remains unclear.

(3) *photoinhibitory quenching* ***(qI)*** is the most slowly forming and relaxing NPQ process, which might persist for several hours in the dark following illumination (Ruban *et al.*,2012).

Although all described here mechanisms of photoprotection are constantly being used if needed, however the fact is that PSII undergoes damage, particularly the D1 subunit of RC is vulnerable and constitutes the main target for light-induced damage (Nixon *et al.,* 2005). The rate of photoinhibition in high light exceeds its repair, while awaiting its repair, it has been suggested that inactive PSII complex might be used as energy sink to protect and subside the energy flux to the neighboring complexes (Aro *et al.,* 1993; Kanervo*et al.,* 2005; Lee *et al.,* 2001; Matsubara and Chow, 2004). This mechanism is called qI quenching. The time of qI strongly depends on the PSII repair rate, which is limited by gene expression and protein translation. D1 protein is encoded by psbA gene, plant and algae genome carry one individual copy of psbA (Zurawski *et al.,* 1982), surprisingly, in cyanobacteria there are various number of *psbA* copies (see under: 1.5) (Golden *et al.,* 1986), additionally the expression level of each *psbA* gene often depends on the illumination (Campbell *et al.,* 1998; Clarke *et al.,* 1995; Clarke *et al.,* 1995). Moreover, each homologue of D1 in cyanobacteria reveal different turnover rate, therefore it seems that in cyanobacteria the qI quenching could be regulated by changes in expression of D1 homologues (Campbell *et al.,* 1998; Komenda *et al.,* 2000).

1.4.4 PSII repair

As described previously in plants, algae and cyanobacteria the photoinhibition is a serious limiting side effect of photosynthesis, therefore various

protective mechanisms were developed upon evolution (see here: 1.4.3). However, the PSII photodamage is an inevitable part of photosynthesis and occurs at all light intensities (Adir *et al.,* 2003; Edelman and Mattoo, 2008). Conclusively, if the photo-protection fails, there must be a reliable and efficient system of repairing the damage.

The main target for irreversible photodamage, particularly in a strong illumination, is the PSII protein complex, precisely the D1 subunits that binds and holds the majority of cofactors. Re-activation of damaged PSII relies on the efficient replacement of degraded D1 with a new copy (i.e. D1 turnover). Although, the D1 turnover is fairly similar in plant and cyanobacteria, the spatial and signalling differences have been reported, as well as various auxiliary factors involved and the number of steps of the process. PSII repair is restricted in chloroplasts of higher plants to the stroma lamellae, where photodamaged PSII migrates when triggered by phosphorylation catalyzed by kinases (Aro *et al.,* 1993; Tikkanen *et al.,* 2008). On the contrary, PSII repair in cyanobacteria most evidently takes place in the thylakoid membranes, this is supported by studies of Schottkowski where fractions of pD1 have been found in the thylakoids membranes (Schottkowski *et al.,* 2009). Studies *in vivo* on localisation of PSII repair in *Synechocystis* sp. PCC 6803 are still to be revealed.

Putative model of PSII repair

In vitro studies proposed that photodamaged D1 in the chloroplast is being degraded in a two-step manner (two-protease model), initiated by a cleavage at the stromally exposed loop by a protease from Deg family (Deg2) in a GTP-dependent manner (Haussuhl *et al.,* 2001), followed by FtsH-mediated removal of the 23-kDa N-terminal D1 fragment still in the mem-

brane (Spetea *et al.,* 1999). However, it is under debate whether this two-protease model of D1 degradation is physiologically relevant, since studies conducted *in vivo* in plants and particular in cyanobacteria support rather a one-protease model. Mutants lacking all Deg proteases homologues in *Synechocystis* 6803 showed unaffected D1 turnover (Barker *et al.,* 2006), suggesting that cyanobacterial system uses exclusively one type of auxiliary proteases family (FtsH-only model) and does not require an initial cleavage (Silva *et al.,* 2003).

Figure 1.6 reflects the general knowledge on PSII repair cycle in the FtsH-only model D1 turnover. Since the RC occupies the core of PSII, in order to removed degraded D1 from the centre, the PSII holoenzyme must be partially disassembled and then reassembled, so that D1 is released and replaced with a newly synthetized copy (Ohad *et al.,* 1984). Light-induced D1 damage triggers monomerisation and partial PSII disassembly, leaving the RC47 complex exposing D1 to the external auxiliary factors. The photoinactivation of D1 results in conformation changes within the N-terminal tail in the D1 structure, most probably allowing FtsH to initiate the degradation (Komenda *et al.,* 2007). The degradation of damaged D1 by hexameric FtsH2/FtsH3 hetero-oligomeric complex is synchronized with an insertion of a new D1 protein. In this scenario the process is completed by the re-attachment of CP43 subunit, followed by Mn_4Ca cluster and of recycled extrinsic PSII proteins re-binding. The D1 turnover is a rapid process, one of the fastest in nature, with a half-time as short as 30 minutes (Tyystjarvi *et al.,* 1994), therefore all steps must happen flawlessly and efficiently. The exact mechanism and all factors being involved in this process are not entirely explored but over 30 years of studies reached some reliable consensuses.

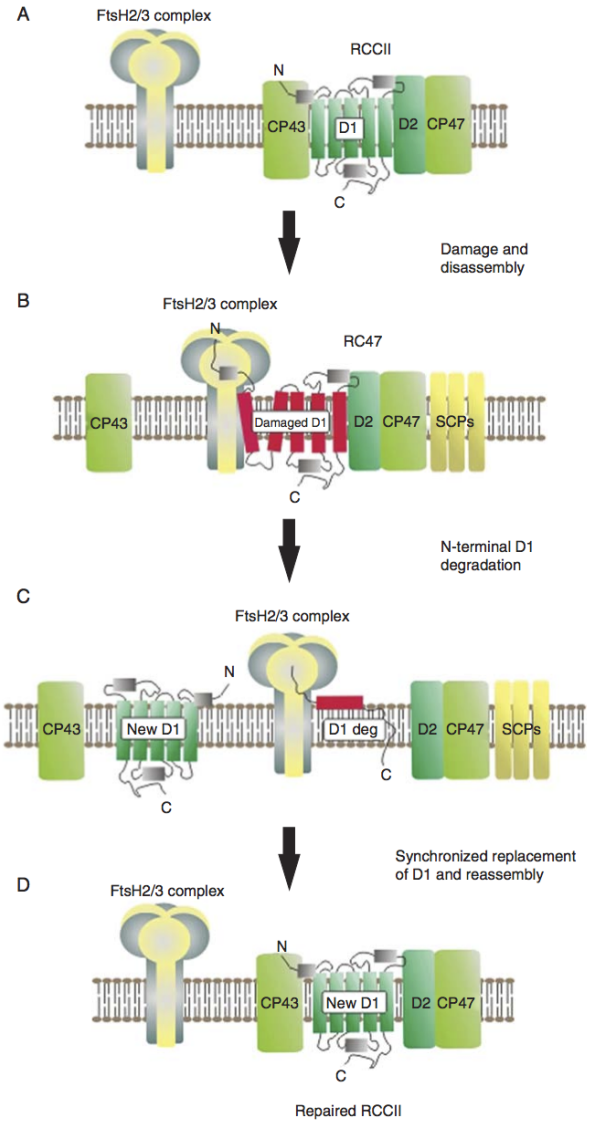

Figure 1.6: **The FtsH-only model of photodamged D1 replacement in the process of PSII repair in *Synechocystis* 6803**
(a) Light-driven damage causes the partial disassembly of PSII holoenzyme to the monomeric RC47 complex exposing the damaged D1 and reattachment of CP43 (b), (c) The hexameric FtsH2/FtsH3 hetero-oligomeric complex initiates the N-terminal D1 degradation and removal (d) Subsequently a new functional copy of D1 is inserted into the RC complex followed by the re-assembly of PSII subunits. Reproduced from Nixon, 2010.

It is evident that FtsH membrane-bound, ATP-dependent metallo-proteases play a crucial role in the D1 degradation. Studies on mutant lacking FtsH2 homologue in *Synechocystis* 6803 (Silva *et al.,* 2003; Komenda *et al.,* 2006), in parallel with disruptions of FtsH2 and FtsH5 homologues in *A. thaliana* (Bailet *et al.,* 2002) have shown an absence of smaller D1 fragments, indicating stabilisation of damaged D1 and an impaired PSII repair. Given the multiplicity of FtsH proteases in chloroplast and cyanobacteria (i.e. *Synechocystis* 6803 genomes encodes four; plant *A. thaliana* contains 12 genes coding fully length FtsH homologues), it cannot be excluded that the process is carried out via several other homologues of FtsH when taking into account that some of FtsH homologues in the chloroplast are able to substitute and complement each other in a complex (Zaltsman *et al.,* 2005; Zhang *et al.,* 2010). Similarly, in *Synechocystis* 6803 FtsH2 homologue has been repeatedly co-purified with FtsH3 (Baker *et al.,* 2008) and further analysing *in vitro* has shown that most likely these two homologues are present in the hetero-oligomeric complexes (Boehm and Yu *et al.,* 2012). However, the characterisation of FtsH proteases revealed its poor unfoldase activity, which is required for the protein turnover, suggesting that the D1 degradation most likely comprises other auxiliary proteins. This work partially covers this issue.

1.5 Proteases of the AAA+ superfamily

The large, functionally diverse family of AAA covers all *ATPasese Associated with diverse cellular Activities*. The AAA+ are involved in a wide variety of cellular functions such as protein unfolding and degradation, bacteri-

ochlorophyll biosynthesis, DNA processing, molecular motor dynein and many other. Therefore AAA+ proteins are found in all subcellular compartments of eukaryotic cells and bacteria (Sinder et al., 2008). The diversity in structural elements within the AAA+ core, divided the AAA+ superfamily into groups, clades and families (Ammelburg *et al.,* 2006 Erzberger *et al.,* 2006). There are five major groups of AAA+ (i) the extended AAA, (ii) the helicases and clamp loaders (HEC), (iii) transport (PACTT), (iv) ExeA group, (v) signal transduction ATPases with numerous domains (STAND). This study is particularly focused on the most abundant (i) extended AAA group, which contains FtsH protease uniquely embedded in the membranes with a function of a proteolytic degradation of membrane proteins. It is evident that AAA+ proteins are present in the membranes as hexameric complexes composed of identical or closely related subunits (70-80 kDa). All subunits are highly conserved and show above 40% of identity in all the species from bacteria to human (Bayer, 1997; Neuwald *et al.,* 1999). However, two different membrane topologies divide the AAA-proteases into two classes in eukaryote. Class I (i-AAA) such Yta1 consists of exclusively one transmembrane domain and therefore its active site is found in the mitochondrial intermembrane space of *S. cerevisiae*. While the two transmembrane domains are characteristic for class II (m-AAA), which is present in all organisms: (i.e. FtsH in both plant and chloroplast, mitochondrial Yta10p, Yta12p and human Paraplegin), and expose their catalytic sites to the cytoplasm or the matrix (Tomoyasu *et al.,* 1993). The AAA proteases quality-control function requires the specific recognition of non-native polypeptides with omission of their folded counterparts, the AAA domain provides domain this specific binding, however it is not ATP-

dependent (Akiyama *et al.,* 1998a; Leonhard *et al.,* 1999). Thus, the ATP hydrolysis induces conformational changes of FtsH and it is essential for the next step of targeted degradation (Arlt *et al.,* 1996). Generally defining proteolysis depends on the availability of water molecules, and since this is trivial to explain the process happening in the cytoplasm, for the protein embedded in the hydrophobic membrane there are two theories attempting to answer this problem. The shedding model based on the view of AAA proteases degrading membrane protein by shedding its solvent-exposed loops, which results in destabilisation in the hydrophobic segment and allows for further proteolysis. The second pulling model suggests that the AAA proteases extract the membrane-embedded parts of the target by binding the unfolded protein and using pulling force supplied by conformational changes in a response to the ATP hydrolysis (Langer, 2000). Such extraction of hydrophobic polypeptide domain must be followed by its traverse through the membrane bilayer, which requires either the protein-translocation channels, for instance found in the ER (Plemper *et al.,* 1999), or the complexes of AAA hydrophilic pores may facilitate this transport (Lenzen *et al.,* 1998; Yu *et al.,* 1998) (Figure 1.8). To better understand the later, the structure of FtsH protease must be explained in detail.

1.5.1 FtsH structure

FtsH proteases are highly conserved in all bacteria and endosymbiosis-derived eukaryotic organelle (i.e. chloroplast and mitochondria) (Wagner *et al.,* 2012). Despite intense studies, the high-resolution structure of intact FtsH protein is still to be obtained. However, there were many successful attempts resolving the soluble part of protease as well as the isolated key

domains derived from *E. coli* and other organisms (Suno *et al.,* 2006; Krzywda *et al.,* 2002), shedding light on its structure and complexity in the membranes. FtsH proteases are the only protease of AAA+ family anchored in the membrane (Tomoyasu *et al.,* 1993) and in *E. coli* essential for cell viability (Jayasekera *et al.,* 2000). As mentioned (1.6) all of FtsH discussed in this project, belong to the m-AAA type with two N-terminal transmembrane (TM) helices (Langklotz *et al.,* 2012), divided by a 70-residues periplasmic domain, essential for the proper regulation of substrate selection (Akiyama *et al.,* 1998b) (Figure 1.7). The cytoplasmic part of the C-terminus protein includes the AAA+ domain linked by a short (12 aa) linker region to the protease domain (PD). The AAA+ domain includes three characteristic motifs Walker A, Walker B and the Second Region of Homology (SRH). The order of residues within Walker A and Walker B provides coordination of ATP in conjunction with Mg^{2+} and water molecules, while the SRH with its *arginine finger* (Arg^{321}/Arg^{318}), catalyzes the ATP hydrolysis (Karata *et al.,* 1999; Karata *et al.,* 2001; Suno *et al.,* 2006). Protease Domain (PD) features a HEXXH (His-Glu-Xaa-Xaa-His, X- any residue) binding motif, where the His residues and Asp facilitate the Zn^{2+} binding (Bieniossek *et al.,* 2009). At the C-terminal end there is a leucine-rich motif that has been implicated in co-recognition of certain substrates (Greaf *et al.,* 2007).

Regardless of sparse information on the native FtsH structure, the structure of soluble FtsH domains was determined via X-ray (Suno *et al.,* 2006; Bieniossek *et al.,* 2009; Ogura *et al.,* 2001), the results indicate unanimously a hexameric assembly of FtsH complexes into a ring structure with a narrow central pore (Figure 1.8B). Although, the structures of proteases domains are very highly conserved across all species and mostly show the pseudo

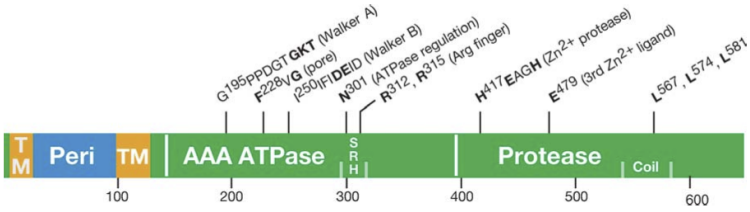

Figure 1.7: **The amino acids sequences of FtsH protease**
Colours divide the protein into the regions of: cytoplasm (green), transmembrane (orange), periplasmic region (blue), respectively. AAA ATPase region includes three characteristic motifs: Second Region of Homology (SRH), Walker A and Walker B, the zinc metalloprotease domain is found within the cytoplasmic domain we all. Some of the key amino acids signed at the top. Reproduced from Ito and Akiyama, 2005.

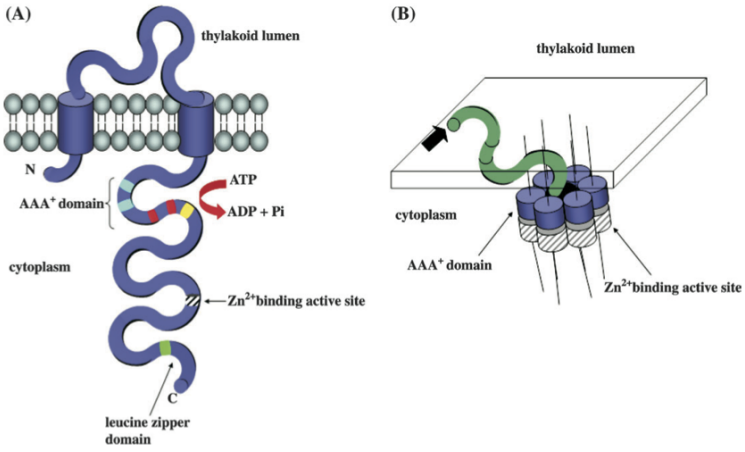

Figure 1.8: **The FtsH topology in the thylakoid membrane of *Synechocystis* 6803**
(A) single FtsH protease subunit in the membrane bilayer, with two transmembrane domains (TM) from N-terminus site, separated by a luminal loop and longer cytoplasmic site with the characteristic AAA+ domain facilitating the ATP hydrolysis, the zinc binding site followed by the leucine zipper domain at the C-terminal end of the protein. (B) Topology of hexameric FtsH holoenzyme in the thylakoid membrane, which forms a ring shape with the central hole where the degradation most presumably happens, the protease catalytic sites are located at the periphery of the hexamer ring, not at the chamber wall. Reproduced from Nixon, 2005.

six-fold symmetry hexameric complex (Niwa *et al.,* 2002), there are significant variations of the AAA+ modules resulting in two- or three-fold symmetry (Langklotz *et al.,* 2012; Suno *et al.,* 2006). Studies on *T. Thermophilus* support the three-fold-symmetric structure and propose that the protease is active only when the exterior subunit of the complex is open. The process initiates when three molecules of ATP dock down in the FtsH complex open pockets, this triggers the closing motion of three AAA+ domains. The closure enables the arginine finger to interact with the γ -phosphate of ATP molecules, leading to its hydrolysis. Closed subunit return to the open form without releasing ADP, while the whole FtsH structure regains its normal state. These open-close synchronized motions of FtsH subunits would in effect drive the translocation of degraded protein through its central pore and, followed by its cleavage into small peptides of 6-25 amino acids in length (Suno *et al.,* 2006).

1.5.2 FtsH in *E. coli*

The details on FtsH originate from studies on *E. coli* mutant associated with the *ftsH* gene (filamentous and temperature-sensitive phenotype). There are five AAA+ proteases encoded in *E. coli*, among: ClpXP, ClpAP, HslUV, Lon and FtsH, yet only the latter is essential for cell viability (Jayasekera *et al.,* 2000). All five classes of proteases form large hexameric complexes but only FtsH in *E. coli* is anchored in the inner cytoplasmic membrane (Tomoyasu *et al.,* 1995). Bacterial trans-location system aims to rescue the overloaded ribosomes, by tagging the incompletely synthetized polypeptides with a C-terminal degradation signal, called SsrA tag (-AAXXXXXALAA) (Gottesman *et al.,* 1998). ClpXP mostly degrades the proteins with exposed

C-terminal residues, however FtsH and Lon proteases are involved as well in the quality control of the membrane proteins (Choy *et al.,* 2007; Lies *et al.,* 2008). Considering that 21% of open reading frames in *E. coli* encodes proteins assembled into the cytoplasmic membrane, FtsH protease holds a crucial role in keeping balance and membrane order (Boyd *et al.,* 1998). So, it is evident that the SecY and F_0a subunits when unassembled into the full complexes of ATPase and SecYEG translocase, are degraded by FtsH (Kihara *et al.,* 1995; Akiyama *et al.,* 1996). Other substrate for FtsH proteases includes YccA a 7 trans-membrane homologue of Bax Inhibitor-1 (BI-1) in eukaryotes (Ito and Akiyama, 2005). Functions of YccA in prokaryotes are not well established, however its high abundance negatively impacts on the FtsH activity (Kihara *et al.,* 1998), YccA therefore displays a double role of a substrate and inhibitor for the FtsH complex.

The other vital role of FtsH in *E. coli* is to maintain balance between lipopolysaccharide (LPS) and phospholipids (PL). LPS are composed of polysaccharide O-antigen, a core polysaccharide and lipid A. LPS are highly abundant in the outer leaflet of outer membrane in order to form a permeable barrier against external agents (Vuorio *et al.,* 1992; Nikaido, 2003). The (R)-3-hydroxymyristoyl-ACP is a precursor for both the LPS and PL synthesis. The reaction for LPS biosynthesis is catalysed by LpxC deacetylase, which is a short-lived enzyme and must be degraded within minutes in FtsH-mediated proteolysis (Young *et al.,* 1995; Ogura *et al.,* 1995). In a *ftsH* mutant the LpxC is stabilized, resulting in over-accumulation of LPS and this state is compensated by increased FabZ activity leading to oversynthesis of PL, rebalancing the LPS to LP ratio (Ogura *et al.,* 1995). Additionally, FtsH role was well characterised in the stress response, including the controlled

response to the heat shock (HS). Induced targeted proteolysis of sigma factor RpoH (σ32) by FtsH under non-HS conditions, keeps the RpoH on the minimum level needed for the rapid induction of the HS response when sensing the temperature upshifts (Langklotz *et al.,* 2012). FtsH protease in *E. coli* is exploited for the proteolysis of λ proteins in response to the viral infection FtsH activity implies on which of the two alternative pathways the λ phage enters. Stabilised CII induces the expression of CI repressor enhancing the entry into lysogeny, while the degradation of CII by FtsH favours the lytic pathway, leading to phage replication and lysis of the host cell (Shotland *et al.,* 1997). In summary, FtsH sole membrane protease in *E. coli* regulates the amount of proteins in a posttranslational mechanism of proteolysis. This is crucial for cell viability to facilitate the immediate response to the internal and external influences.

1.5.3 FtsH in *Synechocystis* sp. PCC 6803

Cyanobacteria are presumably the oldest preserved prokaryotes able to perform the oxygenic photosynthesis. All four photosynthetic complexes are embedded in the thylakoid membrane system, which is similar to single unstacked thylakoid of chloroplast in higher plants. There are four putative FtsH homologues encoded by *Synechocystis* sp. PCC 6803 genome FtsH1 (*slr1390*), FtsH2 (*slr0228*), FtsH3 (*slr1604*) and FtsH4 (*sll1463*) (Kaneko and Tabata, 1997; Mann *et al.,* 2000). FtsH1 and FtsH3 are essential for cell viability, while disruption of FtsH4 showed no detectable phenotype (alike the wild-type). Deletion of *slr0228* results in light-sensitive phenotype and reduced level of PSI with wild-type level of PSII was maintained (Mann *et al.,* 2000). The role of FtsH2 was assigned to the selective D1 degradation

during the repair of PSII complex. Other suspected role of FtsH2 in the photosynthetic apparatus involved degradation of other PSII misassembled subunits (Silva *et al.,* 2003; Komenda *et al.,* 2006). Otherwise, FtsH2 protease was recognised to respond to other external stresses such: UV-B exposure (Cheregi *et al.,* 2007), deficiency in inorganic carbon (Zhang *et al.,* 2007), heat stress (Kamata *et al.,* 2005), osmotic stress (Stirnberg *et al.,* 2007). The indispensible role of FtsH2 in *Synechocystis* may be comparable to the sole membrane anchored protease found in *E. coli*. Studies on organisation of FtsH proteases suggest that it is likely that FtsH2 plays a role of scaffolding and is present exclusively in the hetero-oligomeric complexes with FtsH3 in a ratio 1:1, whilst FtsH3 might be found also in FtsH3/FtsH1 complex within plasma membrane. FtsH4 is said to form a homo-complex in the thylakoid membrane (Boehm *et al.,* 2012). According to the phylogenetic tree (Figure 1.9) prepared for protein sequences of FtsH homologues in *Synechocystis* sp. PCC 6803 and the ortholog found in *E. coli* (K-12 strain), it might be predicted that FtsH1 (*slr1390*) and FtsH2 (*slr0228*) share more similarities, than FtsH3 (*slr1604*) and FtsH4 (*sll1463*). Interestingly, FtsH4 seems to have closer evolutionary relationship to FtsH found in *E. coli*, than the other three homologues.

1.5.4 FtsH in plants

The plant model organism for the photosynthetic studies *Arabidopsis thaliana* contains 17 FtsH sequences, 12 of these genes are coding for active FtsH homologues (Garcia-Lorezno *et al.,* 2006), five produce inactive forms lacking the zinc binding motif (Sokolenko *et al.,* 2002). Eight active and all inactive forms are targeted to the chloroplast (Ferro *et al.,* 2010), whilst three are

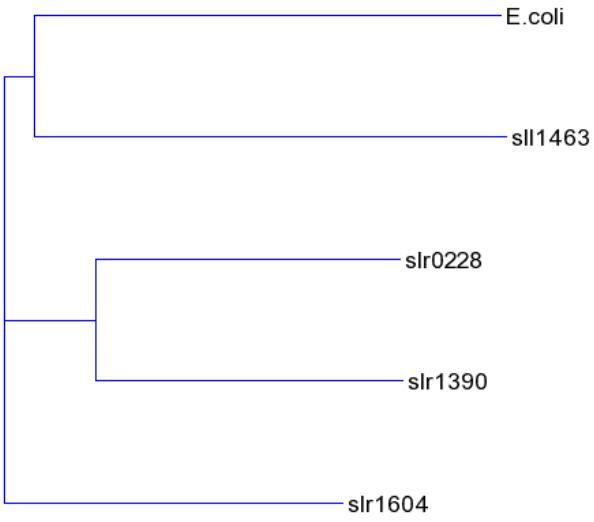

Figure 1.9: **Phylogeny of FtsH**
Phylogenetic tree for FtsH orthologs found in *E. coli* and *Synechocystis* sp. PCC 6803 (FtsH1 = slr1390, FtsH2 = slr0228, FtsH3 = slr1604, FtsH4 = sll1643). Alignments were made in ClustalX, phylogenetic tree generated in server TREX (http://www.trex.uqam.ca)

exported into the mitochondria (Janska *et al.*, 2005) and remaining FtsH11 is found in both organelles (Urantowka *et al.*, 2005). Moreover, encoding genes tend to form pairs and produced proteins are able to substitute for each other in a hexameric complexes (Yu *et al.*, 2004). Chloroplast FtsH homologues are located either in the thylakoid membranes or in the envelope. It is evident that the thylakoid FtsH homologues are involved in degradation of many major proteins of PSII and PSI, like well-established D1 turn-over in PSII repair cycle, most likely in a two-step manner (1.5.4) in a cooperation with the luminal Deg protease (Lindahl *et al.*, 2000). Similarly to FtsH found in *E. coli* plasma membrane, FtsH in chloroplast responds to heat stress by mediating D1 degradation observed in spinach (Yoshioka *et al.*, 2006) and degrades the Rieske FeS protein in pea (Osterset-

zer and Adam, 1997). Additionally, FtsH homologues found in the chloroplast envelope are essential for embryogenesis (Wagner *et al.,* 2012). The mitochondrial FtsH are divided into two groups (1.6) depending on the location m-AAA in the inner envelope of mitochondria, with proteases active domains facing the mitochondrial matrix (Kolodziejczak *et al.,* 2002) and i-AAA proteases where the active side faces the inner membrane space (Gibala *et al.,* 2009). FtsH proteases in plant mitochondria play a key role in ATPase complex assembly and stability as well as protection against oxidation (Kolodziejczak *et al.,* 2007 Gibala *et al.,* 2009).

1.6 Study the biological membrane *in vivo*

Singer and Nicolson described biological membranes as two-dimensional fluid mosaics (Singer and Nicolson, 1972), however it is known now that their highly organised composition is remarkable (Figure 1.10). Biological membranes contain a complex array of lipids, proteins, sugars and small molecules and although the proportions and kind of components vary between the species, the general prototype seems to be alike in all living organisms: the amphipathic two-layered sheets of lipids, embedding the proteins. According to Gorter and Grendel (Gortel and Grendel 1925) the dual nature of lipids: polar heads and acyl carbon chains of hydrophobic tails results in the structure of lipid bilayer. The beauty of this theory is that such formation is caused by spontaneous increase in water entropy, which results in arrangement of the head groups in contact with aqueous surrounding, while facing each other tails are packed inside bilayer. In most cases the latter is true, however more studies have shown that many lipids in na-

ture do not form the bilayer when they are on their own. Membrane lipids comprise a large number of lipid species and more than 600 species are considered to build the biological membranes (Dowhan 1997). However, the lipid lateral organisation into the bilayer plane happens in nonrandom fashion and leads to existance of lipid domains (lipid heterogeneity) in cell membranes (Simmons and Vaz, 2004). Fluid-mosaic model of membranes emphasises that membrane lipids passive role is to ensure the fluid ocean in which the membrane proteins float and provide structural heterogeneity.

At least one-quarter of genes code for membrane proteins (Wallin and von Heijne, 1998), which within the membrane may be either embedded in the bilayer, covalently attached to the inner surface or as peripherally bound to other membrane-anchored protein. Constant movements are observed within the membranes; proteins and lipids are held by non-covalent interactions, however whilst lipids move *laterally* and also slowly across in a *transverse diffusion*, most proteins are limited to a constant lateral diffusion. These dynamic motions often lead to organisation into micro- and macro-scale clusters. The scale of movements varies in time and distance, for instance phospholipids with diffusion coefficient of 1 μm^2. s^{-1} travelling up to 2 μm in 1s, whereas proteins mobility may be as fast as lipid with remarkable diffusion coefficient 0.4 μm^2. s^{-1} for membrane bound proteins e.g. rhodopsin or in extreme cases proteins seem to be virtually immobile like bounded to extracellular matrix fibronectin with diffusion coefficient lower than $10^{-4} m^2.s^{-1}$ (Berg *et al*., 2002). Either rapid or slow motions all play an important role in cell signaling, cell recognition, transport, response, adhesion and other physiological cellular functions (Vereb *et al.,* 2003). Study-

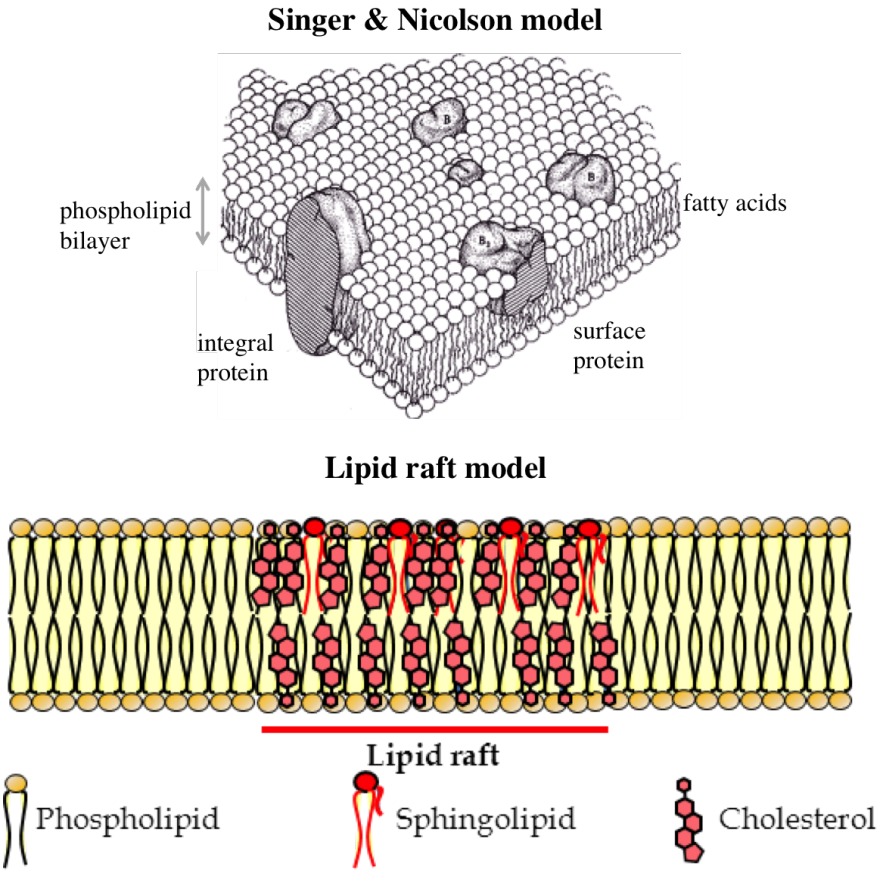

Figure 1.10: **Membrane models**
Comparison of the Singer & Nicolson membrane model (Reproduced from Singer & Nicolson, 1972), with the lipid raft model well described in animal cell membranes, without proteins (Sergent *et al.*, 2012)

ing membrane dynamics *in vivo* became possible with the implementation of *state-of-the-art* techniques, listing among: use of fluorophores combined with fluorescence microscopy i.e. the fluorescence recovery after photobleaching (FRAP) (Edidin *et al.,* 1997), single-particle tracking (Kusumi *et al.,* 1993), optical trapping by laser tweezers (Sako *et al.,* 1995), as well as spectroscopic methods (i.e. fluorescence correlation spectroscopy) (Magde *et al.,* 1979). These methodologies supported by digital image processing add valuable information on protein dynamics, interactions and the spatial distributions. This study uses the Green Fluorescent Protein fusion in order to explore the localisation of membrane-associated proteins. The outcome provides another evidence for existence of microdomains in bacterial membranes (Vereb *et al.,* 2003; Lopez and Kolter, 2010).

1.6.1 Membranes in *Synechocystis* sp. PCC 6803

Classified as Gram-negative bacteria, the cell envelope of cyanobacteria consists of a plasma membrane, peptidoglycan and the outer membrane. Additionally, these organisms hold the internal system of thylakoid membranes, which house all photosynthetic and some of the respiratory complexes (Figure 1.11). It is still under a debate whether the inner thylakoid membranes exist as separate cell compartments or there are connections with the plasma membrane. High-resolution images of *Synechocystis* structures imply that the thylakoid membranes are rather discontinuous from the plasma membrane (Liberton *et al.,* 2006), whilst other data proposes a continuity model. These two models, however, implicate significant disparities in physiological processes including protein targeting, thylakoid

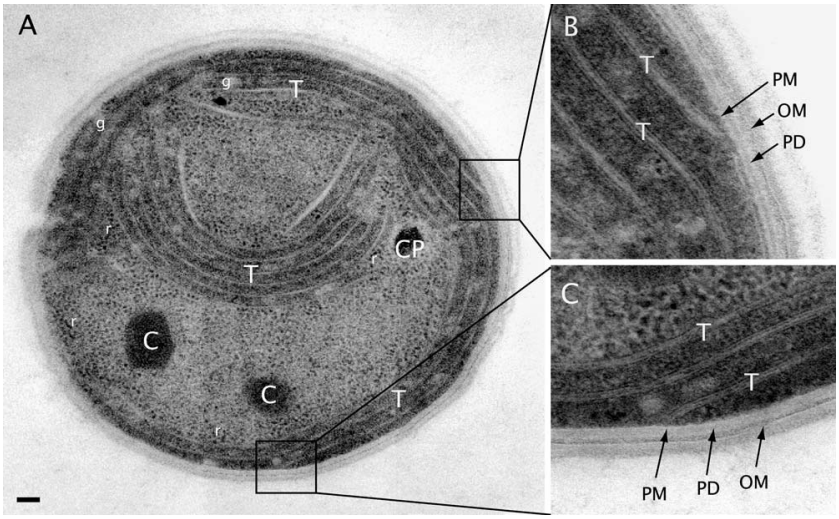

Figure 1.11: **Membranes in Synechocystis 6803**
Thin section of *Synechocystis* cell visualised under electron microscope. Enraged areas show details of thylakoid membranes (T), plasma membrane (PM), outer membrane, peptidoglycan (PD), carboxysome (C), cyanophycin granule (CG) and ribosome (r) (Reproduced from Liberton *et al.*, 2006).

membrane biogenesis as well as maintenance of a proton gradient across the thylakoid membranes.

Despite what remains uncertain, there is a common interest in learning functions of each membrane, which is often dictated by proteins found within. Thus, proteomics studies of plasma membrane isolated from *Synechocystis* 6803 contains important proteins involved in nutrient uptake, efflux and secretory pumps (Pisareva *et al.,* 2006), while thylakoid fractions comprise proteins of PSI, PSII, NADH, ATP (Srivastava *et al.,* 2005). However, systematic protein identification in differentiated prokaryotic membrane system is challenging and not always trivial. Even careful and time consuming separation of membrane fractionations often carries across trace of undesired proteins (Komenda *et al.,* 2008). Identification of proteins in

such manner does not shed light whether the studied proteins are homo- or heterogeneous with respect to their distributions (Srivastava *et al.,* 2006). Particularly interesting, but not yet well understood is described in many studies organisation of protein complexes into the distinct areas within the bacterial membrane. Recent studies revealed that OXPHOS complexes carrying out the oxidative phosphorylation in *E. coli* exclusively in the specific regions of plasma membrane, rather than in the entire plasma membrane (Lenn *et al.,* 2008). Similarly, the visualisation of key respiratory electron donors (i.e. NDH-1 and SDH) in cyanobacterium *Synechococcus* sp. PCC 7942 has shown both complexes concentrated in discrete patches in the thylakoid membranes, approximately 100-300 nm in size. The redistribution of such large complex clusters occurs under some conditions, but the mechanism behind is still be to explored (Liu *et al.,* 2012). This project exposes other evidence supporting the presence of micro-domains within bacterial membranes, most likely these structures resemble the membrane-rafts in the eukaryotic cells, which not only contain the specific proteins building up the complex but very likely are supported by indispensible lipids coordinating such structures. Such scenario has been described for many bacterial organisms, for example the holoenzyme PSII is associated with 20 molecules of four class of lipids, where only 6 of phosphatidylglycerol (PG) molecules are essential for PSII assembly and stability in the thylakoid membranes (Sakurai *et al.,* 2006; Umena *et al.,* 2011).

Lipids in thylakoid membranes of *Synechocystis*

Lipid composition of thylakoid membranes is highly conserved among oxygenic photosynthetic organisms. *Synechocystis* thylakoid membranes

contain four major groups of lipids, which comprise: unchared monogalactosyldiacyglycerol (MGDG) and digalactosyldiacylglycerol (DGDG) and two anionic lipids: sulfoquinovosyldiacylglycerol (SQDG) and phosphattidylglycerol (PG) (details and lipid structures might be found in Chapter 4, Figure 4.1) (Wada and Murata 1998). In contrast to other membranes, the majority of lipids found in thylakoids are glycolipids. Each of four kind of lipids has its own role in the photosynthetic membranes. MGDG and DGDG are considered as "bulky lipids" and function mainly as structural lipids (Murata and Siegenthaler 1998). Interestingly, the headgroup of MGDG is quite large and it is expected to have a cone shape rather then cylindrical form. Such shape, in an absence of proteins, favours the hexagonal phase rather than a standard bilayer. However if for example LHC-II molecules are mixed with MGDG in appropriate ratio, MGDG rapidly adopts into a bilayer structure (Simidjiev *et al.,* 2000). Negatively charged SQDG and PG are important for indispensable lipid-protein interactions within photosynthetic complexes (Wada and Murata 2007; Domonkos *et al.*, 2008) as well as to maintain the anionic charge on the thylakoid surface (Apostolova *et al.,* 2008). Additinally, PG-less mutant showed decreased level of PSI but not PSII complexes, further tests implied that loss in PG impacts on PSI synthesis rather than stability of mature complexes (Sato *et al.*, 2004). Similar conclusions were proposed for PG-derivate cardiolipin in *Sacchoromyces cervisiae*, where its presence was essential for translation of protein components building the electron-transport chain in mitochondria (Ostrander *et al.*, 2001).

1.6.2 Protein translocation across membranes

The architecture of cyanobacterial membranes systems still misses unambiguous information on the connectivity between distinct bilayers, little is therefore known about the process of extracytoplasmic protein sorting. Typically half of the proteins in a living organism have to be translocated across the membranes (Schatz and Dobberstein, 1996). In cyanobacteria this process occurs in a very similar manner to *Escherichia coli* targeting system (Spence *et al.,* 2003), where two types of translocation system are employed. In order to route the polypeptide into correct secretion pathway, it has to be labeled with some sort of appropriate signal. The general secretory **Sec** and twin-arginine translocation **TAT** systems are in use for extracytosolic protein transport (Mori *et al.,* 2001; Berks *et al.,* 2003). It has been shown that in both mechanisms, export across the inner membranes requires an N-terminal signal peptide (leader peptide), which is a non-functional part of a mature protein and is often removed by either signal peptidase I (leader peptidase) or signal peptidase II (lipoprotein signal peptidase). The leader peptide is characterized by a hydrophilic positively charged N-terminal region (n), a hydrophobic central domain (h) and a polar C-terminal (cleavage site) region (c) (Dalbey and Robinson, 1999). The translocation is an energy-dependent process, which depends either on ATP hydrolysis or in case of bacterial membranes the proton gradient (Dalbey and Robinson, 1999). In cyanobacteria newly synthesised proteins for export are directed either to the thylakoid or plasma membrane. Sec pathway transports unfolded proteins through a SecYE channel into the membrane which is unable to transport folded domains (Henry *et al.,* 1997) There are six putative genes coding components of Sec-dependent path-

way: secA, secY, secE, secG, secD, SecF, whilst the first three are found and involved in chloroplast Sec transport in plants. Another bacterial protein translocation system Twin-arginine translocation (Tat) is independent from Sec and homologous to pH-dependent protein translocation well described in chloroplast. The Tat signal peptide contains additionally a conserved twin-arginine motif in the N-terminal end. The protein transport is carried out on the expense of the pH-gradient across thylakoid membranes (Henry *et al.,* 1994). Both pH-dependent and Tat-dependent systems translocate folded proteins. Tat signal peptides are cleaved by signal peptidase type 1, encoded by two genes in *Synechocystis* 6803, one of peptidases present in the thylakoid membranes and second in the plasma membrane, taking part in protein sorting process (Huang *et al.,* 2002).

1.7 A high-resolution insight into the cell

A fundamental goal in biology is to determine how cellular organisation is coupled to function. Recent advances in visualisation techniques focus on resolution improvement in order to determine cell structures in great details. Imaging *in vivo* became a common tool in biology, with many advantages, mainly enables visualisation of cellular processes in real time without perturbing organism physiology. High-resolution visualisation approaches listing among: electron microscopy (EM) and atomic force microscopy (AFM) solve the cellular structures with reaching resolution in the Ångström scale (0.1 nm). However obtaining such details using EM requires sample to be stabilized, its thickness reduced and contrast enhanced, the latter is achieved by addition of heavy metal atoms (lead, uranium), in other words

the biological material must be fixed prior to be used. EM spectacularly improves the resolution in the xy plane, but deprives users the t scale. Particularly useful for structural biology is the cryo-EM, which enables observation of specimens in their native environment without staining or fixation. Whereas AFM limitation is the single scan size, typically only area of 150 x 150 μm might be recorded, as well as the time in which the signal is registered.

This project exploits the fluorescence microscopy to visualise enhanced green fluorescent protein (eGFP) in the background of naturally red chlorophyll and localise several key enzymes in the cyanobacterium *Synechocystis* 6803.

1.7.1 Fluorescence and confocal fluorescence microscopy

The fundamental principle in fluorescence microscopy is based on the *Stokes fluorescence law*, according to which a fluorescent molecule (fluorophore) emits longer wavelength photons when excited by photon of shorter wavelength (higher frequency). In this concept a fluorophore is excited by filter-selected monochromatic light (xenon arc/mercury lamp) or by coherent laser light focused on the specimen by objective lens. The excited molecule emits a fluorescence signal, and the same objective is used for illumination and detection. Dichromic mirrors separate excitation and emitted lights. User might observe filtered signal using ocular lens or it reaches the detector (CCD) and generate the image. Relatively poor resolution in z-axis and contrast obtained by standard fluorescence microscope is mainly a result of interference of fluorescence emitted by the specimen that appears out of the focal plane.

A step forward and better resolution was achieved in a confocal microscope, where a laser beam is used in order to generate a point illumination together with a pinhole in optically conjugate plane in front of the detector to eliminate out-of-focus signal (Fig. 1.12). Therefore, only fluorescent signal produced by fluorophore nearby the focal plane is detected. Lasers of various wavelengths are used in this system to excite the appropriate fluorophore. In a Laser Scanning Confocal Microscopy (LS-CM) used in this study, a pair of oscillating mirrors scan a point of laser light across the specimen via the objective. Fluorescence emitted by the specimen passes back through the mirror systems to a beam splitter, which rejects any reflected excitation wavelengths and then through the pinhole to generate the image of optical slice. The emitted signal is detected by a Photomultiplier (PMT), which records the brightness of fluorescence at each scanning point and maps this into a 2-dimentional (XY) image.

Additionally, confocal microscope facilitates automated collection of 3-dimensional (Z-series) data, which might be obtained *in silico* by reconstruction of consecutively collected 2-dimensional vertical image stacks. According to Abbe's diffraction limits are dictated by used wavelength and numerical aperture (d= λ/2NA). In this study, where 488 nm was used as excitation wavelength, together with immersion oil objective with 1.4 NA, the theoretical maximum resolution in XY plane is expected at round 139 nm, with lower resolution in Z-axis 528 nm. However, many aberrations decrease the effective resolution and as a result two fluorescent molecules distanced by 250 nm in lateral plane and 750 nm in axial are distinguished in this system. There are many limitations in fluorescent imaging techniques caused by laser limited speed scanning, its alignment, as well as

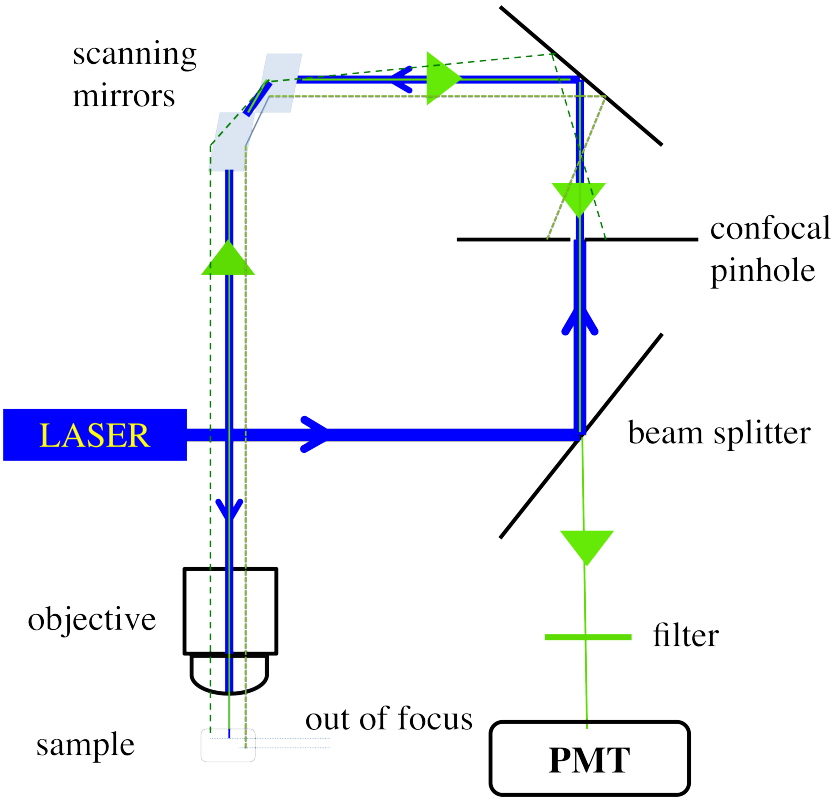

Figure 1.12: **Confocal microscope**

any aberrations of other features building the optical system. Fluorophore excited states have significant lifetime (nanoseconds). Scanning confocal microscope excites and collects information from a small volume of a sample (< cubic micron), therefore if number of molecules found in a unit is too low to obtain signal, user will increase the excitation level. This leads to saturation of excited state and depletion in ground state effecting the image as well as irreversible photobleaching of fluorophore. More signal might be registered by decrease in laser power and simultaneous opening the pinhole, however this allows more signal from out-of-focus planes, decreasing resolution in Z-plane. While collecting data it is wise to compromise between the quality and quantity of registered signal.

1.7.2 GFP

Discovered in 1962 by Shimomura (Shimomura *et al.*, 1962), Green Fluorescent Protein (GFP) originates from jellyfish *Aequorea victoria* with its fluorescence properties became one of the most useful proteins in biology and biochemistry. GFP molecule consists of 238 amino acid residues (26.9 kDa). The wild-type GFP isolated from *Aequorea victoria* with major excitation peak at 395 nm and emission peak shifted towards green wavelength at 509 nm (Tsien *et al.,* 1998).
GFP shows a β-barrel structure, built up from 11 of β-sheets enclosing six α helices (Fig. 1.13).

The centre of molecule buries the chromophore 4-(p-hydroxybenzylidene) imidazolidin-5-one (HBI) formed by residues 65-67, which are Ser-Tyr-Gly (Ormo *et al.,* 1996; Yang *et al.,* 1996; Tsien, 1998,). Chromophore is non-

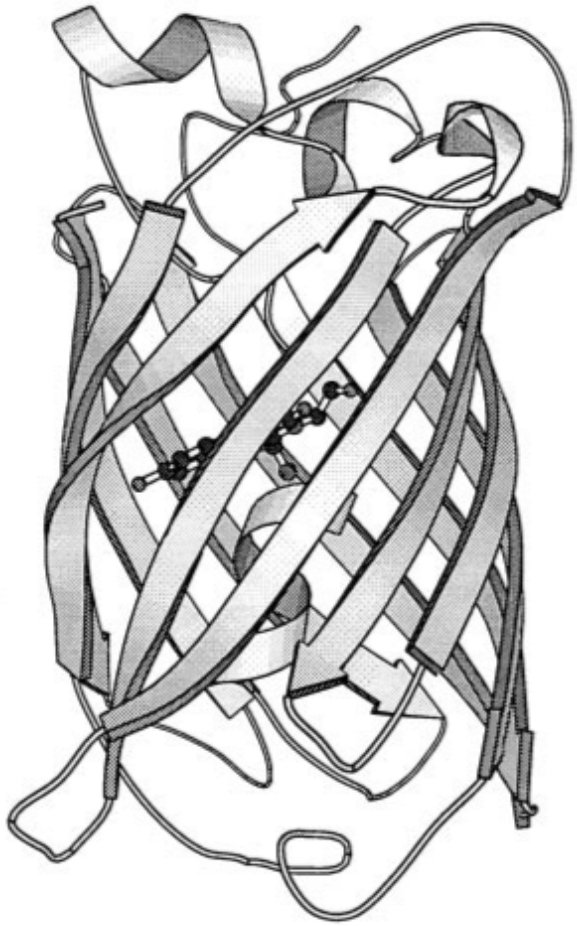

Figure 1.13: **GFP structure**
Schematic drawing of GFP backbone, the chromophore is shown as a ball and stick model. Reproduced from Omro *et al.*, 1996.

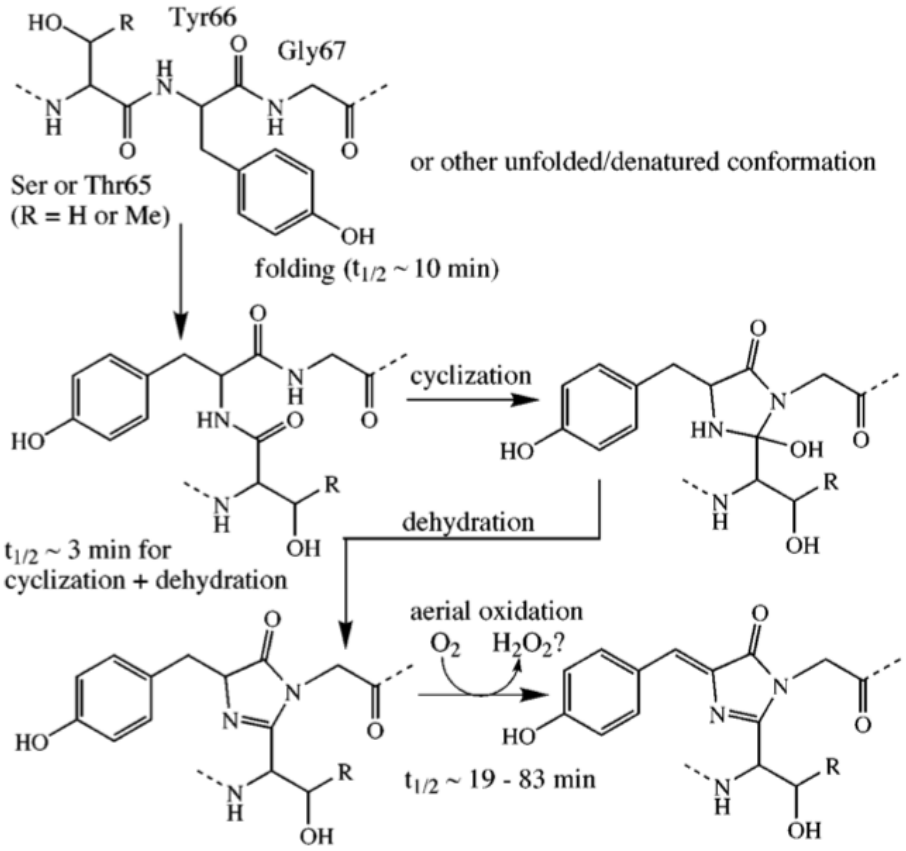

Figure 1.14: **Biosynthesis of GFP chromophore**
Steps leading to activation of GFP chromophore:
(1) Protein folding, (2)cyclization, (3) dehydration and (4) oxidation. Figure courtesy of Tsien 1998.

fluorescent if GFP molecule is not properly folded and active state requires following steps to occur (Fig. 1.14): (1) GFP folds into native conformation, (2) the imidazolinone is formed by nucleophilic attack of the amide of Gly67 on the carbonyl of residue 65, (3) followed by dehydration, (4) molecular oxygen dehydrogenates the α-β bond of residue 66 to put its aromatic group into conjugation with the imidazolinone (Tsien, 1998). These steps are essential for the chromophore to absorb and fluoresce.

However, wild-type GFP folding properties decline steeply at higher than room temperatures. To preserve the wild-type spectrum and enable of the use molecule in other organisms many recombinant techniques have been used. As results there are many various GFP mutants with altered physio-chemical properties. Single amino acid replacements: triple mutation: F99S, M153T, V163A improved folding properties at 37° and reduced its aggregation inside the cell (cite Yokoe 1996); S65T resulted in brighter fluorescence with excitation at 488 nm (Heim *et al.,* 1995). Other alterations of chromophore three amino acids and residues in contact with chromophore resulted in new derivatives of GFP. Y66W mutagenesis modified GFP to its blue emission form (Cyan Fluorescent Protein CFP), while replacement of Threonine203 with Tyrosine (T203Y) produced Yellow Fluorescent Protein (YFP) with a largest shift in emission to 529 nm (Miyawaki *et al.,* 1997).

GFP is used widely as a non-invasive fluorescent marker for gene expression, protein localisation, intracellular protein targeting and protein-protein interactions (Gerdes and Kaether, 1996; Chalfie *et al.,* 1994; Cubitt *et al.,* 1995). It has been reported that GFP *in vivo* and *in vitro* may be used as an indicator of pH changes (Bizzarri *et al.,* 2009). Similarly, GFP-based fluorescence sensor of calcium was described (Miyawaki *et al.,* 1997). It has been successfully expressed in bacteria, plants, yeast, mammalian cells, whole organisms and subcellular organelles (Lim *et al.,* 1995; Zolotukhin *et al.,* 1996; Hampton *et al.,* 1996; Rizzuto *et al.,* 1995). GFP labeling is achieved by chimeric fusion with appropriate targeting sequences. The fluorescent protein is linked to either C or N terminus of native protein, depending on target structures and function. In most cases a short linker up to 10

amino acids is required. In some cases GFP might disturb the function of tagged protein or might be cleaved off during post-translational modification. In order to avoid misinterpretation, successful mutants must be carefully tested for expression on genomic and proteomic levels.

1.8 Aims of this project

In order to shed more light on PSII repair and assembly, the initial aim of this study was to investigate the sub-cellular localisations of key proteases found in *Synechocystis* sp. PCC 6803. GFP chimeric fusion to five proteins involved in D1 repair, early stages of PSII assembly and three of unknown but vital functions, was employed.

Several hypotheses were formulated here, firstly all membrane associated proteases studied here were found to be located to dedicated areas within thylakoid or cytoplasmic membranes. Secondly, FtsH2 involved in PSII repair is found in large patches and remains immobile when activated by high light, suggesting existence of *repair centres*.

In order to assess more information on specialised *repair centres* proposed here, a novel pull-down assay was optimised in this study, which allowed for isolation of membrane fractions enriched in specific epitag. In order to access information on the protein membrane clustering and changes within *repair centres*, protein content was identified via mass spectrometry in both light conditions.

Additionally to complement thylakoid heterogeneity model, samples were set to identify lipids associated within these isolated FtsH2-enriched membrane fractions.

In a parallel study ctpA protease, involved in PSII biogenesis, was localised using the same approaches. Its presence in different cellular compartments suggests slightly different concept to what has been suggested in other studies.

Chapter 2

Materials and Methods

2.1 Bioinformatics tools

Protein and gene database

KEGG (Kyoto Encyclopedia of Genes and Genomes) GenomeNet

(release: Release 0.1, December 1, 1995 by Kanehisa Laboratories)

http://www.genome.jp/kegg/

CyanoBase (Version 2006.9.12; Nakamura *et al.,* 1998)

http://www.kazusa.or.jp.cyanobase/

UniProt (Release 8.8; Bairoch *et al.,* 2005)

http://www.ebi.uniprot.org.index.shtml

BLAST (Release 2.2.14; Altschul *et al.,* 1990)

http://www.ncbi.nlm.nih.gov.BLAST/

Protein properties prediction servers

CBS Centre for Biological Sequence Analysis, 1993. TMHMM Server v. 2.0
Prediction of transmembrane helices in proteins
http://www.cbs.dtu.dk/services/TMHMM/

CBS Centre for Biological Sequence Analysis, 1993. TatP 1.0 Server
http://http://www.cbs.dtu.dk/services/TatP/

EXPASY (Wilkins *et al.*, 1999)
http://us.expasy.org/tools/

STRINGS 9.05
http://string-db.org/newstring.pl

Alignment and Phylogenetic Tree

Server TREX http://www.trex.uqam.ca

ClustalX (WorkBench 3.2 environment) (Thompson *et al.*, 1994; Gonnet *et al.*, 1992)

Primer design

Primer3 v. 0.4.0
Pick primers from a DNA sequence (Steve Rozen and Helen J. Skaletsky, 2000)
http://frodo.wi.mit.edu

Cloning tools

Sci-Ed Software, Software for the Molecular Biologist Clone Manager Basic, Ver 9.2, Copyright 1994-2010

Serial Cloner 2.6 (Serial Basics, Mac)

NEB Cutter (New England BioLabs)

Other database

PubMed
http://www.ncbi.nlm.nih.gov/pubmed

2.2 Strains and growth conditions

2.2.1 *E. coli* strains

a). a non-pathogenic K12 derivative DH5α *E. coli* strain was used to propagate plasmids [kindly provided by Genetics of Biofilms Laboratory] (Taylor *et al.*, 1993)
b) BW25113 *E. coli* strain contains λ Red plasmid and was used as a host for homologous recombination. *E. coli* strain [kindly provided by Genetics of Biofilms Laboratory] (Datsenko and Wanner 2000)

2.2.2 Growth conditions

Liquid cultivation According to (Sambrook *et al.*, 1989) all strains of *E. coli*, were grown in liquid media Luria-Bertani (LB: 1 % (w/v) NaCl, 1 % (w/v) bacto-tryptone, 0.5 % (w/v) yeast extract) in plastic flasks on the orbital shaker at 180 rpm in 37° C. BW25113 was grown in 30°C.
Cultivation Strains were cultivated on LB 1.5% (w/v) agar plates cultivated in the static incubator.

Long-term storage For cryopreservation cells were suspended in liquid LB with addition of 15% glycerol/DMSO, following with a flash cooled in liquid nitrogen and placed for storage in -80°C (Sambrook *et al.,* 1989). For *E. coli* strains hosting plasmids/vectors antibiotic for selective growth were added either to liquid or solid LB in concentrations of: Ampicillin (10μl.ml^{-1}), Chloramphenicol (30μl.ml^{-1}), Spectinomycin (5μl.ml^{-1}), Apramycin (10μl.ml^{-1}).

2.2.3 *Synechocystis* sp. PCC 6803 strains and growth conditions

Table 2.2 lists all *Synechocystis* strains used in this study.

2.2.4 Growth conditions

Liquid cultivation *Synechocystis* strains were grown in liquid medium BG-11 (For 1000ml of 1x BG-11: 10ml of 100X BG-11: ($NaNO_3$, $MgSO_4{\cdot}7H_2O$, $CaCl_2$, citric acid, Na_2EDTA; 1ml of Trace element: H_3BO_3, $MnCl_2{\cdot}4H_2O$, $ZnSO_4{\cdot}7H_2O$, $Na_2MoO_4{\cdot}2H_2O$, $CuSO_4{\cdot}5H_2O$, $Co(NO_3)_2{\cdot}6H_2O$; 1ml of Iron Stock: Ferric citrate; 1ml of K_2HPO_4 stock; 1ml of Na_2CO_3 stock) (Stanier et al., 1971) in Nunc sterile filter-cup tissue flasks in a rotation incubator (New Brunswick Scientific, Model G25 USA and Multitron, Infros HT) at 30°C, illuminated with an incident fluorescent white light of average intensity of 7 μE. m^{-2}. s^{-1}. Appropriate antibiotics were added to liquid or solid media. **Cultivation** on the solid agar 1.5% (w/v) BG-11 plates (BG-11 basic mineral medium (Stanier et al., 1971) with supplementation of 0.3% (w/v) sodium thiosulphate and addition of antibiotics after autoclave sterilization. In order to maintain the strains were restreaked onto the new plates on average

Table 2.1: *E. coli* strains

Strain	Relevant Genotype	Reference
BW25113	*F-, DE(araD-araB)567,lacZ4787(del)::rrnB-3, LAM-, rph-1, DE(rhaD-rhaB)568, hsdR514*	Datsenko and Wanner 2000
DH5α	*F$_-$, endA1, deoR, hsdR17(rK- mK+), supE44, thi-1, recA1, gyrA96, (NaI1), relA1, Δ(lacZYA-argF)U169, (m80lacZΔM15) λ-*	Taylor *et al.*, 1993

Table 2.2: *Synechocystis* sp. PCC 6803 strains

Strain	Relevant Genotype	Reference
WT	PCC 6803 wild-type **glucose sensitive strain**	Stanier (1973)
FtsH1-GFP	WT + *slr1390-GFP-Acc(5)III*	This work
FtsH2-GFP	WT + *slr0228GFP-Acc(5)III*	This work
FtsH3-GFP	WT + *slr1604GFP-Acc(5)III*	This work
FtsH4-GFP	WT + *sll1463GFP-Acc(5)III*	This work
CtpA-GFP	WT *slr0008GFP-Acc(5)III*	This work
FutA1-GFP	WT + *slr1295GFP-Acc(5)III*	Spence, not published

every 2 weeks.

Long term storage strains were suspended in 1 ml of liquid BG-11 with 10% DMSO for preservation, then flash cooled in liquid nitrogen and stored at -80° C.

2.2.5 Stress conditions

All stress conditions to which strains of *Synechocystis* sp. PCC 6803 were exposed are listed in the Table 2.3.

Synechocystis sp. PCC 6803 was grown in Nunc flasks were wrapped in aluminium foil and Dark Adapted (DA) in a black box with no light access at 30°C for 48 hours. High Light (HL) treatments were performed by illuminating previously Dark Adapted (DA) and Low Light (LL) cells for 1 hour in light box under white light 600 μE.m^{-2}s^{-1} (hand-made: BOX LIGHT). To investigate if any of observed phenomenon was reversible, strains exposed to HL were moved back to the initial conditions (weather DA or LL). Lincomycin/chloraphenicol treatment was performed on strains grown previously in Low Light following either prolonged Low Light exposure or High Light treatment for 30 min, control experiment was repeated for WT.

2.3 Cell concentration of *E. coli* and *Synechocystis* sp. PCC 6803 cultures

The optical density of liquid *E. coli* cultures was determined at 600 nm (OD_{600}), whereas the optical density of liquid *Synechocystis* sp. PCC 6803

Table 2.3: Stress conditions

Stress	**Treatment**	**Time course**
High Light	600 μ E.m^{-2}.s^{-1}, 35°C	10, 20, 30, 45, 60 min
Dark Adaptation	No light access, 30°C	24-hours
Iron Deprivation$*$	BG-11 (-Fe) + addition of Chelex 100 sodium (Sigma-Aldrich)	2-5 days
Copper Deprivation$*$	BG-11 (-Cu)	up to 7 days
Phosphate Deprivation$*$	BG-11 (-P) flasks washed with 10% HCL	up to 7 days
Zinc Deprivation$*$	BG-11 (-Zn)	up to 7 days
Inhibition of elongation factor G	lincomycin/chlorophenicol at final concentration of 400 μM	30-minutes prior to the experiments

$*$to wash off all traces of microelements strains were washed and pelleted 3 times with the final media lacking the tested ion and grown in the shaking incubator under low light (7-10 μEm^{-2}s^{-1})

cultures was measured at 730 nm ($OD7_{730}$). For both cultures a 1 mL disposable cuvette was used. OD_{730} of 0.25 for *Synechocystis* sp. PCC 6803 corresponds to approximately 1x 10^8 cells ml^{-1} (Williams, 1988).

2.4 Molecular biology

2.4.1 Buffers and solutions

All used chemicals and standard buffers were prepared using reagents from Sigma-Aldrich, if not stated otherwise. All media were prepared according to the protocols cited or described in this work.

2.4.2 DNA transformation

Transformation of *E. coli*

a) Preparation of chemically competent *E. coli* cells

E. coli DH5(α) cells (2.2.1.a), were streaked onto the Luria-Bertani, (LB) plates (1 g NaCl, 0.5 g yeast extract, 1 g tryptone, 100 ml) (Sambrook *et al.*, 1989) and incubated at 37° C over night in a shaking incubator (Orbital Incubator S1500, Stuart). A single colony was used to inoculate in 10 ml of LB media. The conical tube was incubated for 2-3 hours while shaking at 37°C. When optical density OD_{600} reached 0.4 - 0.6 cells were put on ice. The cells were harvested at 4000 g at 4°C (Eppendorf) for 10 min and the pellet was washed with 5 ml of ice-cold 100 mM $MgCl_2$. The cell suspension was left on ice for approximately 5 min and further harvesting was

Table 2.4: Plasmids and vectors

Plasmid	**Antibiotic resistance**	**Genotype**	**Reference**
PIJ790	chloraphenicol (CamR)	λ-RED (gam, bet, exo), cat, araC, rep101ts	Gust 2003
PIJ786	Aparmycin (ApraR)	egfp-P1-FRT-oriT-aac(3)IV- FRT-P2	Gust 2010
pGEM T-Easy	Ampicilin (AmpR)	found in Promega Corporation, USA	Marcus *et al.*, 1996
FL_1390_GFP_APRA_FR	Aparmycin (ApraR)	FL- slr1390- eGFP-P1-FRT-oriT- aac(3)IV-FRT-P2- FR in PGEM	This study
FL_0228_GFP_APRA_FR	Aparmycin (ApraR)	FL- slr0228- eGFP-P1-FRT-oriT- aac(3)IV-FRT-P2- FR in pGEM	This study
FL_1604_GFP_APRA_FR	Aparmycin (ApraR)	FL- slr1604- eGFP-P1-FRT-oriT- aac(3)IV-FRT-P2- FR in PGEM	This study
FL_1463_GFP_APRA_FR	Aparmycin (ApraR)	FL- sll1463- eGFP-P1-FRT-oriT- aac(3)IV-FRT-P2- FR in PGEM	This study
FL_0008_GFP_APRA_FR	Aparmycin (ApraR)	FL- slr0008- eGFP-P1-FRT-oriT- aac(3)IV-FRT-P2- FR in PGEM	This study

repeated. The pelleted was resuspended in 1 ml of ice-cold 100 mM $CaCl_2$ and left on ice for at least 30 min. Aliquots were flash cooled in the liquid nitrogen and stored at -80°C or used as prepared.

b) Transformation of chemically competent cells via *Heat shock*

DH5α cells were thawed on ice. 1-5μg of plasmid DNA together with plasmids of positive and negative controls were added to 50μl DH5α cells and incubated on ice for 30 min. The cells were then *heat shocked* by floating in the water bath at 42° C for 1 min and incubated on ice for 2 min. 500μl LB media was added to the cells, which were then incubated shaking at 37° C for 1-2 hours. 150μl of the aliquots were spread onto the LB plates supplemented with appropriate antibiotics and incubated overnight at 37° C.

c) Preparation of electrocompetent *E. coli* cells

Stock of BW25113 was streaked out onto the 1.5% (w/v) LB plate and grown overnight at 30°C. Selected single colonies were inoculated in a 10 ml starting culture with addition of chlorophenicol (10 μl.ml^{-1}) and incubated over night shaking at 30°C. The following day a 100 μl of starting culture was moved into 4x10 ml fresh LB media and grown in a shaking incubator at 30°C, for about 3 hours, till the OD_{600} reached 0.4. The cultures were moved immediately onto ice, harvested at 4000 rpm at 4°C for 10 min. The pellets were resuspended in 1 ml of 10% ice-cold glycerol, and this step of harvesting and washing with glycerol was repeated 3 times. Finally, the harvested cells were resuspended in 100 μl of 10% glycerol, further cells were either snap frozen in the liquid nitrogen or kept on ice for 30 min prior to use.

d) Transformation of electrocompetent *E. coli* cells via electroporation

All tubes, media tips and the cuvettes were chilled on ice or in the refrigerator in advance. 50 μl of eletrocompetent cells were mixed with 1-2 μl of plasmid (in Elution Buffer or water solution) and moved into the 0.2 cm gap cuvette (Gene Pulser MicroPulser Cuvettes, Bio-Rad, UK). Instrument settings were adjusted, with a choice of exponential growth and the following parameters: Voltage (V) = 2500 V, Capacitance (C) = 25 μF, Resistivity (R) = 200 $\Omega \cdot$m , Gap size = 2 mm. The cuvette was wiped off any trace of condensed water and placed in the electroporator chamber (Gene Pulser MXcell Electroporation System, Bio-Rad, UK). The pulse was applied aiming for time constant round 5.0 ms. Immediately after the pulse, the cuvette was washed with 1ml of ice-cold LB and the content was placed in the 1.5 ml eppendorf tube left in the shaking incubator for 2 hours at 30°C, due

to temperature sensitive pIJ790 plasmid in BW25113. 150 μl of the aliquot was pelleted onto the 1.5% LB agar plate with the appropriate antibiotic. The plate was left overnight at 30°C and single colonies were screened the following day.

Transformation of *Synechocystis* sp. PCC 6803

Synechocystis sp. PCC 6803 cells were transformed according to the original work by (Chauvat *et al.*, 1989). Wild-type culture in the exponential growth phase was harvested and spun down at 6000rpm washed by resuspension in fresh BG-11 medium, step was repeated two times. Solution of plasmid DNA was added to 100 μl of cells and incubated under 50 μE.m^{-2}.s^{-1} white light at 30°C over night before being spread onto the BG-11 plates. The plates were incubated under 50 μE.m^{-2}.s^{-1} white light at 30°C until confluent green growth was observed (one day). Antibiotics in appropriate concentration was added beneath the solid agar (diluted in 1ml of BG-11 in appropriate concentration) and left for a longer period (5-7 days) allowing the selection process to occur. New single colonies were then restreacted onto a new agar plate and when grown transferred to the liquid BG$-$11 media with appropriate antibiotic with the final concentration of 100μM. The process of transferring to fresh media with antibiotic was repeated 3-5 times. The strains were screened via PCR to confirm the segregation stage. The primers used for genotyping screen can be found in Table 2.7. The DNA was extracted from *Synechocystis* cells using the Fungal/Bacterial DNA Kit, following the manufacturer instructions of the (Zymo Research Europe GmbH, The Epigenetics Company, Germany). PCR prgram was chosen individually according to primers annealing temperatures. Primer were design that they amplify entire *ftsH* ORF and 650bp downstream se-

quence, therefore expected size for WT round 2.5kbp for *ftsH-GFP-Apra* round 4.6kbp.

2.4.3 Extraction and purification of DNA

Total genomic DNA extraction from *Synechocystis* sp. PCC 6803

Total genomic DNA was extracted from *Synechocystis* cells using the Fungal/Bacterial DNA Kit, following the manufacturer instructions of the (Zymo Research Europe GmbH, The Epigenetics Company, Germany).

Mini plasmid DNA preparation from *E. coli*

A single colony from LB agar plate was inoculated into a 10 ml liquid LB culture supplemented with appropriate antibiotic. The culture was grown over night at 30°C or 37°C depending on *E.coli* strain, with shaking at 180 rpm. The culture was harvested and by following the steps of Qiagen Plasmid Purification Handbook (QiaGEN Limited, UK), plasmids were eluted and either stored at -20°C or used immediately.

2.4.4 DNA work and techniques

Agarose gel electrophoresis

DNA separation according to the size was performed by running samples on the agarose gel. Gel was prepared with Agarose Powder (Agarose Type II, Sigma-Aldrich) to the final concentration of 0.8-1.5% (w/v), dissolved in 1x Tris-Acetate-EDTA buffer (TAE: 40 mM Tris-Acetate, 1 mM EDTA at pH = 8.0). When partially cooled, SYBR Safe DNA Stain (Invitrogen) was added to the final concentration of 0.1 μg.ml^{-1}. Samples were mixed in ratio of 5:1 with 6x DNA Loading Dye (ThermoScientific, UK: 10 mM Tris-HCL (pH = 7.6), 0.03% (w/v) bromophenol blue, 0.03% (w/v) xylene cyanol FF, 60% (v/v) glycerol, 60 mM EDTA). Gels were run in gel tanks (peQLAB, Biotechnologie, GmbH) with TAE buffer using constant voltage 70-120 V. DNA could be visualised by UV transilluminator (manufacturer) and photographs were taken (G:BOX, Syngene, Division of Synoptics Group, UK). To estimate the size of unknown DNA fragments a DNA marker (2-log DNA marker ladder, N3200S; New England Biolabs Limited, UK) was loaded in one lane of each agarose gel.

DNA recovery from agarose gel

DNA products from the PCR reactions were purified from the PCR mixture by running the samples on the agarose electrophoresis gel and excising the appropriate bands with a scalpel under transilluminator. Qiagen Gel Extraction Kit was used according to the manufacturer instructions to clean the DNA from residues of primers, dimers and other components of PCR buffer. Extracted DNA was used for the purpose of cloning and sequencing.

DNA fragment amplification via Polymerase Chain Reaction (PCR)

Enzymes and Reagents for PCR reactions

The thermo-stable DNA polymerases used in this study were:

- Taq DNA polymerase (PCR Master Mix, Promega, Promega Corporation, USA)

- Taq DNA and Tgo DNA polymerase (Expand High Fidelity PCR System, Roche, USA)

- PHUSION (F-530L, New England Biolabs Limited, UK)

Taq DNA polymerase (Promega) was used for routine optimisation of primers annealing temperatures as well as for screening of *Synechocystis* genomic DNA and single colony screens. Expand High Fidelity PCR System and PHUSION with proofreading activities were used for precise DNA fragments amplification for further cloning. Expand High Fidelity System adds A - overhangs for TA cloning, while PHUSION leaves blunt ends of the PCR products.

PCR temperature and time conditions

PCR thermocycler was used in this study (C1000 Thermal Cycler Bio-Rad, My Cycler, Bio-Rad). Depending on the step and gene amplification differ-

Table 2.5: Thermocycler conditions for Master Mix

Step	Temperature	Time	Number of cycles
Initial denaturation	95°C	2 min	1
Denaturation	95°C	30 sec	
Primers Annealing	45-60°C	30 sec	25-35∗
Extension	72°C	1 min per 1kb	
Final Extension	72°C	5 min	

∗- steps were optimised if the standard procedure led to decreased product yield or failure

ent polymerases were used in constructions of new plasmids.

a) During routine screening with Taq polymerase (Promega), typically 25 μl reaction mixture was used, contained: 12,5 μl PCR Master Mix 2x, 2 μl of 10 μM upstream primer, 2 μl of 10 μM of downstream primer (Table 2.7), 1-2 μl of template DNA, adjusted to approximately 25 μl with nuclease-free water.

The lid of thermo-cycler was warmed up to 104°C to prevent sample evaporation and condensation in the top of the PCR tube. Table 2.5 contains all steps for termocycler.

b) amplifications of genes and cassettes used for cloning into vectors acquired using the High Fidelity PCR System (Roche). PCR reaction varied from the standard one (Table 2.5). Reaction volume 50μl consisting of: 1μl Deoxynucleotide mix (10 mM of each dNTP), 2μl upstream primer (10μM), 2μl downstream primer (10μM) (Table X), Template DNA 2-5μl (0.1-250 ng), 5μl of 10x High Fidelity Buffer with 15 mM $MgCl_2$, topped with nuclease-free water to 50μl and 0.75μl Expand High Fidelity enzyme Mix. Thermal cycling set up for this system is gathered in the Table 2.6.

Table 2.6: Thermocycler conditions for Expand High Fidelity

Step	Temperature	Time	Number of cycles
Initial denaturation	94°C	2 min	1
Denaturation	95°C	15 sec	
Primers Annealing	45-65°C	30 sec	15-20∗
Extension	68°C	45sec- 8min/1kb*	
Final Extension	72°C	7 min	1

∗- steps were optimised if the standard procedure led to decreased product yield or failure

Oligonucleotide PCR primers

Table 2.7 presents all oligonucleotide sequences used in this study. Primers were purchased from Eurofins MWG Operon.

Restriction digest

Restriction DNA digestion were performed according to the manufacturer instructions (New England Biolabs Limited, UK) EcoRI endonuclease recognised and cut the GÂATT_C sequence, in pGEM-T Easy EcoRI cuts in MSC region in result leaving flanking the A/T cloning site. Approximately 1 μg of DNA (10μl) was digested in 1 unit of EcoRI in 1 hour at 37°C with NEBuffer EcoRI containing: 100 mM Tris-HCl, 50 mM NaCl, 10mM $MgCl_2$, 0.025% Triton X-100, pH = 7.5.

DNA ligation

Amplified in 2.8.3 and digested in 2.8.4 DNA fragments were further cloned into cloning vectors. pGEM T-Easy (Promega, Promega Corporation, USA) was used in this study. pGEM vector is a linearized with a single 3-terminal thymidine at both ends, this allows using the TA cloning technique. Ligation into pGEM was performed according to manufacturer instructions

(Promega), where 5 μl of 2X Rapid Ligation Buffer, 1 μl of pGEM T-Easy vector (50 ng) and an excess of PCR product (3:1), 1 μl T4 DNA Ligase (3Weiss units/μl), mixture was topped up to the final volume of 10 μl with nuclease-free water and left at RT for 30 min.

Amplification of eGFP cassettes

eGFP together with antibiotic marker Apramycin (GFP-ApraR) cassettes were amplified from pIJ786 plasmid (PBL, Biomedical Laboratories) by using long primers (Table 2.7). Each forward and reverse primer has a 39 nt matching *Synechocystis* sequence at the 5- end, either side of the stop codon, not including the TAA (stop codon of the target gene) and a 3- sequence of 19 nt or 20 nt matching nt the right or left end of the cassette. (Figure 2.7).

ReDIRECT λ Red recombination system

All GFP-tagged strains were generated following the ReDIRECT system described in (Gust *et al.*, 2003). This system allows transformation with linear DNA. Used in this study the BW25113 *E. coli* strain hosts the pIJ790, a derivative of the pDK46 plasmid (Datsenko and Wanner, 2000). pIJ790 is controlled under an inducible arabinose promoter and provides chloramphenicol resistance, however the origin of replication is temperature-sensitive, therefore replication of the plasmid only occurs at 30°C.

The pJI790 plasmid encodes the phage derived λ Red recombination genes, including three proteins which when expressed induces increased recombination in *E. coli* (Murphy, 1998) (Figure 2.1). The loci of these three recombination enhancing genes: *gam* (γ), *bet* (β) and *exo* genes are under control of one pL promoter on the pL operon. Each of these proteins: Exo, Bet and Gam have their particular functions. Exo is a 5'- to 3'- dsDNA (double stranded DNA) dependent exonuclease with ability to generate 3-ended

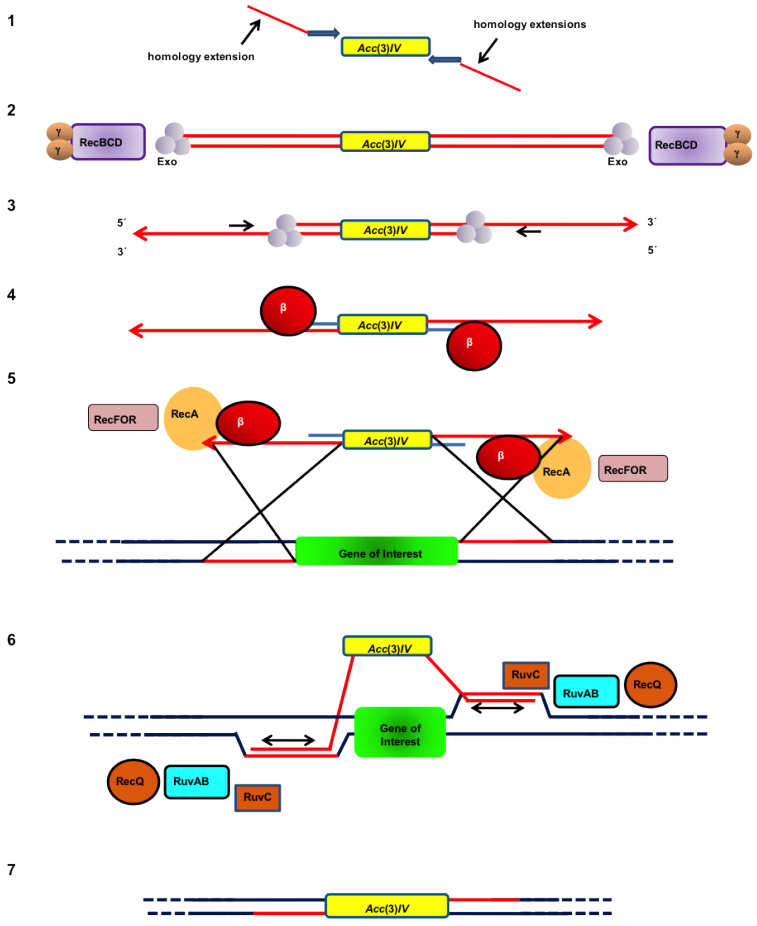

Figure 2.1: **RED recombination**
Scheme of the λ RED recombination of short sequences of homologous DNA, in an example generation of gene deletion constructs. Reproduced from (Poteete, 2001). Function of Exo, Beta and Gam explained in the text.

overhangs. Exo forms a trimer with a central hole, which is entered by dsDNA. The exonuclease entirely degrades one of the strands leaving the other one intact, therefore resulting in an ssDNA (single stranded DNA) leaving the complex (Mosberg JA *et al.,* 2010 Genetics). The bet gene encodes Beta protein, which binds the ssDNA and protects DNA from exonuclease degradation. The Beta protein also promotes recombination of complementary strands of ssDNA. Finally, the Gam protein forms a dimer that binds and inhibits the host RecBCD complex.

Using ReDIRECT system for homologous recombination in this study

The target genes were amplified with left and right flanked region of 1kb (Table 2.7), ligated into pGEM T-Easy cloning vector and *E. coli* BW25113 was transformed via electroporation with obtained plasmid. Linear DNA (GFP-ApraR) amplified from pIJ786 plasmid was introduced to the same host BW25113 via electroporation, where λ Red recombination system enhanced the homologous recombination resulting with a full in-frame GFP fusion to the target gene (Figure 2.2).

Screening single colonies via PCR

Single colonies obtained after heat shock/electroporation were picked by sterile tip into 50μl of nuclease free water and boiled in 100°C for 5 min. Such resuspension was treated as DNA concentrated stock and used in amount of 5μl into the PCR reaction mixture (Master Mix Promega). Run in appropriate PCR program (Table 2.5, 2.6).

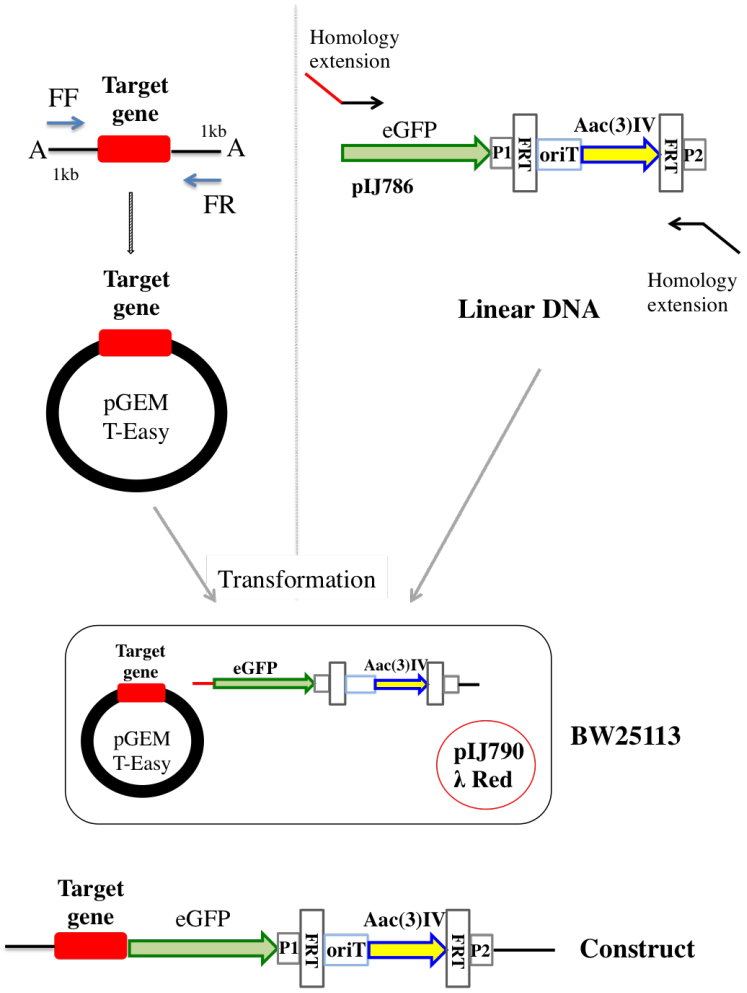

Figure 2.2: **Mutant engineering**
Steps to obtain the in-frame gene-GFP fusion while using the ReDIRECT protocol. Cloning into pGEM-T Easy vector cut with EcoRI which left flanking the A/T cloning sites. Cloned fragment with *ftsH* was amplified with PCR by Taq Polymerase with Adenine overhangs at 3′ ends. Homologous sequence for homologous recombination into *Synechpcystis* genome was 1kb long, upstream was at the beginning of sequence cloned to pGEM vector, and 1kb downstream at the end of the linear *GFP-Aac(3)IV* gene. Aac(3)IV states for the apramycin resistance gene. Details in the main text.

2.5 Biophysical characterisation of *Synechocystis* mutants

2.5.1 Growth controls

Obtained mutants were grown in the shaking incubator under low light 7-10 μE.m^{-2}.s^{-1} at 30°C. Optical density was measured at 730 nm (manufacturer) every day throughout the 2-week period.

2.5.2 Oxygen evolution

Oxygen production was measured in a 30°C chamber in Clarke-type light-controlled oxygen electrode (OxyLab Hansatech, King Lynn, UK). 1 mL of each sample was centrifuged and resuspended in methanol to determine chlorophyll light absorption measured by spectrophotometer at 666 nm and 750 nm. Formula: OD = (OD_{666} - OD_{750}) x 12.63 was applied to normalise chlorophyll a concentration to 10 μM. Each sample (wild-type, GFP mutants) was placed in an air-isolated chamber. The measurements were performed in the presence of an artificial electron acceptor: 1 mM DCBQ and 3 mM potassium ferricyanide, while sample was illuminated with 1000 μE.m^{-2}.s^{-1} of white light until the oxygen production achieved its maximum. Values at T_1 and T_2 times were registered and used to calculate the oxygen production rates. All oxygen production measurements were performed for cultures grown in LL and following 40-minutes treatment in HL with and without addition of lincomycin (inhibitor of new protein synthesis).

2.5.3 Optical spectroscopy-Absorption

Optical spectroscopy-absorption spectra of intact cells in the BG-11 media at the final chlorophyll concentration of 5 μM were recorded at RT on DW2000 spectrophotometer (SLM Aminco) in a split beam mode across 400-750 nm.

2.5.4 77K fluorescence measurements

Fluorescence emission spectra were measured on the whole cells of all GFP-tagged mutants. Samples were optimised to the final concentration of 5 μg.ml^{-1} chlorophyll *a*. Cell suspensions were injected into 4 mm diameter quartz capillary tubes and kept in dark (5 min) prior to the experiment, finally snap-frozen in liquid nitrogen. Steady-state fluorescence spectra were obtained using a Perkin Elmer LS50 luminescence spectrometer equipped with a liquid-nitrogen sample holder keeping 77K. The excitation wavelengths used were 435 nm and 600 nm, and emission registered in a range of 620 to 750 nm. Fluorescence ratios were averaged from spectra obtained from three samples.

2.6 Protein analytical techniques

2.6.1 Preparation of small-scale crude membranes

Preparation of the crude thylakoid membranes was carried out according to the protocol supplied by Nixon (Imperial College London, UK) slightly

changed for further pull-down assay procedure. All procedures were performed in a cold and dark room (4°C). 50 ml of fresh cell cultures (75-100μg chlorophyll *a* concentration) were harvested at 4000 rpm for 20-30 min. The cell pellet was either snap-frozen in the liquid nitrogen and stored at -80°C or moved to a 2 ml tube containing 200-300μl of glass beads (212-300 μm, Sigma Aldrich G1277) and spun down for 1min at 13,000 rpm. The supernatant was discard and pelleted cells were resuspended in 500 μl of buffer A (40 mM K-phosphate, pH = 8.0, 10 mM Tris buffer pH = 6.8, 1 mM EDTA, pH = 7.0, 100 mM NaCl, supplemented with Complete Protease Inhibitor Mini 1 tablet per every 10 ml). Breakage was carried out by vortexing each tube for 1 min and leaving it for 1 min on ice, the sequence was performed for 3-5 times depending on the success of procedure. The supernatant (S1) was transferred to a new tube and pellet with beads was washed with 800 μl of buffer A and collected and combined with the (S1). The supernatants were cleaned up from the unbroken cells and glass beads by centrifugation at 10,000 rpm for 1 min, repeated 3 times. To pellet crude membranes the clean fractions were centrifuged for 30 min at max speed of 14, 000 rpm. Blue supernatant containing soluble proteins was moved into a new tube, green pellets (membranes) were diluted in 50 μl buffer B (10mM Tris, pH = 6.8, EDTA, pH = 8.0, supplemented with Complete Protease Inhibitor Mini 1 tablet per every 10 ml (Roche, USA)). Chlorophyll *a* concentration was measured. The suspensions were snap-frozen in the liquid nitrogen and stored at -80°C or proceeded.

2.6.2 Isolation of membrane sub-fractions

Prepared membranes (2.6.1) were diluted down to desired chlorophyll concentration and incubated with 50 μl of α-GFP MicroBeads (anti-GFP antibodies coupled with micro beads)rotating for 1 hour on ice in a cold room (4°C). Manufacturer columns (μMACS Epitope Tag Protein Isolation Kit) were placed into the magnetic field stand, washed with supplied 200 μl Lysis Buffer (150mM NaCl, 1% Triton X-100, 50mM Tris HCl PH = 8.0), following the wash with 200 μl Buffer B (10mM Tris, pH = 6.8, EDTA, pH = 8.0, supplemented with Complete Protease Inhibitor Mini 1 tablet per every 10 ml). The membrane solutions with antibody mixture were loaded onto the column and the flow through fraction was collected. The column was washed six times with 200 μl of Wash 1 Buffer (150mM NaCl, 1% (v/v) Igepal CA-630, 0.5% (w/v) sodium deoxycholate, 0.1% (w/v) SDS, 50mM Tris HCl pH = 8.0), and twice with 100 μl of Wash 2 Buffer (20mM Tris HCl PH = 7.5). 20μl of Elution Buffer (50mM Tris HCl pH = 6.8, 50mM DTT, 1% (w/v) SDS, 1mM EDTA, 0.005% (w/v) bromophenol blue, 10% (v/v) glycerol) warmed up to 95°C was applied onto the column and left for 5 min, finally columns were washed with 50 μl of 95°C Elution buffer. All fractions of: flow through, washes and elution were collected and concentrated to the final volume of 50 μl with sample concentrators with cutoff= 10kDa (VivaSpin, Generon). Samples were analysed via SDS-PAGE and mass spectroscopy, as described.

2.6.3 Chlorophyll determination

Chlorophyll concentration was determined for whole cells (2.5.3, 2.5.4), the crude membranes (2.6.2) using the equations derived by Arnon (1949). For whole cells a 100 μl aliquot of cells was added to 900 μl 100% (v/v) methanol and incubated in the dark for 10 minutes. Cells were then pelleted by centrifugation to remove debris and the absorbance of the supernatants was registered at 666 and 750 nm. Pure membranes extracts (2.6.2) were diluted 200x, 5 μl of solutions with membranes was added to 995 μl 100% (v/v) methanol and measured as above.

2.6.4 SDS-Polyacrylamide gel electrophoresis (PAGE)

SDS-PAGE (Shaprio., *et al* 1967, Weber., *et al*., 1969) with Laemmlii buffers (Laemmli UK, 1970) was used to analyse and separate proteins. Typically according to the size of target proteins: 10%-12.5% (v/v) acrylamid resolving gels with or without 6M urea were prepared (40% Acrylamide, 3M Tris-HCl pH = 8.9, 10% (w/v) SDS, 6M Urea, TEMED, 10% APS), topped up with 1,5-2cm of 5% of stacking gel (40% (v/v) Acrylamide, 1M Tris-HCl pH = 6.8, 10% (w/v) SDS, TEMED, 10% (w/v) APS). Gels were run in Bio-Rad gel tanks in Laemmlii running buffer (250mM Tris Base, 1.9M Glycine, 1% (w/v) SDS). Samples containing membrane proteins were solubilised for 30 min at RT prior to loading using solubilisation buffer (0.03 M Tris-HCl pH = 6.8, 5% glycerol, 1% SDS, 10% β-mercaptoethanol, 0.001% bromophenol blue), and span down for 3 min. 5μg chlorophyll per lane was loaded onto 10 or 15 gels wells. 3μl of low range pre-stained molecular weight

standards were run alongside samples (Bio-Rad). Gels were run at 100 V for 1.5-2 hours (PowerPac, Basic Power Supply, Bio-Rad, UK).

2.6.5 Visualisation of proteins resolved by SDS-PAGE

Coomassie R-250 staining

Gels were stained (Coomassie brilliant blue R 0.2% (w/v), 5 volumes methanol, 2 volumes glacial acetic acid, 5 volumes H_2O) for 24 hours and washed several times in the destain solution (10% (v/v) acetic acid) to be visualised.

Instant Blue

Gels were removed from the gel tanks and moved directly into 20 ml solution of Instant Blue (Expedeon), incubated for 15-20 min while gently shaking. Protein bands were visible and gel was photographed. Bands cut out of gel stained with Instant Blue were cleaned up in 1.5 ml tube by 20 min incubation with either 1 ml of 30% (v/v) ethanol or 30% (v/v) acetic acid solution. In order to rapidly destain, the solution was warmed up to 60°C, supernatant was decanted and washing step was repeated 3 times until gel became clear.

Silver staining

Gels were removed from the gel tanks, washed briefly with ddH_2O and fixed for at least 1.5 hour in 40% (v/v) methanol and 10% (v/v) acetic acid solution, following 20 min wash repeated 3 times with 30% (v/v) ethanol and 1 min reduction step with 0.02% (w/v) $Na_2S_2O_3$. Gels were incubated for 20 min with 0.2% (w/v) $AgNO_3$ and 0.02% (v/v) formaldehyde and washed 3 times for 20 sec with dH_2O, finally gels were developed while shaking vigorously for 3-5 min in a developing solution (3% (w/v) Na_2CO_3, 0.05% (v/v) formaldehyde, 0.0005% (w/v) $Na_2S_2O_3$, first portion

of developing solution was discarded and replaced with fresh when became yellow. The staining was terminated by stop solution containing 0.5% (w/v) glycine. Gels were washed 2 times in ddH_2O for 30 min. Afterwards gels were photographed and kept for mass spectrometry analysis.

2.6.6 Western Blotting

After protein separations by SDS-PAGE (2.6.5) identification was completed by a well established method of immuno-detection of specific proteins (Renart *et al.*, 1979; Towbin *et al.*, 1979). Gels were blotted into the 0.2 μm pore size PVDF membrane using the iBlot system (Invitrogen). After protein transfer, the PVDF membranes were incubated in 5% (w$\check{}$) Marvel milk powder in TBS + Tween (50mM Tris-HCl, 150mM NaCl, pH = 7.6, 0.1% (v/v) Tween 20) for 30 min, blocking non-specific protein binding. Membranes were then washed 3 times for 5 min with TBS + Tween and incubated with the primary antibody over night in cold room (4°C).

After incubation, the membranes were washed in TBS + Tween three times for 10 min to remove the unbound primary antibody. The secondary antibody conjugated with horseradish peroxidase HRP (Novagen) was applied for 1 hour at RT. Unbound secondary antibody was removed by washing 3 times for 5 min in TBS + Tween following 2 times in pure TBS for 5 min. Immuno-detection of HRP was carried out using the manufacturers detection kits (Amersham ECL Prime Western Blotting Detection Reagent, GE Healthcare Life Sciences).
Immunoblotting analysis was performed using specific primary antibodies as listed: α-GFP antibody supplied by Gentaur Molecular Products, Bel-

gium; α-gFtsH a polyclonal antibody raised against residues 297 to 312 of *E. coli* FtsH (Tomoyasu *et al.,* 1993), which potentially cross-reacts with all *Synechocystis* sp. PCC 6803 FtsH homologues, kindly provided by Teru Ogura (University of Kumamoto, Japan); α-FtsH1 polyclonal antibodies raised against residues 578 to 592 of FtsH1, α-FtsH2 residues specific for 98 to 115 of *Synechocystis* FtsH2, α-FtsH3 against residues 59 to 75 of *Synechocystis* FtsH3, all at 1 in 1000 dilution, and α-FtsH4 against residues 556 to 574 of *Synechocystis* FtsH4, at 1 in 10,000 dilution; α-D1 a rabbit polyclonal antiserum (#304-F) raised against residues 325 to 353 of precursor D1 from pea (Pisum sativum; Nixon *et al.,* 1990) at a dilution of 1 in 5000; α-SbtA rabbit polyclonal antiserum raised against residues 184-203 of *Synechocystis* SbtA, dilution 1:200,000 (kindly provided by T. Ogawa). Secondary anti-rabbit and anti-mouse antibodies were horseradish peroxidase-conjugated (GE Healthcare). Signal was visualized using the chemiluminescent kit (GE Healthcare).

2.6.7 Mass spectrometry

Sample preparation

Elution fractions eluted from anti-GFP pull-down columns were cleaned up by running samples on SDS-PAGE gradient pre-cast gel (Invitrogen) allowing migration for about 1-1.5 cm at constant voltage 80 V. Proteins in gel were visualised with Instant Blue (2.6.6) and cut out with scalpel on light box. Only small fragments (1mm^2) of total bands were used for the mass spectrometry analysis. Experiment was carried out on two biological replicates.

MALDI TOF/TOF MS

Matrix-assisted laser desorption/ionization on Time-of-flight mass spectrometry (TOF MS) Mass spectrometry (LC-MS) was used to identify the protein compositions within the isolated membrane fractions. All procedure was performed by Dr Paul Hitchin (CISBIO mass spectrometry facility, Imperial College).

In preparation for mass spectrometry samples were digested with trypsin (E.C.3.4.21.4, Promega) overnight. Tryptic peptides were separated on an offline Ultimate 3000 nanoLC system using a PepMap 100 75 mm x 15-cm fused silica C18 analytical column (Dionex), coupled to a Probot for fraction collection and matrix addition with α-cyano-4-hydroxycinnamic acidas the matrix. A gradient of 2-60 % ACN in 0.1 % TFA was delivered over 60 min at a flow rate of 0.300 nL/min. MALDI TOF/TOF MS was performed using a AB Sciex 4800 mass spectrometer (Foster City, CA) in the positive reflectron mode with Delayed Extraction. MS precursor acquisition was followed by interpretation and data-dependent MS/MS acquisition with the CID on. Data interpretation was configured to select a maximum of 10 precursor ions per fraction with a minimum signal-to-noise ratio of 50. The data were processed using GPS Explorer (Applied Biosystems, CA) against the Swiss-Prot database. Search parameters were: enzyme = trypsin: fixed modifications = carboxymethyl (C), variable modifications = oxidation (M), mass tolerance +/- 100 ppm: fragment mass tolerance = 0.3 Da: maximum missed cleavages = 1, mass values = monoisotopic.

2.7 Lipid analysis

2.7.1 Lipid extraction

Lipids were extracted from crude membranes (2.6.1) or from elution of GFP pull-downs (2.6.2). Lipids were prepared according to methods described in Bligh and Dyer (1959). Thylakoid membranes of *Synechocystis* or elution collected from pull-down anti-GFP/GST affinity column were diluted in 1 ml of distilled water. Suspension was mixed with 3.75 ml of chloroform:methanol (1:2, v/v), vortexed and incubated in RT for 20 min. 1.25 ml of milliQ water and 1.25 ml of chloroform was added, content was vortexed and spun down at 300 rpm for 5 min. The top and bottom phases were transfered to new tubes seperately, the bottom contained lipids. The latter step of lipid extraction was repeated by adding to water fraction 2 ml of chloroform, vortexing and spinning down. Again top phase was removed and bottom lipid phase combined with that previously obtained. 0.5 ml of ethanol was added to lipid fraction and it was vacuumed at 30°C, 3000 rpm with pressure: 100 mPa for 2.5-3 hours. Pellet of lipids was resuspended in chloroform:methanol solution (2:1, v/v), for small scale extracts in 50μl, for large scale 100μl.

2.7.2 Thin-Layer Chromatographic Separation

Pre-coated silica gel plate without fluorescent dye plate (Merck 5721) was prepared by drying and marking loading path with a pencil. Plate was developed with solvent solution : chloroform:methanol:ammonia 13:7:1, by volume, paper filter (20x20 cm) was placed inside the glass tank for even

saturation. Tank was saturaed with lipid extraction solution for about an hour prior to run. Suspensions of extracted lipids were applied to the TLC plate with Hamiltonian syringe, with a gap of 1 cm in between each sample. Lipid separation was completed by 1.5 hour. The TLC plate was dried in the fume hood for 10 min, then it was sprayed evenly with solution of 1 % (w/v)primiludine and when dry visualised under UV light. Lipids patterns were marked with pencil and recovered from the TLC plate by scraping silica of marked area into a long glass flask with teflon cap. The weights of dry silica were registered. Silica powders containing lipids were subjected to methanolysis with 2 ml of methanol-HCL (5% (v/v)), approximately 10μl of lipid marker (15:0) was used in each sample. Tubes were incubated for 2.5 hours in 85°C. 2.5 ml of hexane was added to lipid and the top phase was transferred to a new glass tube. Hexane was evaporated by centrifugal evaporator for 1.5 hour at 30°C, 3000 rpm. Lipid were resuspended in 10 μl of hexane.

2.7.3 Gas Chromatography. Analysis of fatty acids in lipids

The resultant methyl esters were anlysed with gas-liquid chromatograph (Shimadzu, GC-4A) equipped with hydrogen flame-ionization detector. Fatty acids methyl esters were seperated on a glass column (2.0 x 4.0 mm internal diameter). Fatty acid methyl esters were separated on a glass column (2.0 m x 4.0 mm internal diameter) packed with 15% diethyleneglycol succinate on Chromosorb W or on a capillary column (Quadrex, CPS-1, 50 m x 0.25 mm internal diameter) coated with cyanopropylmethyl silicone at a thickness of 0.25 μm. Temperatures of the column and the flame-ionization detector were 170 and 260°C, respectively. The relative amounts of fatty acid

methyl esters were determined by comparison of areas under the peaks on the chromatogram, as calculated with a data processor (Shimadzu, C-R3A). The fatty acid methyl esters were identified by a gas chromatograph-mass spectrometer (JEOL, JMS-DX-300) equipped with a mass data-analysis system (JEOL, BJMS-3100) and the same columns as used for GLC. Positions of double bonds in fatty acids were determined by GC-MS on a column (1.0 m x 2.5 mm internal diameter) packed with 3% OV-1 (Gasukuro Kogyo) at a column temperature of 230°C. The distribution of fatty acids at the sn-position of the glycerol moiety of lipids was analyzed by selective hydrolysis at the sn-1 position by Rhizopus delemar lipase.

2.8 *In vivo* Imaging

2.8.1 Chemical fluorophores

FM-1 43

Lipophilic styryl green fluorescent FM 1-43 dye (Molecular Probes, Invitrogen) was used to stain the plasma membrane of intact *Synechocystis* cells. Dye was prepared in HBSS (Hanks Balanced Salt Solution, Invitrogen) to the final concentration of 5 μg.m^{-1}, kept on ice. 90 μl of cells were mixed with 10 μl of the staining stock solution. The drops of aliquot of cells were placed on the 1.5% (w/v) BG-11 agar plate, dried and visualised under the microscope using argon laser at 488 nm, the emission was registered in range of 560–600 nm.

2.8.2 Confocal fluorescence microscope

Cells were immobilised by their adhesion to BG-11 agar plates. Laser scanning confocal microscope (Leica TCS-SP5) with a 63x immersion oil objective (NA 1.4) was used in all experiments. Samples were excited by 488 nm Argon laser (30% power) with confocal pinhole set to give resolution in the z-direction of 1 μm. Fluorescence emission of GFP was selected and natural fluorescence from the chlorophyll were collected at 502-51 2nm and 670-720 nm respectively (wavelength ranges selected by monochromators). All images were recorded at 12-bit resolution (512 x 512 pixels), with laser scanning at 400 Hz and with line average of n = 2. Each frame was recorded twice, second image called: post-bleached GFP, was recorded after 10x with laser increased by a factor of 2.4 to bleach GFP fluorescence. Clean GFP images were obtained by subtracting the post-bleach image from the pre-bleach image. For purpose of this procedure images from both channels were merged and smoothed.

2.8.3 Data processing

ImageJ

ImageJ with the package of MBF plugins (McMac Biophotonics Facility) and JACoP plugin was used to process the data. Only raw data of images in 8–bit/12–bit grey scale have been analysed. Following pluggins were used in this study: Interactive 3D Surface Plot, Live Histogram, Colocalisation Analysis and JACoP.

The graphs of fluorescence profiles in the radial function were obtained by interpolation of values obtained from single cells to one scale.

Imaris

Imaris (BITPLANE Scientific Software) was used for determination of two fluorochromes (GFP and chlorophyll) in the same physical location. The threshold values were set for each channel manually. The percentage of channel A pixels overlapping channel B pixels and *vice versa* were estimated. Pearson and Mander correlations of channel A and channel B inside the colocalised region (ROI) were estimated and analysed according to criteria: -1 for perfect inverse correlation, 0 no correlation and 1 perfect correlation.

Quantifications of a patch size

FtsH2-4 patches observed in thylakoid membranes appeard in irregular shapes and different sizes. Method presented in work of Rexroth *et al*., inspired me to use similar approach in order to obtain approximate size. Observed in this study FtsH fluorescent patches appeared bright and wide in both x and y axis. Biological membranes are approximately 30-50 nm thick, these values are smaller than the resolution of this optical system, therefore GFP-signal blurr in Y-dimension is significant. The Cartesian system was introduced for each patch, where x-axis was traced along the membrane and y-axis was perpendicular to thylakoid membrane. Two line profiles were extracted across each distinct patch: in x and y dimensions. The full widths were measured at half maximum of Gaussian function. In order to get the real dimensions of patches, the width of the point spread function (in y-axis) was subtracted from the diameter in x-axis. One assumtion that was made was that observed FtsH patch occupies one out of n-thylakoid membranes. It was alos no assumed that visible patches are round within the membrane but rather irregularly shaped, therefore I could not calculate

approximate total surface which FtsH occupies in a single cell.

MATLAB

According to Prof NJ Burroughs method, radial fluorescence profiles were determined for each cell by using the chlorophyll fluorescence to define the cell geometry, i.e. radial coordinates were used to allow cell fluorescence to be averaged over rotation angle in each cell. Images were segregated into cells using chlorophyll fluorescence to demarcate approximate cell boundaries. Averaging over cells was performed by rescaling to a standard 1/2 maximum radius, filtering out cells that were not sufficiently circular (i.e. undergoing cell division). A bleached image was used to calibrate the auto fluorescence, i.e. levels of GFP protein were defined as relative to the bleached image.

Table 2.7: Primers used in the study

Primer name	Sequence (5′==>3′)
Cloning primers	
slr1390-3kb-F	TTACTTTGATAATCAGGTTCAT
slr1390-3kb-R	CTGGGAGCATTGCTGTAGATCGC
slr0228-3kb-F	GCCAGATAATCCAAAGCCTTTTGG
slr0228-3kb-R	CTCCGTTGCAATTAGGGAACTTCC
slr1604-3kb-F	GAGGATTTGGAAGAAAAACGCTG
slr1604-3kb-R	CTGTGAGTCCAAACAACCAGCAC
sll1463-3kb-F	CAGCGTTGGTTTTATCCTCGAAG
sll1463-3kb-R	CATCGGAGTTGGAGCCAGAAACC
slr0008-3kb-F	GACGTTACCGTGGTCATTTTGGC
slr0008-3kb-R	GACCAAGTTTGGGTTTGATGGTAC
Cassette primers	
slr1390-GFP-APRA-F	TTATCAACAATCTCAAAAACAGCCTGCTCTAGCCGGTAACTGCCGGGCCCGGAGCTGCC
slr1390-GFP-APRA-R	ATAGATTGTACGAGGATCGGACATTGCACAGATAGGGGGATTCCGGGGATCCGTCGACC
slr0228-GFP-APRA-F	CGCCGAGGTTCCCGTCAAGGAACAGTTAATTCCCCAACTCTGCCGGGCCCGGAGCTGCC
slr0228-GFP-APRA-R	CCTTGCTGACCATACTAAATTGGTTGGAGAAGGGAATTTATTCCGGGGATCCGTCGACC
slr1604-GFP-APRA-F	CTCCTGGCTAACAACAATGCCAAATTGGCACTTCTAGTTCTGCCGGGCCCGGAGCTGCC
slr1604-GFP-APRA-R	ATCAGAGTTTTAACTCTAGGAATTCCAATGCTTGGATTCATTCCGGGGATCCGTCGACC
sll1463-GFP-APRA-F	CTATTGGGCCAGGTTCAAGCTCCTGGCACCCTAGTGGTACTGCCGGGCCCGGAGCTGCC
sll1463-GFP-APRA-R	TGCAAACAGGTTTTTAAAGGGAGCAAAAAAGCAAGTTCCATTCCGGGGATCCGTCGACC
slr0008-GFP-APRA-F	TCTTCAATTCCCGCCATGGCAACGGCTCACAAGCCCAACCTGCCGGGCCCGGAGCTGCC
slr0008-GFP-APRA-R	TTTCTAATTAGAATTCCTGATGTTTTGTCCAAATGGTGAATTCCGGGGATCCGTCGACC

Screening primers (5′==>3′)	
slr1390-SCREEN-F	TGACAACAGATGAACATTACC
slr1390-SCREEN-R	GTGCGGCCATTTTGGTTAGTGC
slr0228-SCREEN-F	AGGAAAATTCCTCCAGGGTG
slr0228-SCREEN-R	CGGGTGCTGGAATATGTGCG
slr1604-SCREEN-F	CACTGGTTTATTTCGTCCAG
slr1604-SCREEN-R	GATGTGATTCAATTTTTTCCAG
sll1463-SCREEN-F	GCCGAAGTACAAGCCGCCTG
sll1463-SCREEN-R	GGATTATATTCACCGAATTG
slr0008-SCREEN-F	TTTGGCTGGGGGCTTTGGCAC
slr0008-SCREEN-R	GACCAAGTTTGGGTTTGATG

Chapter 3

Localisation of FtsH proteases under high light suggests existence of *repair centres*

This chapter is an outcome of work submitted recently to press, where subcellular localisations of four FtsH homologues in *Synechocystis* sp. PCC 6803 cells were visualised *in vivo*. Three of which, are concentrated mainly in distinct patches within the thylakoid, whereas one appeared in the plasma membrane. All four proteases do not show any spatial changes when PSII repair is at its maximum. The visible patches of FtsH2, a key proteolytic protein directly involved in the PSII repair, may correspond to the PSII *repair centres*. Novel approach in anti-GFP affinity pull-downs of FtsH2-gfp from isolated thylakoid membranes, revealed the protein content within these membrane zones, suggesting membrane heterogeneity and rearrangement after high light treatment.

3.1 FtsH homologues and their roles

FtsH proteases are membrane-integral proteins found across all the species from bacteria to eukaryotes (details in 1.5). In *Synechocystis* 6803 there are four homologues of FtsH proteases: FtsH1 (*slr1390*), FtsH2 (*slr0228*), FtsH3 (*slr1604*) and FtsH4 (*sll1463*) (details found in 1.5.3). Biochemical studies where membrane fractions were used, indicate that FtsH2 and FtsH4 are located mainly in the thylakoids (Pisareva, *et al.,* 2006), while FtsH1 and FtsH3 are found in the plasma membrane (Pisareva *et al.,* 2005; Pisareva *et al.*, 2006). The current models based on membranes fragmentation and affinity glutathione-S-transferase tag (GST) pull downs assays propose that FtsH proteases operate as homo- or hetero-oligomeric complexes, occupying distinct membrane systems in the cyanobacterium (Barker *et al.,* 2008; Boehm *et al.,* 2012). However, studying protein interactions which often omit some of the key domains *in vitro* may not always precisely reflect the behaviour of a native proteins in a living organism. It is therefore crucial that information obtained using methods *in vitro* and *in vivo* are complementary, rather then propose various concepts.

To investigate the roles and interactions of FtsH proteases and to find subcellular localisation in *Synechocystis* cell *in vivo*, chimeric fusions of Green Fluorescent Protein (GFP) to the C-terminus of each FtsH homologue were constructed.

3.2 Molecular engineering: GFP fusion

In order to generate in-frame GFP-fusion to the C-terminal end of FtsH proteases and to ensure that expression of the FtsH proteins was in context, the gene fusions were introduced into the native chromosomal *loci*, replacing the wild-type genes: *slr1390*, *slr0228*, *slr1604* and *sll1463* with *slr1390-GFP*, *slr0228-GFP*, *slr1604-GFP*, *sll1463-GFP*, respectively. The resultant strains remained under the transcriptional control of native promoters ensuring their yield at physiological levels. The constructs were obtained with incorporation of modified ReDirect method (Gust *et al.*, 2004) (refer to: 2.4.4). Each of FtsHx genes with 1 kb down- and up-stream flanking regions of homology were amplified *via* PCR using the genomic DNA of *Synechocystis* sp. PCC 6803 as template (FtsHx-3kb-F/R primer pairs). 3-4 kb PCR products were ligated into the EcoRI site of pGEM T-Easy via TA-cloning. The GFP-Aac(3)IV, including FRT and oriT fragments was amplified from PIJ786 plasmid (available from PBL Biomedical Laboratories), using the long primers (FtsHx-GFP-APRA-F/R), each containing a homology extension of 39 nt matching *Synechocystis*. 2,5 kb product was introduced as linear DNA into the BW25113 *E. coli*, to where FtsHx-pGEM (x-individual homologue) was also introduced. BW25113 hosts the PIJ790 plasmid expressing the λ red proteins (details in 2.4.4), which enhanced the rocombination between GFP-Aac(3)IV and pGEM-FtsHx (Figure 3.1).

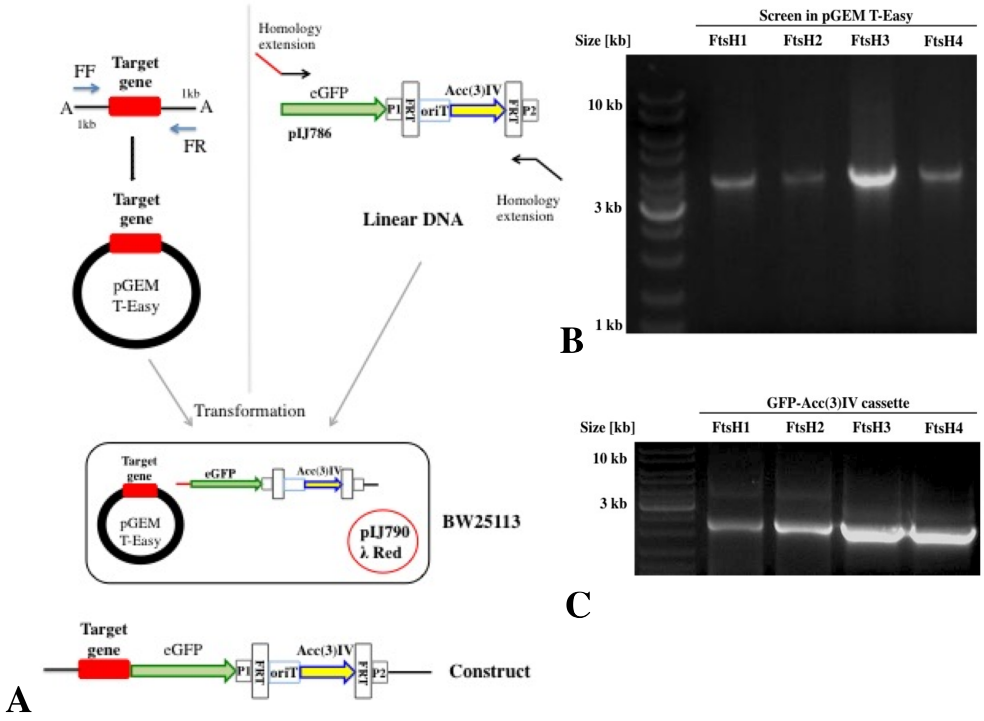

Figure 3.1: **Scheme of FtsHx-eGFP-Aac(3)IV constructs engeenering** PCR amplifications for all FtsHx genes with 1kb left and right flanking regions and eGFP-Aac(3)IV cassette with homologous extension to each of FtsHx gene. Adopted from Sacharz *et al.*, 2014.

3.3 Tests on successful mutants

Genotyping

The cell of *Synechocystis* is highly polyploid and contains several genome copies. In order to confirm that all native *loci* in each of multiple copies of chromosome in *Synechocystis* cells were replaced with GFP-tagged version, the segregation testes were preformed. The status and progress of segregation was tested via PCR on the extracted genomic DNA. PCR primers amplified the native gene and its flanking regions (2.5 kb) for mutants the products were bigger due to the insertion of GFP and apramycin-resistance

cassette (4.5 kb) (Figure 3.2).

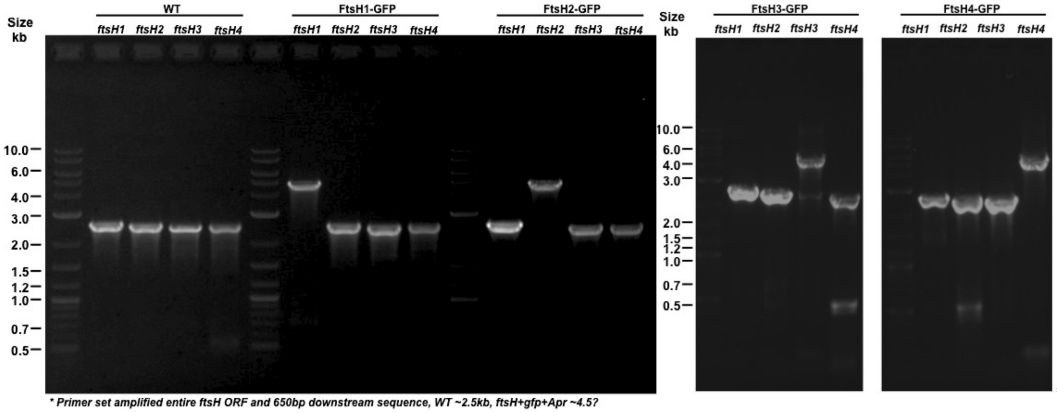

Figure 3.2: **Genotyping. Segregation status screen.**

Protein expression

Immunoblotting was used to examine the expression level and size of the FtsH-GFP recombinant proteins in the mutants. Both the soluble and membrane proteins were analysed on the SDS PAGE gels. Membranes were extracted in a crude membrane preparation (details: 2.6.1). After electrophoresis, proteins were either stained in gel (2.6.6) or transferred to a PVDF membrane for immunoblotting with specific antibodies (details in: 2.6.7). Experiments have shown that all four FtsH-tagged mutants expressed full-length FtsH-GFP fusion proteins (Figure 3.3). The expression levels of FtsH1 was significantly lower, with consistency to wild-type this homologue shows lower abundance than other three. For FtsH1-GFP a doublet band round 100 kDa appeared when probed with global FtsH and GFP antibodies, being most probably a results of loss in protein trans-membrane region. Similarly, FtsH2-GFP and FtsH4-GFP a cleavage of 10 kDa was registered, both partially cleaved forms were detected by GFP antibody, suggesting that proteins lost part of the trans-membrane region. Degra-

dation might have occurred during sample preparation, however other *in vivo* mechanisms may not be ruled out, especially for FtsH4, which is of unclear function. It can not be stated that the expression of GFP-tagged FtsH proteins did not vary from the wild-type, as an increase was registered for *ftsH2-GFP* when compared to native FtsH2. In *ftsH4-GFP* strain protein abundance seemed to be about 40% lower in GFP-tagged strain. Antibodies used for detection of each individual FtsH were not specific and some abnormalities were registered as well in previous studies. However, no free GFP was observed in any of the strains, suggesting that GFP might somehow affect FtsH4 expression and function.

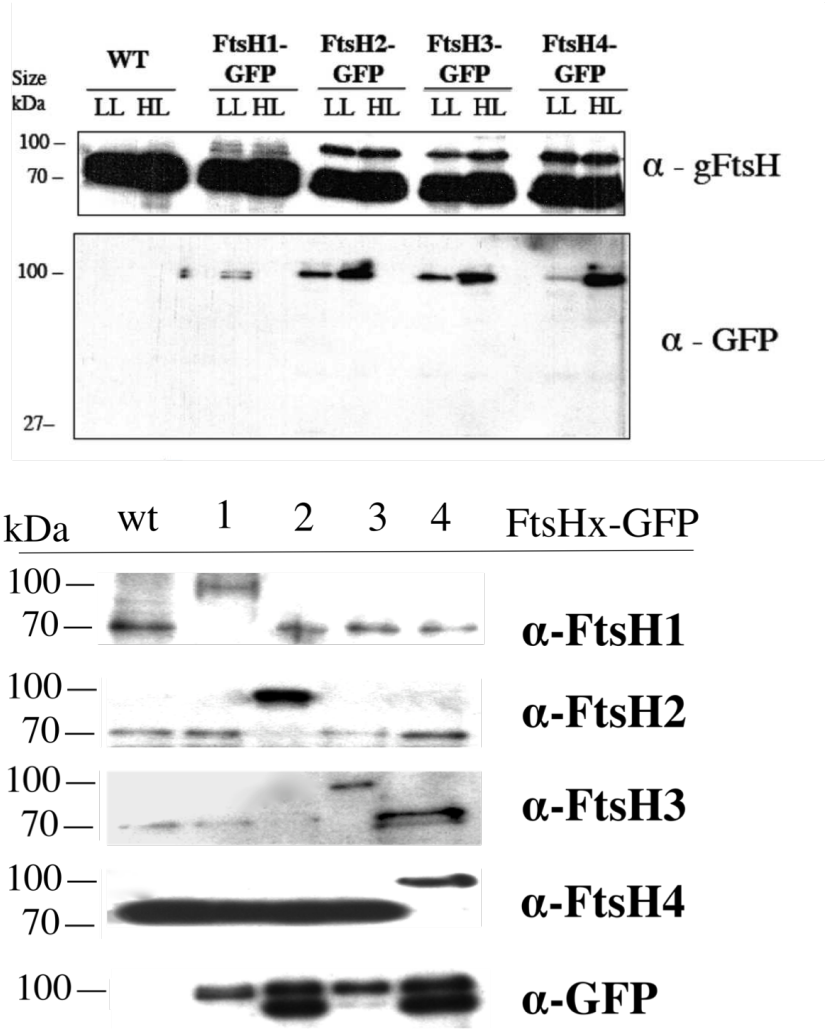

Figure 3.3: **Immunoblotting analysis**
Immunoblotting analysis of the tagged strains using antibodies specific for all FtsH homologues (global FtsH), specific to each individual FtsH homologue, GFP. Wild-type was used as a control in all tests. Protein samples were separated by SDS-PAGE using 10% (w/v) polyacrylamide gels.

Biophysical characteristics of the mutants

Genomic test and biochemical analysis confirmed that all obtained mutants were fully segregated and expressed GFP-tagged proteins at the expected sizes. Affinity (e.g. GST) and visualization (GFP) tagging are both powerful tools in biology, however any protein tag (GFP is 27 kDa) may in same cases impact on the target protein, affecting its insertion into the membrane, mobility and most importantly functions. Insertional disruptions of three out of four FtsH in *Synechocystis* were either lethal (FtsH1, FtsH3) or led to observable changes in the phenotype (FtsH2) (Mann 2000). To assure that GFP fusion did not impact on phenotype and proteins' functions, phenotype and PSII function tests were performed.

Growth

In order to identify potential aberrations in the mutants' phenotype, comparative photoautotrophic growth analyses were performed between the *Synechocystis* sp. PCC 6803 wild-type and all four FtsH-GFP tagged strains. Knowing that malfunction of FtsH1, FtsH2 and FtsH3 is either lethal or results in a light sensitive phenotype, a comparative growth analysis was performed under photoautotrophic growth conditions in moderate light (30 μE m^{-2} s^{-1}) for 10 days, in order to increase the dependency of the cells on PSII repair. The resulting growth curves, based on daily measurements of optical density at 730 nm (OD_{730}) were plotted against time on a semi-logarithmic scale. Experiment was repeated for three replicates in the same conditions. Growth of each mutant was almost identical when compared to wild-type (Figure 3.4).

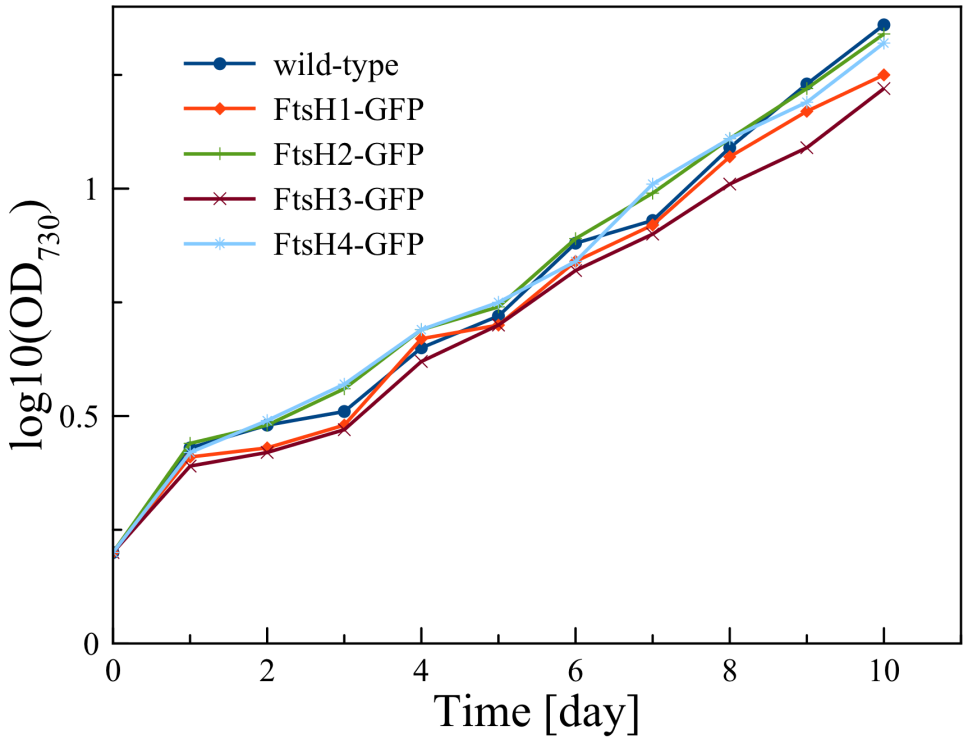

Figure 3.4: **Photoautotrophic growth of wild-type and FtsHx-GFP strains** Cells grown in BG-11 medium were inoculated to fresh BG-11 medium at cell concentration where optical density at 730 nm = 0.1. Growth curve was plotted based on the values of OD_{730} measured on each day for all strains. Cultures illuminated by 30 $\mu E.m^{-2}.s^{-1}$ for 10 days.

Absorption at RT and fluorescence emission at 77K

To characterise physiological activity of all mutants, which potentially may be impaired by GFP tag, spectral properties were monitored by testing RT (room temperature) absorption and low temperature (77K) fluorescence emission of intact cells (Materials and methods 2.5.3, 2.5.4). Figures 3.5 and 3.6 show the RT absorption spectrum and the 77 K fluorescence emission spectrum of wild-type and GFP-tagged strains respectively. Both spec-

tra display the characteristic features related to PSII and PSI. The peaks of absorption spectra at RT in the visible region might be assigned to Chl a (418 nm, 436 nm, 678 nm), carotenoids (490 nm) and phycobilisomes (625 nm), respectively. While in cyanobacteria, the fluorescence spectrum at 77K when upon excitation by 435 nm contains four main emission bands, with peak at 650 nm related to PC, 685 and 695 nm from CP43 and CP47 chlorophyll antenna of PSII respectively, and PSI peak at 725 nm. The RT absorption and 77K fluorescence emission spectra of all tested mutants were practically identical to the wild-type, indicating no significant perturbations caused by GFP tag. In particular, showing that FtsH2-GFP function was not impaired (Mann et al., 2000).

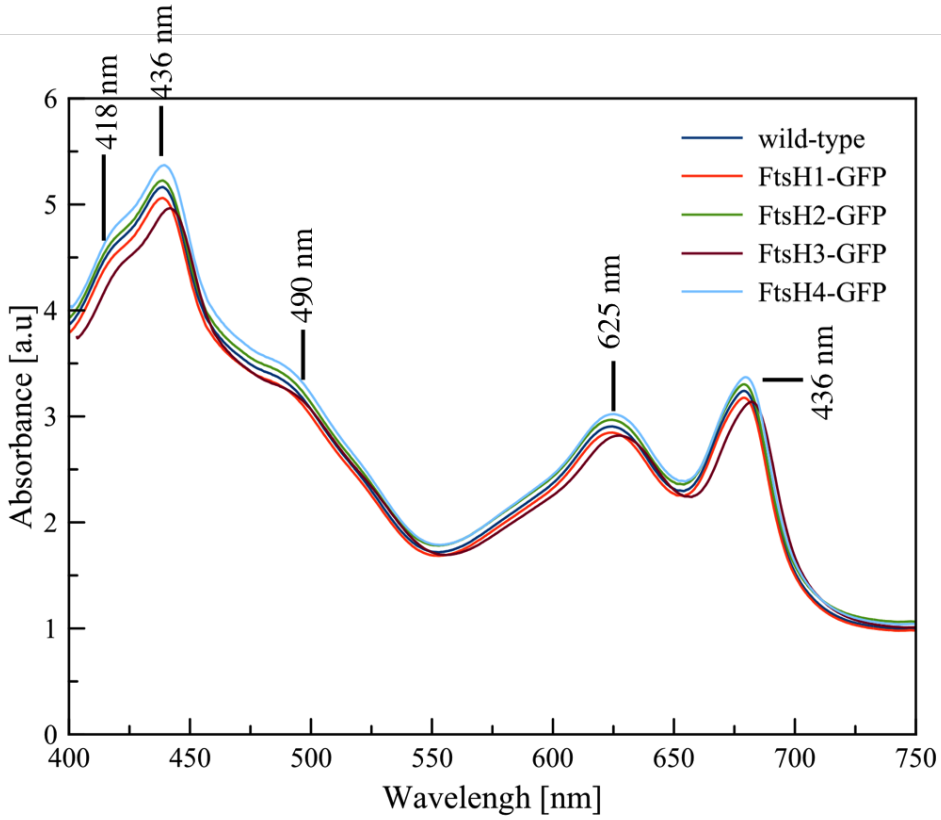

Figure 3.5: **Biophysical characterisation of GFP-tagged strains**
RT absorption spectra of whole *Synechocystis* cells, all spectra normalised to minimum at 750 nm. Absorption peaks marked according to details in text.

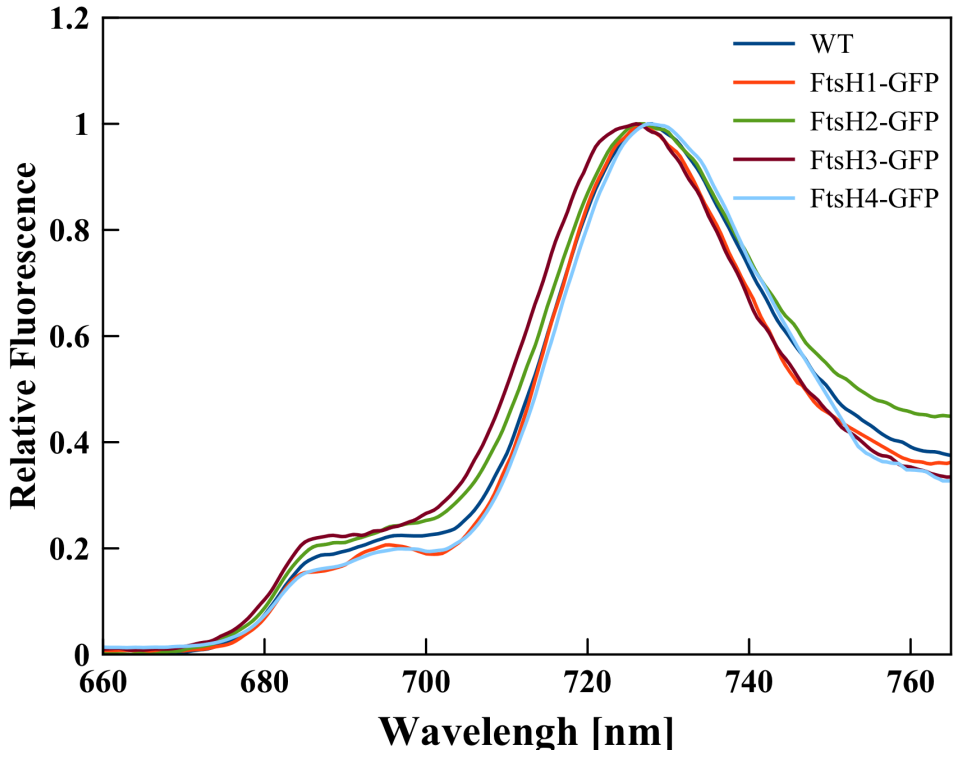

Figure 3.6: **77K fluorescence emission spectra**
77 K fluorescence emission spectra for whole cells of *Synechocystis* 6803 wild-type and strains with FtsHx-GFP. Fluorescence spectra recorded with excitation at 435 nm and normalised to the PSI fluorescence peak (720 nm). Cells were kept in dark 10 min prior to freezing.

Oxygen evolving activity

Given that ΔftsH2 shows a light-sensitive phenotype and strong impairment of the PSII repair cycle (Silva *et al.*, 2003), the susceptibility to photoinhibition was compared in the wild-type and *ftsH2-GFP* to check for the functionality of the tagged protease. Under photoinhibitory conditions, there was no significant difference in the maintenance of PSII oxygen-evolving activity between the wild-type and *ftsH2-gfp* (Figure 3.7). This is

in marked contrast to *ftsH2* null mutants (Silva *et al.*, 2003), and it demonstrates that the GFP tag does not disturb the function of FtsH2 in the PSII repair cycle. In high light exposure and in the presence of lincomycin to inhibit protein synthesis (Dalla Chiesa *et al.*, 1997), the loss of PSII activity is significantly higher for both wild-type and GFP-tagged strain (T-test for n=3, $p<0.05$), indicating that protein synthesis is mitigating the effects of PSII photodamage, and therefore that the PSII repair cycle is active.

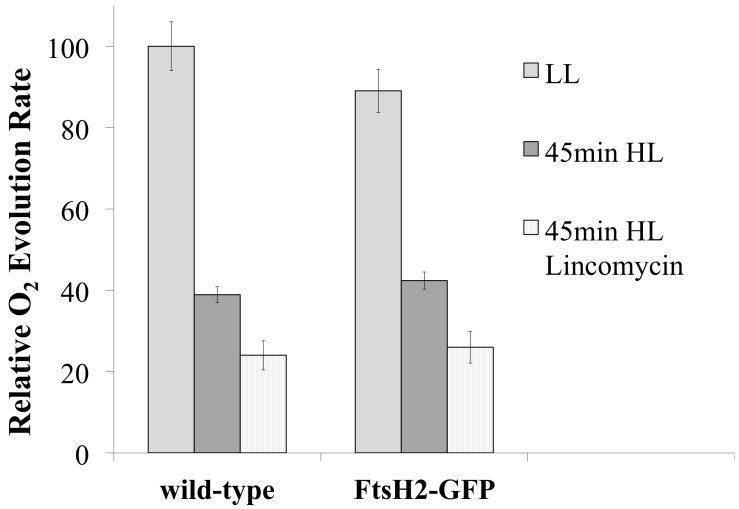

Figure 3.7: **Photoinhibition and the PSII repair cycle in wild-type and ftsH2-gfp cells.**
Relative oxygen evolution rates (light-saturated and in the presence of PSII electron acceptor) for cells grown in low light (LL) and exposed to high light for 45 min, w/o presence of lincomycin (400 μM) to inhibit protein synthesis (PSII repair cycle). Oxygen evolution rates were first calculated in units of μmol oxygen mg chlorophyll a^{-1} h^{-1} and then the rates were normalised (100% corresponds to the O_2 evolution rate of WT cells grown in LL mean = 237$\pm$ 7 (n=3)). Two-tailed T-test for n = 3, $p<0.05$.

3.4 Localisation of FtsH *in vivo*

Optimisation and data processing

Confocal fluorescence microscopy was used to visualise the localisation of the FtsH proteases in cells of *Synechocystis* sp. PCC 6803 grown under low light (LL, $7\mu E.m^2.s^{-1}$), as described in Materials and Methods (2.8). Fluorescence microscopy aims to register fluorescence of excited fluorophores. In cyanobacteria naturally fluorescent chlorophyll is useful for defining the region of the thylakoid membranes (Mullineaux *et al.,* 2002). However, in *Synechocystis*, membrane proteins may be located in either of the distinct membrane systems, therefore to comprehensively determine protein location in such a small organism ($2.32\mu m \pm 0.09$, n = 30), another set of references have been introduced. According to methods of Prof Nigel Burroughs in order to distinguish cell membranes, images were recorded on wild-type cells stained with FM 1-43 (details in 2.8.1), which specifically stains the cytoplasmic membrane (Schneider *et al.,* 2007), and on a strain in which the periplasmic FutA1 protein was GFP-labeled (Figure 3.8A). Each frame was recorded twice. A second image after bleaching GFP was recorded after 10x scans with 2.4x laser intensity. For the purposes of data analysing, the post-bleached GFP scan was subtracted from pre-bleached GFP image in order to get the clean GFP signal.

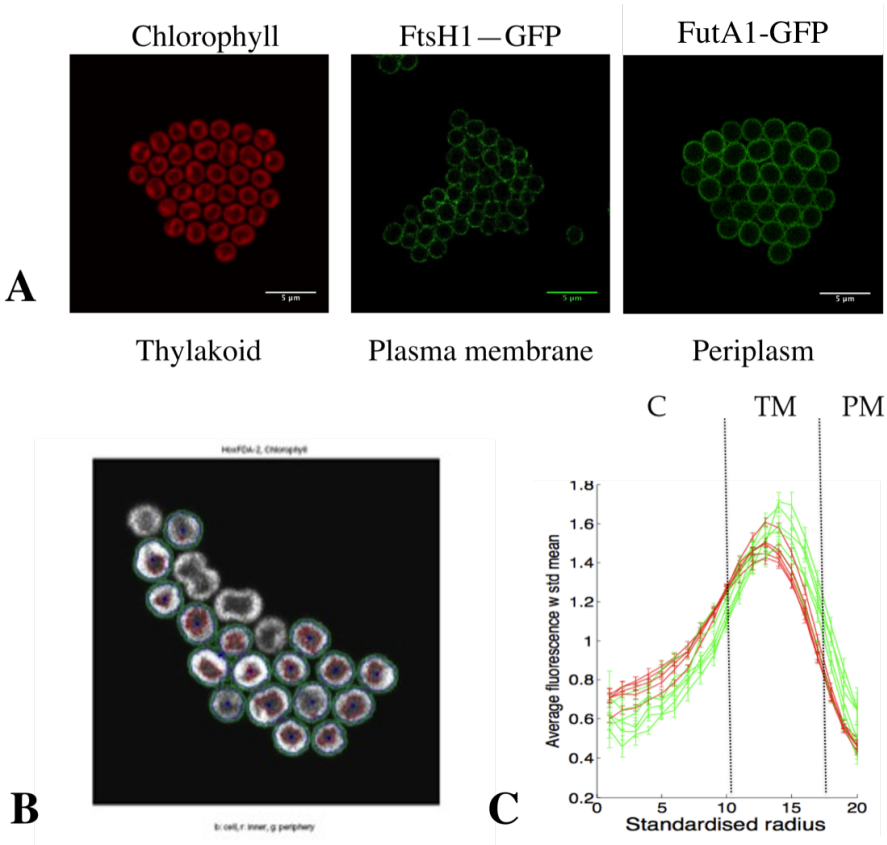

Figure 3.8: **Regional fluorescence quantifications**
(A) Defining cell compartments, with reference to: thylakoid (T) - red chlorophyll fluorescence, plasma membrane (PM): FtsH1-GFP, periplasm (PP): FutA1-GFP (data not published). (B) Image analysis according to Prof Burroughs, cell segmentation procedure and use of radial functions in individual cells in the micrographs. (C) Radial function of fluorescence intensities, separation into compartments of: C: cytoplasm TM: thylakoid membranes PM: plasma membrane, analysis by Prof. Nigel Burroughs.

For analysis purposes *Synechocystis* cells were treated as approximately spherical. Therefore, to quantify the localisation of GFP fluorescence, cell images were segmented into cytoplasmic, thylakoid, and periplasmic/plasma membrane regions based on the radial distribution of fluorescence relative to a standardised cell radius (Figure 3.8 B, C).

In order to obtain the profile plots of fluorescence, the diameter of each cell (n = 50) was traced out and fluorescent values registered and normalized to one standardised size. The visible patches were picked by hand and the total cell fluorescence was compared to the fluorescence of all summed up spots/puncta. All data were registered for at least three biological replicates.

Patchy distributions

Figures 3.9(A)–3.12(A) show fluorescence micrographs of red and green channels for wild-type and the each FtsH-GFP strain grown in low light. Based on comparison of GFP signal to the radial distributions of chlorophyll and FutA1-GFP fluorescence (representing periplasm region)(Figure 3.7, 3.9 and 3.13 and 3.14), it may be assumed that FtsH1 is present mainly in the plasma membrane. However, FtsH1 shows more fluorescence in the thylakoid region than FutA1-GFP (data not published, with courtesy of Dr Edward Spence) (Figure 3.14), suggesting the possibility of a minor population of FtsH1 in the thylakoids.

The radial distribution of FtsH2 corresponds closely to the radial distribution of chlorophyll (Figure 3.10 and 3.14), indicating that this protein is predominantly found in the thylakoid membrane. The same method assigned FtsH3 and FtsH4 mainly to the thylakoids (Figure 3.11, 3.12), however the

fluorescence signals of both homologues are rather shifted to more distal from the cell centre than the chlorophyll fluorescence, suggesting populations at the distal edge of the thylakoids or possibly in the cytoplasmic membrane. Prof Burroughs' method was used for the localisation of fluorophore in a spherical cell, however it failed to recognise patterns in distributions. To demonstrate uneven distributions of observed proteins, GFP signals were measured across each individual GFP tagged cells and averaged GFP values for 30 cells are presented in a form of plotted 3D profiles (Figure 3.13). It is rather clear that none of FtsH proteins are evenly distributed within the membrane. FtsH1 in comparison to FutA1-GFP, which equally fills the periplasm, shows a rather small puncta distribution within the cytoplasmic membrane, while FtsH2 is concentrated in distinct relatively large (200–600 nm) patches in the thylakoid membranes. The number of FtsH2 patches per cell varies from about 2 to 5 in the 1 μm optical sections observed at the set confocal pinhole, which will include roughly 60% of the cell volume. Therefore cells must typically contain about 3-8 distinct patches of FtsH2 in the entire thylakoid membranes. In extreme cases, big patches or clusters of smaller patches of FtsH2 occupy a significant part of the thylakoid, however this might occur in cells at different life stages, in response to stress or undergoing apoptosis.

FtsH3 is concentrated in small spots usually at the periphery of the thylakoid membranes (130–200 nm), 2-3 spots observed per cell, which implies 3-5 spots of FtsH3 in the entire cell. Averaged line profiles for fluorescence confirm that a significant proportion of FtsH3-GFP fluorescence is more distal to the cell centre than chlorophyll fluorescence, indicating that some FtsH3-GFP spots are either at the outer periphery of the thylakoids, or

in the cytoplasmic membrane. FtsH4 shows similar distribution to FtsH3, with on average 2 spots visible in the plane, mainly occupying the outer periphery of the thylakoid membranes, where the chlorophyll fluorescence is dimmer.

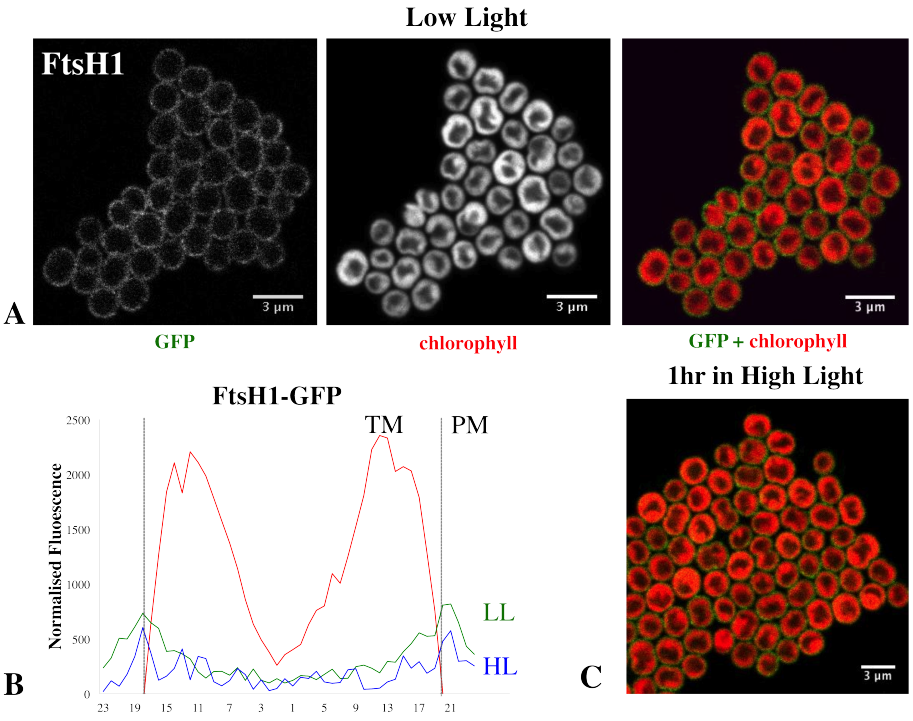

Figure 3.9: **Localisation of FtsH1 in High Light**
(A) Confocal fluorescence images showing GFP fluorescence, chlorophyll fluorescence (8-bit) and merged image of both (RGB) in Low Light (B). Averaged fluorescence line profiles across cells (n = 50, for 3 biological replicates), standardized to cell radius, for chlorophyll fluorescence (red); GFP fluorescence in low-light cells (green); GFP fluorescence in high-light cells (blue). (C) Merged image of FtsH1-GFP in High Light. Scale bar: 3 μm.

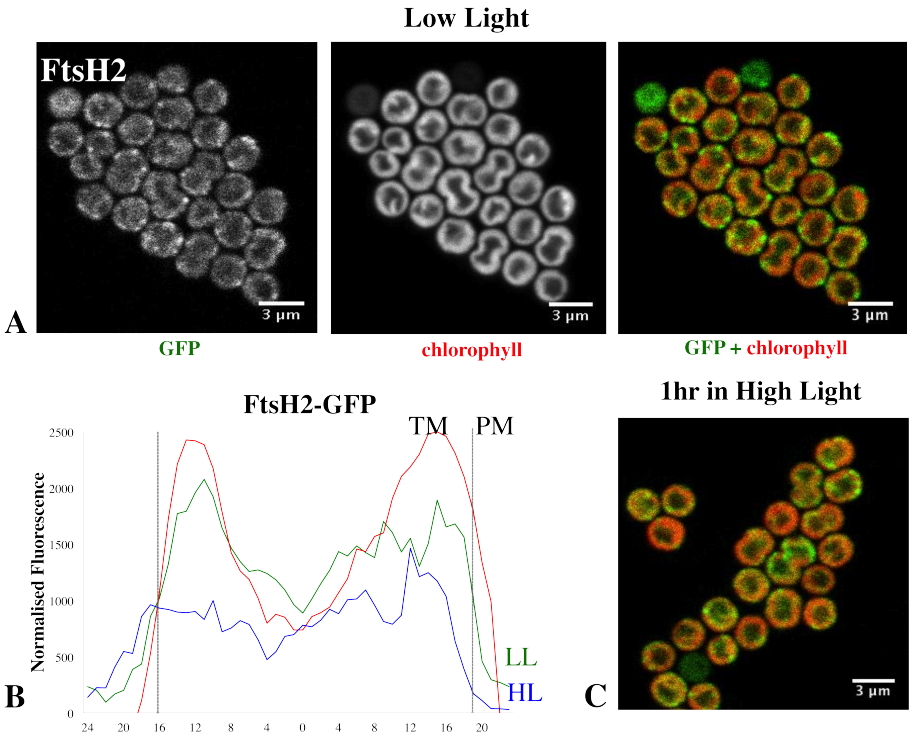

Figure 3.10: **Localisation of FtsH2 in High Light**
(A) Confocal fluorescence images showing GFP fluorescence, chlorophyll fluorescence (8-bit) and merged image of both (RGB) in Low Light (B). Averaged fluorescence line profiles across cells (n = 50, for 3 biological replicates), standardized to cell radius, for chlorophyll fluorescence (red); GFP fluorescence in low-light cells (green); GFP fluorescence in high-light cells (blue). (C) Merged image of FtsH2-GFP in High Light. Scale bar: 3 μm.

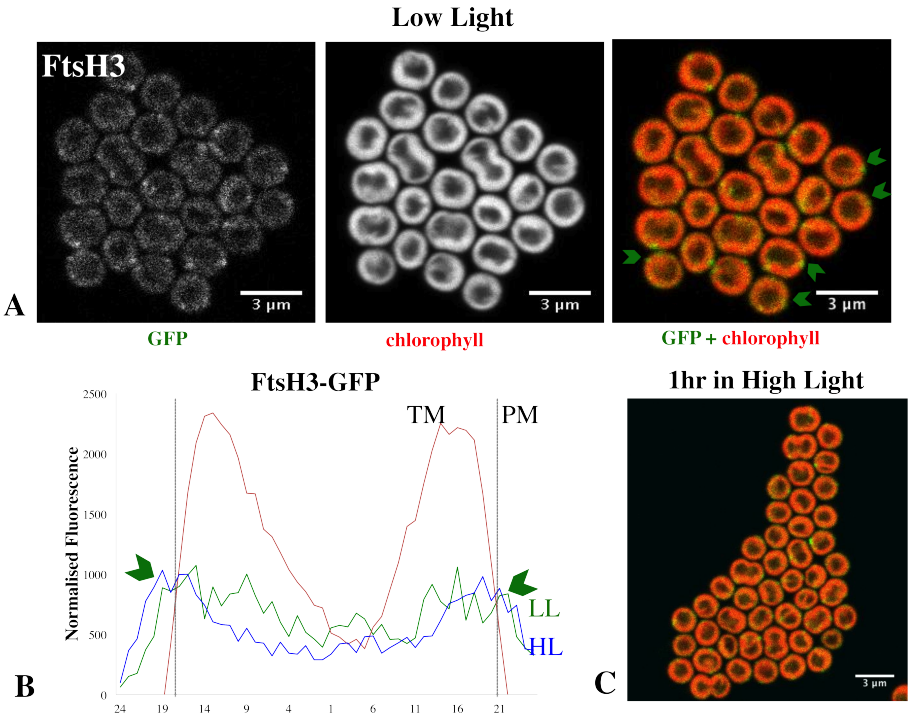

Figure 3.11: **Localisation of FtsH3 in High Light**
(A) Confocal fluorescence images showing GFP fluorescence, chlorophyll fluorescence (8-bit) and merged image of both (RGB) in Low Light (B). Averaged fluorescence line profiles across cells (n = 50, for 3 biological replicates), standardized to cell radius, for chlorophyll fluorescence (red); GFP fluorescence in low-light cells (green); GFP fluorescence in high-light cells (blue). (C) Merged image of FtsH3-GFP in High Light. Scale bar: 3 μm.

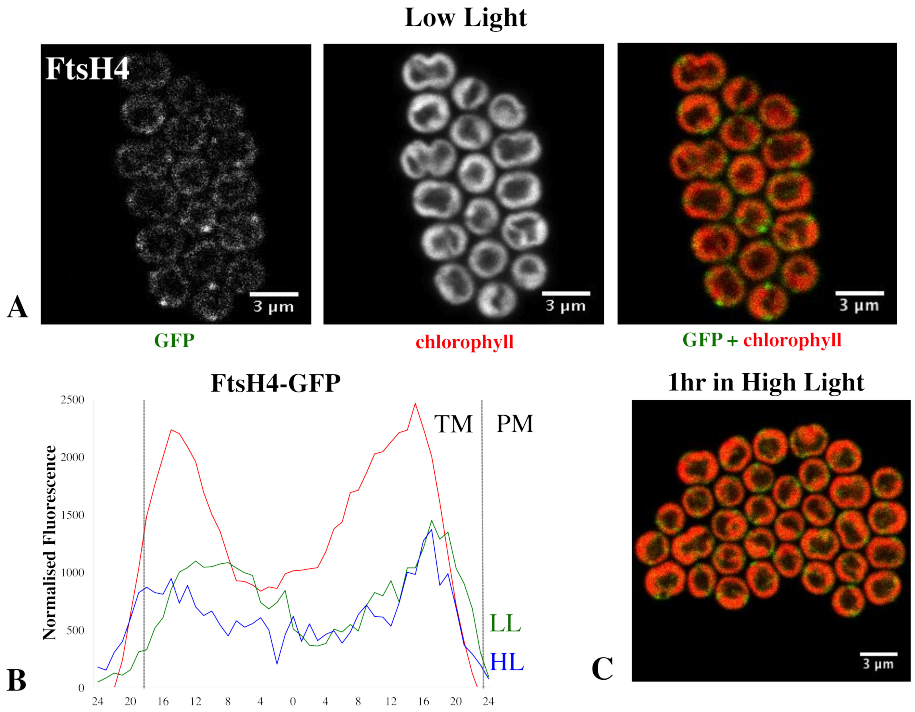

Figure 3.12: **Localisation of FtsH4 in High Light**
(A) Confocal fluorescence images showing GFP fluorescence, chlorophyll fluorescence (8-bit) and merged image of both (RGB) in Low Light (B). Averaged fluorescence line profiles across cells (n = 50, for 3 biological replicates), standardized to cell radius, for chlorophyll fluorescence (red); GFP fluorescence in low-light cells (green); GFP fluorescence in high-light cells (blue). (C) Merged image of FtsH4-GFP in High Light. Scale bar: 3 μm.

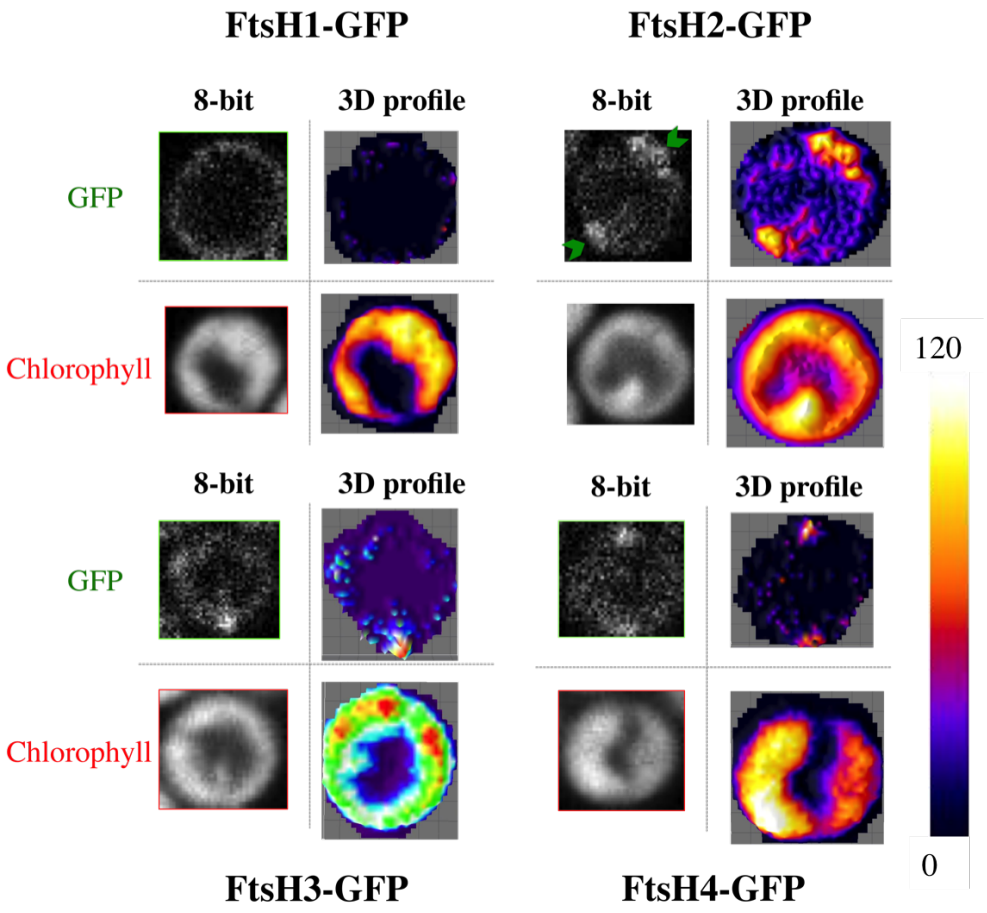

Figure 3.13: **Plotted 3-dimensional profiles of the whole cell in low light** Confocal images showing chlorophyll and GFP fluorescence (8-bit) from cells in low light and same signals in false-colour 3D surface plots (with linear colour scale) of GFP and chlorophyll fluorescence in low-light exposed *Synechocystis* cells.

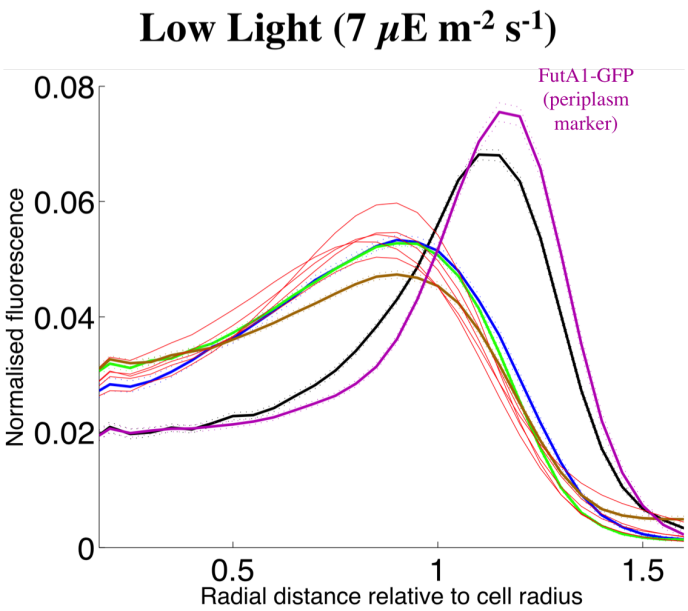

Figure 3.14: **Radial distribution of FtsH under Low Light**
Normalised fluorescence relative to standardised cell radius, for references: FutA1-GFP (magenta) (Spence, not published), FtsH1-GFP (black), FtsH2-GFP (green), FtsH3-GFP (brown), FtsH4-GFP (blue). Data averaged from a minimum of 443 cells and normalised to total fluorescence from each species. A standardised cell radius is defined by chlorophyll fluorescence. Graph prepared by Prof Nigel Burroughs.

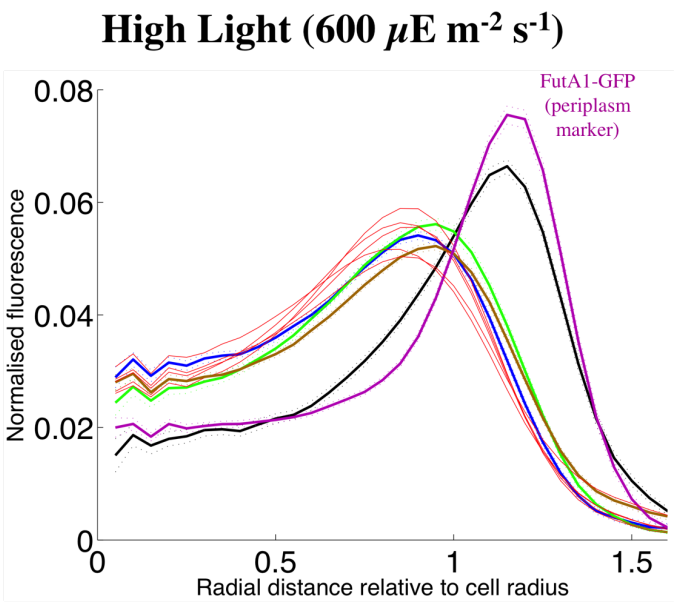

Figure 3.15: **Radial distribution of FtsH under High Light**
Normalised fluorescence relative to standardised cell radius, for references: periplasmic FutA1-GFP (magenta) (Spence, not published), chlorophyll (multiple red lines), FtsH1-GFP (black), FtsH2-GFP (green), FtsH3-GFP (brown), FtsH4-GFP (blue). Data averaged from a minimum of 443 cells and normalised to total fluorescence from each species. A standardised cell radius is defined by chlorophyll fluorescence. Refer to Fig. 3.14 for comparison in low light. Graph prepared by Prof Nigel Burroughs.

Table 3.1: Localisations of FtsH homologues in *Synechocystis* 6803

FtsH homologue	**Localisation *in vivo* in LL**	**Localisation *in vivo* in HL**	**Ratio* of HL/LL GFP singal**	**Distribution**
FtsH1-GFP	PM	PM	0.95	even
FtsH2-GFP	TM	TM	1.3	heterogenous
FtsH3-GFP	TM/PM	TM/PM	0.94	heterogenous
FtsH4-GFP	TM	TM	0.88	heterogenous

PM = plasma membrane, TM = thylakoid membranes,

$*$ - based on the Corrected Total Cell Fluorescence registered in GFP channel, n = 30 cells.

3.5 Effect of High Light on FtsH distribution

The role of FtsH2 in the PSII repair cycle has been well-established (Komenda, *et al.*, 2006), however details that could explain the proccess better are still missing. Some intriguing questions remain unaswered:

Where does D1 turnover happen?

Does FtsH2 move from visible patches in order to access PSII and assist in its repair when activity of repair cycle is high?

Are other FtsH homologues involved in D1 repair process?

To answer these questions we performed straightforward experiments where low light grown strains were exposed for up to 1 hour to high light at 600 μE.m^{-2}.s^{-1}. Given that such prolonged exposure leads to acceleration of D1 damage, we expect to impact on FtsH2 activity.

However, the radial distributions of all four FtsH proteases were not significantly altered by high light treatment, with FtsH1 still occupying the plasma membrane, FtsH2 found in the thylakoid region, while FtsH3 and FtsH4 were mainly at the periphery of the thylakoid membranes. High Light did not impact on spatial distribution of the observed proteins, nor did it greatly impact on proteins' overall expression (Figure 3.3). Fluorescence quantifications showed slight decrease in FtsH1 fluorescence per cell (Figure 3.9) while overall mean FtsH2 fluorescence per cell increased by 20-40% (Figure 3.10). FtsH3 and FtsH4 distribution and fluorescence intensities per cell remained unaffected by high light (Figure 3.11, 3.12). Notably, all FtsH proteases remained in their patchy regions seen under Low Light. Results from immunoblots showed a slight increase in FtsH2 content after HL treatment (Fig. 3.3).

Importantly, FtsH2 in HL remained concentrated in the thylakoid membrane patches similar to its location under LL (Figure 3.16A, B). In order to quantify the extent to which FtsH2 is localised in dedicated thylakoid membrane patches as opposed to being evenly spread in the thylakoid membranes, correlation coefficients for co-localisation of chlorophyll and GFP fluorescence were calculated in the two conditions. According to correlation coefficient formulae (Appendix 1) , segregation of FtsH2 into distinct thylakoid membrane zones would decrease the correlation between GFP and chlorophyll fluorescence, while a more even distribution of FtsH2 in the membrane would have the opposite effect. However, neither Pearson's correlation coefficient nor Manders' overlap coefficient (n = 30, $p < 10^{-6}$) (Zinchuk *et al.,* 2007; Manders *et al.,* 1993) were significantly affected by HL treatment (Fig. 3.16 C), indicating that the relative distribution of

FtsH2-GFP and chlorophyll fluorescence remains unchanged under conditions when the PSII repair cycle is most active (Student's t-test comparisons of HL vs LL for both coefficients gives $p = 0.3$).

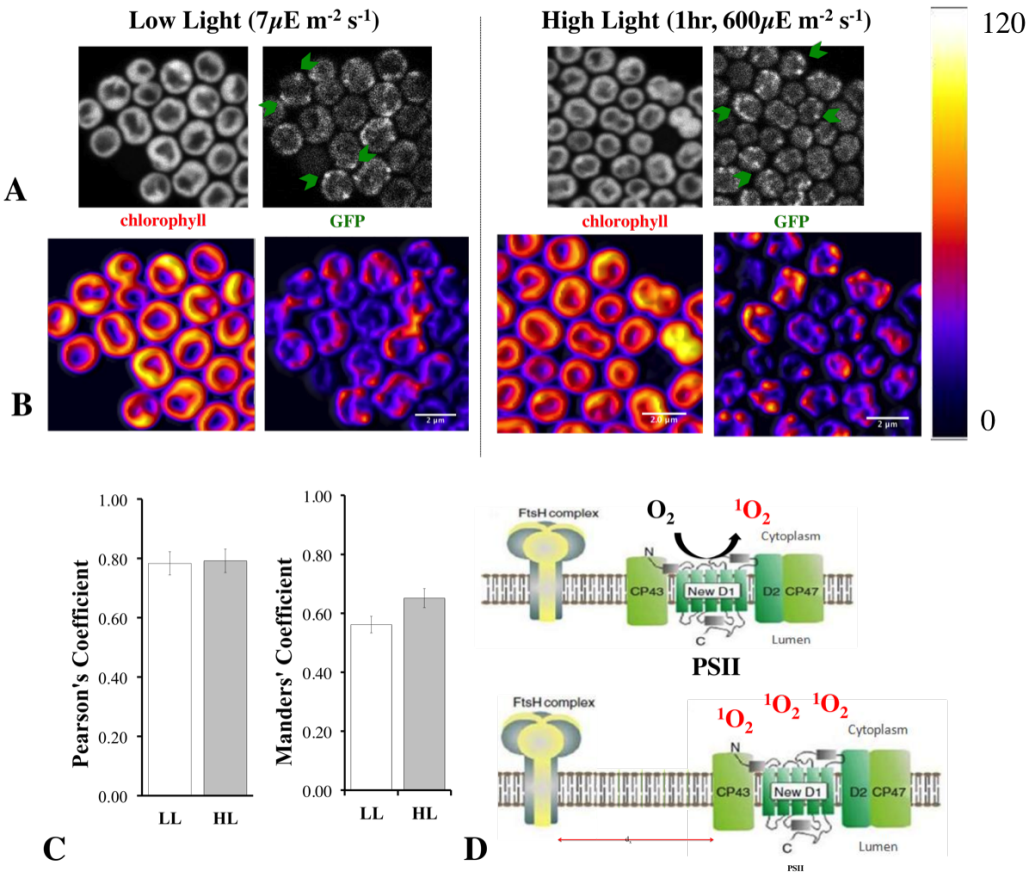

Figure 3.16: **Patchy localisation of FtsH2**
Effect of high-light exposure on the relative distributions of chlorophyll and FtsH2-GFP in *Synechocystis* cells (A) Confocal images showing chlorophyll and GFP fluorescence (8-bit) from cells in low and high light, (B) False-colour 3D surface plots (with linear colour scale) of GFP and chlorophyll fluorescence in low-light and high light-exposed *Synechocystis* cells (C) Co-localisation of GFP and chlorophyll fluorescence assessed by Pearson's and Manders' coefficients. There are no significant differences between HL and LL (n = 30, p = 0.30 for Pearson's coefficient and 0.26 for Manders' coefficient, error bars show standard deviation, tested and averaged for 3 biological replicates), (D) Model trying to explain the existence of localised repair centres in the thylakoid membranes and impact of ROS (singlet oxygen) on biogenesis of protein *de novo*.

3.6 Altered distribution of FtsH in response to nutrient stress

Other functions of FtsH homologues in *Synechocystis* are not established, however their irreplaceable role (FtsH1 and FtsH3) in cell viability has been previously described (Mann *et al.*, 2000). On the contrary, multiple important roles of FtsH in *E. coli* have been reported (Boyd *et al.*, 1998). In order to find other potential functions or factors triggering FtsH's activity, simple experiments were to test the localisations of FtsH homologues under stress conditions different than high light. Verbal communications with experts in this field, including Dr Samantha Bryan, Prof Joseph Komenda and Prof Peter Nixon, inspired the use of macro- and micro-elements deprivation as another way of triggering cellular stress.

Micro- and macro-elements play various important roles in all living organisms. Macro-elements are required by every cell in relatively large quantities to build the organic compounds of cellular structure and to be utilised in metabolic pathways. On the contrary, individual cell needs micro-elements (trace metals) in only trace amounts, however the demand is as important as for macro-elements. There are many roles of micro-elements, they are for example essential for redox-factors in enzymes involved in multiple metabolic pathways. There are seven trace metals used in the basic BG-11 medium, supplemented in order to maintain stable growth of *Synechocystis*, including: iron, boron, manganese, molybdenum, zinc, copper and cobalt. Transport of each of these metals into the cell is strictly regulated. In *Synechocystis* some metal importers residue in the plasma membrane (zinc, iron and manganese). In this study shortage in phosphate, iron, zinc and copper

was tested. The cells were observed after deprivation of each of element for certain period of time (Chapter 2: 2.2.5, Table 2.3).

Phosphate is important for cell viability. It was chosen for this project as a control, based on knowledge that organic phosphate impacts on ATP synthesis, it was reasoned that this element when absent in the cell will impact on overall protein expression and activity including protease FtsH.

Zinc is an important, essential trace. More than 100 zinc dependent or zinc-binding proteins have been described in *E. coli* with its importance for enzymes such DNA primase and RNA polymerase (Nies *et al.*, 2009). FtsH is a zinc-dependent protein, therefore, shortage in zinc may have a catastrophic impact on its presence and function.

Proper functioning of oxygen photosynthesis requires several membrane complexes as well as soluble proteins which contain either iron or copper (Hervas *et al*., 2003). Copper and iron are crucial for photosynthetic organisms and the requirement for both elements exceeds that of non-photosynthetic ones (De la Cerda *at el*., 2008). For instance *Synechocystis* demands for iron is 10 times greater than *E. coli* (Keren *et al*., 2004). Testing iron on FtsH function was inspired by Prof Joseph Komenda, according to whose preliminary data, the absence of iron impacted on the FtsH4 activity (not published).

Copper was another choice as it is highly important for photosynthetic organisms. Thylakoid membranes require copper for the electron carrier plastocyanin and cytochrome oxidase.

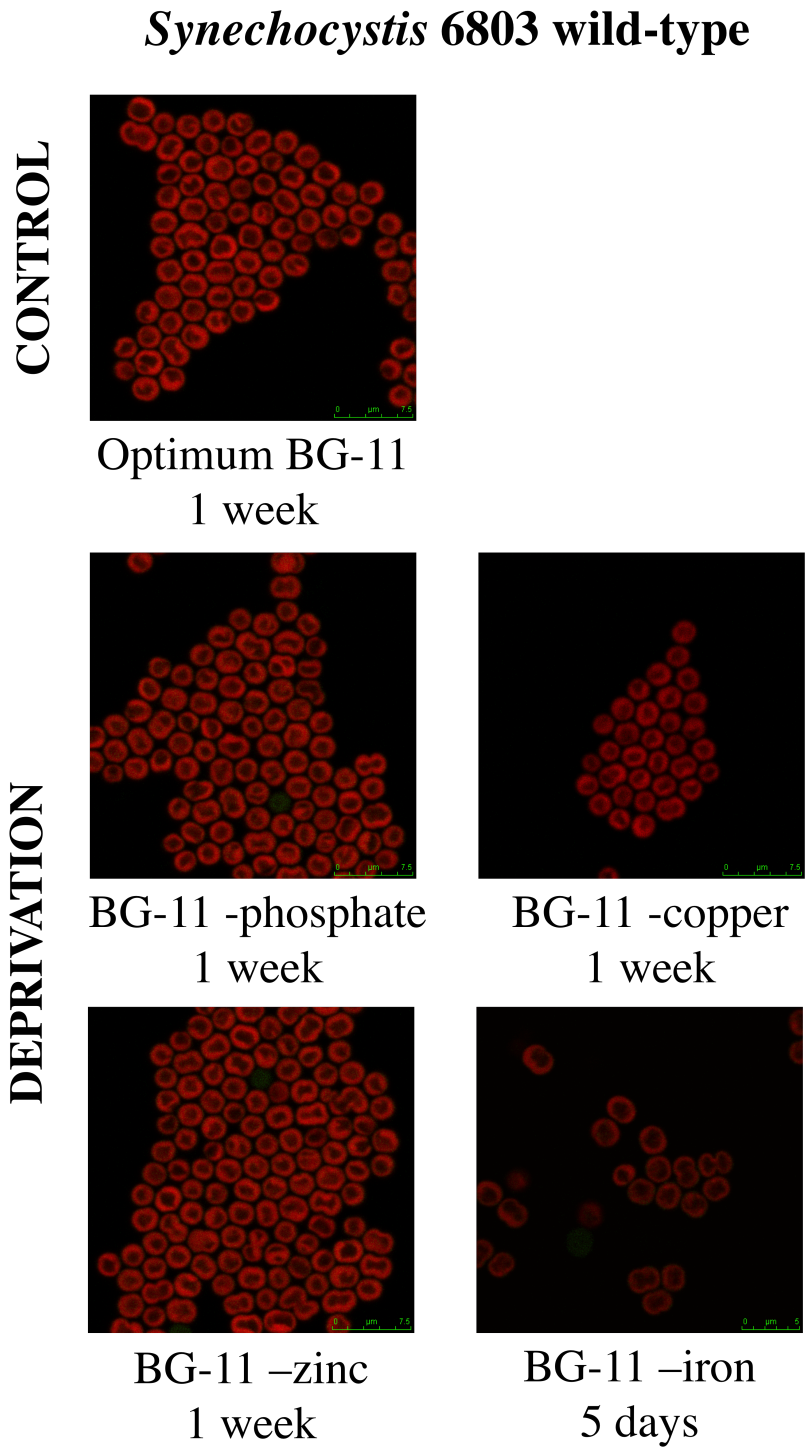

Figure 3.17: **Wild-type under nutrition stress**
Micrographs of *Synechocystis* where red fluorescence comes from chlorophyll.

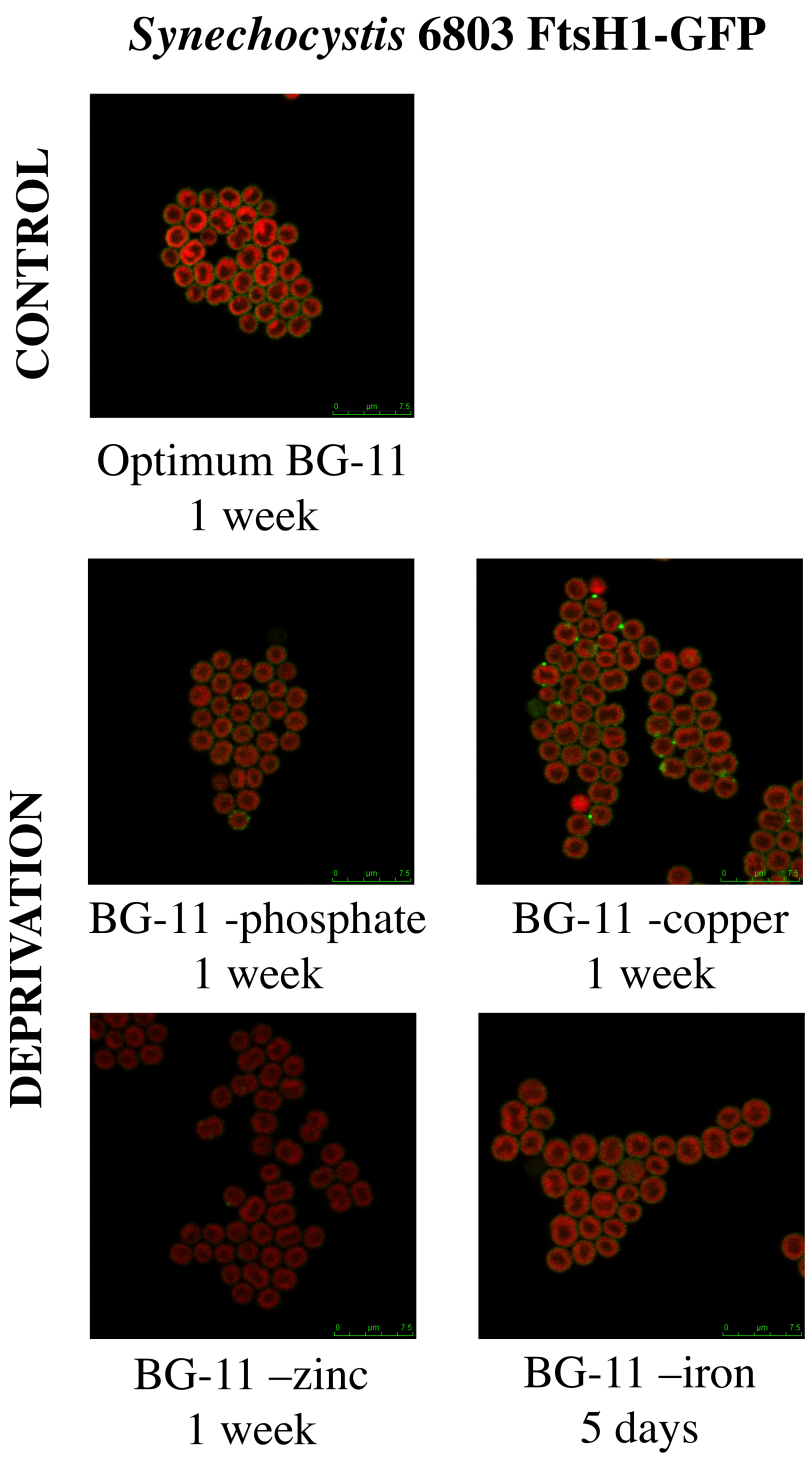

Figure 3.18: **FtsH1-GFP under nutrition stress**
Micrographs of *Synechocystis* where red fluorescence comes from chlorophyll.

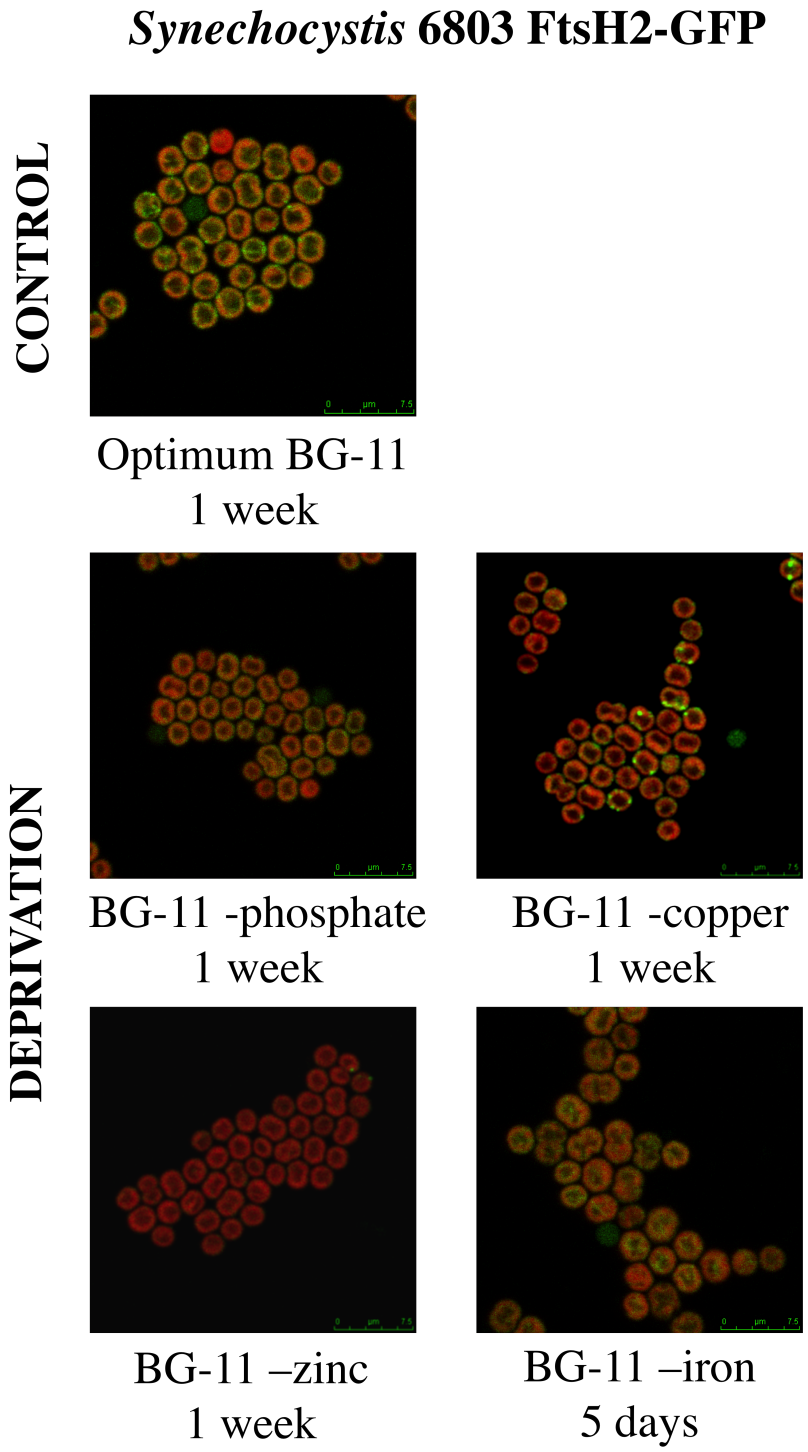

Figure 3.19: **FtsH2-GFP under nutrition stress**
Micrographs of *Synechocystis* where red fluorescence comes from chlorophyll, green - GFP signal.

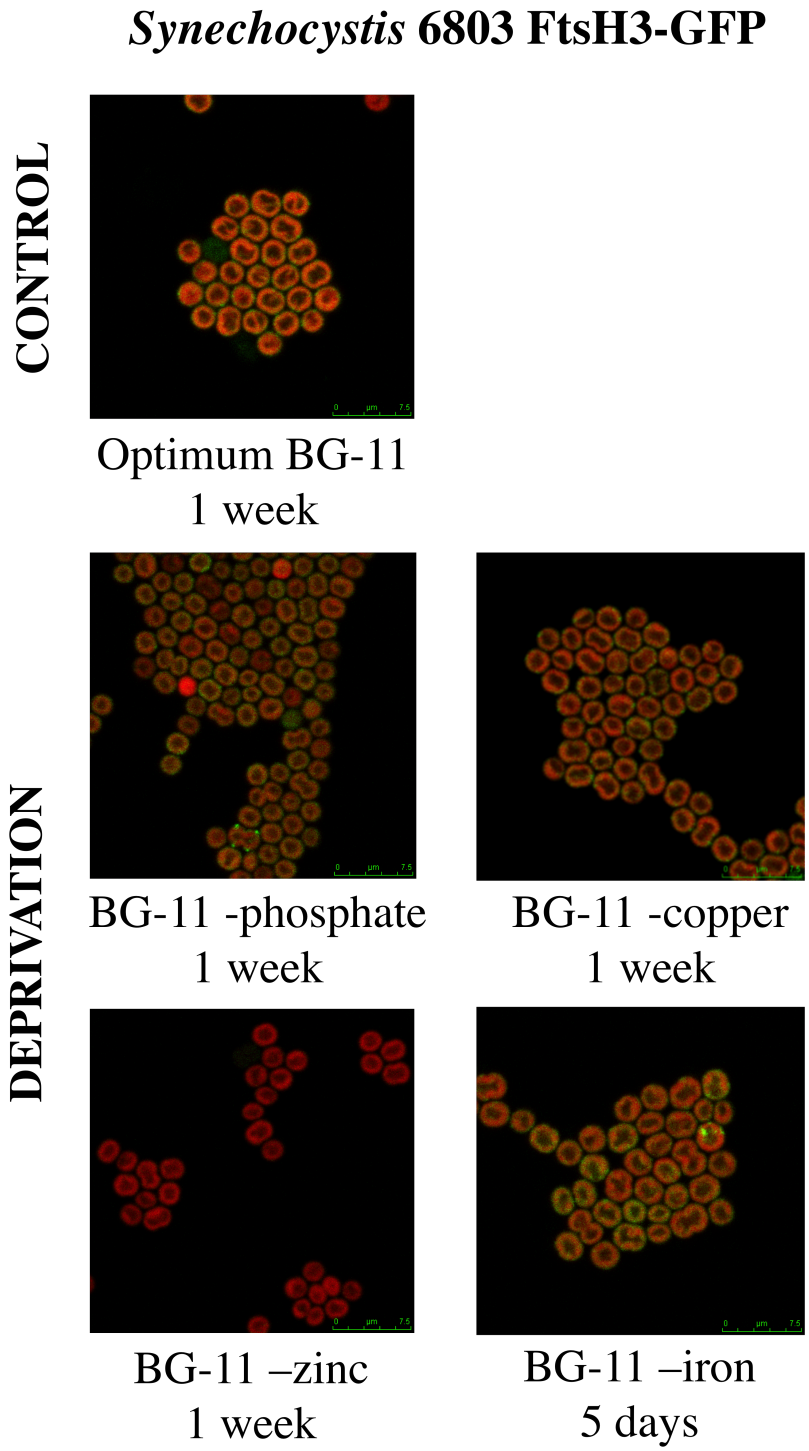

Figure 3.20: **FtsH3-GFP under nutrition stress**
Micrographs of *Synechocystis* where red fluorescence comes from chlorophyll, green - GFP signal.

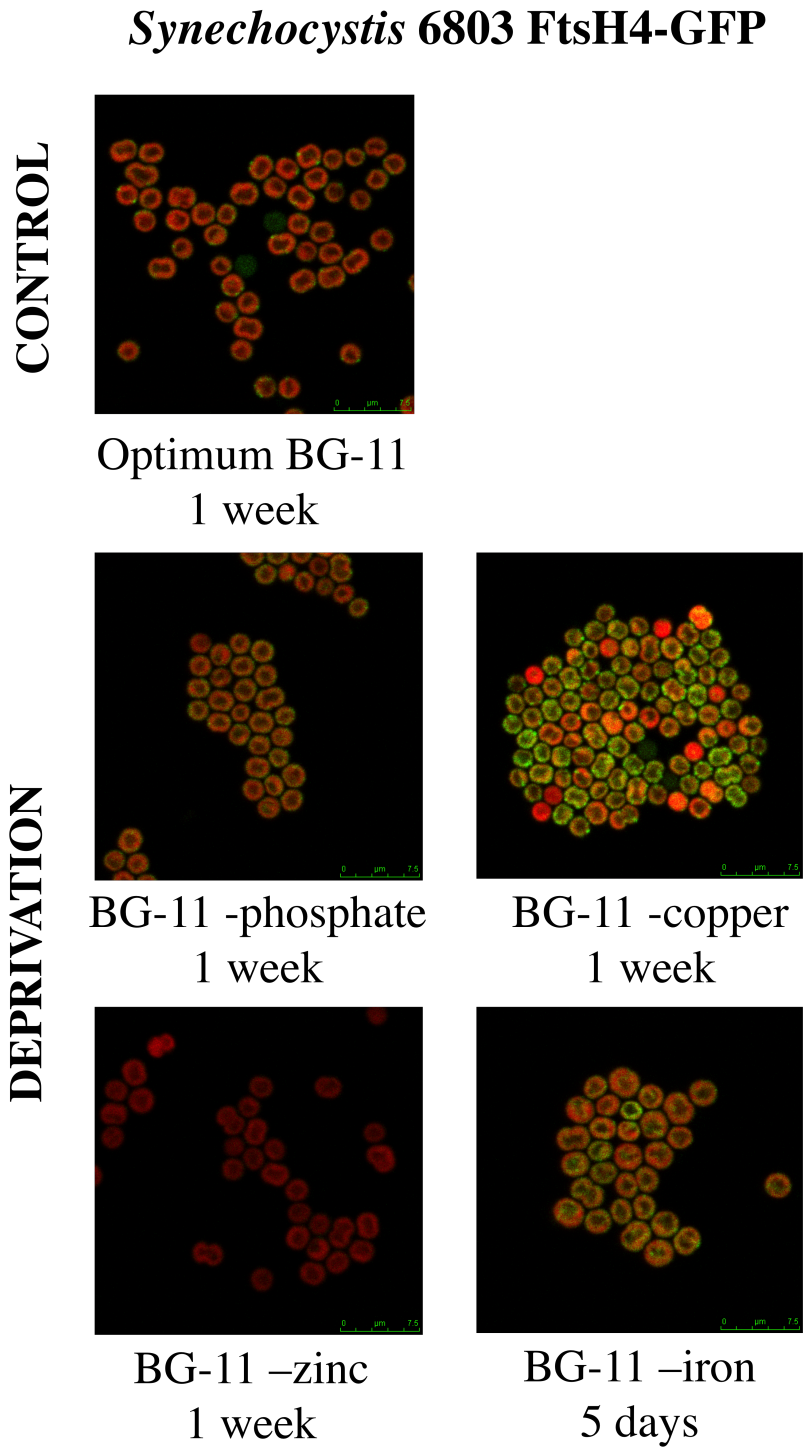

Figure 3.21: **FtsH4-GFP under nutrition stress**
Micrographs of *Synechocystis* where red fluorescence comes from chlorophyll, green - GFP signal.

Table 3.2: Corrected Total FtsH-GFP Cell Relative Fluorescence

Strain	Phosphate	Zinc	Copper	Iron
FtsH1-GFP	0.21	0.09	0.88	0.65
FtsH2-GFP	0.28	0.13	0.71	0.86
FtsH3-GFP	0.31	0.13	0.97	1.24
FtsH4-GFP	0.33	0.1	1.68	1.28

$*$- Corrected Total Cell Fluorescence calculated based on equations found in Appendix 2. Values = CTCF (stress condition)/CTCF (Optimum)

Changes in FtsH fluorescence under nutritions stress

Figures 3.17 - 3.21 illustrate chlorophyll and GFP (in FtsH-GFP tagged strains) signals registered in *Synechocystis* cells after nutrient stress. Micrographs in Figure 3.17 show the chlorophyll distribution in thylakoid membranes in wild-type *Synechocystis* cells after growth in media lacking: phosphate, zinc, copper and iron respectively. No significant changes either in level of chlorophyll fluorescence signal or its distribution were registered. In the case of iron, the phenotype started to change after 5 days of its deprivation, cells growth was decreased and cultures became yellow a week after inoculation. Test was therefore performed for 5 consecutive days. Cells deprived of iron were also on average about 15% bigger in diameter (measured along the longer axis) when compared to growth in optimum BG-11 (from average 2.2 μm to 2.65 μm). Thylakoid membranes seemed rather to retain their original shape in all cases.

Table 3.2 contains values of Corrected Total Cell Fluorescence (CTCF, Appendix 2) (in GFP-tagged strains) calculated for all nutrient stress conditions. The values represent the ratio of avarage CTCF in each set stress to

Table 3.3: Pearson's Correlation Coefficient (PCC) and Mander's Overlap Coefficient (MOC)

Strain	**Optimum**	**Phosphate**	**Zinc**	**Copper**	**Iron**
FtsH1-GFP					
PCC	0.575	0.532	0.3	0.648	0.613
MOC1 GFP/chl	0.189	0.176	0.06	0.166	0.23
MOC2 chl/GFP	0.038	0.023	0.011	0.016	0.037
FtsH2-GFP					
PCC	0.783	0.973	0.508	0.851	0.485
MOC1 GFP/chl	0.553	0.595	0.168	0.59	0.327
MOC2 chl/GFP	0.112	0.353	0.004	0.091	0.132
FtsH3-GFP					
PCC	0.805	0.834	0.485	0.8	0.863
MOC1 GFP/chl	0.68	0.39	0.086	0.314	0.73
MOC2 chl/GFP	0.234	0.164	0.01	0.085	0.425
FtsH4-GFP					
PCC	0.858	0.923	0.537	0.817	0.869
MOC1 GFP/chl	0.76	0.607	0.146	0.873	0.574
MOC2 chl/GFP	0.38	0.208	0.019	0.782	0.168

$*$- Pearson's and Manders' coefficients, additional infromation found in Appendix 1.

CTCF calculated in optimum condition, reasoning that the closer to 1, the smaller the difference. Table 3.3 lists values for calculated co-localisation coefficients (Pearson's and Manders', Appendix 1), which indicates the degree of overlap of GFP and chlorophyll channels. Two different Manders' Overlap Coefficients (MOC1 and MOC2) were generated. MOC1 evaluates the fraction of G (Green: GFP) in compartment containing R (Red: chlorophyll) and MOC2 calculates fraction of R in compartment of G. In other words, by providing measures of the fraction of total probe fluorescence that colocalises with the fluorescence of a second probe, MOCs provide an intuitive and direct metric of the signals overlap. Based on information, that the total fluorescence of chlorophyll was constant (CTCF calculations), then MOC2 informs on how much of the total of chlorophyll signal overlaps with signal of GFP, therefore if the latter variable alternates, then MOC2 indicated that either GFP signal has changed, this may be confirmed by CTCF. However if CTCF remains consistent then it may indicate that part of GFP signal has shifted away from chlorophyll.

FtsH1-GFP was found originally in the region of plasma membrane and under all nutrient stresses majority of GFP was registered similarly from in the outside of the thylakoid region. However, according to Table 3.2 and Table 3.3 CTCF for GFP decreased significantly for cells growth in both phosphate and zinc lacking media, respectively to 21% and 9% of original GFP signal in normal condition. For copper and iron deprivation GFP signals decreased slightly to 88% and 65%. For copper starvation, FtsH1-GFP was visible in the plasma membrane but seemed to undergo changes in distribution. Most of GFP signal was visible in bright spots (1-2 per cell) round the cell contour. Both Manders' coefficients indicate that most of

GFP signal did not overlap with chlorophyll. Values were lower for zinc as there was a significant loss in GFP signal overall.

The GFP signal in FtsH2-GFP, similarly to previous observation, diminished when grown in BG-11 without supplementation of phosphate and zinc (28% and 13%). Slight decreases were also observed for copper and iron stress. However, mostly noticeable for the last two conditions, were the changes in the patterns of distributions. The copper starved cells showed GFP fluorescence in bright spots in the thylakoids, these spots seemed to be brighter and less dispersed than patches observed in optimum conditions. Pearson's Correlation Coefficient (PCC) for FtsH2-GFP was in the same range for normal, minus-phosphate and minus-copper conditions but these values were lower for minus-zinc and minus-iron conditons, suggesting that correlation of GFP and chlorophyll channels decreased. In iron deprived cells FtsH2-GFP was visible shifted from the thylakoid membranes into the region of cytoplasm and the pattern seemed more dispersed.

For FtsH3-GFP the changes were rather subtle. FtsH3-GFP in optimal condition is visible in small patches/spots on the edge of the thylakoid and plasma membrane. The abundance is much lower when compared to FtsH2-GFP and FtsH4-GFP. Nutrient stress caused in all cases loss in signal for minus-phosphate and minus-zinc cultivations. However it did not change for copper stress and increased 1.24x for iron deprivation, GFP was visible in both thylakoid/plasma membrane region as well as the thylakoid membranes. PCC remained the same, except for zinc. M1 and M2 were lower for phosphate, copper and zinc and both increased for iron deprivation, suggesting more GFP signal within the thylakoid.

Observations for changes in FtsH4-GFP are most evident. Consistently

without zinc presence of FtsH4-GFP decreased drastically, illustrated by drop in all values: CTCF, PCC, MOC1 and MOC2. Cultivation without phosphate seemed not to have much of an effect on any of these parameters, however data for minus-copper and minus-iron reflectes their impact on this protease. Copper-starved cells have shown an increase in FtsH4-GFP fluorescence of 1.68x, for iron 1.28x. Consistently, MOC1 and MOC2 increased suggesting almost total correletion in overlapping of GFP/chl and chl/GFP. Interestingly, immunoblots did not show any increase in the FtsH4 abundance after iron starvation, neither was any free GFP signal detected. For minus-copper incubated cells FtsH4-GFP signal has been registered, once again (alike for FtsH2-GFP with no iron) towards the cytoplasm region, hence leading to a slight decrease in both MOC1 and MOC2 parameters.

These experiments have not explicitly provided or suggested any new function of FtsH homologues in the *Synechocystis* cells, however they have shown that under some particular conditions FtsH may disperse and move from their patchy locations, which is in contrast to invariant distribution registered under high light.

3.7 What is building up the repair centres?

The patchy clusters of FtsH were present in all light conditions and no dispersal was registered. Such restricted mobility, indicates that FtsH proteases, particularly FtsH2, are confined to the distinct membrane regions, even when highly active. FtsH2 dedicated location is another evidence for lateral heterogeneity of *Synechocystis* thylakoid membranes. Thus, it was proposed to call these FtsH2 patches the PSII *repair centres*.

Knowing that each molecule of GFP represents approximately one molecule of FtsH protease (Figure 3.3), it raises a question of how many of FtsH molecules and what else is building and holding the visible bright patches. Answering the first question was not trivial for this model, however study focused on the latter problem. In order to investigate the structure of *repair centres*, find potential interacting partners, as well as shed some light on what actually holds the patch together, this project exploited a novel and effective way of isolating sub-fractions of thylakoid membranes of *Synechocystis*. The Epitope Tag Isolation technique, previously used mainly for soluble protein-protein interactions analysis (Greaves et al., 2009), has been optimised for cyanobacterial membranes (Materials and Methods 2.6.2). An advantage of this system over the standard purification methods, is that the magnetic field provides a strong force immobilizing complexes of: micro-beads- α-GFP-FtsHx. Importantly membranes are not treated with detergent prior to loading onto the column. However in order to get rid of all nonspecifically bounded these fractions are multiply washed on the column with buffer containing various low concentrations of detergents (1% Igepal CA-630 (NP-40), 0.5% sodium deoxycholate, 0.1% SDS). This re-

sulted in isolation not only the interacting proteins but also, most evidently, small-scale membrane fragments. SDS-PAGE separation visualised via silver staining reveals presence of proteins other than tagged FtsH, in the elution fractions (Figure 3.22) and very little material found in the elution of wild-type control. The polypeptide profile of the bound fraction is significantly different from that of the crude membrane preparation (Fig. 3.22). In addition, the alteration of composition in different light conditions implies this might be a neat approach to monitor content and changes in functions of protein complexes (Fig. 3.23).

Proteins associated with repair centres

Figures 3.22 and 3.23 show the immunoblots for identification of proteins associated within close proximity to FtsH2. It is shown that bound material included FtsH2-GFP as expected, corresponding to bands under 100 kDa probed with α-GFP, α-FtsH2 and α-gFtsH. The α-gFtsH antibody indicated the presence of an other not-tagged FtsH homologue. The less abundant band under 30 kDa represents high proportion of D1 protein retained on the column. The purity of isolated thylakoid fractions was tested by probing with α-SbtA antibody (a sodium- dependent bicarbonate transporter), a marker for the plasma membrane (Srivastava *et al.*, 2006). To further characterise bound fractions, in particular to assess information on differences in polypeptide profiles in low and high light mass spectrometry was exploited (Table 3.5).

A significant number of key proteins were identified in these micro-membrane domains bounded in the pull-down method. Proteins eluted from the col-

umn from crude membranes of wild-type were treated as negative control for non-specific background contamination. Therefore single protein of CcmM (Carbon dioxide concentrating mechanism protein) identified in these samples was treated as contamination if found bound on the column from FtsH2-GFP strain.

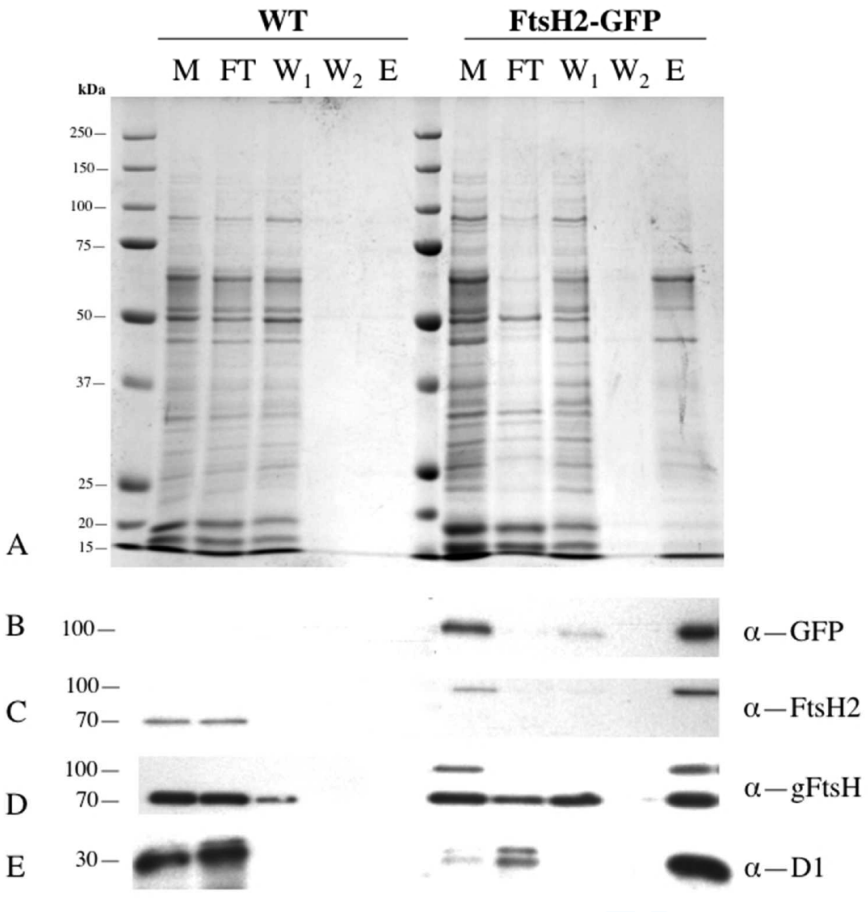

Figure 3.22: **Optimisation of pull-down assay**
Use of anti-GFP pull-downs to isolate a thylakoid membrane fraction from low-light *Synechocystis* ftsH2-gfp cells. (A.) Silver-stained SDS-PAGE gel for membrane fractions from wild-type and ftsH2-gfp. M: crude membrane preparation (material containing 0.1 nmol chlorophyll loaded per lane); FT: flow-through (i.e. unbound material) from the column; W1, W2: first and second column washes; E: final elute of bound material. Each of lanes FT, W1, W2, and E contains the appropriate fraction from material containing 0.2 nmol chlorophyll loaded onto the column. (B-E) immunoblots with antibodies against GFP (B); FtsH2 (C); FtsH (global) (D); D1 protein of PSII (E).

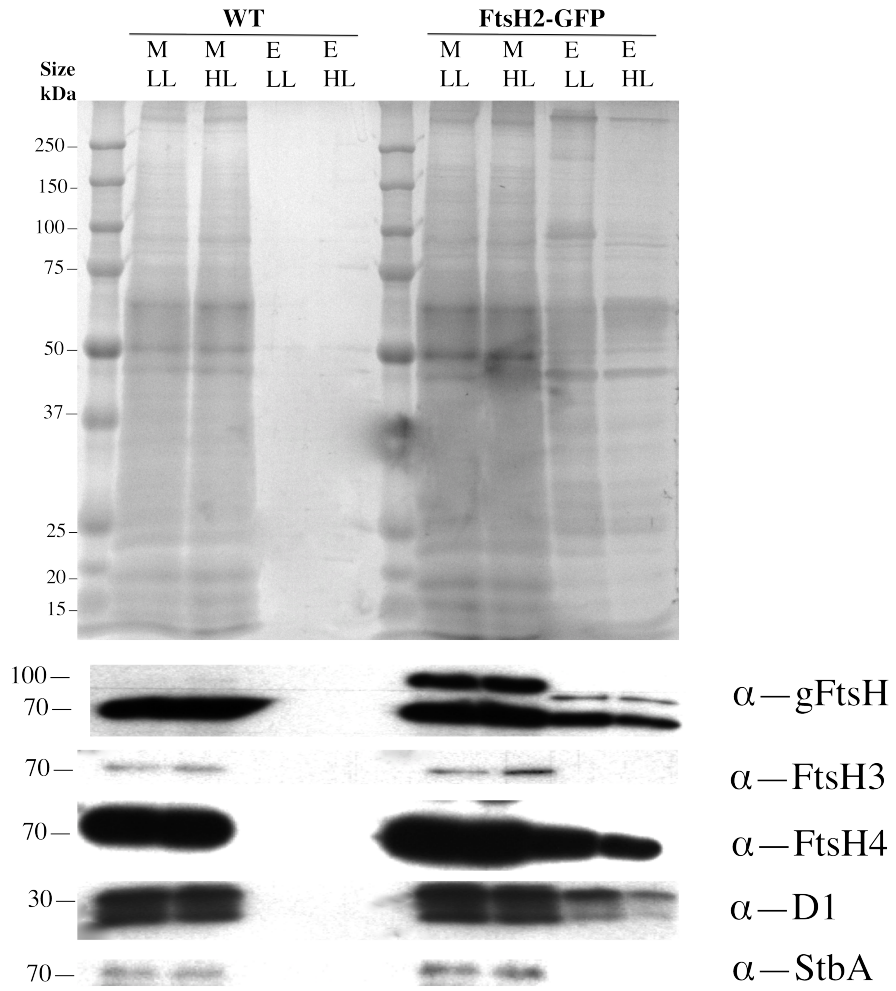

Figure 3.23: **Protein bound in pull-down in low and high light**
Effects of high-light pre-treatment on anti-GFP pull-downs from membranes of Synechocystis ftsH2-gfp cells (wild-type cells used as control). M: crude membrane fraction (sample containing 0.1 nmol chlorophyll loaded per lane); E: final elute of bound material, each lane containing the bound fraction from material containing 0.2 nmol chlorophyll loaded onto the column. Silver-stained gel and immunoblots with antibodies to global FtsH, FtsH3, FtsH4, D1 and the plasma membrane marker StbA. (Srivastava *et al.*, 2006).

Retained proteins of FtsH2-GFP identified via mass spectrometry were divided into six groups with most abundant associated to (i) Photosystem I

and (ii) Photosystem II. Five subunits of PSI were found in association with repair centres (psaC, psaI, psaE and psaL) and another five main subunits of PSII Reaction Centre were distinguished in low light (CP43, CP47, psbH, psbE, D1), (iii) three subunits building up the ATPase complex, (iv) FtsH2 and its FtsH4 homologue and additionally (v) isiA (iron stress-induced protein), two never associated with FtsH2 (vi) spcA and slr gene product. The latter member of Band 7 stomatin-like protein was reported to be important for survival of *Synechocystis* under high light and is a potential interaction partner for the HLIP proteins that stabilise PSI trimers (Wang *et al.*, 2008). In comparison, a group of proteins bound from membrane of FtsH2-GFP after high light, identified five proteins (i) a subunit of PSI (psaI), with (ii) CP43, CP47, D1 and absent in low light D2, however none of other proteins of (iii) ATPase subunits or (iv) FtsH4 homologue and (v) isiA protein were found in this fraction.

Table 3.4: Protein identification via Mass Spectrometry

ORF	Protein	Protein Role	FtsH2-GFP LL	FtsH2-GFP HL	WT LL
slr0335	ApcE	Phycobiliprotein ApcE	+	-	+
slr1311	CcmM	Carbon dioxide concentrating mechanism protein	+	-	+
slr0012	RbcL	Ribulose bisphosphate carboxylase large chain	-	-	+
slr1834	PsaA	Photosystem I P700 chlorophyll a apoprotein A1	+	+	-
slr1835	PsaB	Photosystem I P700 chlorophyll a apoprotein A2	+	+	+
ssl0563	PsaC	Photosystem I iron-sulfur center OS	+	-	-
smr0004	PsaI	Photosystem I reaction center subunit II	+	+	-
ssr2831	PsaE	Photosystem I reaction centre subuunit IV	+	-	-
slr1655	PsaL	Photosystem I reaction centre subuunit XI	+	+	-
sll0851	CP43	Photosystem II 44 kDa reaction center protein	+	+	-
slr0906	CP47	Photosystem II CP47 chlorophyll apoprotein	+	+	-
ssl2598	psbH	Photosystem II reaction center protein H	+	-	-
ssr3451	psbE	Cytochrome b559 subunit alpha	+	-	-
sll0849	psbD	Photosystem II D2 protein	-	+	-
slr1311	PsbA2	Photosystem Q(B) protein (D1)	+	+	-
slr1326	AtpA	ATP synthesis subunit alpha	+	-	-
slr1329	AtpB	ATP synthesis subunit beta	+	-	-
slr1327	AtpC	ATP synthesis subunit gamma chain	+	-	-
slr0228	FtsH2	ATP-dependent zinc metalloprotease FtsH2	+	+	-
sll1463	FtsH4	ATP-dependent zinc metalloprotease FtsH4	+	-	-
sll0247	IsiA	Iron stress-insuced chlorophyll-binding protein	+	-	-
sll1578	cpcA	C-phycocyanin α chain	+	-	-
slr1128	hypothetical	Protein of Band 7, stomatin homolog	+	-	-

MALDI TOF LS-MS. 10 precursor ions, minimum signal-to-noise ratio = 50

3.8 Conclusions and future work

In summary, four mutants have been generated in *Synechocystis* sp. PCC 6803, each expressing functional GFP-tagged FtsH protease. This study showed that GFP did not disturb their function, with exception to FtsH4-GFP whose function is unclear.

Sub-cellular localisation *in vivo* showed that all FtsH homologues in low light are localised to the specific system of membrane, either plasma (FtsH1, FtsH3) or thylakoid membrane (FtsH2), or periphery of thylakoid in close proximity to cytoplasmic membrane (FtsH3, FtsH4). Previously similar results have been reported based on biochemical studies of membrane separation, as well as experiments *in vitro* (Pisavera *et al.*, 2006; Boehm *et al.*, 2012). It has been confirmed here that all four proteases do not evenly occupy cyanobacterial membranes but rather are localised into dedicated patches in some cases occupying over 70% of the membrane area. Such segregated protein distributions give yet further evidence for heterogeneity in *Synechocystis* membranes.

High Light experiments revealed that positions of these proteolytic enzymes do not change, even for PSII increased activity (FtsH2). These findings might elucidate that the PSII *repair centres* proposed here most likely play a role of specialised proteolytic garage where proteins of big complexes are degraded.

It has been proposed that variations in protein composition associated to FtsH2-enriched regions might be caused by multiple functions of FtsH2 homologue, which may switch, to focus mainly on PSII repair when illuminated by high light.

Preliminary studies showing the altered distributions of FtsH proteases in nutrient deficiency open a question of what role might FtsH2 and FtsH4 play when triggered by iron stress. However, to address this, other studies must be conducted.

Most importantly these findings support the hypothesis of heterogeneity of thylakoid membranes and existence of micro-compartmentations in *Synechocystis* sp. PCC 6803 as well as non-homogeneous distributions of proteins in the plasma membrane.

Chapter 4

Identification of lipids within FtsH *repair centres*

The aim of this work was to explore the concept of membrane heterogeneity in prokaryotic organisms. Based on results presented in Chapter 3, we postulated that FtsH is only one example of a membrane protein in *Synechocystis* cells showing segregation to localised patches of thylakoid membranes. The literature lists more examples of similar organisation of membrane proteins in prokaryote. Whilst, the phenomenon of *latheral heterogenoity* is well established in eukaryotes, we are still missing solid evidence for prokaryotic models. Notably, the thylakoid membrane heterogeneity is a newly emerging hypothesis, based only on recent *in vivo* studies. Therefore, studying lipid composition associated with FtsH protein complexes may be a good starting point to shed more light on the thylakoid membrane topology.

4.1 Lateral membrane heterogenity in prokaryota

The concept proposed by Singer and Nicolson (1972) on the membranes fluid mosaic structure, described as a two-dimensional oriented solution of integral proteins floating in the viscous phospholipid bilayer solvent is out of date. It has been established that lipids play an important role, not only as the structural matrix holding proteins but their particular compositions indicate that they are indispensable in biogenesis and functional regulation of membrane proteins (Sato 2004).

Recent studies have been paying more attention to the importance of lipids in the thylakoid membranes of oxygenic organisms, these membranes are said to be the most abundant membranes found in nature. Cyanobacterial membranes' lipid composition is unlike that of any other membranes, latter dominated by the phospholipids, while cyanobacterial cells contain mainly uncharged galactolipids (MGDG) and digalactosyldiacylglycerol (DGDG) and minor population of unique sulfolipid, sulfoquinovosyldiacylglycerol (SQDG) and phospholipids (PG) (Figure 4.1, details 1.6.1). Whereas MGDG and DGDG are assigned to perform rather role of scaffolding, PG and SQDG are anionic and often enhance protein-protein interactions to stabilise large membrane complexes. In principal composition of lipids within protein complexes depends on species. PSII structure of *Synechocystis* obtained at 1.9Å resolution in X-ray crystallography showed that 6 MGDG, 3 DGDG, 5 SQDG and 5 PG moleclues are present within the complex. Further studies carried out on mutant with disturbed PG synthesis have shown impaired function of PSII due to its incomplete assembly and loss in stability (Sakurai *et al.,* 2007). Similarly for PSI, its lipid composition was identified by

X-ray crystallography at 2.5Å resolution confirmed further via thin layer chromatography (TLC) combined with gas chromatography. PSI complex derived from *Synechocystis* contains 2 MGDG, one DGDG, one SQDG and two PG molecules per monomer (Kubota *et al.*, 2010). Most information has been obtained based on studies conducted on *T. elongatus*, it has been proposed that one of PG lipids is involved in PSI monomer-monomer interaction as a mutant not expressing PG shows PSI monomer accumulation, whereas other PG stablilises PSI via co-ordination of PsaX to the complex (Domonokos *et al.,* 2004). Other studies identified lipids associated with remaining photosynthetic complexes with the exception of ATP synthase (Jordan *et al.,* 2001; Guskov *et al.,* 2009).

There are many other reports based on other prokaryotic membranes showing evidence of heterogeneous systems with respect to lipid composition and localisation. Membrane proteins, however, often make up nearly half of the weight of the biological envelope. It also has been discussed that lipids are essential for protein assembly and functions in the membranes, for example closely related to this study established by Nowaczyk *et al.*, lipoprotein Pbs27 is part of a preassembled PSII subcomplex that represents a distinct intermediate in the repair cycle of PSII (Nowaczyk, *et al.*, 2006).

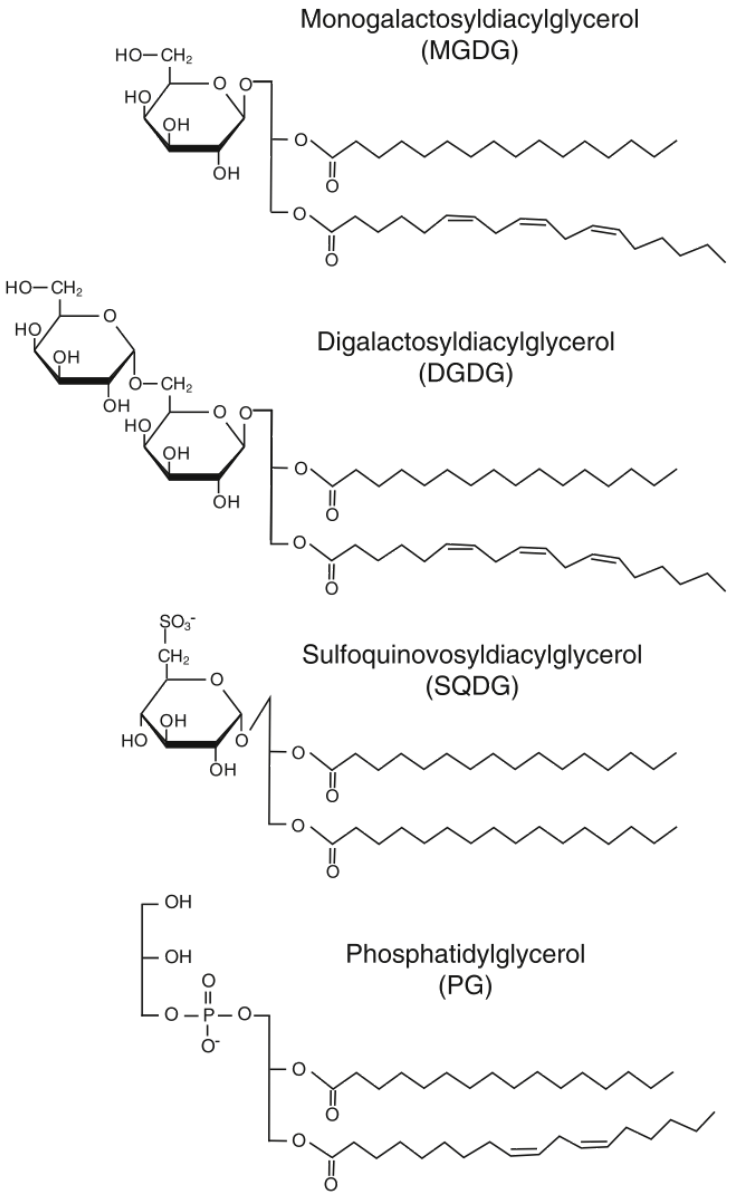

Figure 4.1: **Structures of lipids in thylakoid membranes** Monogalactosyldiacylglycerol (MGDG), diagalactosyldiacylglyceril (DGDG), sulfoquinovosyldiacylglycerol (SQDG), and phosphatidylglycerol (PG). Fatty acids are esterified to the sn-1 and sn-2 positions of the glycerol backbone in each lipid. (Reproduced from Mizusawa and Wada, 2012)

Chapter 3 of this thesis shows four examples of membrane proteins being distributed unevenly in the *Synechocystis* cells. Whilst FtsH1 was registered in small spots in the cytoplasmic membrane, three other FtsH homologues were found in patches/spots within thylakoids. Additionally, recent studies demonstrated similar cases for localised respiratory complexes in another cyanobacterium *Synechococcus* sp. PCC 7942 (Liu *et al.,* 2012). Membrane heterogeneity and protein aggregation into specific zones has been proposed in *E. coli* (Lenn *et al.,* 2008).

In this study, notably unchanged localisation of FtsH2, when moved from low to high light, inspired us to call these localised proteins patches the *repair centres*. We have managed to identify proteins present nearby FtsH2 complex, however the intriguing question of *what holds these patches together* remains. It was therefore a great opportunity for us to collaborate with experts in the field of lipids involved in photosynthesis to identify lipids associated with FtsH *repair centres*. This approach of studying lipids within membrane fractions isolated on small scale allowed for preliminary identification of lipids supporting the structures of specific thylakoid regions, however the small quantities of obtained material were not sufficient for quantitative analysis of bound lipids.

4.2 Strains and experimental procedure

Wild-type 6803, *ftsH2-GFP*, *ftsH3-GFP*, *ftsH4-GFP* tagged strains (engineered in Chapter 3) were used in lipid work.
WT was used for large scale lipid isolation from crude membranes. FtsH-GFP tagged strains were prepared according to methods described in 2.6.2.

Lipids were extracted and analysed according to modified method of Bligh and Dyer (1959) (Details in 2.7).

4.3 Lipid identified associated with FtsH complexes

Table 4.1 presents a percentage proportion of lipids detected in fractions of FtsH-GFP pull downs. Table 4.2 presents the major fatty acids of wild-type and fractions obtained from FtsH-GFP strains.

Sample	Lipid			
	MGDG	DGDG	SQDG	PG
	mol %			
WT membranes	44.3 ± 1.2	21.8 ± 0.8	26.7 ± 1.0	7.2 ± 0.9
FtsH2 LL	8.4 ± 0.97	10.6 ± 1.09	62.7 ± 1.26	18.3 ± 3.9
FtsH2 HL	16.5 ± 2.18	20.2 ± 2.09	10.9 ± 3.3	52.4 ± 4.1
FtsH3 LL	31.5	12.3	19.9	36.3
FtsH3 HL	20.5	14.8	17.7	47
FtsH4 LL	12.1	37.3	16.3	34.3
FtsH4 HL	22.4	18.4	20.1	39.1

Table 4.1
Percentage lipid content identified within FtsH complexes, colours show the most abundant type of lipids found in analysed samples. SD for FtsH2 in LL and HL, n = 5

MGDG	Fatty acid (mol%)										
Sample	14:0	16:0	16:1 (9)	18:0	18:1 (9)	18:1 (11)	18:2 (9,12)	18:3 (6,9,12)	18:3 (9,12,15)	18:4	
TM		**0.25**	**54.13**	**4.65**	**0.19**	**6.74**	**0.1**	**13.28**	**20.38**	**0.15**	**0.32**
FtsH2 LL		5.94	42.99	8.81	11.71	13.04	1.14	5.01	3.57	NA	7.8
FtsH2 HL		9.92	49.12	7.98	19.55	8.49	NA	NA	NA	NA	4.95
FtsH3 LL		12.05	39.06	17.74	13.61	13.74	2.18	NA	NA	NA	1.62
FtsH3 HL		6.79	49.82	8.92	15.4	14.27	NA	1.36	NA	NA	3.44
FtsH4 LL		10.61	46.17	7.75	16.73	13.36	NA	1.42	NA	NA	3.97
FtsH4 HL		23.84	36.88	3.47	19.55	9.31	3.56	NA	NA	NA	3.39

DGDG	Fatty acid (mol%)										
Sample	14:0	16:0	16:1 (9)	18:0	18:1 (9)	18:1 (11)	18:2 (9,12)	18:3 (6,9,12)	18:3 (9,12,15)	18:4	
TM		**0.33**	**53.86**	**5.26**	**0.35**	**3.8**	**0.1**	**10.06**	**25.46**	**0.1**	**0.69**
FtsH2 LL		7.69	43.66	5.86	20.64	10.73	NA	1.95	NA	NA	9.47
FtsH2 HL		7.91	45.53	5.94	19.77	8.82	NA	2.19	NA	NA	9.84
FtsH3 LL		15.38	48.25	5.61	19.46	7.4	NA	NA	NA	NA	3.9
FtsH3 HL		9.78	45.8	6.22	17.9	15.24	NA	NA	NA	NA	5.06
FtsH4 LL		17.78	29.62	10.17	17.47	7.86	7.51	1.59	5.53	NA	2.46
FtsH4 HL		7.4	50.14	6.45	17.57	14	NA	1.79	NA	NA	2.67

SQDG	Fatty acid (mol%)										
Sample	14:0	16:0	16:1 (9)	18:0	18:1 (9)	18:1 (11)	18:2 (9,12)	18:3 (6,9,12)	18:3 (9,12,15)	18:4	
TM		**0.27**	**74.27**	**7.39**	**0.7**	**9.89**	**0.1**	**6.4**	**0.71**	**0.17**	**0.1**
FtsH2 LL		2.09	26.48	27.98	24.45	9.24	3.09	2.65	1.24	0.47	2.31
FtsH2 HL		13.73	56.04	NA	14.61	8.63	NA	NA	NA	NA	6.99
FtsH3 LL		15.88	43.08	8.82	16.95	10.99	NA	1.72	NA	NA	2.57
FtsH3 HL		7.49	49.79	8.27	17.69	12.02	NA	1.83	NA	NA	2.92
FtsH4 LL		7.1	48.89	9.83	15.48	13.44	0.66	1.86	NA	NA	2.73
FtsH4 HL		7.71	45.36	12.58	14.51	14.87	NA	2.01	NA	NA	2.97

PG	Fatty acid (mol%)										
Sample	14:0	16:0	16:1 (9)	18:0	18:1 (9)	18:1 (11)	18:2 (9,12)	18:3 (6,9,12)	18:3 (9,12,15)	18:4	
TM		**0.5**	**55.44**	**3.4**	**0.59**	**10.43**	**0.1**	**25.97**	**1.19**	**2.26**	**0.22**
FtsH2 LL		10.72	47.33	6.57	21.35	7.08	0.4	2.35	NA	NA	4.19
FtsH2 HL		6.86	45.4	3.17	36.3	3.66	0.48	1.02	NA	0.98	2.13
FtsH3 LL		12.68	41.3	9.85	22.94	10.27	NA	1.35	NA	NA	1.6
FtsH3 HL		8.54	43.33	3.03	36.92	5.82	NA	0.65	NA	NA	1.7
FtsH4 LL		9.59	41.04	11.32	22.86	11.42	NA	1.66	NA	NA	2.11
FtsH4 HL		12.4	43.14	9.15	21.37	9.73	NA	1.33	NA	NA	2.89

Table 4.2 Percentage in fatty acid content within FtsH complexes

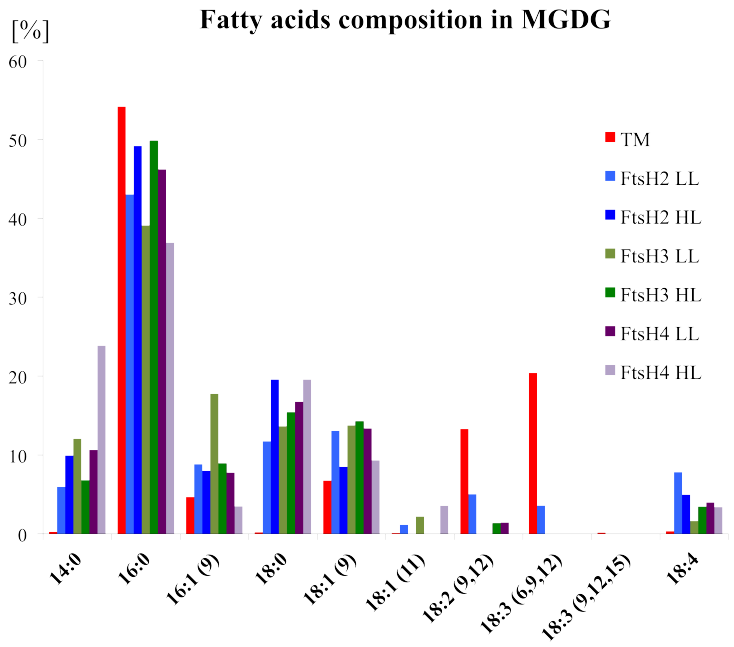

Figure 4.2: **Percentage of fatty acids of MGDG associated with FtsH complexes**

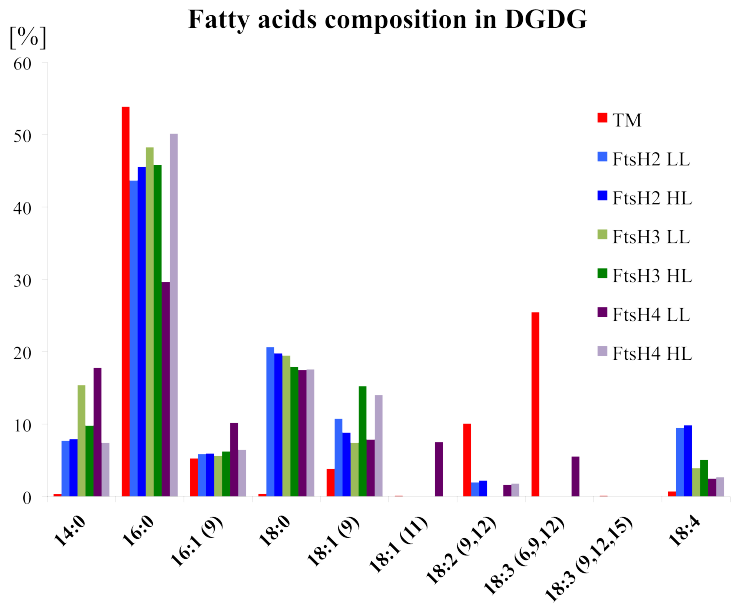

Figure 4.3: **Percentage of fatty acids of DGDG associated with FtsH complexes**

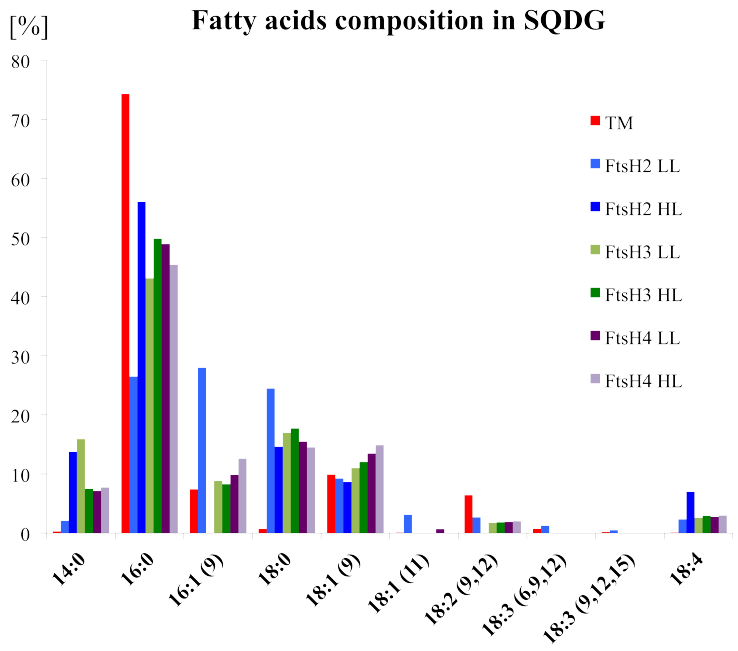

Figure 4.4: **Percentage of fatty acids of SQDG associated with FtsH complexes**

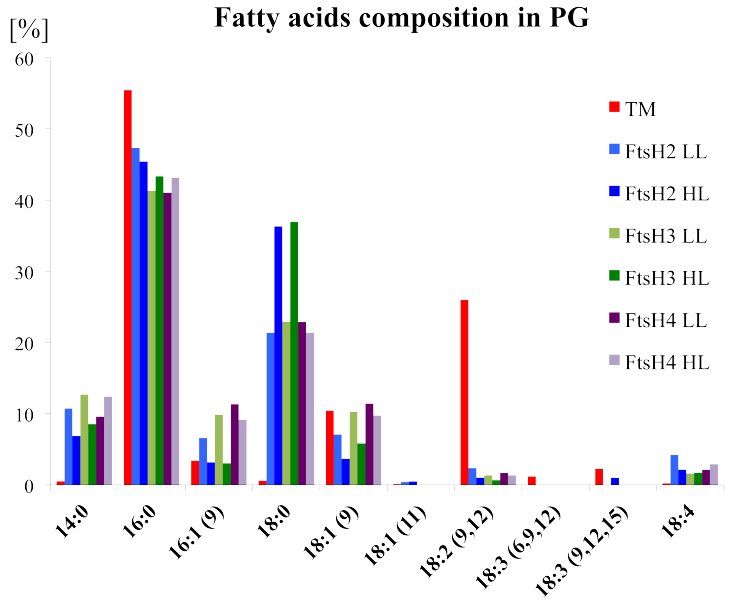

Figure 4.5: **Percentage of fatty acids of PG associated with FtsH complexes**

According to litarature (Sato *et al.*, 1979; Sato, 2004) *Synechocystis* sp. PCC 6803 membranes are made up from four main lipid groups. Top row of Table 4.1 shows the percentage composition of lipids in crude membranes of wild-type 6803 in LL with predominant presence of MGDG (44.3%), followed by DGDG and SQDG constituting for 21.8% and 26.7%, respectively and PG being only a 7.2% fraction of all. Interestingly, in contrast to general lipid composition found in membranes of wild-type, significant number of lipids identified bound to FtsH2-GFP, FtsH3-GFP and FtsH4-GFP belong to the anionic group. PG and SQDG were the most abundant lipids present in isolated membrane fractions, taking up to 80% of the total identified lipids. The lipid content has changed after high light treatement, however for FtsH2 and FtsH3 anionic lipids either SQDG or PG were represented by highest numbers in both light conditions. Remarkable changes in both PG and SQDG contents happened for FtsH2 for two different light condtions. SQDG mostly abundant in FtsH2 in low light decreases 6x after high light treatment, while PG increased nearly 3x. For FtsH4 in low light DGDG constitutes for 37% followed by 34.3% of PG. Membrane fractions isolated from FtsH4-GFP after high light exposure were mostly composed of PG (39.1%). Overall for three cases exposure to high light shifted balance towards PG lipids.

For all four groups of isolated lipids, the relative amounts of fatty acids were calculated by comparing areas under chromatographic peaks with a set of standard data (Appendix 5). Fatty acids of cyanobacteria are mainly unbranched chains containing 14, 16 or 18 carbon atoms and 0, 1, 2, 3 or 4 double bonds (Sato *et al.*, 1979). In contrast to galactolipids (DGDG and MGDG), which include substential amounts of highly unsaturated fatty

acids such as α-linolenic acid [18:3(9,12,15)] or hexadecatrienoic acid [16:3(7,10,13)] cyanobacterial PG and SQDG contain fatty acids with lower levels of unsaturation such as palmitic acid (16:0) (Sato 2004). The most abundant fatty acids identified in the wild-type *Synechocystis* were as follows: 16:0, 18:1(9), 18:2(9,12) and 18(6,9,12) (Table 4.2 and Figures: 4.2-4.5). Both MGDG and DGDG are mostly represented by palmitic acid (16:0) and linolenic acids (18:3). For PG and SQDG 16:0, 18:1 and 18:2 were most predominant. For membranes pulled-down with FtsH both for MGDG and DGDG 16:0 was mostly abundant, followed by 18:0 and 18:1. An interesting trend was observed in all FtsH fractions in low and high light where 14:0 myristic acid made up up to 23% of all fatty acids, however its presence in the total membranes is limited to under 1% in both MGDG and DGDG. The main and significant difference was registered for considerable amounts of highly unsaturated stearidonic acid [18:4], these rich in double bonds chains are very rare in thylakoids and in total do not exceed 0.5%. All FtsH fractions contained 18:4 and in most extreme case for FtsH2 in low and high light it comprised to over 9%. SQDG and PG lipid were mainly found within FtsH complexes and proteins associated with these membrane fractions. Both lipid groups are negatively charged because of their sulfo- and phosphate groups. Percentage composition of fatty acid found in SQDG and PG in wild-type membranes is represented mainly by 16:0, 18:1 and 18:2. For FtsH membrane clusters the ratios vary and are slightly different for each FtsH. SQDG fatty acids of 16:1(9) take up to 27% in FtsH2 low light, similarly 18:0 reaches 24%. However, for high light saturated shorter chain 14:0 (13.73%) as well as poly-unsaturated longer chains 18:4 (6.99%) are significantly higher. FtsH3 and FtsH4 fractions are enriched in 18:0 and

18:4. Identified PG lipids are composed mainly of 14:0, 16:0, while 18:0 contribute up to over 10% of whole fatty acids. Content of 18:2 is however lowered compared to total amounts found in wild-type, on the contrary 18:4 once again was found on significantly high level.

These results may demonstrate that lipid composition associated with isolated FtsH varies within thylakoid membranes depending on proteins associated with. Isolated fragments of thylakoid membranes contain not only specific proteins (Chapter 3) but are enriched or deprived of some type of lipids. Therefore these lipid compositions do not display general lipid composition found in total thylakoid membranes, this indicates that isolation of membranes fragaments is not random and specific lipids may be essential for membrane formation and division of thylakoid membranes into specialised areas. We have also shown that there are slight changes in the composition of lipid classes as well as fatty acids within same proteins after high light treatment. Noteworthy, the lipids types idenitified in membranes fractions derived from FtsH2-GFP and FtsH3-GFP vary. It may suggest that these two proteins may not exclusively be present in hetero-oligomeric FtsH2/FtsH3 complexes.

4.4 Conclusions

For long time studying membrane proteins was the major way of studying membrane properties. The S-N (Singer and Nicolson) theory of lipid embedding floating proteins in the cellular bilayer is too simplistic and it has been shown that localisations of lipid and proteins in membranes are not random, instead various specialised membrane areas are present in

many organisms. It has been also repeatedly reported that lipids do not constitute exclusively the matrix for proteins, they play role in proteins' assembly into the membrane, stabilisation of protein complexes, membrane transport, cellular signalling and often divide membrane into speficic areas called in eukaryota: lipid rafts without equivalent name in bacteria, might be described as: microdomians. Therefore, analysis of lipid composition within protein complexes and their spatial distribution is important part of looking into the membrane structure and its stability. Membrane heterogeneity is not exclusively the merit of proteins but rather a consequence of close and mutual protein-lipid interactions. If lipids building up such structures are removed, then these are not stable and functional in most cases. Importantly, these results reassured that the novel method of membrane isolation resulted in separation of epitope-tagged proteins together with associated lipids. Lipid analysis requires considerable amounts of lipids in tested samples and these fractions did not contain such amounts, however, it was still possible to separate lipids groups into four typical groups found in *Synechocystis*, to further identified them *via* gas spectrometry and calculate the ratio.

Preliminary results on lipid composition found within isolated FtsH-enriched membranes fractions in low and high light may suggest that lipid distributions in cyanbacterial thylakoid membranes are heterogeneous. The ratio of major lipids class found in these membrane fragments is significantly different to lipid percentage content found in total membranes obtained from the wild-type. Particularly interesting was observed increased amounts of anionic lipids SQDG and PG, with the latter being the least abundant lipids in cyanobacterial cells.

Chapter 5

Sub-cellular localisation of ctpA proteases

Work presented in this chapter is in preparation for publication, where the localisation of ctpA protease, one of the PSII assembly factors is shown here *in vivo* in cyanobacterium *Synechocystis* sp. PCC 6803. Various protein localisations suggest that D1 processing and possibly insertion into PSII complex occurs in more than one cellular compartment. Disruption in proteins translation led to visible changes in localisation of ctpA protease, indicating possible changes in regulation of PSII complexes.

5.1 Putative models of PSII assembly and repair. CtpA protease role

Complexes of photosystem I (PSI) and photosystem II (PSII) reaction centres (RC) are housed in the thylakoid membranes of cyanobacteria (Wollman *et al*., 1999). Due to constant damage and frequent recovery of PSII complex, its step-wise re-construction requires many auxiliary assembly factors (Rokka *et al.,* 2005). The total number of PSII complexes is regulated in two manners, by *de novo* synthesis and repair, localisations of these two processes in the cell are still to be revealed. Active PSII complexes are housed in the thylakoid membranes (Gantt 1994; Wollman *et al*., 1999), but their distribution in cyanobacterial membranes is not established with such detail as in plant chloroplasts (Boekema *et al*., 2000; Dekker and Boekema, 2005). Thus the spatial asymmetry in PSII and PSI distributions in cyanobacteria has been reported, (Sherman *et al*., 1994; Vermaas *et al*., 2008, Agarwal *et al*., 2012), yet there is no uniform model. Additionally, attempts at labelling and visualising subunits of PSII reaction centre *in vivo* failed (Bryan, Sacharz, unpublished). Similarly, there is no one consensus on sub-cellular localisation of PSII assembly *de novo*. While some biochemical data has elucidated that initial steps in the process may occur in plasma membrane (PM) (Zak *et al*., 2001; Keren *et al*., 2005), other assigned them to the specialised structures of thylakoid membranes (TM) called thylakoid centres (TC) found in close proximity to PM (Kunkel *et al*., 1982). According to these models pre-PSII complexes must be transferred from PM to TMs via either lateral fusion or mobile vesicles (Nickelsen *et al*., 2011). Compromising these two theories, a new one emerged, as identified

by Schottkowski in *Synechocystis* sp. PCC 6803 an intermediate membrane subfractions (PDM), defined by presence of some of auxiliary PSII factors (Schottkowski *et al*., 2009). Noteworthy, these fractions showed substantial amounts of pD1 protein and PratA binding Mn^{2+}, and therefore named: PratA-defined membrane, now being studied in detail for PSII biosynthesis (Stengel *et al*., 2012). PSII assembly begins with D2 and cyt b_{559} incorporation into the membrane, followed by D1 attachment into such core complex. D1, similarly to many other proteins, is synthesised with cleavable C-terminal extension of unknown function (Anbudurai *et al*., 1994). pD1 in higher plants iso 9 amino acids long (Satoh *et al*., 2007), while for cyanobacteria the extension is 16 amino acids (Diner *et al*., 1988; Zhang *et al*., 2002). Regardless of the length, pD1 must be cleaved before or right after entering the RC (Reaction Centre). It is not clear whether mature or precursor (pD1) form of D1 is used in this early stage, however only shortened D1 is able to annex Mn_4CaO_5 by interacting with manganese binding soluble protein PratA (Schottkowski *et al*., 2009, Stengel *et al*., 2012) and to construct RC, which may bind other PSII subunits (Roose *et al*., 2004). The post-translational modifications of pD1 *Synechocystis* occur in a two-step cleavage. The first close to the middle of the extension at Ala352 residue, results in the first product: intermediate D1 (iD1) (Komenda *et al*., 2007), followed by second cleavage at Ala344 residue. Endoprotease ctpA is considered to play a direct role in this process (Anbudurai *et al*., 1994). Studies on a mutant where gene *slr0008*, encoding ctpA protease, was disturbed (ΔctpA) showed decreased cleavage of pD1, thus pD1 assembly into the PSII was not affected. ΔctpA mutant showed a decreased PSII activity, loss in its stability and increased photoinhibition (Ivleva *et al*., 2000; Kuvikova *et*

al., 2005). It has been also suggested that ctpB homologue of ctpA and other proteases may be involved in this two-step maturation of pD1 (Komenda *et al.*, 2007).

In parallel to synthesis of new PSII complexes, the active PSII pool in the thylakoid membranes is regularly being damaged. Particularly D1 polypeptide is targeted for turnover at unusually high rate (Ohad *et al.*, 1984). Localisation of PSII repair cycle was proposed recently to the specialised thylakoid membrane domains called repair centres enriched in FtsH proteases (Chapter 3). Partial disassembly of PSII to RC47* stage is followed by removal of damaged D1 and replacement with a new functional copy (Komenda *et al.*, 2012; Nixon *et al.*, 2010). Inserted pD1 polypeptide is most likely being processed by ctpA protease, after its assembly into RC, however some hypotheses propose that pD1 cleavage is performed before its insertion and this may happen in proximity to PDMs (Komenda *et al.*, 2012). It is not clear whether the new D1 polypeptides for PSII repair are synthesised and processed in the biogenesis centres or rather close to each active repaired PSII in TM. To address the above, we visualised ctpA protease *in vivo* by labelling it with enhanced green fluorescent protein (eGFP). We observed that, indeed, there are three populations of ctpA proteases in *Synechocystis*, radially distributed in the cell. Central population present in the regions of cytoplasm and at the edge of thylakoid membranes, second in the thylakoid membranes presumably in thylakoid lumen, and another concentrated in distinct puncta outside of thylakoids, towards plasma membrane region. Noteworthy, the ratio of ctpA populations may depend on the process, which is currently in favour: the *de novo* synthesis or repair of the existing PSII.

5.2 CtpA translocation through the membrane

CtpA protease sequence found in *Synechocystis* analysed by prediction algorithms (TatP 1.0 Server) is suspected to be lacking trans-membrane motifs and according to literature is found in the lumenal side of the thylakoid membranes (Shestakov *et al.*, 1994). N-terminal signal peptide (TAT signal in ctpA: MGKRTRRFWALAFSLLMGALIYLGNTPSALAF) is cleaved after the 31st amino acid, after Alanine (A) before phenylalanine (F). The signal peptide sequence contains a characteristic stretch of short hydrophobic amino acids, with the average hydrophobicity: -0.202. Positively charged amino acids at the beginning of the sequence help to enforce its proper topology, according to the positive-inside rule. The 31 amino acid long signal peptide sequence was predicted to form a single alpha-helix. It was therefore important to avoid fusion protein being cleaved before ctpA insertion into the membrane, the GFP was fused at its C-terminal end.

5.3 Mutant engineered for this study

GFP fusion to *slr0008* was generated by use of modified ReDirect method (Gust *et al.*, 2002). *Slr0008* gene was amplified from genomic DNA of *Synechocystis* sp. PCC 6803 with left and right flanking regions, using following primers: F: 5'- CGTTGATGGGGTAATTTTGG - 3', R: 5'- GGTGACGGAACCTTCTTCAA -3' 2.5 kb kb product was cloned into pGEM T-easy vector (PROMEGA) and introduced to *E. coli* strain BW25113, hosting PIJ790 plasmid with λ red system. Two long primers were used to amplify the GFP apramycin cassette flanked by FRT (Flipase Recognition Target) sites

from pIJ786 plasmid (provided by PBL Biomedical Laboratories). A pair of long primers, had at the 5- end 39 nt matching *Synechocystis* sequence either side of but not including the stop codon and a 3- sequence (19 nt or 20 nt) matching the right or left end of the cassette. The product was introduced by electroporation into BW25113, where homologous recombination assisted by PIJ790 results in incorporation of GFP and the 20 nt linker region at the C-terminus *slr0008*. Successful transformants were screened via PCR amplifying 4.7 kbp product (Figure 5.1 and 5.2).

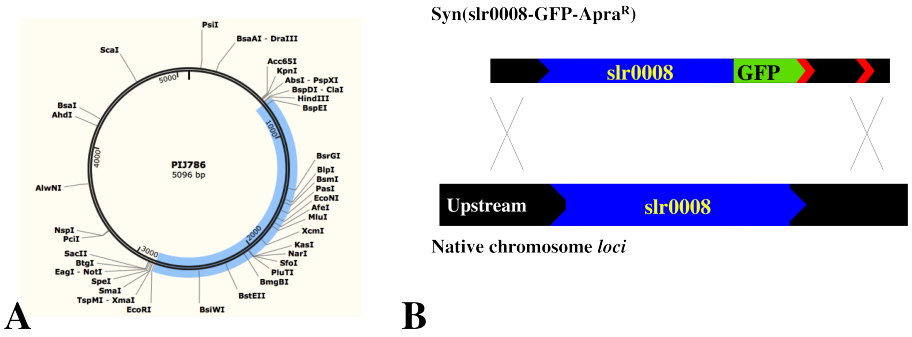

Figure 5.1: **slr0008-GFP construct**
PIJ 786 plasmid used for GFP-Aac(3)IV amplification (Gust 2004) (A), a schematic construction and replacement of native gene *slr0008* by *slr0008-GFP-Apra*^{R} (B).

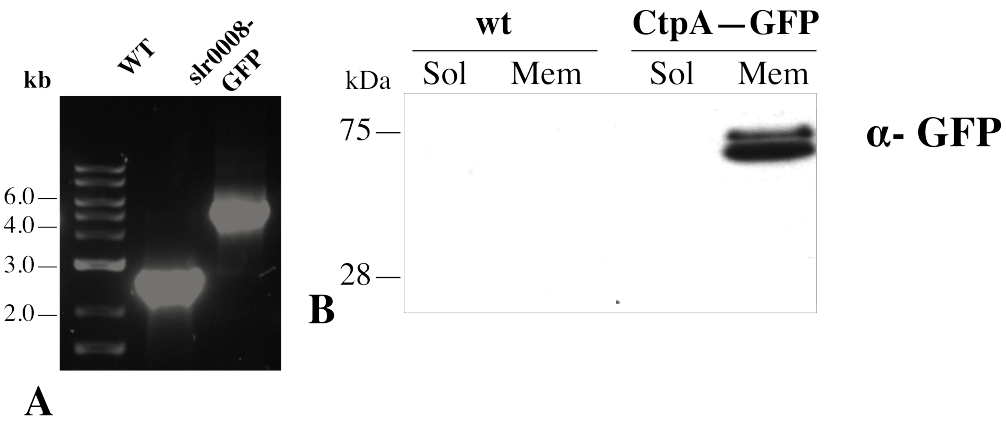

Figure 5.2: **Confirmation of slr0008-GFP construct**
PCR genotyping screen, 2.9 kb product for wt and 4.7 kb where *slr0008* was replaced by *slr0008-GFP* (A), immunoblot analysis. All detected GFP was bound to ctpA at expected size 76 kDa present exclusively in the crude membrane fraction. 1.0 μg of chlorophyll a was loaded per each lane (B).

5.4 Characteristic of *slr0008-GFP* mutant

Genotyping and biochemistry

In order to investigate the sub-cellular localisation of PSII assembly and repair, we engineered a chimeric fusion of GFP to *slr0008* gene in *Synechocystis* sp. PCC 6803. Absence of the wild-type band in *slr0008-gfp* strain, provided evidence of full segregation and replacement of all gene *loci* in all multiple copies of chromosome (Figure 5.2). Enhanced green fluorescent protein (eGFP) was expressed at the C-terminal end of ctpA protein. The fully segregated mutant of ctpA-GFP showed a similar phenotype to the wild-type. The measurement of oxygen-evolving activity is prerequisite for testing PSII activity. Data comparisons for wild-type and *ctpA-GFP* strain in low, high light and with addition of lincomycin, revealed that there were no significant differences (T-test for n = 3 with $p<0.05$) (Figure 5.6). This is in contrast with Δslr0008 mutant, which showed PSII vulnerability to photoinhibition when exposed to higher irradiance (Komenda *et al.*, 2007).

The immunoblots with antibody against GFP showed that all detectable GFP was bound to ctpA proteases and no free GFP was present (Figure 5.2). Interestingly, the GFP signal was detected only from the crude membrane fractions, however ctpA is known as a lumenal protein. This observation might be explained by either ctpA attachment to other membrane proteins (such D1) or membrane preparation of crude membranes from *Synechocystis* is not perfect and results in lumen content retained in the thylakoid membranes. Two bands were recognised by GFP antibody at 75 kDa and just below (74 kDa), the latter might be a consequnece of loss of protein fragment, or protein degradation but the reason for this is unknown.

Unfortunately, lacking specific anti-ctpA antibody, we failed to present that all ctpA is labelled with GFP tag. However, according to genotyping tests all native *slr0008* was replaced with *slr0008-GFP*, if all population leaves ribosomes with GFP tag and there was no free GFP detected in the fractions, then the remaining unknown is the quantification of ctpA in wild-type and GFP labelled strains.

Epitope tag affinity pull-downs have been used to inverstigate potential interactions of ctpA with either pre- or mature form of D1 (pD1, D1) or other proteins. According to immunoblots with anti-D1 anitbody (Figure 5.3), elution fraction obtained in protein pull-down assay from small scale crude membranes of ctpA-GFP strain showed that ctpA-GFP was co-purified with upper D1 band (pD1), when compared to membranes fractions and presence of three bands (pD1, iD1, D1). This may suggest that observed ctpA-GFP localisation may correspond to presence of pD1 either prior to its insertion into PSII complex or just after its assembly before modification.

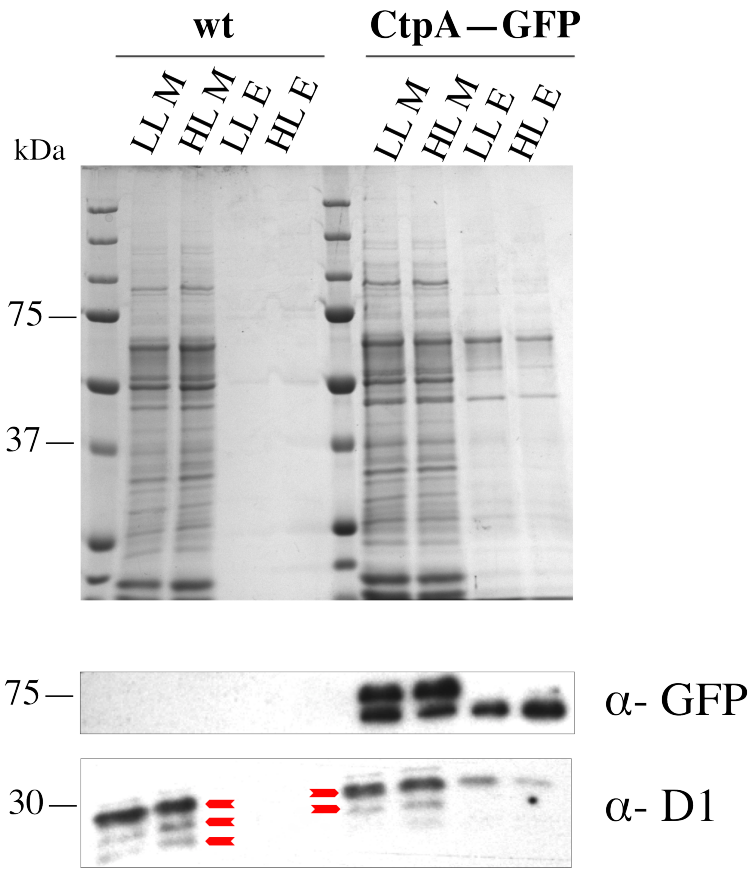

Figure 5.3: **ctpA interactions**
Anti-GFP affinity pull-downs of small scale crude membranes, comparisons of membrane fractions and elution fractions in LL and HL, proteins run on 10% SDS PAGE and visualised by silver staining. Wild-type elution fraction treated as a negative control, probing the elution fractions with antibodies, with band recognised by α-GFP at 76 kDa and just below 75 kDa suggesting cleavage of ctpA protease, and several bands (labelled with red arrows) for three forms of D1 probed with α-D1 antibody.

Biophysical characteristic

Absorption spectra at RT were registered for whole *Synechocystis* cells of wild-type and *ctpA-GFP* strain (Figure 5.4). For measurements of the fluorescence emission spectra at low temperature 77K, whole *Synechocystis* cells were adapted to State 2 by incubation in dark for 5 min prior to recording (Mullineaux, 1990). Figure 5.5 shows the 77K emission spectra for wild-type and *ctpA-GFP* strain recorded for excitation of phycocyanin by 600 nm and chlorophyll by 435 nm. The differences in PS I/PS II stoichiometries between *ctpA-GFP* and WT were minor.

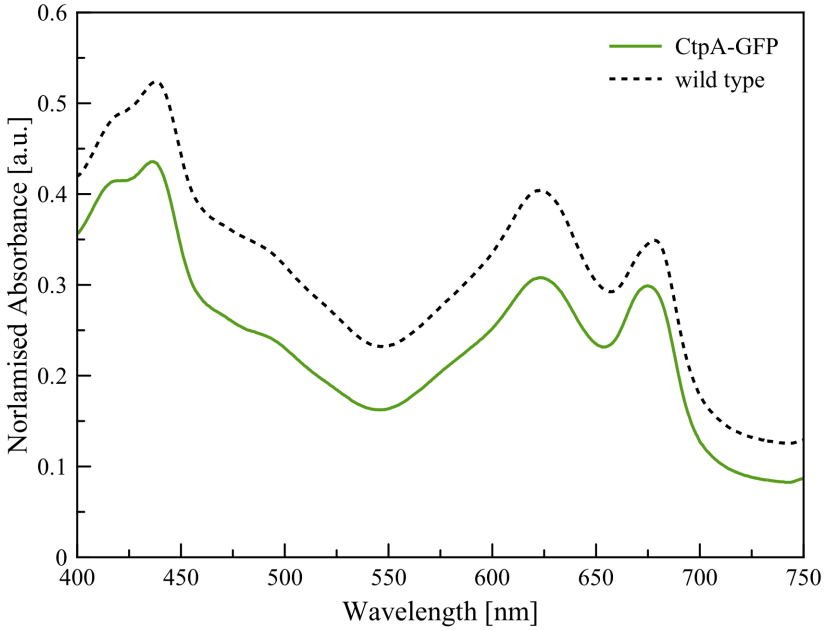

Figure 5.4: **Absorption spectra for ctpA-GFP**
Comparative absorption spectra of whole wild-type *Synechocystis* 6803 cells and *ctpA-GFP* strain. Spectra were recorded in RT using cell suspension of 5 μM chlorophyll concentration, using a split beam mode across 400-750 nm and then normalised to minimum value at 750 nm.

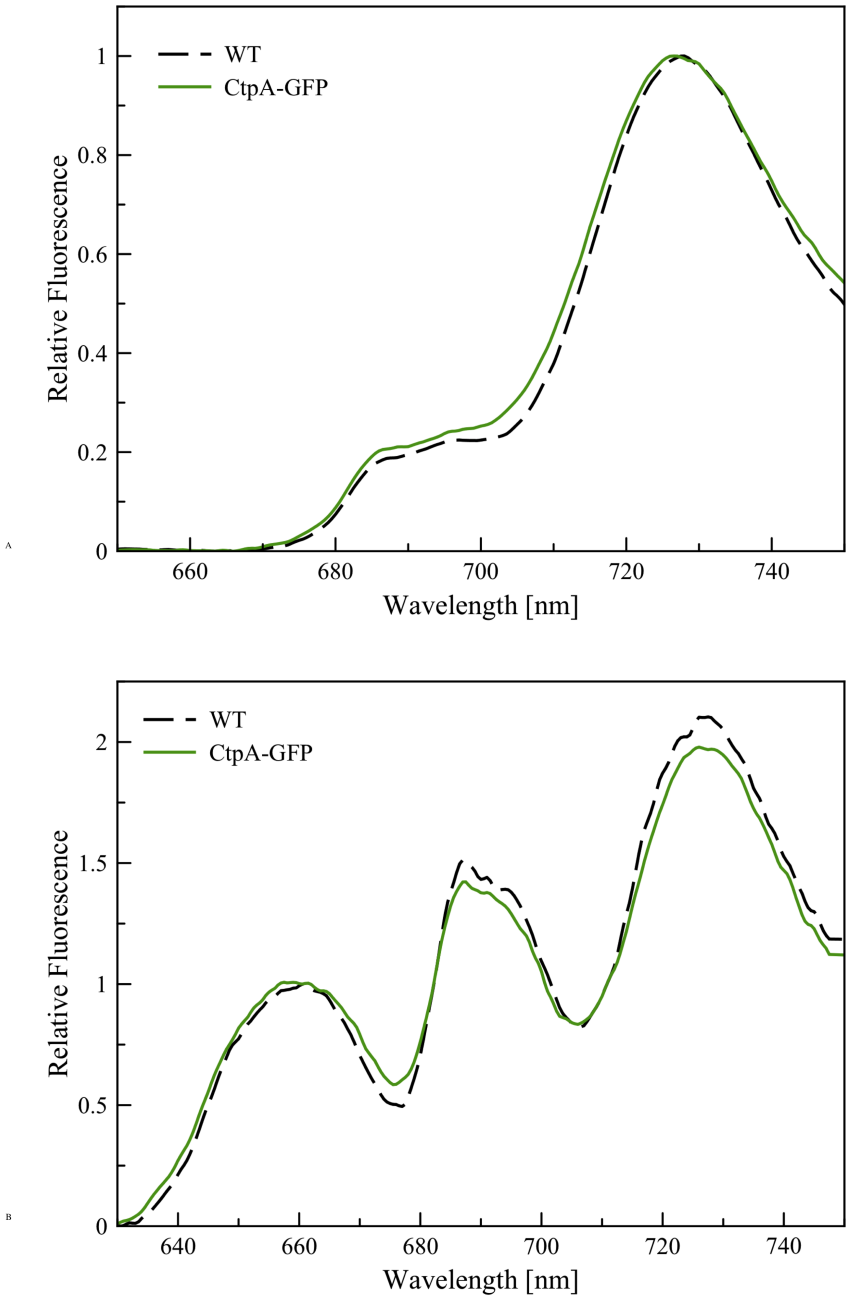

Figure 5.5: **The 77K fluorescence emission for ctpA-GFP strain**
The 77K fluorescence emission for wild-type *Synechocystis* 6803 and *ctpA-GFP* strain. Spectra recorded with excitation at 435 nm normalised to PSI fluorescence peak at 720 nm (A) and 600 nm normalised to the phycocyanin fluorescence peak 654 nm (B) respectively. Cells suspension at concentration of 5 μM chlorophyll were adapted to dark for 5 min prior to freezing and recording the spectra.

Oxygen evolution

Oxygen production was measured in a 30°C chamber by using a Clarke-type oxygen electrode (OxyLab Hansatech, Kings Lynn, UK) with intensity saturating illumination. 1 ml of samples was centrifuged and re-suspended in methanol to determine chlorophyll light absorption measured by spectrophotometer at 666 nm and 750 nm. Formula OD = (OD_{666} - OD_{750}) x 12.63 (Lichtenthaler and Wellburn 1983) was applied to normalise chlorophyll *a* concentration to 10 μM. Each sample (wild-type, GFP mutant) was placed in an air-isolated chamber. The measurements were performed in the presence of an artificial PSII electron acceptor: 1 mM DCBQ and 3 mM potassium ferricyanide, while sample was illuminated with 1000 $\mu E.m^{-2}$ s^{-1} of white light until the oxygen production achieved its maximum. Values at T_1 and T_2 times were registered and used to calculate the oxygen production rates. In order to inhibit translation cell suspensions (wild-type, *ctpA-GFP* mutant), prepared as above, were incubated with lincomycin at a final concentration of 400 $\mu g.ml^{-1}$. All oxygen production measurements were performed 3 times for three biological replicates for cultures grown in LL and following 45–minutes treatment in HL +/- lincomycin. Bar graph (Figure 5.6) was prepared based on averaged values for 3 biological replicates, $p<0.05$ for two tailed T-test. There are no significant differences in all three conditions registered for WT and *ctpA-GFP* strain, indicating that GFP tag did not impact on PSII activity.

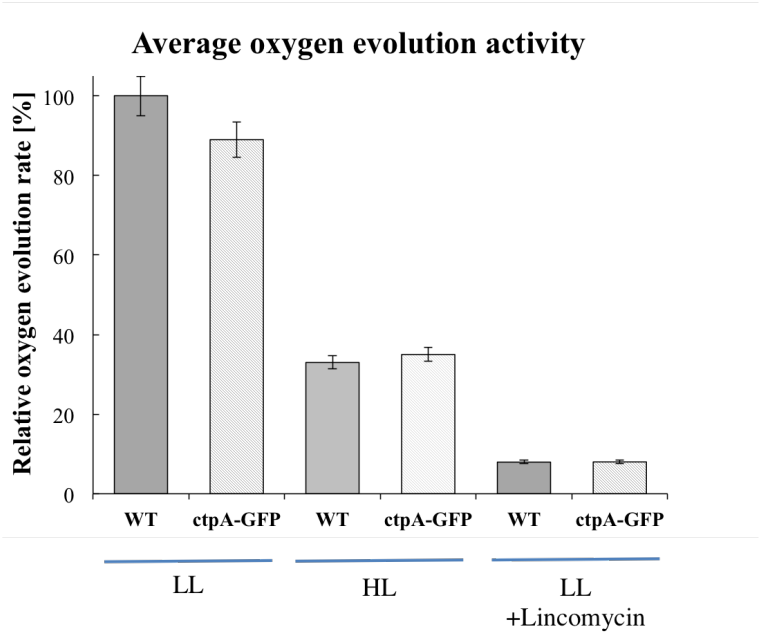

Figure 5.6: **Oxygen evolving activity of ctpA-GFP strain**
Relative oxygen evolution rates (light-saturated and in the presence of PSII electron acceptor) for cell grown in LL and exposed to HL (45-min), the thrid set shows rates for LL and addition of lincomycin (400 μM). Oxygen evolution rates were calculated in units of μmol oxygen mg chlorophyll a^{-1}. h^{-1} and were normalised (100% corresponds to the o_2 evolution rate of WT cells grown in LL, mean = 251 $\pm$11 (n=3)). Two-tailed T-test for n=3, $p<0.05$ indicates that diffrences between WT and *ctpA-GFP* strains are not significant.

5.5 Localisation of ctpA protease *in vivo*

Figure 5.7 shows confocal fluorescence micrographs of *Synechocystis* cells with GFP tag on ctpA. The native chlorophyll fluorescence (shown in red) indicates the distribution of the photosynthetic complexes in the thylakoid membranes (Mullineaux *et al.*, 2002).

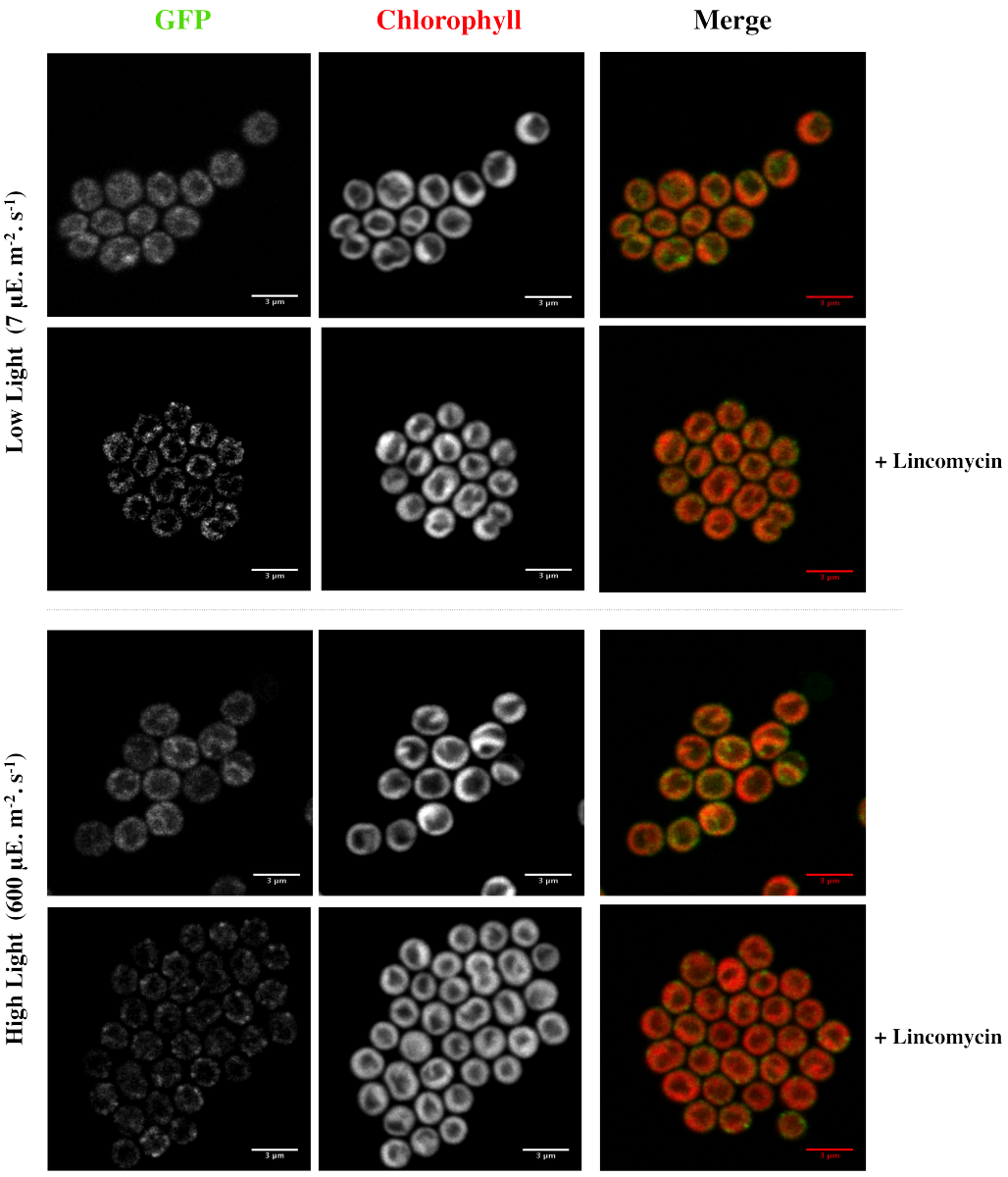

Figure 5.7: **Localisation of ctpA protease**
Micrographs presenting the localisation of ctpA *in vivo* as follows: Low Light (LL) ($7\mu E.m^{-2}.s^{-1}$), LL with addition of lincomycin to final concentration of 400 μM, High Light (HL) 60 min in $600\mu E.m^{-2}.s^{-1}$, HL + lincomycin. First two columns show fluorescent signals in 8–bit grayscale recorded subsequently from GFP and chlorophyll, the third column is a result of merging two channels.

The first two columns of micrographs show two channels in 8–bit grayscale, recorded simultaneously for the chlorophyll, which represents PSI and PSII and therefore marks the thylakoid membranes (Mullineaux *et al*., 2002) and green fluorescence of ctpA-GFP (Figure 5.7). Last column shows images in RGB mode where chlorophyll and GFP channels are merged and yellow indicates where both signals overlap.

CtpA visualised by GFP is not found in exclusively one cell compartment, nor is it evenly distributed in the cell. In low light it is visible predominantly in the central part of the thylakoid, with some extension to the cytosolic side, some spots are visible on the edge of thylakoid/plasma membrane. It is noticeable that these ratios change depending on tested condtions. It was therefore decided to manually divide cells into three cellular compartments regions of : cytoplasm, thylakoids and thylakoid/plasma membrane where ctpA-GFP was visible in accumulated spots (Figure 5.8).

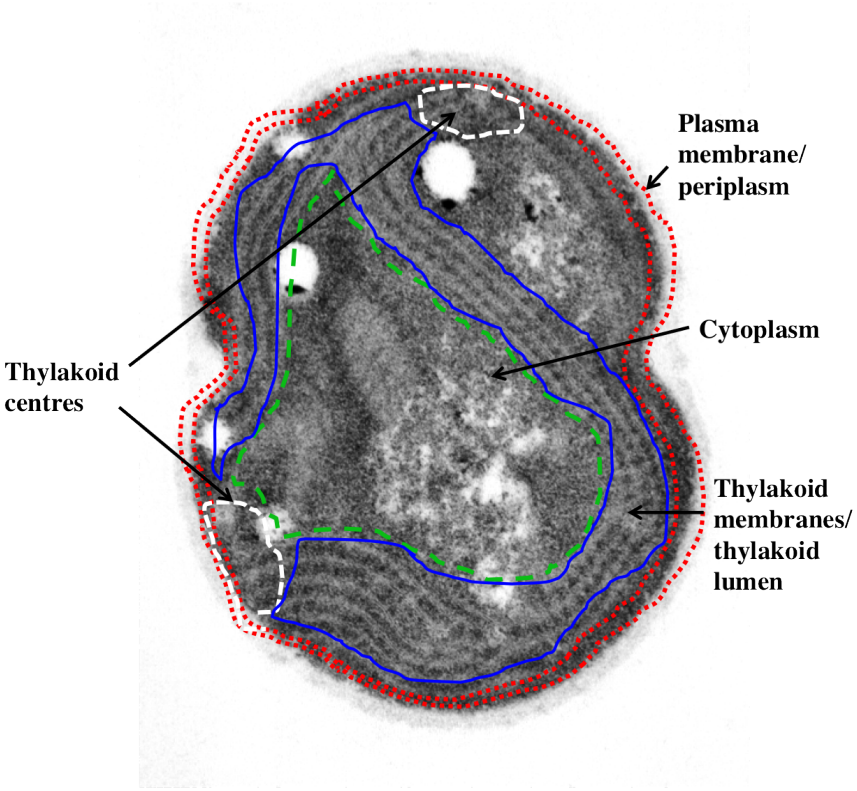

Figure 5.8: **Dividing into cellular regions**
Thin section electron micrograph of *Synechocystis* 6803 cell, (Adapted from Mullineaux). Colour dashed/dotted lines were used to present various cellular regions: red - plasma membrane (PM), white - thylakoid centres, blue - region of thylakoid membranes/lumen, green - cytoplasm.

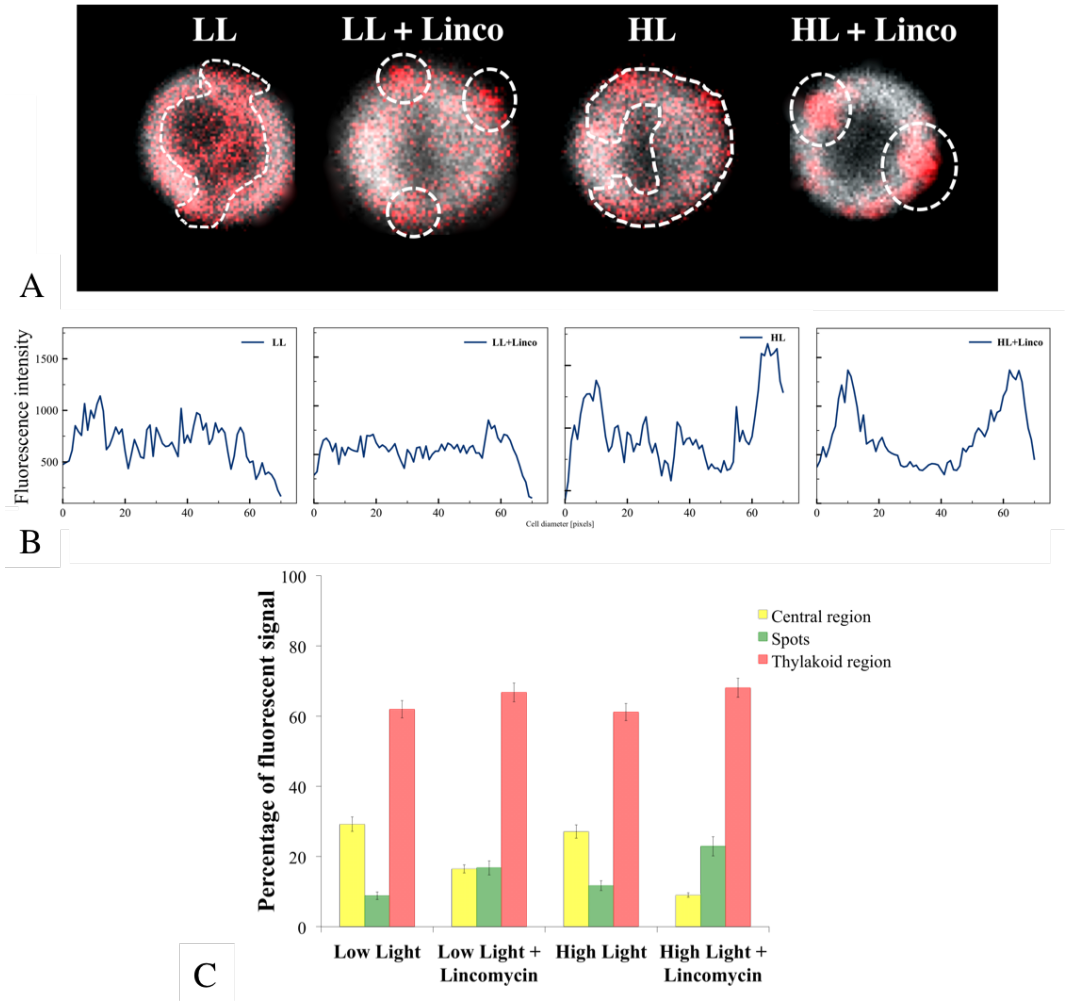

Figure 5.9: **Sub-cellular distribution of ctpA protease**
Cellular localisations of ctpA–GFP in different treatments. Examples of single cells found under different conditions, red LUT used for GFP signal, grayscale (8–bit) signal defines the thylakoid area (A). Averaged plot profile of GFP signal through a single cell from each population (for n=30 cells) (B). Bar graph showing the percentage of GFP signals registered in the regions of: internal cytoplasm, thylakoid and external region thylakoid/plasma membrane (n = 30 cells, three biological replicates) (C).

Table 5.1: Percentage of ctpA-GFP fluorescence across cellular compartments

Cellular region	**Low Light [%]**	**Low Light +Lincomycin [%]**	**High Light [%]**	**High Light +Lincomycin [%]**
PM/TC	9± 1.2	17±2.8	12±2.2	23±3.5
TM/TL	62±3.5	67±3.8	61±3.7	68±4.0
Cytoplasm	29±3.6	16±2.7	27±3.8	9±1.4

Standard Deviation for n=30 across 3 biological replicates

Figure 5.9 outlines ctpA-GFP distribution within a single randomly chosen cell in four tested conditions. Signal from ctpA-GFP is rather low when compared to other proteins visualised in *Synechocystis* (FtsH in Chapter 3), therefore red LUT with grayscale background was used to represent ctpA-GFP and chlorophyll, respectively. Inspection of images in Figure 5.7 suggests that ctpA-GFP distribution is altered when cells were moved from low to high light as well as after treatment with lincomycin. Simple profile plots across cells were prepared to show the inhomogeneity of GFP signal across the cell (Figure 5.9). CtpA-GFP signals from cells in low light show that most of fluorescence comes from thylakoids (62%), however significantly high fluorescent signal was registered for the cytoplasmic region (29%), no global fluorescence peaks appeared suggesting rather disperse distribution. In high light some redistribution in ctpA-GFP localisation was observed. Similar to low light the main fluorescent signal comes from thylakoid region (61%) however formation of ctpA-GFP spots on the periphery of thylakoid can be distinguished and constitutes 12% of total GFP signal. According to profile plots in high light, averaged mean fluorescence across the cell overall increased compared to low light and substantial population of ctpA-GFP in puncta around thylakoids is represented by two fluores-

cence peaks.

To check whether the ctpA redistribution depends on *de novo* protein synthesis, the same experiments in low and high light were carried out in the presence of the protein synthesis inhibitor lincomycin (Chang *et al*., 1965). Such stress caused overall decrease of around 25% in GFP signal compared to low light, confirming that no new ctpA-GFP was expressed and existing proteins might have undergone turnover. Interestingly, for cells treated with lincomycin ctpA redistribution was altered. In low light fluorescence peaks appeared more distinct in the external regions of the thylakoids, on average there were three spotty locations visible per cell, constituting for 17% of ctpA-GFP signal. Most predominant changes appeared for high light followed by treatment with lincomycin, GFP signal registered in the cytoplasmic region decreased 3 times compared to cells low and high light without lincomycin. On the contrary mean fluorescence calculated for sum of puncta round the cell edge increased 2 times (23%). Noteworthy, the spots seen in number of 2-3 per cell doubled their size after lincomycin incubation to 400 nm suggesting that the existing pool of ctpA-GFP may have moved into these locations.

In all conditions ctpA-GFP appeared to occupy at least three cellular locations, however fluorescence ratios varied. In low light ctpA seems to spread equally within the surface of the thylakoid membranes (lumen), with disperse signals registered from areas in close proximity to the cytoplasm and to plasma membrane. While in high light, most of signal registered came from the central part of thylakoid and plasma membrane. Nevertheless, the most drastic changes were registered after addition of linocmycin and illumination under high light, where spotty population of ctpA-GFP in plasma

membrane almost tripled in abundance compared to low light (Table 5.1). It would be interesting to test whether redistribution of ctpA-GFP observed after lincomycin treatment occurs as a result of mobility and shift into specific spotty areas or an effect of increased ctpA turnover in the thylakoid membranes. To test the latter the short-time lapse experiments were employed, however prolonged laser exposure lead to significant irreversible photobleaching of GFP. Therefore testing ctpA mobility in between cell region is still to be revealed.

5.6 Conclusions

In summary, *Synechocystis* strain expressing functional ctpA-GFP was generated and used to reveal sub-cellular localisation of D1-proceeding protease. Our results show the thylakoid lumen to be the main site where ctpA is found in low light. When PSII photodamage accelerates, after high light exposure, ctpA is visible additionally concentrating to the areas on the edge of thylakoid or within plasma membrane. It is an interesting observation as previous putative models suggest pD1 processing happening exclusively in the plasma membrane (Zak *et al.*, 2001). We show here that it is likely that posttranslational modification of pD1 may happen within both membranes. Combining our and previous data, we could hypothesise that the repair of PSII happens in the thylakoid membranes (Chapter 3), and it is coupled with synthesis of pD1 and its assembly into PSII core complexes during the light-activated repair. Additionally, based on previous views and our data, the PSII synthesis *de novo* might be localised to other regions (presumably plamsa membrane) where we observed accumulation of ctpA

protease in treatments with lincomycin. The latter, however needs further verification.

Chapter 6

Discussion and Conclusions

6.1 Non-homogenous distribution of proteins in thylakoid membranes

Based on the visualised localisation of FtsH proteases *in vivo* combined with biochemical data, we establish that all but the FtsH4-GFP homologue of FtsH labelled with GFP are expressed at the physiological level in *Synechocystis* (Chapter 3). Additionally all of FtsH1-3 seem to be fully functional, however FtsH4 function cannot be confirmed, since the *sll1463 null* mutant shows no obvious phenotype (Mann *et al.*, 2000).

This study reveals that FtsH proteases occupy either the plasma membrane (FtsH1, FtsH3) or the thylakoids (FtsH2) (Komenda *et al.*, 2006), or in the case of FtsH3 and FtsH4, where location on the edge of thylakoid may not exclude a minor presence in the cytoplasmic membrane. These findings are in accord with previous studies based on cell fractionation and proteomics (Pisareva *et al.*, 2007) as well as with the recent data on the organisation of

FtsH subunits (Boehm *et al*., 2012). Based on work of Boehm *et al*., and results of this study, it might be assumed that hetero-oligomeric complexes of FtsH1/FtsH3 and FtsH2/FtsH3 are located in regions where FtsH3 signal overlaps with these of FtsH1 and FtsH2.

Observing localisation of proteins *in vivo* allows the monitoring of any changes in distribution of a labeled protein in real time. With improvements of optical resolution, it has become possible to register non-random patterns in which often proteins aggregate within the membranes. Detailed analysis of individual cells shows that in low light all FtsH proteases do not evenly and randomly occupy the membranes but rather stay within specific patchy locations, indicating a tendency to segregate into localised membrane zones. Patterns of these patches differ in size and number for each of FtsH protease. FtsH1 occupies the area of the plasma membrane but in comparison to FutA1-GFP (Spence, not published), which evenly spreads in the periplasmic region it is rather seen in small spots around the periphery of the cell. Similarly to what we observed, it has previously been reported that proteins in the *Synechocystis* plasma membrane are found rather in the non-homogeneous distribution in micro-domains (Pisavera *et al.,* 2011). On the contrary highly expressed FtsH2 and FtsH4 very distinctively mark the region of thylakoids, with relatively large and bright patches of FtsH2-GFP in some cases occupying a significant part of the membrane. Similarly, FtsH4 high expression allowed assigning this homologue exclusively to thylakoids, visible in 2-3 rather peripheral spots per cell. The localisation of FtsH3 was similar but not quite the same and it is likely that these two homologues are not associated together. However, the peripheral distribution of FtsH3 and FtsH4 somehow matches described

previously PSII assembly centres (Schottkowski *et al.*, 2009). It would be interesting to test whether either of FtsH3 or FtsH4 interacts with assembly factors such PratA (Schottkowski *et al.*, 2009).

Dedicated patchy locations in low light indicate that either protease complexes are assigned to specific regions of the *Synechocystis* membranes or accumulate in these while not active. The latter would suggest that after activation FtsH proteases may either leave their primary patch- location in order to perform their function or stay in the zones to perform a role of *protein garage*. However, not many functions of the FtsH proteases in *Synechocystis* are established. Light is one known factor triggering the involvement of FtsH2 in PSII repair. Additionally, as FtsH3 has been reported to be present in FtsH2/FtsH3 hetero-oligomeric complexes (Boehm and Yu, *et al.*, 2012), hence by increasing light intensity, we impact on D1 turnover rate and therefore we should activate both FtsH2 and FtsH3. Nevertheless, high light illumination did not impact on the localisation or distribution of any of the four FtsH's, which remained stable even after 60 minutes of exposure to 600 μE.m^{-2}.s^{-1}.

However, under other stress conditions caused by nutrient deprivation, FtsH homologues have demonstrated different distributions in comparison to both low and high light. In particular, cultivation of *Synechocystis* cells in media lacking copper and iron had a visible impact on all of four homologues. These observations can not be explained in details without further tests but it is posisble that FtsH proteases (for example FtsH1 found in the plasma membrane) might be invoved in the degradation of copper/iron transporters or other proteins associated with metal regulation. Prolonged growth of *Synechocystis* in media lacking these primary

micro-elements might trigger a cellular response, such negative feedback, may lead to increased production of copper/iron metallochaperones which would be sent to the regions of the periplasm and plasma membrane in order to bind these missing metals. Such cascade of events must be eventually followed by protein degradation. We did not test for protein expressions under such conditions. Thus these observation are rather interesting than revealing any potentially new roles of FtsH proteases. These changes, however, demonstrate that FtsH complexes may leave their primary localisations, but such movement does not happen in high light when FtsH2 is activated.

Localised *repair centres* in the thylakoid membranes

As stated, data comparisons of all FtsH patterns in low and high light indicate no clear changes in distribution. Factors other than light may be activating FtsH1 and FtsH4, unfortunately functions of those proteases are not yet described. Yet, in the case of FtsH2, light is the obvious trigger. Stressing the importance of both homologues' functions and showing their immobile patchy locations in response to high light, we propose here to call the visible patching zones (Figure 3.16): *repair centres*, where D1 and possibly other proteins (Komenda *et al.*, 2006) are being degraded. Based on *in vivo* visualisation and other studies (Boehm *et al.*, 2012) we expect that proposed *repair centres* may include FtsH3, however the membrane occupation of FtsH2 and FtsH3 within the thylakoid varies and in this study no FtsH3 was detected bound in the pull-down tests on FtsH2-GFP. We therefore set to identify what other proteins are associated with *repair centres* (Chapter 3). According to some unpublished sources and verbal communications (Prof. Nixon, Imperial College, London) FtsH2 is suspected

to perform a role of membrane scaffolding to support hetero-oligomeric complex of FtsH2/FtsH3 and possibly other associated proteins (Boehm *et al.,* 2012). This study used a different way of pulling-down proteins which aimed to isolate fragments of thylakoid membranes. The plan was to separate membrane fragments corresponding to FtsH2-enriched thylakoid membranes zones observed *in vivo*. This method does not involve treating membranes with any detergent before loading on the column. Therefore fractions bound on the magnetic column in theory should contain mixure of proteins and lipids. Further steps involved using a mixture of low concentration of detergents: 1% Igepal CA-630 (NP-40), 0.5% sodium deoxycholate and 0.1% SDS to wash off random proteins and lipids. The method was good enough to isolate distinctive membrane protein clusters only from *ftsh2-gfp* cells but not from wild-type control, indicating that isolation happened as a consequence of direct and indirect association with FtsH2-GFP. The membrane fractions included numerous thylakoid membrane components, but did not contain the cytoplasmic membrane marker SbtA (Norling *et al.,* 1998) at detectable levels. It resulted in co-purification of other proteins most likely present nearby the *repair centres*. Using a group of available antibodies some obvious and expected proteins were identified including: FtsH2-GFP, GFP and D1. Identification of proteins via mass spectrometry shed more light on composition of the micro-membrane domains enriched in FtsH2 (Table 3.1). In low light proteins associated and co-purified with FtsH2-GFP are derived mainly from PSII and PSI system, as well as the ATPase complex. It is clear that FtsH2 homologue is involved in PSI biogenesis (Mann *et al.,* 2000), hence subunits psaC, psaI, psaE and psaL. Presence of D1 together with CP43 and CP47 might be a

result of FtsH2 role in PSII partial disassembly and D1 degradation (Silva *et al.*, 2003). In addition to photosynthetic proteins and FtsH2 itself, FtsH4, IsiA and Slr1128 were detected. Slr1128 is a Band 7 stomatin-like protein reported to be important for survival of *Synechocystis* under high light and to potentially interact with HLIP protein and stabilise PSI trimers in order to protect cell under high light (Wang *et al.*, 2008). IsiA the iron stress induced protein was co-purified, it has not been reported to interact with FtsH2 itself, however experiments with iron deprivation show that FtsH2 undergoes redistribution when under such stress (Chapter 3). The lack of FtsH3 present within isolated FtsH2-bound fragments was the main discrepancy to results obtained in FtsH structural studies by Boehm and collegues. However, if the protein levels of FtsH2 and FtsH3 are compared in wild-type and GST-tagged strains (Boehm *et al.*, 2012) as well as GFP level *in vivo* (Chapter 3), it is rather apparent that FtsH2 is more abundant. It is possible that smaller patches or big patches of FtsH2 overlap to some extend with FtsH3 spots, the latter often seen on the periphery of thylakoid. It can not be ruled out that FtsH2 might be also present as a homocomplex and our protein isolation method results in separation of FtsH2 homocomplexes rather than less abundant FtsH2/FtsH3 complexes. It is worth consideration that GFP tag on FtsH2 may impact on FtsH2/FtsH3 complex formation and stability.

It also appears that the population of photosynthetic membrane proteins in proximity to FtsH2 changes according to light intensity. High light treatment resulted in loss of proteins bound on the column, with a higher proportion of the core components of the photosynthetic reaction centres present when repair cycle is active. Such changes in protein content around *repair*

centres under high light may suggest dissociation of proteins from the complex and may indicate that FtsH2 plays multiple roles and switches on/off its activity according to particular stress.

Repair centres distanced from PSII

Chlorophyll fluorescence indicates mostly PSII distribution, which appears to be even in the thylakoid membrane. The present model of FtsH2 D1 degradation pictures at least one FtsH complex in proximity to PSII, suggesting that in either low or high light, FtsH2 would be found in the entire thylakoid space (Figure 3.16D). Surprisingly, FtsH2 localisation does not completely correlate with PSII even in conditions of intensified protease activity (Figure 3.16). The pattern of patches visible under high light suggests specific areas where cellular processes such D1 degradation happen. Distancing the PSII repair process from its target location makes mainly sense if there are obstacles to avoid. One reason for such a shift might be explained on the basis that PSII is a potent source of reactive oxygen species (ROS) such as singlet oxygen (Krieger-Liszkay, 2005). $^1O_2$ is a highly reactive form that rapidly oxidises cell components (Triantaphylides *et al.*, 2008) and affects translation of new proteins by direct damage of elongation factor G (Murata *et al.*, 2012). The same study claims that D1 *de novo* synthesis is affected by high concentration of ROS. ROS species diffuse rapidly but are also rapidly quenched in the cytoplasm, giving them a limited lifetime and diffusion range (Skovsen *et al.*, 2005). Singlet oxygen has a range of diffusion round 200–300 nm in the cytoplasm (Skovsen *et al.*, 2005). In a cell as small as *Synechocystis* it will still be impossible to completely avoid ROS generated by active PSII, but nevertheless there must be significant

variation in ROS concentration within the cell on 100 nm scales. Shift of repair zones away from PSII could serve to reduce the damaging effects of ROS on PSII repair.

If the hypothesis of distanced repair centres proposed here is correct, an intriguing question appears:

How does PSII discard the unfunctional D1 polypeptide and pass it to the immobile FtsH2* repair garage*?

PSII represented by chlorophyll fluorescence is mostly distributed evenly within the thylakoid membranes. D1 subunit is a 5 transmembrane α -helix protein located in the heart of PSII in the thylakoid membrane, surrounded by multiple proteins and cofactors. The mechanism of D1 disassembly from PSII was proposed (review by Nixon *et al.,* 2009). Thus, since changes in FtsH2 position were not detected even after high light stress, and as large transmembrane proteins occupy the same area in the thylakoid, then either the entire PSII complex might be mobile or another unknown chaperone may be involved in the process. **FRAP** (Fluorescence Recovery After Photobleaching) is a well established method applied to assess protein mobility *in vivo*. Unfortunately, these conducted FRAP experiments failed to reveal any reliable information on whether PSII complexes are mobile or not, due to the irregular shape of *Synechocystis* thylakoids (Mullineaux, unpublished). On the contrary, there have been many studies conducted on mobility of the photosystem centres in other photosynthetic organisms, showing that under some conditions these big complexes diffuse within

the thylakoids. In cyanobacterium *Synechococcus* sp. PCC 7942 movements of chlorophyll was registered after treatment with intense red light (Sarcina *et al.*, 2006). These studies found also that PSII complexes, after long exposure to intense red light, concentrate in specific zones, possibly similar to the *repair centres* proposed here. In the chloroplast of *Arabidopsis thaliana* the photodamaged PSII reaction centre must migrate from the grana to stroma lamellae to be repaired (Aro *et al.*, 1993). Studies on *Arabidopsis* mutants lacking STN7 and STN8 protein kinases, essential for PSII phosphorylation, registered lower mobility of chlorophyll binding proteins (Goral *et al.*, 2010). Chloroplast models for the PSII repair cycle imply the migration of photodamaged PSII reaction centres from the grana to the stroma lamellae for repair (Tikkanen *et al.*, 2008). Such explanation of PSII repair movement toward *repair centres* would make a clear model of D1 turnover in *Synechocystis* sp. PCC 6803, however, the exact mechanism of PSII mobility remains to be revealed.

6.2 Specific lipid species may stabilise protein clusters within thylakoid membranes and facilitate PSII repair

Chapter 3 and 4 show that the unconventional method of membrane proteins isolation resulted in separation of protein clusters most probably found nearby the epitope-tagged protein (FtsH) all bound by lipids. Our studies do not answer whether the lipids associate with proteins or it is the opposite, however with only four main lipid groups in the thylakoid membrane

system and various proteins, the latter solution is more likely to happen.

Lipids found within analysed FtsH-associated domains seem to be specific for these protein aggregations and are represented by considerable amounts of anionic sulfoquinovosyl diacylglycerols (SQDG) and phosphatidylglycerols (PG). Together with decreased amounts of glycolipids: monogalactosyl diacylglycerol (MGDG), digalactosyl diacylglycerol (DGDG) identified within the *FtsH zones* indicate that identified lipids were not random. On the contrary MGDG and DGDG build up the integral matrix (Murata and Siegenthaler 1998) and therefore contribute most to the total content of lipids in cyanobacterial membranes (MGDG 62%, DGDG 14%). Charged SQDG and PG however maintain membrane complexes by protein-lipid interactions. SQDG lipids are essential for autotrophic growth in *Synechocystis* 6803 and mutant with *sqdB* gene disruption (SD1) requires SQDG supplementation (Aoki *et al*., 2004). Studies have shown that deprivation of SQDG had little effect on structure of PSI and PSII complexes but it brought about 37% more severe photodamage to PSII (Aoki *et al*., 2004). SQDG found in protein micro-domains may therefore play a role in stabilising other complexes (such as FtsH itself).

Demand for PG lipids in cyanobacteria is crucial. Studies where depletion of PG is tested are always conducted with external presence of PG in growth media (Sato *et al*., 2000). PG lipids were identified as indispensable molecules of mature PSI and PSII complexes in *Synechocystis* (Kubota *et al*., 2010, Sakurai *et al*., 2006). PG-deficient mutants showed impaired PSII assembly and decreased dimerization of PSII monomers (Sakurai *et al*., 2007, Guskov *et al*., 2007).

PG therefore seem to be the least abundant but the most important for for-

mation and functioning of photosynthetic complexes.

The main lipids associated with the FtsH patches switches from SQDG in low light to PG after high light treatment. For FtsH2 SQDG content decreased for high light, while PG increased and overall anionic lipid content dropped from 80% in low light to 64% in high light. For FtsH3 and FtsH4 however in low light anionic lipids constitude about 50% and the proportion in high light increased to over 60%. Noteworthy, FtsH2 and FtsH3 were proposed to be present in heterocomplexes in *Synechocystis* (Boehm *et al.*, 2012), however lipid compositions found with associacion with these proteins are slightly different especially in low light. FtsH3 was assigned to build FtsH1/FtsH3 heterocomplexes in the plasma membrane, thus this may explain the contribution of different kinds of lipids in comparison to those found in association with FtsH2.

Given that MGDG and DGDG are the main architectural lipids embedding proteins, the emerging question is: why after exposure to high light does the total percentage of MGDG and DGDG double for FtsH2 if according to mass spectrometric results protein content decreased? Confocal images of FtsH2 (Figure 3.10 and 3.16) show that in high light these proteins are visible in brighter patches than these observed in low light, suggesting further agglomeration and increased number of molecules when activated. In theory after high light treatment we may be pulling down smaller fragments of membranes, since less proteins were found in these fractions (with lower chlorophyll content marked by faint elution colours compared to low light elution). Similarly the small size of isolated membranes might be supported by both lower content of anionic lipids and increased number of bulky structural lipids (DGDG and MGDG). The anionic lipids seem

to play a role in protein interactions, therefore the decrease in PG, SQDG and proteins presence after high light treatments may be a result of re-organisation and changes in interactions within these clusters, one of which may be disassembly of PSII complexes followed by D1 turnover.

Another observation to consider is the fairly high content of unsaturated fatty acids lipids in all four lipid groups (18:2, 18:3 and 18:4) found within FtsH2-bound fractions. It might be an important result when combined with experiments carried out by Jansen *et al.*, showing that fatty acid unsaturation is critical for pD1 maturation to D1 protein (Jansen *et al.*, 2002). pD1 accumulation was observed in a $desA^{-}/desD^{-}$ mutant kept in low-temperature and illuminated with high-light (Kanervo *et al.*, 1997; Jansen *et al.*, 2002). According to studies on D1 processing, the initial insertion of pD1 into the Reaction Centre is followed by its cleavage and then manganese cluster binding. Then without incorporation into the thylakoid membrane it can not be modified and shortened. It is therefore important for PSII repair to keep the thylakoid membranes' fluidity and it makes sense that this flexibility would be especially maintained within the FtsH *repair centres* studied here.

Thus, all FtsH membrane fractions were enriched in SQDG and PG. It must be considered that such phenomenon may face some technical issues. It may be possible that SQDG and PG lipids due to their negatively charged sulfo- and phospho-groups interact with protein complexes stronger than other lipids. As a result multiple detergent washing of membrane fractions bound on the column may lead to effective loss of neutral lipids. On the other hand experiments with high light performed in the same manner and detergents showed differences in lipid content even for negatively charged

lipids.

Studying these results it is implied that we have succeeded in pulling down membrane fragments which may be illustrated by centrally bound FtsH complex (epitope-tagged) and proteins found around FtsH, which include: subunits of PSI, PSII and ATP (in low light) and other, all bounded by lipids. Confocal analysis shows that FtsH2 protein clusters range from 200–600 nm in diameter. Absolute resolution of fluorescence microscope defines the distance where two bright spots are distinguished as separate, so measuring the size of visible patches required the assumption that fluorescence measured in Y axis (perpendicular to the membrane) is an artefact and spot would only have its real size in X axis (along the membrane). However while analysing data it was uncertain whether fluorescence of such a spot originated from one single membrane, the signal could be collected across all thylakoid membranes. According to Abbe's theory if small molecules are separated by < 300 nm (and this is the case for distance between thylakoid membranes), then two or more Airy discs may merge and give the impression of one brighter spot. Based on the fact that both of our biochemical methods (i.e. for protein identification and lipid identification) are not quantitative, we are missing a tool that would allow us to define the single unit building up such membrane fragment. It would be very informative to estimate which and how many other protein and lipid moleclues are associated with one FtsH complex. Therefore the only hypothesis emerging here is that thylakoid membranes show lateral heterogeneity in respect to proteins and lipids. For these experiments we may assume that high light exposure causes changes in this heterogeneous system in both protein and lipid distribution, the scale and range however are unknown. It would

be very informative to quantitatively determine the number of molecules within isolated microdomains *in situ* in both light conditions by employing techniques such Atomic Force Microscopy (AFM) or Near Field Scanning Microscopy (NSOM). Both of these complement fluorescence microscopy, and might be useful in determining the size of the studied membrane clusters.

6.3 Distribution of ctpA protease as an evidence for localised PSII repair and assembly *de novo*

The lumenal ctpA protease was localised *in vivo* by visualisation of GFP at its C-terminal end in *Synechocystis* sp. PCC 6803. We show that ctpA-GFP was simultaneously observed in at least three subcellular localisations: the region on cytoplasm side, thylakoid membranes/lumen (TMTL) and on the edge of thylakoid towards the region of plasma membrane (PM). PSII assembly and repair has been extensively studied, and whereas the cellular localisation of PSII repair was assigned to thylakoid membranes (Komenda, *et al*., 2006; Jansen *et al*., 2002; Chapter 3) the PSII assembly and disassembly, in particular the localisation of D1 processing and its integration into Reaction Centre (RC) has remained rather elusive. Two theories have been proposed on new D1 insertion into the repaired PSII. The first suggests the repair cycle happens close to specialised areas for *de novo* biogenesis. According to this theory, damaged PSII would re-locate in proximity to the PM where D1 would be assembled into the RC. The second supports the spatial separation of D1 insertion happening in special re-

gions called PratA Defined Membranes (PDM) for newly synthetized PSII and in TM directly delivered into matured repaired PSII (Schottkowski *et al*., 2009). According to our findings, ctpA proteases associated with pD1 processing are present in three cellular regions, suggesting that PSII repair might be spatially separated from PSII synthesis *de novo*. Combining with other results, we propose that the fraction of ctpA visible close to the cytoplasmic membrane is suspected to assist the PSII assembly *de novo*, whereas the populations found within the central thylakoid and thylakoid region at the cytoplasm side may process the pD1 for damaged PSII. Studies where structure of the *Synechocystis* cells was revealed with resolution of 5 nm reported an intriguing discovery of sheet-like structures 5–8 nm in diameter decorated with ribosomes (van de Meene, *et al*., 2006). Interestingly, these ribosome-enriched small membrane structures appeared within the interior of the cell and most evidently formed fusions with connections to thylakoid. Such agglomerations of ribosomes close to the membrane suggest a role in direct protein insertion into the thylakoid membranes (van de Meene, *et al*., 2006). It might be then possible that ctpA-GFP visible nearby the cytoplasmic region interacts immediately with pD1 co-translationally inserted into the thyalkoid membrane. Such an arrangement would enable quick and direct pD1 processing for damaged PSII. Similar roles for ribosomes found within either thylakoid or cytoplasmic membranes has been previously associated with proteins for thylakoid biogenesis in plants (Wollman, *et al*., 1999; Robinson, *et al*., 2000). Changes in protease abundance registered for different treatments indicate rapid cellular responses to on-going stress. In low light, 90% of the ctpA-GFP signal comes from the region of thylakoid and cytoplasm; it may suggest that either the re-

pair predominates over *de novo* synthesis, or ctpA proteases remain at low activity as in such conditions D1 is quite stable and PSII in low light is damaged at slower rate. High light treatment segregates the ctpA pool to be more evenly distributed within thylakoid membranes as well as shifting to the small (200 nm) puncta on the periphery. In this situation, the thylakoid population may be involved in cleaving pD1 inserted into partially disassembled PSII under repair. Whereas, remaining ctpA in the plasma membrane likely assists PSII synthesis *de novo*. However, after addition of lincomycin, which effectively blocks the translation of new proteins (Chen, *et al.*, 1965), we observed the expected suppression in GFP signal, as well as a three fold increase in ctpA abundance in the puncta round the cell contour in both LL and HL. Noteworthy, the absolute fluorescence intensity registered from the visible spots doubled in HL while the overall signal decreased. CtpA functions other than in pD1 posttranslational modification have not been reported. Therefore how the shortage of pD1 in presence of lincomycin impacts on ctpA redistribution to spots close to plasma membrane is not clear. However, studies by Jansen *et al.*, showed that for *Synechocystis* cultures at logarithmic growth phase pD1 was found exclusively in thylakoid membrane and after 60 minutes incubation with lincomycin a dramatical pD1 decrease was observed (Jansen *et al.*, 2002). Jansen's finding could help to explain the reasons for the observed ctpA shifts. CtpA may follow pD1 and if there is no new pD1 pool within thylakoids then it may be suspected that these specific ctpA accumulations may happen close to PDM domains (PratA-defined membranes), which are significantly richer in pD1 and D1 protein (Schottkowski *et al.*, 2009; Rengstl *et al.*, 2011). Hence the D1 supply within thylakoid drops suddenly, ctpA might be signalled

to move to the remaining pD1 pool in PDM. Schottkowski and co-authors showed very similar phenomenon. In their study they constructed a plasmid where eCFP (enhanced Cyan Fluorescent Protein) was fused to N-terminal of D1 (coded by *psbA2*, *slr1311*). Such plasmid was introduced (by conjugation) into the wild-type and *pratA*$^{-}$ mutant *Synechocystis* and functional D1-eCFP was observed using confocal micorscope. Interestingly, in wild-type the D1-eCFP was seen distributed very similarly to ctpA-GFP in low and high light, mainly in the thylakoid region on the side of the cytoplasm. However, for *pratA*$^{-}$ mutant the D1-eCFP emission did not colocalize with thylakoids. Similarly to ctpA-GFP treated with linocomycin, it was mainly registered in the periphery of cells (Schottkowski *et al.*, 2009). In Schottkowski's experiment the shifts of D1 to the thylakoid periphery were observed in cells deficient in PratA, that means that D1 would be post-transitionally processed but the step of manganese cluster assembly would be impaired. In our case ctpA shifted into similar locations when overall protein translation was inhibited, that would also include lower level of PratA. Combining both *in vivo* experiments and our pull-downs results, we show that ctpA protease follows pD1 or D1 and in limiting conditions, therefore such shifts might be triggered by changes in D1 locations.

The experiment with linomycin was performed within 60 minutes, in such short time we registered that absolute signal from puncta after addition of lincomycin was 1.5 fold brighter than from cells in LL. The difference was more prominent for lincomycin and HL treatment, in such conditions fluorescence from peripheral spots was 2.5 fold greater than registered in these cellular areas in low light (Table 5.1).

It is therefore not clear how proteins being found in thylakoid lumen can es-

cape and are translocate into another cell compartment in such a short time scale. The internal multiple concentric shells of the thylakoid system are surrounded by the cytoplasmic membrane which seperates the cell from the extracellular environment (Nierzwickibauer *et al*., 1983). The problem of membrane connectivity in cyanobacteria is still debatable (Liberton *et al*., 2006; van de Meene *et al*., 2006) . It is not clear whether direct connections exist between the different membrane systems and many state-of-art techniques have been intensively employed to investigate this problem. Nevo and co-workers showed that membranes are not connected *per se*, they showed, however, that individual thylakoid membranes create a network which contain continuous lumen. Interestingly, they also discovered multiple perforations through the thylakoid membranes, which assure cytoplasmic continuity and enable transport in the entire cell (Nevo, *et al*., 2007). Others like Gantt speculate about physical connections between the plasma membrane and thylakoid membranes, stating that thylakoids are derived from the plasma membrane (reviewed by Gantt 1994). Our findings can not clearly state that observed accumulation of the remaining ctpA protease is coupled with escape to another membrane lumen. In response to stress, ctpA might move closer to PDM but rather stay inside thylakoid lumen.

Similarly, we do not have any direct information on proteins diffusion and fluidity inside the thylakoid lumen. Studies where the mobility of phycoerythrin in thylakoid lumen of cryptophyte alga was measured directly by Fluorescence Recovery After Photobleaching (FRAP) showed no detectable diffusion (Kana *et al*., 2009). However the latter may suggest that limitations occur due to the size and type of observed protein-pigments. The

phycobiliprotein complex's mobility may be restricted sterically but the situation might be different for soluble plastocyanin or ctpA.
It is also worth considering that in response to light, stress cell regulation may alter the priority of PSII complex synthesis *de novo* over its repair. This implication is however a subject for further studies. Our study answers one of frequently asked question: Where does the PSII repair take place and is it coupled with its assembly *de novo*? If taking for granted that PSII repair happens only in the thylakoid membranes then by looking at visualised ctpA protease *in vivo* we may postulate that these two processes may be happening simultaneously in *Synechocystis* in different cell compartments. The latter suggests that cyanobacteria share similar solutions to these adapted by plants. However, the exact mechanism of D1 insertion into new growing reaction centre and replacement of damage D1 in partially disassembled PSII in thylakoid membrane, where most subunits are recycled, may differ and needs further verification. It is also worth considering that ctpA proteases may be turnover and this process may be allocated to visible spots on the edge of thylakoids.

6.4 Prokaryotic membranes as heterogenous systems

The essence of the Singer and Nicolson (1972) membrane model is that membranes are two-dimensional solutions of oriented lipids and globular proteins. The lipid bilayer has a dual role: it is both a solvent for integral membrane proteins and a permeability barrier. Membrane proteins are free to diffuse laterally in the lipid matrix unless restricted by special interactions. Therefore in order to study biological membranes we

employ protein or lipid-related techniques. In this study localisations of proteins in membranes or membrane lumen were demonstrated *in vivo*. FtsH homologues were visible in fairly large (FtsH2) clusters occupying thylakoid membranes (with exception for FtsH1). Based on preliminary observations this work aimed to gather evidence for lateral heterogeneity in thylakoid membranes in cyanobacteria. Biochemical data, where epitope-enriched membrane fragments were isolated and studied for protein and lipid content, showed that subunits of PSII and PSI complexes are found in close proximity to FtsH2 complexes, however not many other proteins were found. Additionally, lipid analysis revealed high content of anionic lipids (SQDG and PG) as well as unsaturated fatty acids in these membrane fragments. These findings shed more light on membrane compartmentalisation into small functional "protein-lipid islands" with possibly "rigid core" stablised by protein-lipid interactions and a disorientated fluid surrounding composed of unsaturated lipids which ensure protein exchange (in the case of PSII repair). Even though the "patch" structure proposed here is only based on identified components and previous structural studies, such arragments make sense as photosynthetic membranes are very crowded and therefore must be well organised.

Similar distinct localisation of the key respiratory electron donors NDH-1 and succinate dehydrogenase (SDH) complexes was revealed in cyanobacterium *Synechococcus* PCC 7942. Both complexes were found under low light in concentrated patches in the thylakoid membranes (Liu *et al.*, 2012). A very interesting example of cyanobacterial membrane domains was investigated by Rexroth *et al.*, who as a model used *Gloeobacter violaceus* PCC 7421, cyanobacterium without an internal membrane system. Specialised

functional membrane domains, which contain both photosynthetic and respiratory complexes, were found within the plasma membrane (Rexroth *et al.*, 2011).

Similar micro-domains composed of specific proteins and lipids were previously described for bacterial cells such as distinct localisation of cardiolipins found in polar and septal regions of *E. coli* (Mileykovskaya and Dowhan 2000) and similarly in *B. subtilis* (Kawai *et al.*, 2004). Both works of Lenn (Lenn *et al.*, 2008; Llorente-Garcia *et al.*, 2014) and recently Nenninger (Nenninger *et al.*, 2014) showed mobile domains of membrane proteins in *E. coli*.

In eukaryotic cells the non-random distributions and hindered diffusion of proteins in membranes was provided by discovery of *lipid rafts*. The latter detergent-resistant membrane domains in submicron range are enriched in cholesterol and sphingolipids, both rather rigid type of lipid molecules (Dietrich *et al.*, 2001). Sphingolipids present within *lipid rafts* contain mostly saturated fatty acids but are surrounded by highly unsaturated lipid to ensure membrane fluidity between domains (Schroeder *et al.*, 1994). What is common for these findings is that each of these membrane domains found across all species are enriched in negatively charged phospholipids suggesting their indispensable role in heterogeneous lateral membrane segregation. Furthermore, significant amounts of unsaturated fatty acids found in samples may suggest that while some membrane areas stay rigid, others remain fluid and flexible. In this case it is possible that membranes between photosynthetic complexes and *repair centres* are fluid to facilitate unrestricted protein migration.

The lateral membrane heterogeneity paradigm has been accepted for bac-

terial plasma membrane and eukaryotic membranes. Our results obtained from both *in vivo* experiments and biochemical protein/lipid analysis support one another and demonstrate that thylakoids may also be considered as well organised non-homogeneous membrane systems. These preliminary but revealing results encourage further investigations of the hypothesis proposed here.

6.5 Future work

(With reference to Chapters)

Chapter 3

It would be challenging and interesting to attempt to co-localise FtsH homologs together by using various fluorescent tags excited by different wavelengths. In order to demonstrate *in vivo* that FtsH2/FtsH3 or FtsH1/FtsH3 are present in thylakoid or plasma membranes in hetero-complexes, a split GFP approach might be employed.

It would also be very informative to collect and analyse data of *Synechocystis* mutants with colocalisation of two (or more) different fluorophores coupled with FtsH homologues.

Chapter 4

It would be interesting to localise FtsH proteases in the absence of SQDG or PG lipids. However, the latter is difficult to obtain as mutant where PG biosynthesis is inhibited requires external supplementation of PG lipids.

As for SQDG, when missing in metabolic pathways they are most probably replaced in the cell by MGDG, therefore visible changes in distribution may not be noticed. It was however planed to compare FtsH localisation in a mutant with disruption of *slr1508* (ΔdgdA) which does not contain DGDG at detectable levels (Sakurai *et al.*, 2007). These bulky lipids contribute 20% to the total thylakoid membrane lipids and their absence may not be without an effect on thylakoid structure, photosynthetic complex distribution and therefore localisation of FtsH repair zones.

It would be revealing to use super-resolution microscopy to test whether these visible patches containing FtsH and mixture of lipids are in fact 200 nm in diameter, as registered under fluorescent microscope, or much smaller. For well identified lipid rafts it was determined that the size of single unit is significantly smaller than it was first assumed <50 nm (Pralle *et al.*, 2000) and visible bigger patches containing proteins/lipids are aggregations of these basic blocks. Other experiments by Edidin and Dietrich revealed that such distinct confined membrane strctures are very not stable and with fast protein-lipid exchange rate (Edidin *et al.*, 2003; Dietrich *et al.*, 2002). It would be interesting to answer what is the residency time for bulk thylakoid domains and if it depends on conditions such as temperature (Kawasaki *et al.*, 2001).

It would be logical to employ biophysical quantitative tools such Atomic Force Microscopy (AFM) as a next step for studying thylakoid topology. It could facilitate the process of mapping FtsH-associated membranes and determine their micro-compositons.

Chapter 5.

CtpA relocation and the shift from thylakoid to plasma membrane region

on time scales of 30 minutes may suggest connections between the two membranes. It would be interesting to explore the subject of membrane connectivity by employing immuno-gold labelling combined with electron microscopy. It would be also revealing to colocalise ctpA and D1-CFP, the latter was previously expressed in a *Synechocystis* strain used in work by Schottkowski *et al.*, (2009). Colocalisation of ctpA and PratA would be also very revealing, however attempts to generate mutants with PratA-GFP/YFP failed.

Bibliography

Adam, Z., Clarke, AK. (2002). Cutting edge of chloroplast proteolysis. *Trends Plant Sci* **7**: 451–456.

Adir, N., Zer, H., Shochat, S., Ohad, I. (2003). Photoinhibition- a historical perspective. *Photosynthesis Research* **76**: 343–370.

Agarwal, R., Maralihalli, G., Sudarsan, V., *et al*., (2012). Differential distribution of pigment-protein complexes in the thylakoid membranes of *Synechocystis* 6803. *J Bioenerg Biomembr* **44:** 399–409.

Allen, JF., Forsberg, J. (2001). Molecular recognition in thylakoid structure and function. *Trends Plant Sci* **6**: 317–326.

Allen, JF. (2003). Botany. State transitions–a question of balance. *Science* **299**: 1530–1532.

Ammelburg, M., Frickey, T., Lupas, AN. (2006). Botany. Classification of AAA+ proteins. *J Struct Biol* **156**: 2–11.

Anbudurai, PR., Mor, TS., Ohad, I., Shestakov, SV., Pakrasi, HB. (1994). The ctpA gene encodes the C-terminal processing protease for the D1 protein of the photosystem II reaction center complex. *Proc Natl Acad Sci USA* **91**: 8082–8086.

Andersson, B., and Anderson, JM. (1980). Lateral heterogeneity in the distribution of chlorophyll-protein complexes of the thylakoid membranes of spinach chloroplasts. *Biochim Biophys Acta* **593**: 427–440.

Anderson, JM. (1986). Photoregulation of the composition, function, and structure of thylakoid membranes. *Ann Rev Plant Physiol* **37**: 93–136.

Antal, TK., Lo, W., Armstrong, WH., Tyystjarvi, E. (2009). Illumination with ultraviolet or visible light induces chemical changes in the water-soluble manganese complex, [Mn(4)O(6)(bpea)(4)]Br(4). *Photochem Photobiol* **85**: 663–668.

Aoki, M., Sato, N., Meguro, A., Tsuzuki, M. (2004). Differing involvement of sulfoquinovosyl diacyloglycerol in photosystem II in two species of unicellular cyanobacteria. *Eur J Biochem* **271**: 685–693.

Apostolova, EL., Domonkos, I., Dobrikova, AG., Sallai, A., Bogos, B., Wada, H., Gombos, Z., Taneva, SG. (2008). Effect of phosphatidylglycerol depletion on the surface electric properties and the fluorescence emission of thylakoid membranes. *J Photochem Photobiol B* **91**: 51–57.

Arlt, H., *et al.,* (1996). Illumination with ultraviolet or visible light induces chemical changes in the water-soluble manganese complex, [Mn(4)O(6)(bpea)(4)]Br(4). *Photochem Photobiol* **85**: 663–668.

Armbruster, U., Zuhlke, J., Rengstl, B., Kreller, R., Makarenko, E., *et al.,* (2010). The *Arabidopsis* thylakoid protein PAM68 is required for efficient D1 biogenesis and photosystem II assembly. *Plant Cell* **22**: 3439–3460.

Aro, EM., Virgin, I., Andersson, B. (1993). Photoinhibition of photosystem II. Inactivation, protein damage and turnover. *Biochim Biophys Acta* **1143**: 113–119.

Asada, K. (1999). THE WATER-WATER CYCLE IN CHLOROPLASTS: Scavenging of Active Oxygens and Dissipation of Excess Photons. *Annu Rev Plant Physiol Plant Mol Biol* **50**: 601–639.
Asada, K. (2000). The water-water cycle as alternative photon and electron sinks. *Philos Trans R Soc Lond B Biol Sci* **355**: 1419–1431.

Barker, M., de Vries, R., Nield, J., Komenda, J., Nixon, PJ. (2006). The Deg proteases protect *Synechocystis* sp. PCC 6803 during heat and light stresses but are not essential for removal of damaged D1 protein during the photosystem two repair cycle. *Nature* **281**: 30347–30355.

Behrenfeld, MJ., Bale, AJ., Kolber, ZS., Aiken, J., Falkowski, PG. (1996). Confirmation of iron limitation of phytoplankton photosynthesis in the

equatorial Pacific Ocean. *Nature* **383**: 508–511.

Berg, JM., Tymoczko, JL., and Stryer L. (2002). Biochemistry. 5th edition. New York: W H Freeman: 12.6. 2002.

Berks, BC., Palmer, T., Sargent, F. (2003). The Tat protein translocation pathway and its role in microbial physiology. *Microb Physiol* **47**: 184–254.

Berthold, DA., babcock, GT., Yocum, CF. (1981). A highly resolved oxygen-evolving Photosystem II preparation from spinach thylakoid membranes. *FEBS Lett* **134**: 231–234.

Beyer, A. (1997). Sequence analysis of the AAA protein family. *FEBS Lett* **6**: 2043–2058.

Bizzarri, R., Serresi, M., Luin, S., Beltram, F. (2009). Green fluorescent protein based pH indicators for *in vivo* use: a review. *Analytical and bioanalytical chemistry* **4**: 1107–1122.

Blankenship, RE. (2002). Molecular Mechanisms of Photosynthesis. *Blackwell Science* Oxford.

Bligh, EG., Dyer, WJ. (1959). A rapid method of total lipid extraction and purification. *Can J Biochem Physiol* **37**: 911–917.

Blobel, G., Sabatini, D. (1971). Dissociation of mammalian polyribosomes

into subunits by puromycin. *Proc Natl Acad Sci USA* **68**: 390–394.

Boehm, M., Romero, E., Reisinger, V., Yu, J., Komenda, J., *et al.,* (2011). Investigating the early stahges of photosystem II assembly in *Synechocystis* sp. pCC 6803: isolation of CP47 and CP43 complexes. *J Biol Chem* **286**: 14812–14819.

Boehm, M., Yu, J., Krynicka, V., Barker, M., Tichy, M., Komenda, J., Nixon, PJ. (2012). Subunit organisation of a *Synechocystis* Hetero-Oligomeric Thyalkoid FtsH complex involved in the Photosystem II Repair. *The Plant Cell* **24**: 3669–3683.

Boekema, EJ., van Breemen, JF., van Roon, H., Dekker, JP. (2000). Arrangement of photosystem II supercomplexes in crystalline macrodomains within the thylakoid membrane of green plant chloroplasts. *J Mol Biol* **301**: 1123–1133.

Bonardi, V., Pesaresi, P., Becker, T., Schleiff, E., Wagner, R., Pfannschmidt, T., Jahns, P., Leister, D. (2005). Photosystem II core phosphorylation and photosynthetic acclimation require two different protein kinases. *Nature* **437**: 1179–1182.

Boyd, D., Schierle, C., Beckwith, J. (1998). How many membrane proteins are there? *Protein Sci* **7**: 201–205.

Bricker, TM., Ghanotakis, DF. (1996). Introduction to oxygen evolution and

the oxygen-evolving complex. *See Ref* **234a**: 113–136.

Campbell, D., Eriksson, MJ., Oquist, G., Gustafsson, P., Clarke, AK. (1998). The cyanobacterium *Synechococcus* resists UV-B by exchanging photosystem II reaction-center D1 proteins. *Proc Natl Acad Sci* **95**: 364–369.

Chang, FN., Sih, CJ., Weisblum, S. (1965). Lincomycin, an inhibitos of aminoacyl SRNA binding to ribosomes. *Proc Natl Acad Sci USA* **55**: 431–438.

Chen, GX., Kazimir, J., Cheniae, GM. (1992). Photoinhibition of hydroxylamine-extracted photosystem II membranes: studies of the mechanism. *Biochemistry* **31**: 11072–11083.

Chen, H., Zhang, D., Guo, J., Wu, H., Jin, M., *et al.,* (2006). A Psb27 homologue in *Arabidopsis thaliana* os required for efficient repair of photodamaged photosystem II. *Plant Mol Biol* **61**: 567–575.

Choy, JS., Aung, LL., Karzai, AW. (2006). Lon protease degrades transfer-messanger RNA-tagged proteins. *J.Bacteriol.* **189**: 6564–6571.

Cheregi, O., Sicora, C., Kos, PB., Barker, M., Nixon, PJ., Vass, I. (2007). The role of the FtsH and Deg proteases in the repair of UV-B radiation-damaged Photosystem II in the cyanobacterium *Synechocystis* PCC 6803. *Biochim Biophys Acta* **1767**: 820–828.

Clarke, AK., Soitamo, A., Gustafsson, P., Oquist, G. (1993). Rapid interchange between two distinct forms of cyanobacterial photosystem II reaction-center protein D1 in response to photoinhibition. *Proc Natl Acad Sci USA* **90**: 9973–9977.

Clarke, AK., Campbell, D., Gustafsson, P., Oquist, G. (1995). Dynamic responses of photosystem II and phycobilisomes to changing light in the cyanobacterium *Synechococcus* sp. PCC 7942. *Planta* **197**: 553–562.

DAndrea, LD., Regan, L. (2003). TPR proteins: the versatile helix. *Trends Biochem Sci* **28**: 655–662.

Dalbey, RE., Robinson, C. (1999). Protein translocation into and across the bacterial plasma membrane and the plant thylakoid membrane. *Trends Biochem Sci* **24**: 17–22.

DallaChiesa, M., Friso, G., Deak, Z., Vass, I., Barber, J. and Nixon, PJ. (1997). Reduced turnover of the D1 polypeptide and photo-activation of electron transfer in novel herbicide resistant mutants of *Synechocystis* sp. PCC 6803. *Eur J Biochem* **248**: 731–740.

Datsenko, KA., and Wanner, BL. (2000). One-step inactivation of chromosomal genes in *Escherichia coli* K-12 using PCR products. *Proc Natl Acad Sci USA* **97**: 6640–6645.

Dekker, JP., Boekema, EJ. (2005), Supramolecular organization of thylakoid

membrane proteins in green plants. *Biochim Biophys Acta* **1706**: 12–39.

Demmig-Adams, B., Adams, III WW. (1996). The role of xanthophyll cycle carotenoids in the protection of photosynthesis. *Trends Biochem Sci* **1**: 21–26.

Dietrich, C., *et al*,. (2001). Lipid rafts reconstituted in model membranes. *Biophys J* **80**: 1417–1428.

Dietrich, C., Yang, B., Fujirawa, T., Kusumi, A. and Jacobson, K. (2002). Relationship of lipid rafts to transient confinement zones detected by single particle tracking. *Biohys J* **82**: 274–284.

Di Mascio, P., Devasagayam, TP., Kaiser, S., Sies, H. (1990). Carotenoids, tocopherols and thiols as biological singlet molecular oxygen quenchers. *Biochem Soc Trans* **18**: 1054–1056.

Diner, BA., Ries, DF., Cohen, BN., Metz, JG. (1988). COOH-terminal processing of polypeptide D1 of the photosystem II reaction center of Scenedesmus obliquus is necessary for the assembly of the oxygen-evolving complex. *J Biol Chem* **263**: 8972–8980.

Dobakova, M., Sobotka, R., Tichy, M., Komenda, J. (2009). Psb28 protein is involved in the biogenesis of the photosystem II inner antenna CP47 (PsbB) in the cyanobacterium *Synechocystis* sp. PCC 6803. *Biochem Soc Trans* **149**: 1076–1086.

Domonokos, J., *et al.*, (2004). Phosphatidylglycerol is essential for oligomerization of photosystem I reaction center. *Plant Physiol* **134**: 1471–1478.

Domonkos, I., Laczko-Dobos, H., Gombos, Z. (2008). Lipid-assisted protein-protein interactions that support photosynthetic and other cellular activities. *Prog Lipid Res* **47**: 422–435.

Dopico, AM., and Tigyi, GJ. (2007). A glance at the structural and functional diversity of membrane lipids. *Methods Mol* **400**: 1–13.

Dowhan, W. (1997). Molecular basis for membrane phospholipids diversity: why are there so many lipids? *Annu Rev Biochem* **66**: 199–232.

Edelman, M., Mattoo, AK. (2008). D1-protein dynamics in photosystem II: the lingering enigma. *Photosynth Res* **98**: 609–620.

Edidin, M., Zuniga, MC., Sheetz, MP. (1994). Truncation mutants define and locate cytoplasmic barriers to lateral mobility of membrane glycoproteins. *Proc Natl Acad Sci USA* **91**: 3378–3382.

Edidin, M. (2003). The state of lipid rafts: From model membranes to cells. *Ann Rev Biophys Biomol* **32**: 257–283.

Escoubas, JM., Lomas, M., LaRoche, J., Falkowski, PG. (1995). Light intensity regulation of cab gene transcription is signaled by the redox state of the plastoquinone pool. *Proc Natl Acad Sci USA* **92**: 10237–10241.

Erzberger, JP., Berger, JM. (2006). Evolutionary relationships and structural mechanisms of AAA+ proteins. *Annu Rev Biophys Biomol Struct* **35**: 93–114.

Fagerlund, RD., and Eaton-Rye, JJ. (2011). Evolutionary relationships and structural mechanisms of AAA+ proteins. *J Photochem Photobiol B Biol* **104**: 191–203.

Ferreira, F., Straus, NA. (1994). Iron Deprivation in Cyanobacteria. *Journal of Applied Phycology* **6**: 199–210.

Ferreira, KN., Iverson, TM., Maghlaoui, K., Barber, J., Iwata, S. (2011). Architecture of the photosynthetic oxygen-evolving center. *Science* **303**: 1831–1838.

Ferro, M., Brugiere, S., Salvi, D., Seigneurin-Berny, *et al.*, (2010). AT-CHLORO, a comprehensive chloroplast proteome database with subplastidial localization and curated information on envelope proteins. *Mol Cell Proteomics* **9**: 1063–1084.

Fufezan, C., Rutherford, AW., Krieger-Liszkay, A. (2002). Singlet oxygen production in herbicide-treated Photosystem II. *FEBS Lett.* **532**: 407–410.

Gal, A., Zer, H., Ohad, I. (1997). Redox-controlled thylakoid protein phosphorylation. News and views. *Physiol Plant* **100**: 869–885.

Gantt, E. (1994). Supramolecular membrane organization. In: DA Bryant eds, The molecular biology of cyanobacteria. *Kluwer, Dordrecht* pp 119–138.

Garab, G. and Manella, CA. (2008). Reply: on three-dimensional models of higher-plant thylakoid networks: elements of consensus, controversies and future experiments. *Plant Cell* **20**: 2549–2551.

Garcia-Lorenzo, M., Sjodin, A., Jansson, S., Funk, C. (2006). Protease gene families in *Populus* and *Arabidopsis*. *BMC Plant Biol* **6**: 30.

Gibala, M., Kicia, M., Sakamoto, W., Gola, EM., Kubrakiewicz, J., Smakowska, E. and Janska, H. (2009). The lack of mitochondrial AtFtsH4 protease alters *Arabidopsis* leaf morphology at the late stage of rosette development under short-day photoperiod. *The Plant Journal for Cell and Mol Biol* **59**: 685–699.

Glazer, AN. (1985). Light Harvesting by Phycobilisomes. *Ann Rev of Biophys and Biophys Chem* **14**: 47–77.

Golden, SS., Brusslan, J. and Haselkorn, R. (1986). Expression of a family of psbA genes encoding a photosystem II polypeptide in the cyanobacterium *Anacystis nidulans* R2. *EMBO J* **5**: 2789–2798.

Golden, SS., and Stearns, GW. (1988). Nucleotide sequence and transcript analysis of three photosystem II genes from the cyanobacterium *Synechococcus* sp. PCC7942. *EMBO J* **67**: 85–96.

Golden, SS. (1995). Light-responsive gene expression in cyanobacteria. *J Bacteriol* **177**: 1651–1654.

Gombos, Z., Wada, H., Murata, N. (1994). The recovery of photosynthesis from low-temperature photoinhibition is accelerated by the unsaturation of membrane lipids: a mechanism of chilling tolerance. *Proc Natl Acad Sci USA* **91**: 8787–8791.

Gonnet, GH., Cohen, MA., and Benner, SA. (1992). Exhaustive matching of the entire protein sequence database. *Science* **256**, 1443–5.

Goral, TK., Johnson, MP., Duffy, CD., Brain, AP., Ruban, AV., Mullineaux, CW. (2012). Light-harvesting antenna composition controls the macrostructure and dynamics of thylakoid membranes in *Arabidopsis*. *Plant J* **69**: 289–301.

Gottesman, S., Roche, E., Zhou, Y., Sauer, RT. (1998). The ClpXP and ClpAP proteases degrade proteins with carboxy-erminal peptide tails added by the SsrA-tagging system. *Genes Dev* **12**: 1338–1347.

Gorter, E., Grendel, F. (1925). On bimolecular layers of lipoids on the chromocytes of the blood. *J Exp Med* **41**: 439–443.

Greaf, M., Seewald, G., Langer, T. (2007). Substrate recognition by AAA+ ATPase: distinct substrate binding modes in ATP-dependent protease Yme1 of the mitochondrial intermembrane space. *Mol Cell Biol* **27**: 2476–2485.

Grossman, AR., Bhaya, D., Apt, KE., Kehoe, DM. (1995). Light-harvesting complexes in oxygenic photosynthesis: diversity, control, and evolution. *Annu Rev Genet* **29**: 231–288.

Grossman, AR., Schaefer, MR., Chiang, GG., Collier, JL. (1993). The phycobilisome, a light-harvesting complex responsive to environmental conditions. *Microbiol Rev* **57**: 725–749.

Guskov, A., Kern, J., Gabdulkhakov, A., Brose, M., Zouni, A., Seanger, W. (2009). Cyanobacterial photosystem II at 2.9 Å resolution and the role of quinones, lipids, channels and chloride. *Nat Struct Mol Biol* **16**: 334–342.

Gust, B., Challis, GL., Fowler, K., Kieser, T., Chater, KF. (2003). PCR-targeted *Streptomyces* gene replacement identifies a protein domain needed for biosynthesis of the sesquiterpene soil odor geosmin. *Proc Natl Acad Sci USA* **100**: 1541–1546.

Gwizdala, M., Wilson, A., Kirilovsky, D. (2011). *In vitro* reconstitution of the cyanobacterial photoprotective mechanism mediated by the Orange Carotenoid Protein in *Synechocystis* PCC 6803. *Plant Cell* **23**: 2631–2643.

Ng, WO., Grossman, AR., Bhaya, D. (2003). Multiple light inputs control phototaxis in *Synechocystis* sp. strain PCC 6803. *J Bacteriol* **185**: 1599–1607.

Hakala, M., Tuominen, I., Keranen, M., Tyystjarvi, T., and Tyystjarvi, E.

(2005). Evidence for the role of the oxygen-evolving manganese complex in photoinhibition of photosystem II. *Biochim Biophys Acta* **1706**: 68–80.

Hakala, M., Rantamaki, S., Puputti, EM., Tyystjarvi, T., Tyystjarvi, E. (2006). Photoinhibition of manganese enzymes: insights into the mechanism of photosystem II photoinhibition. *J Exp Bot* **57**: 1809–1816.

Haussuhl, K., Andersson, B., Adamska, I. (2001). A chloroplast DegP2 protease performs the primary cleavage of the photodamaged D1 protein in plant photosystem II. *EMBO J* **20**: 713–722.

Havaux, M., Eymery, F., Porfirova, S., Rey, P., Dormann, P. (2005). Vitamin E protects against photoinhibition and photooxidative stress in *Arabidopsis thaliana*. *Plant Cell* **17**: 3451–3469.

Heim, R., Cubitt, AB., Tsien, RY. (1995). Improved green fluorescence. *Nature* **373**: 663–664.

Hervas, M., Navarro, JA., De la Rosa, MA. (2003). Electron transport between membrane complexes and solebile proteins in photosynthesis. *Nature* **36**: 798–805.

Huang, F., Parmryd, I., Nilsson, F., Persson, B. (2002). Proteomics of *Synechocystis* sp. strain PCC 6803: Identification of Plasma Membrane Proteins. *Mol Cell Proteomics* **1**: 956–966.

Henry, R., Carrigan, M., McCaffrey, M., Ma, X., Cline, K. (1997). Targeting determinants and proposed evolutionary basis for the Sec and the Delta pH protein transport systems in chloroplast thylakoid membranes. *J Cell Biol* **136**: 823–832.

Hill, R., and Bendall, F. (1960). Function of the two cytochrome components in chloroplasts - A working hypothesis. *Nature* **186**: 136–137.

Ingen-Hausz, J. (1779). Experiments upon vegetables: discovering their great power of purifying the common air in the sunshine and of injuring it in the shade. Book:Experiments upon vegatables. *Release by:Emsly and Payne, London Oct*.

Ito, K., Akiyama, Y. (2005). Cellular functions, mechanism of action, and regulation of FtsH protease. *Annu Rev Microbiol* **59**: 211–231.

Ivleva, NB., Shestakov, SV., Pakrasi, HB. (2000). The carboxyl-terminal extension of the precursor D1 protein of photosystem II is required for optimal photosynthetic performance of the cyanobacterium *Synechocystis* sp. PCC 6803. *Plant Physiol* **124**: 1403–1412.

Jansen, T., Kanervo, E., Aro EM, Maenpaa, P. (2002). Localisation and processing of the precursor form of photosystem II protein D1 in *Synechocystis* 6803. *J Plant Physiol* **159**: 1205–1211.

Janska, H., Kwasniak, M., Szczepanowska, J. (2013). Protein quality con-

trol in organelles - AAA/FtsH story. *Biochim Biophys Acta* **1833**: 381–387.

Jayasekera, MM., Foltin, SK., Olson, ER., Holler, TP. (2000).*Escherichia coli* requires the protease activity FtsH for growth. *Arch Biochem Biophys* **380**: 103–107.

Jordan, P., Fromme, J., Witt HT., Klukas, O., Saenger, W., Krauss, N. (2001). Three-dimensional structure of cyanobacterial photosystem I at 2.5 Å resolution. *Nature* **411**: 909–917.

Kamata, T., Hiramoto, H., Morita, N., Shen, JR., Mann, NH., Yamamoto, Y. (2005).Quality control of Photosystem II: an FtsH protease plays an essential role in the turnover of the reaction center D1 protein in *Synechocystis* PCC 6803 under heat stress as well as light stress conditions. *Photochem Photobiol* **4**: 983–990.

Kana, R., Prasil, O., Mullineaux, CW. (2009). Immobility of phycobilins in the thylakoid lumen of cryptophyte suggests that protein diffusion in the lumen is very restricted. *FEBS Letters* **583**: 670–674.

Kaneko, T., and Tabata, S. (1997).Complete genome structure of the unicellular cyanobacterium *Synechocystis* sp. PCC 6803. *Photochem Photobiol* **38**: 1171–1176.

Kanervo, E., Suorsa, M., Aro, EM. (2005).Functional flexibility and acclimation of the thylakoid membrane. *Photochem Photobiol Sci* **4**: 1072–1080.

Karata, K., Inagawa, T., Wilkinson, AJ., Tatsuta, T., Ogura, T. (1999). Dissecting role of a conserved motif (the second region of homology) in the AAA familt of ATPases. Site-directed mutagenesis of the ATP-dependent protease FtsH. *J Biol Chem* **274**: 26225-26232.

Karata, K., Verma, CS., Wilkinson, AJ., Ogura, T. (2001). Probing the mechanism of ATP hydrolysis and substrate translocation in the AAA protease FtsH by modelling and mutagenesis. *Mol Microbiol* **39**: 890-903.

Kashino, Y., Lauber, WM., Carroll, JA., Wang, Q., Whitmarsh, J., *et al.* (2002). Proteomic analysis of a highly active photosystem II preparation form the cyanobacterium *Synechocystis* sp. PCC 6803 revea;s the presence of novel polypeptides. *Biochemistry* **41**: 8004-8012.

Kawai, F., Shoda, M., Harashima, R., Sadaie, Y., Hara, H., and Matsumoto, K. (2004). Cardiolipin domains in *Bacillus subtilis Marburg* membranes. *J Bacteriol* **186**: 1475–1483.

Kawasaki, K., Yin, J.J., Subczynski, W.K., Hyde, J.S. and Kusumi, A. (2001). Pulse EPR detection of lipid exchange between protein-rich raft and bulk domains in the membrane: methodology development and its application to studies of influenza viral membrane. *Biophys J* **80**: 738–748.

Keren, N., Berg, A., van Kan, PJ., Levanon, H., and Ohad, II. (1997). Mechanism of photosystem II photoinactivation and D1 protein degradation at

low light: The role of back electron flow. *Proc Natl Acad Sci USA* **94**:1579–1584.

Keren, N., Aurora, R., Pakrasi, HB. (2004). Critical roles of bacterioferritins in iron storage and profliferation of cyanobacteria. *American Society of Plant Biologists*. **131**: 1666–1673.

Keren, N., Liberton, M., Pakrasi, HB. (2005). Photochemical competence of assembled photosystem II core complex in cyanobacterial plasma membrane. *J Biol Chem* **280**: 6548–6553.

Kihara, A., Akiyama, Y., Ito, K. (1995). FtsH is required for proteolytic elimination of uncomplexed forms of SecY, an essential protein translocase subunit. *Proc Natl Acad Sci USA* **92**: 4532–4536.

Kihara, A., Akiyama, Y., Ito, K. (1995). Different pathways for protein degradation by the FtsH/HflKC membrane-embedded protease complex: an implication from the interference by a mutant form of a new substrate protein, YccA. *J Mol Biol* **279**: 175–188.

Klimov VV, Shafiev MA, Allakhverdiev SI (1990). Photoinactivation of the reactivation capacity of photosystem II in pea subchloroplast particles after a complete removal of manganese. *Photosynthetic Research* **23**: 59–65.

Klinkert, B., Ossenbuhl, F., Sikorski, M., Berry, S., Eichacker, L., Nickelsen, J. (2004). PratA, a periplasmic tetratricopeptide repeat protein involved in

biogenesis of photosystem II in *Synechocystis* sp. PCC 6803. *J Biol Chem* **279**: 44639–44644.

Kolodziejczak, M., Kolaczowska, A., Szczesny, B., Urantowka, A., Knorpp, C., Kielczawa, J. and Janska, H. (2002). Higher plant mitochondrial homologue of the yeast m-AAA protease. Molecular cloning, localization and putative function. *The Journal of Biol Chem* **277**: 43792–43798.

Kolodziejczak, M., Gibala M., Urantowka, A., Janska, H. (2007). The significance of *Arabidopsis* AAA proteases for activity and assembly/stability of mitochondrial OXPHOS complexes. *Physiol Plant* **129**: 135–142.

Komenda, J., Barker, M., Kuvikova, S., de Vries, R., Mullineaux, CW., Tichy, M., Nixon, PJ. (2006). The FtsH protease *slr0228* is important for quality control of photosystem II in the thylakoid membrane of *Synechocystis* sp. PCC 6803. *J Biol Chem* **281**: 1145–1151.

Komenda, J., Tichy, M., Prasil, O., Knoppova, J., Kuvikova, S., de Vries, R., Nixon, PJ. (2007). The exposed N-terminal tail of the D1 subunit is required for rapid D1 degradation during photosystem II repair in *Synechocystis* sp. PCC 6803. *Plant Cell* **19**: 2839–2854.

Komenda, J., Kuvikova, S., Granvogl, B., Eichacker, L., Diner, B., Nixon, PJ. (2007). Cleavage after residue Ala352 in the C-terminal extension is an early step in the maturation of the D1 subunit of Photosystem II in *Synechocystis* PCC 6803. *Biochimica et Biophys Acta* **1767**: 829–837.

Komenda, J., Nickelsen, J., Tichy, M., Prasil, O., Eichacker, LA., Nixon, PJ. (2008). The cyanobacterial homologue of HCF136/YCF48 is a component of an early photosystem II assembly complex and is important for both the efficient assembly and repair of photosystem II in *Synechocystis* sp. PCC 6803. *J Biol Chem* **283**: 22390–22399.

Komenda, J., Sobotka, R., Nixon, PJ. (2012). Assembling and maintaining the photosystem II complex in chloroplasts and cyanobacteria. *Curr Opin Plant Biol* **15**: 245–251.

Krieger-Liszkay, A., Rutherford, AW. (1998). Influence of herbicide binding on the redox potential of the quinone acceptor in Photosystem II: relevance to photodamage and phytotoxicity. *Biochemistry* **37**: 17339–17344.

Kruger, TP., Ilioaia, C., Johnson, MP., Ruban, AV., Papagiannakis, E., Horton, P., van Grondelle, R. (2012). Controlled disorder in plant light-harvesting complex II explains its photoprotective role. *Biochemistry* **102**: 2669–2676.

Krzywda, S., Brzozowski, AM., Verma, C., Karata, K., Ogura, T., Wilkinson, AJ. (2002). The crystal structure of the AAA domain of the ATP-dependent protease FtsH of *Escherichia coli* at 1.5A resolution. *Structure* **10**: 1073–1083.

Kubota, H., Sakurai, I., Katayama, K., Mizusaw, N., Ohashi, S., Kobayashi, M., Zhang, P., Aro E.M., Wada, H. (2010). Purification and charcterisation of photosystem I complex from *Synechocystis* sp. pCC 6803 by expressing

histidine-tagged subunits. *Biochm Biophys Acta* **1797**: 98–105.

Kudoh, H., Sonoike, K. (2002). Irreversible damage to Photosystem I by chilling in the light: cause of the degradation of chlorophyll after returning to normal growth temperature. *Planta* **215**: 541–548.

Kufryk, GI., Vermaas, WF. (2001). A novel protein involved in the functional assembly of the oxygen- evolving complex of photosystem II in *Synechocystis* sp. PCC 6803. *Biochemistry* **40**: 9247–9255.

Kunkel, DD. (1982). Thylakoid centers: structures associated with the cyanobacterial photosynthetic membrane system. *Arch Microbiol* **133**: 97–99.

Kusumi, A., Sako, Y., Yamamoto, M. (1993). Confined lateral diffusion of membrane receptors as studied by single particle tracking (nanovid microscopy). Effects of calcium-induced differentiation in cultured epithelial cells. *Biophys J* **65**: 2012–2024.

Kuvikova, S., Tichy, M., Komenda, J. (2005). A role of the C-terminal extension of the photosystem II D1 protein in sensitivity of the cyanobacterium *Synechocystis* PCC 6803 to photoinhibition. *Photochem Photobiol Sci* **4**: 1044–1048.

Kuwabara, T., Murata, N. (1983). Quantitative-analysis of the inactivation of photosyn- thetic oxygen evolution and the release of polypeptides and manganese in the photosystem II particles of spinach-chloroplasts. *Plant*

Cell Physiol **24**: 741–747.

Langklotz, S., Baumann, U., Narberhaus, F. (2012). Structure and function of the bacterial AAA protease FtsH. *Bioch At Bioph Acta* **1823**: 40–48.

Lee, H-Y., Hong, Y-N., Chow, WS. (2001). Photoinactivation of photosystem II complexes and photoprotection by non-functional neighbors in *Capsicum annuum* L. leaves. *Bioch At Bioph Acta* **212**: 332–342.

Lenn, T., Leake, MC., Mullineaux, CW. (2008). Are *Escherichia coli* OXPHOS complexes concentrated in specialized zones within the plasma membrane? *Biochem Soc Trans* **36**: 1-32–1036.

Lenzen D *et al.,* (1998). Crystal structure of the hexamerization domain of N-ethylmaleimide-sensitive fusion protein. *Cell* **94**: 525–536.

Leonhard, K., *et al.,* (1999). Chaperone-like activity of the AAA domain of the yeast Yme1 AAA protease. *Nature* **398**: 348–351.

Liberton, M., Berg, RH., Heuser, J., Roth, R., Pakrasi, HB. (2006). Ultrastructure of the membrane systems in the unicellular cyanobacterium *Synechocystis* sp. strain PCC 6803. *Protoplasma* **227**: 129–138.

Lichtenthaler, HK., Wellburn, AR. (1983). Determinations of total carotenoids and chlorophylls a and b of leaf extracts in different solvents. *Biochem Soc Trans* **11**: 591–592.

Lies, M., Maurizi, MR. (2008). Turover of endogenous SsrA-tagged proteins mediated by ATP-dependent proteases in *Escherichia coli J Biol Chem* **283**: 22918–22929.

Lima, A., Lima, S., Wong, JH., Phillips, RS., Buchanan, BB., Luan, S. (2006). A redox-active FKBP-type immunophilin functions in accumulation of the photosystem II supercomplex in *Arabidopsis thaliana*. *Proc Natl Acad Sci USA* **103**: 12631–12636.

Lindahl, M., Yang, D-H., Andersson, B. (1995). Regulatory proteolysis of the major light-harvesting chlorophyll a/b protein of Photosystem II by a light-induced membrane-associated enzymic system. *Eur J Biochm* **231**: 503–509.

Lindahl, M., Spetea, C., Hundal, T., Oppenheim, AB., Adam, Z., Andersson, B. (2000). The thylakoid FtsH protease plays a role in the light-induced turnover of the photosystem II D1 protein. *Plant Cell* **12**: 419–431.

Liu, L-N., Bryan, SJ., Huang, F., Yu, J., Nixon, PJ., Rich, PR., Mullineaux, CW. (2012). Control of electron transport routes through redox-regulated redistribution of respiratory complexes. *Proc Natl Acad Sci USA* **109**: 11431–11436.

Llorenta-Garcia, I., *et al*., (2014). Single-molecule *in vivo* imaging of bacterial respiratory complexes indicates delocalized oxidative phosphoryla-

tion. *Biochimica et Biophys Acta* **1837**: 811–824.

Lopez, D., and Kolter, R. (2010). Functional microdomains in bacterial membranes. *Genes Dev* **24**: 1893–1902.

Magde, D., Elson, EL., Webb, WW. (1974). Fluorescence correlation spectroscopy. *An experimental realization Biopolymers* **13**: 29–61.

Manders, EMM., Verbeek, FJ. and Aten, JA. (1993). Measurement of colocalization of objects in dual-colour confocal images. *J Microsc* **169**: 375–382.

Mann, NH., Novac, N., Mullineaux, CW., Newman, J., Bailey, S., Robinson, C. (2000). Involvement of an FtsH homologue in the assembly of functional photosystem I in the cyanobacterium *Synechocystis* sp. PCC 6803. *FEBS Lett* **479**: 72-77.

Matsubara, S., Chow, WS. (2004). Populations of photoinactivated photosystem II reaction centers characterized by chlorophyll a fluorescence lifetime *in vivo*. *Proc Natl Acad Sci USA* **101**: 18234–18239.

Mattoo, AK., Hoffman-Falk, H., Marder, JB., Edelman, M. (1984). Regulation of protein metabolism: Coupling of photosynthetic electron transport to *in vivo* degradation of the rapidly metabolized 32-kilodalton protein of the chloroplast membranes. *Proc Natl Acad Sci USA* **81**: 1380–1384.

Merchant, S., Dreyfuss, BW. (1998). Post-translational assembly of pho-

tosynthetic metalloproteins. *Ann Rev of Plant Physiol and Plant Mol Biol* **49**: 25–51.

Merchant, S., Dreyfuss, BW. (1905). Uber Natur und Ursprung der Chromatophoren im Pflanzenreiche *Biol Centralbl* **25**: 593–604.

Mileykovskaya, E., and Dowhan, W. (2000) Visualization of phospholipid domains in *Escherichia coli* by using the cardiolipin-specific fluorescent dye 10-N-nonyl acridine orange. *J Bacteriol* **182**: 1172–1175.

Miyagawa, Y., Tamoi, M., Shigeoka, S. (2000). Evaluation of the defense system in chloroplasts to photooxidative stress caused by paraquat using transgenic tobacco plants expressing catalase from *Escherichia coli*. *Plant Cell Physiol* **41**: 311–332.

Miyawaki, A., Llopis, J., Heim, R., McCaffery, JM., Adams, JA., *et al.,* (1997). Fluorescent indicators for Ca2+ based on green fluorescent proteins and calmodulin. *Nature* **388**: 882–887.

Moore, M., Harrison, MS., Peterson, EC., Henry, R. (2000). Chloroplast Oxa1p homolog Albino3 is required for post-translational integration of the light harvesting chlorophyll-binding protein into thylakoid membranes. *J Biol Chem* **275**: 1529–1532.

Mori, H., Ito, K. (2001). The Sec protein-translocation pathway. *Trends Microbiol* **9**: 494–500.

Mullineaux, CW., Allen, JF. (1990). State 1-state 2 transitions in the cyanobacterium *Synechococcus* 6301 are controlled by the redox state of electron carriers between photosystems I and II. *Photosynth Res* **22**: 157–166.

Mullineaux, CW. (1999). The thylakoid membranes of cyanobacteria: structure, dynamics and function. *Aust J Plant Physiol* **26**: 671–677.

Mullineaux, CW., Sarcina, M. (2002). Probing the dynamics of photosynthetic membranes with fluorescence recovery after photobleaching. *Trends Plant Sci* **7**: 237–240.

Mullineaux, CW., Emlyn-Jones, D. (2005). State transitions: an example of acclimation to low-light stress. *J Exp Bot* **56**: 389–393.

Murata, N., Siegenthaler, PS. (1998). Lipids in photosynthesis: an overview, in: Siegenthaler PA, MurataN (Eds.), Lipids in Photosynthesis, Kulwer Academic Publishers, Dordrecht, pp. 1–20.

Neely, WC., Martin, JM., Barker, SA. (1988). Products and relative reaction rates of the oxidation of tocopherols with singlet molecular oxygen. *Photochem Photobiol* **48**: 423–428.

Nenninger, A., Mastroianni, G., Robson, A., Lenn, T., Xue, Q., Leake, MC., Mullineaux, CW. (2014). Independent mobility of proteins and lipids in the plasma membrane of *Escherichia coli*. *Mol Microbiol* **92**: 1142–1153.

Neuwald, AF. *et al.*, (1999). AAA+: a class of chaperone- like ATPases associated with the assembly, operation and disassembly of protein complexes. *Genome Res* **9**: 27–43.

Nevo, R., Charuvi, D., Shimoni, E., *et al.*, (2007). Thylakoid membrane perforations and connectivity enable intracellular traffic in cyanobacteria. *EMBO J* **26**: 1467–1473.

Nickelsen, J., Rengstl, B., Stengel, A., Schottkowski, M., Soll, J., Ankele, E. (2011). Biogenesis of the cyanobacterial thylakoid membrane system an update. *FEMS Microbiol Lett* **315**: 1–5.

Nickelsen, J. and Rengstl, B. (2013). Photosystem II assembly: from cyanobacteria to plants. *Annual review of plant biology* **64**: 609–635.

Nierzwickibauer, SA., Balkwill, DL., Stevens, SE. (1983). 3-Dimensional ultrastructure of a unicellular cyanobacterium. *J Cell Biol* **97**: 713–722.

Nies, DH., Grass, G. (2009). Transition metal homeostasis., EcoSal *Escherichia coli* and *Salmonella*: cellular and molecular biology. *SM Press, Washington, DC* **Chapter 5.4.4.3**.

Nikaido, H. (2003). Molecular basis of bacterial outer membrane permeability revisited. *Microbiol Mol Bio Rev* **67**: 593–656.

Nishiyama, Y., Yamamoto, H., Allakhverdiev, SI., Inaba, M., Yokota, A., Murata, N. (2001). Oxidative stress inhibits the repair of photodamage to the photosynthetic machinery. *EMBO J* **20**: 5587–5594.

Nishiyama, Y., Allakhverdiev, SI., Yamamoto, H., Hayashi, H., Murata, N. (2004). Singlet oxygen inhibits the repair of photosystem II by suppressing the translation elongation of the D1 protein in *Synechocystis* sp. PCC 6803. *Biochemistry* **43**: 11321–11330.

Niwa, H., Tsuchiya, D., Makyio, H., Yoshida, M. and Morikawa, K. (2002). Hexameric ring structure of the ATPase domain of the membrane-integrated matallo-protease FtsH from *Thermus thermophiles* HB8. *Structure* **10**: 1415–1423.

Niyogi, KK., Truong, TB. (2013). Evolution of flexible non-photochemical quenching mechanisms that regulate light harvesting in oxygenic photosynthesis. *Curr Opin Plant Biol* **16**: 307–314.

Nixon, PJ., Michoux, F., Yu, J., Boehm, M., Komenda, J. (2010). Recent advances in understanding the assembly and repair of photosystem II. *Ann Bot* **106**: 1–16.

Norling, B., Zak, E., Andersson, B., Pakrasi, H. (1998). 2D-isolation of pure plasma and thylakoid membranes from the cyanobacterium *Synechocystis* sp. PCC 6803. *FEBS Lett* **436**: 189–192.

Nowaczyk, MM., Hebeler, R., Schlodder, E., Meyer, HE., Warscheid, B., Rogner, M. (2006). Pbs27 a cyanobacterial lipoprotein, is involved in the repair cycle of photosystem II. *Plant Cell* **18**: 3121-3131.

Murata, N., Suleyman, I., Allakhverdievb, C., Nishiyama, Y. (2012). The mechanism of photoinhibition *in vivo*: Re-evaluation of the roles of catalase, α-tocopherol, non-photochemical quenching, and electron transport. *Bioch Bioph Acta Bioener* **8**: 1127–1133.

Nowaczyk, MM., Hebeler, R., Schlodder, E., Meyer, HE., Warscheid, B., Rogner, M. (2006). Psb27, a cyanobacterial lipoprotein, is involved in the repair cycle of photosystem II. *Plant Cell* **18**: 3121–3131.

Mustardy, L., Buttle, K., Steinbach, G., Garab, G. (2008). The Three-Dimensional Network of the Thylakoid Membranes in Plants: Quasihelical Model of the Granum-Stroma Assembly. *Plant Cell* **20**: 2552–2557.

Ogura, T., Inoue, K., Tatsuta, T., Suzaki, T., Karata, K., Young, K., Su, LH., Fierke, CA., Jackman, JE., Raetz, CR., Coleman, J., Tomoyasu, T., Matsuzawa, H. (1999). Balanced biosynthesis of major membrane components through regulated degradation of the committed enzyme of lipid A biosynthesis by the AAA protease FtsH (HflB) in *Escherichia coli*. *Mol Microbiol* **31**: 833–844.

Ogura, T., Wilkinson, AJ. (2001). AAA+ superfamily ATPases: common structure-diverse function. *Genes Cells* **6**: 575–597.

Ohad, I., Kyle, DJ., Arntzen, CJ. (1984). Membrane protein damage and repair: removal and replacement of inactivated 32-kilodalton polypeptides in chloroplast membranes. *J Cell Biol* **99**: 481–485.

Ormo, M., Cubitt, AB., Kallio, K., Gross, LA., Tsien, RY., Remington, SJ. (1996). Crystal structure of the *Aequorea victoria* green fluorescent protein. *Science* **273**: 1392–1395.

Ossenbuhl, F., Gohre, V., Meurer, J., Krieger-Liszkay, A., Rochaix, JD., Eichacker, LA. (2004). Efficient assembly of photosystem II in *Chlamydomonas reinhardtii* requires Alb3.1p, a homolog of *Arabidopsis* ALBINO3. *Plant Cell* **16**: 1790–1800.

Ossenbuhl, F., Inaba-Sulpice, M., Meurer, J., Soll, J., Eichacker, LA. (2006). The *Synechocystis* sp. PCC 6803 oxa1 homolog is essential for membrane integration of reaction center precursor protein pD1. *Plant Cell* **18**: 2236–2246.

Ostersetzer, O., Adam, Z. (1997). Light-stimulated degradation of an unassembled Rieske FeS protein by a thylakoid-bound protease: the possible role of the FtsH protease. *Plant Cell* **9**: 957–965.

Pisareva, T., Shumskaya, M., Maddalo, G., Ilag, L., and Norling, B. (2007). Proteomics of *Synechocystis* sp. PCC 6803. Identification of novel integral plasma membrane proteins. *The FEBS Journal* **274**: 791–804.

Plemper, RK., and Wolf, DH. (1999). Retrograde protein translocation: ERADication of secretory proteins in health and disease. *Trends Biochem Sci* **24**: 266–270.

Plucken, H., Muller, B., Grohmann, D., Westhoff, P., Eichacker, LA. (2002). The HCF136 protein is essential for assembly of the photosystem II reaction center in *Arabidopsis thaliana*. *FEBS Lett* **532**: 85–90.

Powles, SB. (1984). Photoinhibition of photosynthesis induced by visible light. *Annu Rev Plant Physiol* **35**: 15–44.

Pralle, A., Keller, P., Florin, E.L., Simons, K., and Horber, J.K. (2000). Sphingolipid-cholesterol rafts diffuse as small entities in the plasma membrane of mammalian cells. *J Cell Biol* **148**: 997–1008.

Pribil, M., Pesaresi, P., Hertle, A., Barbato, R., Leister, D. (2010). Role of plastid protein phosphatase TAP38 in LHCII dephosphorylation and thylakoid electron flow. *PLoS Biol* **8**: e1000288.

Priestley, J. (1774). Experiments and Observations on Different Kinds of Airs. *Book, 1st Ed. 1774, 2nd Ed. 1776*.

Rengstl, B., Oster, U., Stengel, A., and Nickelsen, J. (2011). An intermediate membrane subfraction in cyanobacteria is involved in an assembly network for photosystem II biogenesis. *J Biol Chem* **286**: 21944–21951.

Rengstl, B., Knoppova, J., Komenda, J., Nickelsen, J. (2013). Characterization of a *Synechocystis* double mutant lacking the photosystem II assembly factors YCF48 and Sll0933. *Planta* **237**: 471–480.

Reuter, W., and Muller, C. (1993). New trends in photobiology : Adaptation of the photosynthetic apparatus of cyanobacteria to light and co2. *J Photochem Photobiol* **21**: 3–27.

Rexroth, S., Mullineaux, CW., Ellinger, D., Sendtko, E., Rogner, M., Koenig, F. (2011). The plasma membrane of the cyanobacterium *Gloeobacter violaceus* contains segregated bioenergetic domains. *The Plant Cell* **23**: 2379–2390.

Robinson, C., Woolhead, C., Edwards, W. (2000). Transport of proteins into and across the thylakoid membrane. *J Exp Bot* **51**: 369–374.

Rokka, A., Suorsa, M., Saleem, A., Battchikova, N., and Aro, EM. (2005). Synthesis and assembly of thylakoid protein complexes: multiple assembly steps of photosystem II. *Biochm J* **380**: 159–168.

Roose, JL., Pakrasi, HB. (2004). Evidence that D1 processing is required for manganese binding and extrinsic protein assembly into photosystem II. *J Biol Chem* **279**: 45417–45422.

Roose, JL., Pakrasi, HB. (2008). The Psb27 protein facilitates manganese cluster assembly in photosystem II. *J Biol Chem* **283**: 4044–4050.

Ruban, AV., Young, AJ., Horton, P. (1993). Induction of Non-photochemical energy dissipation and absorbance changes in leaves (Evidence for changes in the state of the light-harvesting system of Photosystem II *in vivo*. *Plant Physiol* **102**: 741–750.

Ruban, AV., Johnson, MP., Duffy, CD. (2012). The photoprotective molecular switch in the photosystem II antenna. *Biochim Biophys Acta* **1817**: 167–181.

Sako, Y., Kusumi, A. (1995). Barriers for lateral diffusion of transferrin receptor in the plasma membrane as characterized by receptor dragging by laser tweezers: fence versus tether. *J Cell Biol* **129**: 1559–1574.

Sakurai, I., Shen, JR., Leng, J., Ohasi, S., Kobayashi, M., Wada, H. (2006). Lipids in oxygen-evolving photosystem II complexes of cyanobacteria and higher plants. *J Biochem* **140**: 201–209.

Sakurai, I., Mizusawa, N., Ohasi, S., Kobayashi, M., Wada, H. (2007). Effect of the lack of phosphatidylglycerol on the donor side of photosystem II. *Plant Physiol* **144**: 1336–1346.

Sakurai, I., Mizusawa, N., Wada, H., Sato, N. (2007). Digalactosyldiacylglycerol is required for stabilization of the oxygen-evolving complex in photosystem II. *Plant Physiol* **145**: 1361–1370.

Samuelsson, G., Lonneborg, A., Rosenqvist, E., Gustafsson, P., Oquist, G.

(1985). Photoinhibition and reactivation of photosynthesis in the cyanobacterium *Anacystis nidulans*. *Plant Physiol* **79**: 992–995.

Sandmann, G., Reck, H., Kessler, E., Boeger, P. (1983). Photoinhibition and reactivation of photosynthesis in the cyanobacterium *Anacystis nidulans*. *Archives of Microbiology* **134**: 23–27.

Sato, N., Murata, Y., Miura, Y, and Ueta, N. (1979). Effect of growth temperature on lipid and fatty acid compositions in the blue-green algae *Anabaena variabilis* and *Anacystis nidulans*. *Biochim Biophy Acta* **572**: 19–28.

Sato, N., Hagio, M., Wada, H., Tsuzuki, M. (2000). Requirement of phophatidylglycerol for photosynthetic function in thylakoid membranes. *proc natl Acad Sci USA* **97**: 10655–10660.

Sato, N. (2004). Roles of the acidic lipids sulfoquinovosyl diacylglycerol and phosphatidylglycerol in photosynthesis: their specificity and evolution. *J Plant Res* **117**: 495–505.

Satoh, K., Yamamoto, Y. (2007). The carboxyl-terminal processing of precursor D1 protein of the photosystem II reaction center. *Phoyosynth Res* **94**: 203–215.

Schatz, G., Dobberstein, B. (1996). Common principles of protein translocation across membranes. *Science* **271**: 1519–1526.

Scheller, HV., Haldrup, A. (2005). Photoinhibition of Photosystem I. *Planta* **221**: 5–8.

Schimper, AFW. (1883). Uber die Entwicklung der Chlorophyllkorner und Farbkorper. *Bot Zeitung* **41**: 5-14, 121-131, 137-146, 153-162.

Schneider, D., Fuhrmann, E., Scholz, I., Hess, WR., Graumann, PL. (2007) Fluorescence staining of live cyanobacterial cells suggest non-stringent chromosome segregation and absence of a connection between cytoplasmic and thylakoid membranes. *BMC Cell Biol* **3**:8 39.

Schottkowski, M., Gkalympoudis, S., Tzekova, N., Stelljes, C., SchÃŒnemann, D., *et al.,* (2009). Interaction of the periplasmic PratA factor and the PsbA (D1) protein during biogenesis of photosystem II in *Synechocystis* sp. PCC 6803. *J Biol Chem* **284**: 1813–1819.

Schroeder, R., London, E. and Brown, D. (1994). Interactions between saturated acyl chains confer detergent resistanceon lipids and glycosylphospatidylinositol (GPI)-anchored proteins: GPI-anchored proteins in liposomes and cells show similat behavior. *Proc Natl Acad Sci USA* **91**: 12130–12134.

Sergent, O., Djoudi-Aliche, F., Lagadic-Gossmann D. (2012). Up-to-data insight about memrane remodeling as a mechanism of action for ethanol-induced liver toxicity. *Trends in Liver Disease Research* **Chapter 9**: 159–178.

Shen, JR. and Inoue, Y. (1993). Binding and functional properties of two

new extrinsic components, cytochrome c550 and a 12-kDa protein, in cyanobacterial photosystem II. *Biochemistry* **32**: 1825–1832.

Sherman, DM., Troyan, TA., Sherman, LA. (1994). Localization of membrane proteins in the cyanobacterium *Synechococcus* sp. PCC 7942. *Plany Physiol* **106**: 251–262.

Shi, LX., Hall, M., Funk, C., Schroder, WP. (2012). Photosystem II, a growing complex: updates on newly discovered components and low molecular mass proteins. *Biochim Biophys Acta* **1817**: 13–25.

Shimomura, O., Johnson, FH., Saiga, Y. (1962). Extraction, purification and properties of aequorin, a bioluminescent protein from the lumi- nous hydromedusan, *Aequorea*. *J Cell Comp Physiol* **59**: 223–239.

Shotland, Y., Koby, S., Teff, D., Mansur, N., Oren, DA., Tatematsu, K., Tomoyasu, T., Kessel, M., Bukau, B., Ogura, T., Oppenheim, AB. (1997). Proteolysis of the phage λ CII egulatory protein by FtsH (HflB) of *Escherichia coli*. *Mol Microbiol* **24**: 1303–1310.

Silva, P., Thompson, E., Bailey, S., Kruse, O., Mullineaux, CW., Robinson, C., Mann, NH., Nixon, PJ. (2003). FtsH is involved in the early stages of repair of photosystem II in *Synechocystis* sp. PCC 6803. *Plant Cell* **15**: 2152–2164.

Simidjiev, I., Stoylova, S., Amenitsch, H., Javorfi, Y., Mustardy, L., Laggner,

P., Holzenburg, A., Garab, G. (2000). Self-assembly of large, ordered lamellae from non-bilayer lipids and integral membranes proteins *in vitro*. *Proc Natl Acad Sci USA* **97**: 1473–1476.

Sinder, J., Thibault, G., and Houry, WA. (2008). The AAA+ superfamily of functionally diverse proteins. *Genome Biology* **9**: 216.

Simmons, K., and Vaz, WLC. (2004). Model systems, lipid rafts, and cell membranes. *Annu Rev Biophys Biomol Struct* **33**: 269–295.

Skovsen, E., Snyder, JW., Lambert, JDC., Ogilby, PR. (2005). Lifetime and Diffusion of Singlet Oxygen in a Cell. *J Phys Chem Letters* **109**: 8570–8573.

Sokolenko, A., Pojidaeva, E., Zinchenko, V., Panichkin, V., Glaser, VM., Herrmann, RG., Shestakov, SV. (2002). The gene complement for proteolysis in the cyanobacterium *Synechocystis* sp. PCC 6803 and *Arabidopsis thaliana* chloroplasts.*Curr Genet* **41**: 291–310.

Spence, E., Sarcina, M., Ray, N., Moller, SG., *et al.,* (2003). Membrane-specific targeting of green fluorescent protein by the Tat pathway in the cyanobacterium *Synechocystis* PCC6803. *Mol Microbiol* **41**: 1481–1489.

Spetea, C., Hundal, T., Lohmann, F., Andersson, B. (1999). GTP bound to chloroplast thylakoid membranes is required for light-induced, multienzyme degradation of the photosystem II D1 protein. *Proc Natl Acad Sci USA* **96**: 6547–6552.

Styring, S., Johannes, S., Mamedov, F. (2011). Two tyrosines that changed the world: Interfacing the oxidizing power of photochemistry to water splitting in photosystem II. *Biochim Biophys Acta* **1817**: 76–87.

Stengel, A., Gugel, IL., Hilger, D., Rengstl, B., Jung, H., Nickelsen, J. (2012). Initial steps of photosystem II de novo assembly and preloading with manganese take place in biogenesis centers in *Synechocystis*. *Plant Cell* **24**: 660–675.

Stirnberg, M., Fulda, S., Huckauf, J., Hagemann, M., Kramer, R., Marin, K. (2007). A membrane-bound FtsH protease is involved in osmoregulation in *Synechocystis* sp. PCC 6803: the compatible solute synthesizing enzyme GgpS is one of the targets for proteolysis. *Mol Microbiol* **63**: 86–102.

Sun, X., Ouyang, M., Guo, J., Ma, J., Lu, C., *et al.,* (2010). The thylakoid protease Deg1 is involved in photosystem-II assembly in *Arabidopsis thaliana*. *Plant J* **62**: 240–249.

Taylor, RG. *et al*,. (1993). *E. coli* host strains significantly affect the quality of small scale plasmid DNA preparations used for sequencing. *Nucleic Acids Res* **21**: 1677–1678.

Thornton, LE., Roose, JL., Pakrasi, HB., Ikeuchi, M. (2005). he low molecular weight proteins of photosystem II. In Photosystem II: The Water/Plastoquinone Oxido-Reductase in Photosynthesis. *The Neth.: Springer, Ed. T. Wydrzynski,*

K Satoh, pp 121–138.

Tikkanen, M., Nurmi, M., Kangasjarvi, S., Aro, EM. (2008). Core protein phosphorylation facilitates the repair of photodamaged photosystem II at high light. *Biochim Biophys Acta* **1777**: 1432–1437.

Tomoyasu, T., Yuki, T., Morimura, S., Mori, H., Yamanaka, K., Niki, H., Hiraga, S. and Ogura, T. (1993a). The *Escherichia coli* FtsH protein is a prokaryotic member of a protein family of putative ATPases involved in membrane functions, cell cycle control and gene expression. *J Bacteriol* **175**: 1344-1351.

Tomoyasu, T. *et al.,* (1993b). Topology and subcellular localization of FtsH protein in *Escherichia coli*. emphJ Bacteriol **175**: 1352–1357.

Tomoyasu, T., Gamer, J., Bukau, B., Kanemori, M., Mori, H., Rutman, AJ., Oppenheim, AB., Yura, T., Yamanaka, K., Niki, H., *et al.,* (1995). *Escherichia coli* FtsH is a membrane-bound, ATP-dependent protease, which degrades the heat-shock transcription factor sigma 32. *EMBO J* **14**: 2551–2560.

Tottey, S., *et al*. (2008). Protein-folding location can regulate manganese-binding versus copper- or zinc-binding. *Nature* **455**: 1138–1142.

Triantaphylides, C., Krischke, M., Hoeberichts, FA., Ksas, B., Gresser, G., Havaux, M., Van Breusegem, F., Mueller, MJ.(2008). Singlet oxygen is the major reactive oxygen species involved in photooxidative damage to plants. *Plant Physiol* **148**: 960–968.

Tsien, RY.(1998). The green fluorescent protein. *EMBO J* **67**: 509–544.

Turcsanyi, E., Vass, I.(2000). Inhibition of photosynthetic electron transport by UV-A radiation targets the Photosystem II complex. *Photochem Photobiol* **72**: 513–520.

Umena, Y. *et al.,* (2011). Crystal structure of oxygen-evolving photosystem II at a resolution of 1.9A. *Nature* **473**: 55–61.

Urantowka, A., Knorpp, C., Olczak, T., Kolodziejczak, M., Janska, H. (2005). Plant mitochondria contain at least two i-AAA-like complexes. *Plant Mol Biol* **59**: 239–252.

van de Meene, AM., Hohmann-Marriott, MF., Vermaas, WF. and Roberson, RW. (2006). The three-dimensional structure of the cyanobacterium *Synechocystis* sp. PCC 6803. *Arch Microbiol* **184**: 259–270.

van de Meene, AM., Sharp, WP., McDaniel, JH., Vermaas, WF. and Roberson, RW. (2012). Gross morphological changes in thylakoid membrane structure are associated with photosystem I deletion in *Synechocystis* sp. PCC 6803. *Biochim Biophys Acta* **1818**: 1427–1434.

Vass, I. (1996a). Adverse effects of UV-B light on the structure and function of the photosynthetic apparatus. *Handbook of Photosynthesis, Marcel Dekker*: 931–950.

Vass, I., Sass, L., Spetea, C., Bakou, A., Ghanotakis, D., Petrouleas, V. (1996b). UV-B induced inhibition of Photosystem II electron transport studied by EPR and chlorophyll fluorescence. Impairment of donor and acceptor side components. *Biochemistry* **35**: 8964–8973.

Vass, I., Cser, K. (2009). Janus-faced charge recombinations in photosystem II photo-inhibition. *Trends Plant Sci* **14**: 200–205.

Vass, I., Cser, K. (2011a). Role of charge recombination processes in photodamage and photo-protection of the photosystem II complex. *Physiol Plant* **142**: 1–11.

Vass, I., Cser, K. (2011b). Molecular mechanisms of photodamage in the Photosystem II complex. *Physiol Plant* **1817**: 209–117.

Verev. G., Szollosi, J., Matko, J., Nagy, P., Farkas, T., Vigh, L., Matyus, L., Waldmann, TA., Damjanovivh, S. (2003. Dynamic, yet structured: The cell membrane three decades after Singer-Nicolson model. *Natl Acad Sci USA* **100**: 8053–8058.

Vermaas, W., Timlin, J., Jones, H., et al., (2008) *In vivo* hyperspectral confocal fluorescence imaging to determine pigment localization and distribution in cyanobacterial cells. *Proc Natl Acad Sci USA* **105**: 4050–4055.

Vuorio, R., Vaar, M. (1992). The lipid A biosynthesis mutation lpxA2 of

Escherichia coli results in drastic antibiotic supersusceptibility. *Antimicrob Agents Chemother* **36**: 826–829.

Wada, H., Murata, N. (1998). membranes lipids in cyanobacteria, in : Siegenthaler PA, Murata N (Eds.), Lipids in Photosynthesis, Kluwer Academic Publishers, Dordrecht, 1998, pp. 65–81.

Wada, H., Murata, N. (2007). The essentail role of phosphatidylglycerol in photosynthesis. *Photosynth Res* **92**: 205–215.

Wagner, R., Aigner, H., Funk, C. (2012). FtsH proteases located in the plant chloroplast. *Physiol Plant* **145**: 203–214.

Wang, Q., Jantaro, S., Lu, B., Majeed, W., Bailey, M. (2008). The high light-inducible polypeptides stabilize trimeric photosystem I complex under high light conditions in *Synechocystis* PCC 6803. *Plant physiology* **147**: 1239–1250.

Wei, L., Guo, J., Ouyang, M., Sun, X., Ma, J., *et al.,* (2010). LPA19, a Psb27 homolog in *Arabidopsis thaliana*, facilitates D1 protein precursor processing during PSII biogenesis. *J Biol Chem* **285**: 21391–21398.

Whitney, S., Andrews, T. (2001). Plastome-encoded bacterial ribulose-1,5-bisphosphate carboxylase/oxygenase (RubisCO) supports photosynthesis and growth in tobacco. *Proc Natl Acad Sci USA* **98**: 14738–14743.

Wollman, FA., Minai, L., Nechushtai, R. (1999). The biogenesis and assem-

bly of photosynthetic proteins in thylakoid membranes. *Biochim Biophys Acta* **1411**: 21–85.

Wise, RR., Hoober, JK. (2006). The structure and function of plastids. *Dordrecht, Springer*: 3–21.

Yang, F., Moss, L,, Phillips, G. (1996). The molecular structure of green fluorescent protein. *Nat Biotechnol* **14**: 1246–1251.

Yerkes, CT., Kramer, DM., Fenton, JM., Crofts, AR. (1990). UV-photoinhibition: studies *in vitro* and in intact plants. *Current research in Photosynthesis* **vol. II**: II. 6.381–II.6.384.

Yokoe, H., Meyer, T. (1996). Spatial dynamics of GFP-tagged proteins investigated by local fluorescence enhancement. *Nat Biotechnol* **14**: 1252–1256.

Young, K., Silver, LL., Bramhill, D., Cameron, P., Eveland, SS., Raetz, CRH., Hyland, SA., Anderson, MS. (1995). The envA permeability/cell division gene of *Escherichia coli* encodes the second enzyme of lipid A biosynthesis. *J Biol Chem* **270**: 30384–30391.

Yu, RC., Hanson, PI., Jahn, R., Brunger, AT. (1998). Structure of the ATP-dependent oligomerization domain of N-ethylmaleimide-sensitive factor complexed with ATP. *Nat Struct Biol* **5**: 803–811.

Yu, F., Park, S., Rodermel, SR. (2004). The *Arabidopsis* FtsH metalloprotease

gene family: interchanageability of subunits in chloroplast oligomeric complexes. *Plant J* **37**: 864–876.

Zak, E., Norling, B., Maitra, R., Huang, F., Andersson, B., Pakrasi, HB. (2001). The initial steps of biogenesis of cyanobacterial photosystems occur in plasma membranes.*Proc Natl Acad Sci USA* **98**: 13443–13448.

Zhang, L., Paakkarinen, V., van Wijk, KJ., Aro, EM. (1999). Co-translational assembly of the D1 protein into photosystem II. *J Biol Chem* **274**: 16062–16067.

Zhang, L., Aro, EM. (2002). Synthesis membrane insertion and assembly of the chloroplast-encoded D1 protein into photosystem II. *FEBS Lett* **512**: 13–18.

Zhang, P., Sicora, CI., Vorontsova, N., Allahverdiyeva, Y., Battchikova, N., Nixon, PJ., Aro, EM. (2007). FtsH protease is required for induction of inorganic carbon acquisition complexes in *Synechocystis* sp. PCC 6803. *Mol Microbiol* **65**: 728–740.

Zinchuk, V., Zinchuk, O., and Okada, T. (2007). Quantitative colocalization analysis of multicolor confocal immunofluorescence microscopy images: pushing pixels to explore biological phenomena. *Acta Histochem Cytochem* **40**: 101–111.

Zurawski, G., Bohnert, HJ., Whitfeld, PR., Bottomley, W. (1982). Nucleotide

sequence of the gene for the M(r) 32,000 thylakoid membrane protein from *Spinacia oleracea* and *Nicotiana debneyi* predicts a totally conserved primary translation product of M(r) 38,950 *Proc Natl Acad Sci USA* **79**: 7699–7703.

Appendix

1. Pearson's Correlation Coefficient (PCC) and Mander's Overlap Coefficient (MOC)

Pearson's Correlation Coefficient (PCC) used in Chapter 3 (Zinchuk *et al.*, 2007).

$$R_r = \frac{\sum_i (S1_i - S1_{aver}) \cdot (S2_i - S2_{aver})}{\sqrt{\sum_i (S1_i - S1_{aver})^2 \cdot \sum_i (S2_i - S2_{aver})^2}}$$

Where:

S1 represents signal intensities of pixels in channel 1

S2 represents signal intensities of pixels in the channel 2

$S1_{aver}$, $S2_{aver}$ reflect the average intensities of these two channels, respectively

R_r value range <-1.0,1.0>, if R_r = -1.0 indicates complete negative correlation, if R_r = 0 indicates no singificant correlation, if R_r = 1.0 then indicates total positive correlation

Mander's Overlap Coefficient (MOC) (Mander *et al.*, 1993)

$$R = \frac{\sum_i S1_i \cdot S2_1}{\sqrt{\sum_i (S1_i)^2 \cdot \sum_i (S2_1)^2}}$$

Colocalisation coefficients m1 and m2:

$$m_1 = \frac{\sum_i S1_{i,\,coloc}}{\sum_i S1_i}$$

$$m_2 = \frac{\sum_i S2_{i,\,coloc}}{\sum_i S2_i}$$

Where:

S1 represents signal intensities of pixels in channel 1

S2 represents signal intensities of pixels in the channel 2

R ranges <0, 1.0> if R = 0.5 that indicates that 50% of both channels pixels overlap.

m1 ans m2 illustrate the contributions of both channels to the pixel of intrest

$S1_{i,coloc}$ and $S2_{i,coloc}$ represent colocalised pixels of channel 1 and 2, respectively

If m1 = 1.0 and m2 = 0.2 that means that all red pixels (channel 1) colocalise with green (channel 2) but only 20% of green pixels colocalise with red ones.

2. Corrected Total Cell Fluorescence

Corrected Total Cell Fluorescence was calculated based on the following formula:

CTCF = Integrated Density - (Area of selected cell x Mean Fluorescence of Background Readings)

The values were averaged for n = 30 cells, randomly choosen for 3 biological replicates, excluding cells at the phase of division. ImageJ was employed for Fluorescence analysis. The Region Of Intrest (ROI) was selected by hand to pick each individual cell using 8-bit micrographs of GFP channel (from which the post-bleach values were substracted ahead). The measurments were setup to show output of: Area, Integrated Density and Mean Gray Values.

3. Distribution of GFP signal in *Synechocystis* 6803 cell

Algorithms in MATLAB were written and exploited by Prof Nigel Bourrough. His data analysis was based on automatical cell segmentations into regions of: thyalkoid membranes, plasma membrane and cytoplasm. All regions were recognised and set by either: chlorophyll fluorescence (thylakoid membranes), or fluorescnece of proteins of well described locations: FutA1-GFP was used to mark the region of periplasm, FtsH1-GFP: plasma membrane, cytoplasm was distunguished by lower signal threshold.

4. Mass spectrometry results, including the ion scores and identified sequences.

ORF	**Protein ID**	**Sequence**	Ion Score
slr0335	ApcE	FVELGQVSAIR	31
		AYSQSISYLESQVR	36
		RFPTLPAANFPNTER	6
		EIQQYNQILASQGLK	31
		EYSDAFGEDTVPYER	31
ccmM	CcmM	NVVAGRSPSSSSASTS	27
slr0012	RbcL	FLFVQEAIEK	51
		WSPELAAACELWK	17
slr1834	PsaA	WGKPGHFDR	56
		LVPDKGQLGFR	41
		DYDPAKNVNNLLDR	53
slr1835	PsaB	FSQDLAQDPTTR	28
		DFGYSFPCDGPGR	27
ssl0563	PsaC	VYLGAETTR	28
		CETACPTDFLSIR	72
		IYDTCIGCTQCVR	78
		ACPLDVLEMVPWDGCK	16
smr0004	PsaI	GSYAASYLPWILIPM	14
ssr2831	PsaE	SGILYPVIVR	50

ORF	**Protein ID**	**Sequence**	Ion Score
slr1655	PsaL	TFIGNLPAYR	70
		TFIGNPAYRK	23
		AESNQVVQAYNGDPFVGHLSTPISDSAFT	5
sll0851	CP43	NDIQPWQVRGPNGLDLDKLR	57
		LGANIASAQGPTGLGK	52
		DLPSTGFAWWSGNAR	94
		GIDRETEPTLFMPDLD	57
		VITNPTLNPAIIFGYLLK	32
slr0906	CP47	GYFQEEIQR	18
		VHTVVLNDPGR	24
		GYFQEEIQRR	92
		LAFYDYVGNSPAK	101
		YQWDKGYFQEEIQR	31
		VDSQLAEGASLSEAWSTIPEK	122
		DVFAGVDPGLEEQVEFGVFAK	102
		AQLGEGFDFDTETFNSDGVFR	78
		KAQLGEGFDFDTETFNSDGVFR	149
		FSVEQTGVTVSFYGGALDGQTFSNPSDVK	22
ssl2598	psbH	LGDILRPLNSEYGK	65
ssr3451	psbE	QELPILQER	57
sll0849	psbD	AYDFVSQELR	23
		AAEDPEFETFYTK	67
slr1311	PsbA2	VIGTWADVLNR	62
		LIFQYASFNNSR	61
slr1326	AtpA	WDSLGRPIDGK	22
		LLESPAPGIIER	51

ORF	Protein ID	Sequence	Ion Score
slr1329	AtpB	FVQAGSEVSALLGR	61
		FVQAGSEVSALLGR	61
		DVNKQDVLLFIDNIFR	47
		MPSAVGYQPTLGTDVGDLQER	20
		NSAGNEVAVTCEVQQLLGDNQVR	34
slr1327	AtpC	LSFAETELPLFEQRFVSLISSQPVVQ	48
		TLFPLSPQGLEAPDDEIFR	13
		SRVDLPTNAPELIAR	22
slr0228	FtsH2	LVDLLIEKETIDGEEFR	41
slr0228	FtsH2	TPGFSGADLANLLNEAAILTAR	7
sll1463	FtsH4	AAEEIVFDSITTGAANDLQR	70
		TPGFAGADLANLVNEAALLEER	25
sll0247	IsiA	RVEQAFDSLQT	83
sll1578	cpcA	FLSSTELQIAFGR	103
slr1128	DSAINSAQGDAQAR	18	

5. Fatty acids calculations

Fatty acids content was evaluated by measuring the areas under chromatographic peaks registered at certain retention time (found on several examples of chromatographic printouts).

6. Lipid molar concentration

Total lipid content was calculated based on percentage of ratio of sum all the fatty acids identified within one group of lipids (MGDG, DGDG, PG or SQDG) to the total sum of all fatty acids found in the sample (MGDG+DGDG+PG+SQDG).

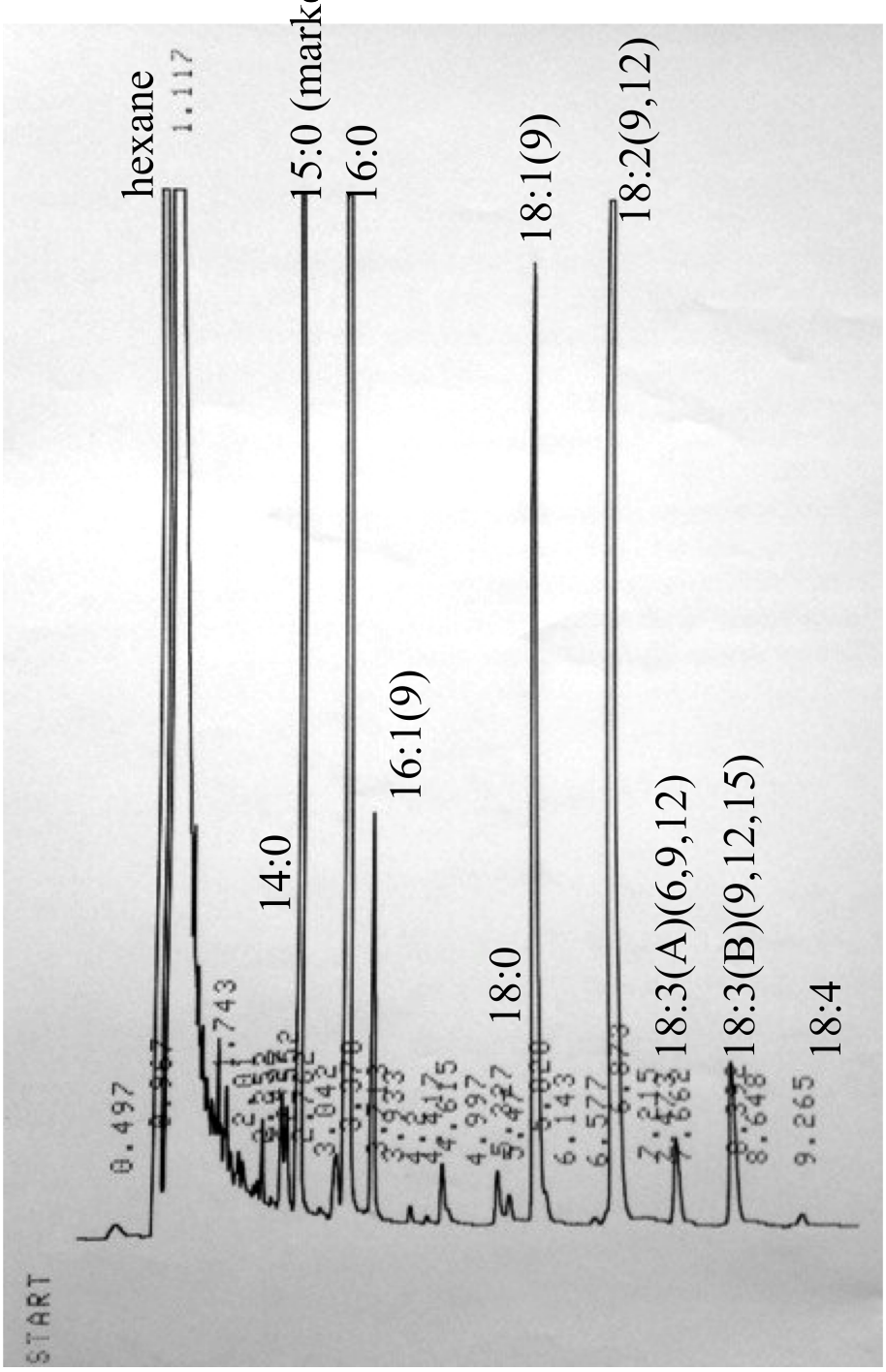

Chromatograph GC separation of lipids derived from wild-type crude membranes. Analysis of fatty acids in PG. X-axis represents the time of retention [min], Y-axis- relative abundance of recognised fatty acids

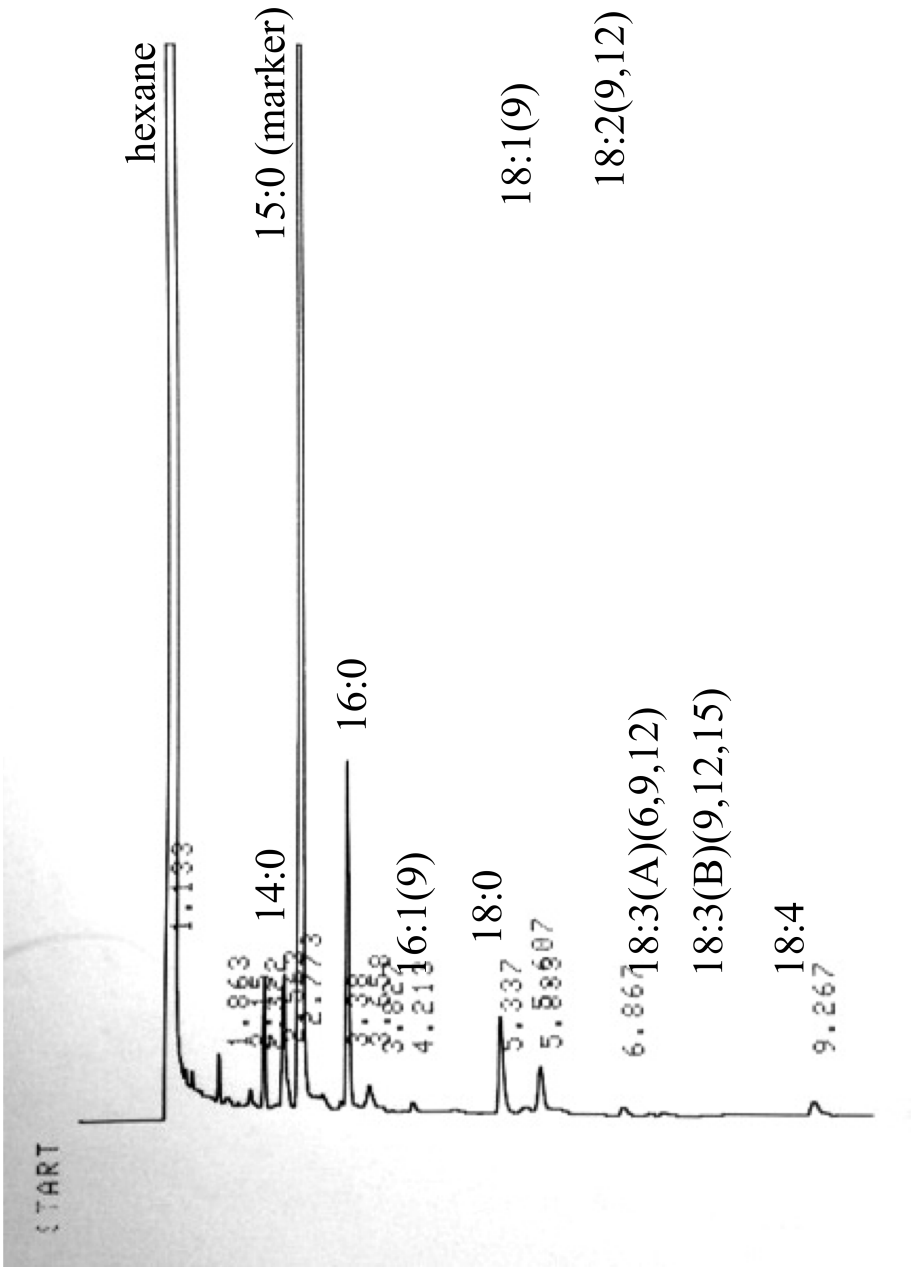

Chromatograph GC separation of lipids derived from membrane fragments isolated from FtsH2-GFP (LL). Analysis of fatty acids in PG, X-axis represents the time of retention [min], Y-axis- relative abundance of recognised fatty acids

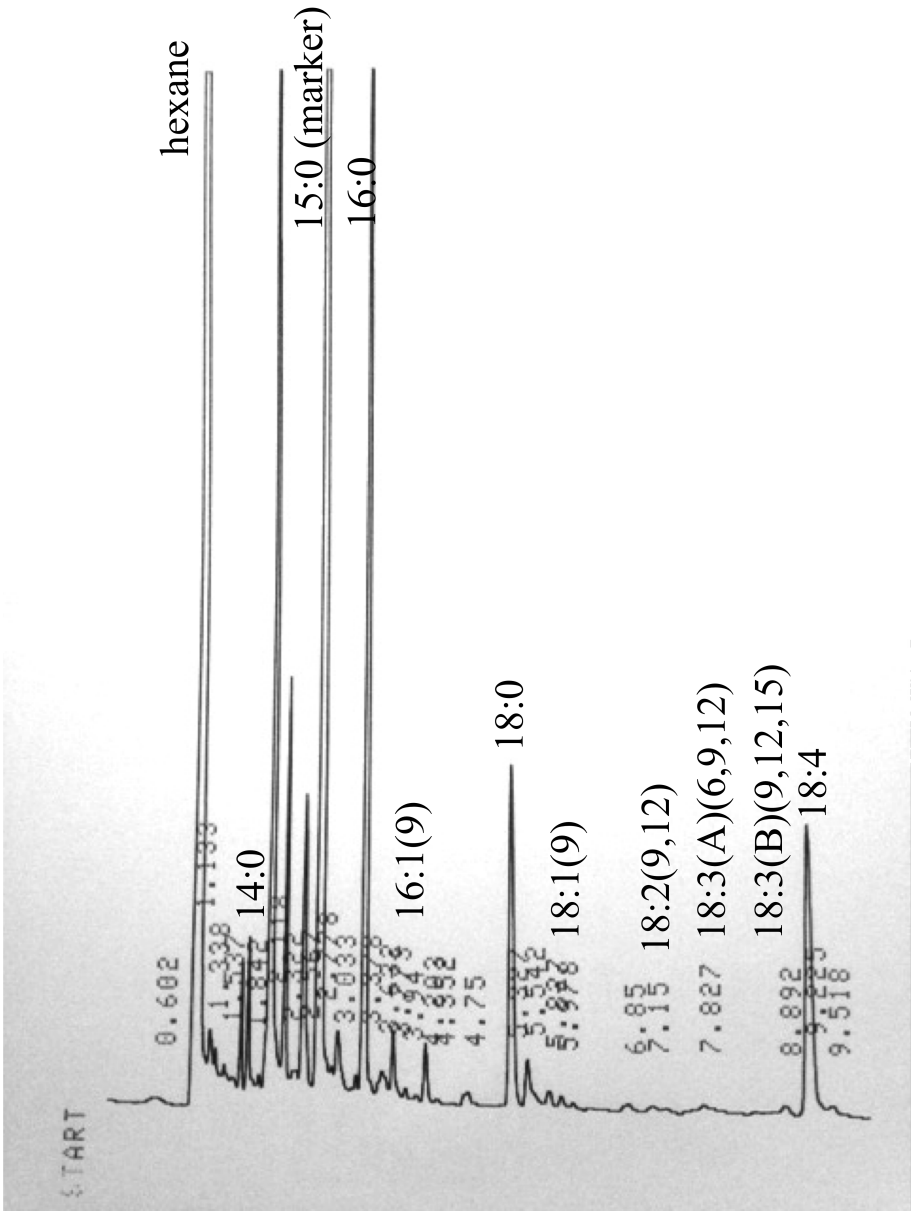

Chromatograph GC separation of lipids derived from membrane fragments isolated from FtsH2-GFP (LL) analysis of fatty acids in DGDG, X-axis represents the time of retention [min], Y-axis- relative abundance of recognised fatty acids